



**HAL**  
open science

# Développement des modèles biomécaniques de l'humain pour l'évaluation ergonomique de commandes automobiles – Application à la pédale d'embrayage

Romain Pannetier

► **To cite this version:**

Romain Pannetier. Développement des modèles biomécaniques de l'humain pour l'évaluation ergonomique de commandes automobiles – Application à la pédale d'embrayage. Biomechanics [physics.med-ph]. UNIVERSITE DE LYON, 2012. English. NNT: . tel-00991439

**HAL Id: tel-00991439**

**<https://theses.hal.science/tel-00991439>**

Submitted on 15 May 2014

**HAL** is a multi-disciplinary open access archive for the deposit and dissemination of scientific research documents, whether they are published or not. The documents may come from teaching and research institutions in France or abroad, or from public or private research centers.

L'archive ouverte pluridisciplinaire **HAL**, est destinée au dépôt et à la diffusion de documents scientifiques de niveau recherche, publiés ou non, émanant des établissements d'enseignement et de recherche français ou étrangers, des laboratoires publics ou privés.

THESE DE L'UNIVERSITE DE LYON

Délivrée par

L'UNIVERSITE CLAUDE BERNARD LYON 1

ECOLE DOCTORALE MEGA

DIPLOME DE DOCTORAT

(arrêté du 7 août 2006)

Spécialité : Mécanique option Biomécanique

soutenue publiquement le 9 novembre 2012

par

**PANNETIER Romain**

**Développement des modèles biomécaniques de l'humain pour  
l'évaluation ergonomique de commandes automobiles – Application à  
la pédale d'embrayage**

Directeur de thèse : WANG Xuguang, IFSTTAR

**JURY**

---

Rapporteur	CHABLAT Damien	Directeur de recherches CNRS, IRCCyN, Centrale Nantes
Rapporteur	PUDLO Philippe	Professeur, LAMIH, ENSIAME
Examineur	CHEZE Laurence	Professeur, LBMC, UCBL 1
Examineur	THIEBAUT Christian	Renault SAS
Examineur	WANG Xuguang	Directeur de recherches, LBMC, IFSTTAR



Ce travail a été réalisé au laboratoire de Biomécanique et Mécanique des chocs, unité mixte de recherche de l'IFSTTAR<sup>1</sup> et de l'université Claude Bernard Lyon 1, dans le cadre d'une convention CIFRE<sup>2</sup> avec le constructeur automobile Renault. Une partie des travaux présentée dans cette thèse a été aussi réalisée dans le cadre du projet européen DHErgo<sup>3</sup>.

---

<sup>1</sup> Institut Français des Sciences et Technologies des Transports, de l'Aménagement et des Réseaux

<sup>2</sup> Convention Industrielle de Formation à la Recherche

<sup>3</sup> Digital Humans for Ergonomic design of products, <http://www.dhergo.org>



# **Développement des modèles biomécaniques de l'humain pour l'évaluation ergonomique de commandes automobiles – Application à la pédale d'embrayage**

## **Résumé**

Ce travail de thèse s'inscrit dans le cadre du développement des mannequins numériques pour l'évaluation ergonomique de la conception de véhicule, plus particulièrement des commandes automobiles. Il vise à développer des modèles biomécaniques permettant la prise en compte de la dynamique du mouvement et de la force exercée lors d'une tâche pour prédire le mouvement et l'inconfort associé. Ce travail s'est focalisé sur la pédale d'embrayage.

Concernant le développement des critères d'inconfort, le concept du mouvement neutre est exploré. Une méthode, basée sur la comparaison entre des mouvements avec des configurations imposées et ceux moins contraintes, est proposée. Elle a permis l'identification de paramètres biomécaniques pertinents et de proposer des indicateurs d'inconfort pour la conception de la pédale d'embrayage.

Les relations entre la posture et la force d'appui ont été étudiées expérimentalement en faisant varier le niveau d'effort exercé sur une pédale statique. Nos résultats montrent que la direction d'effort et l'ajustement postural suivent le principe de minimisation des couples articulaires. Par ailleurs l'utilisation d'un critère de minimisation de l'activité musculaire a montré une amélioration de la prédiction de la direction d'effort pour les efforts peu élevés.

Les indicateurs d'inconfort proposés dans cette étude fournissent des informations objectives permettant aux ingénieurs de conception de comparer des solutions alternatives de design. Le travail sur les mécanismes de contrôle de l'effort et de la posture constitue, quant à lui, une première étape dans l'optique de prendre en compte la force exercée dans la simulation de posture.

## **Mots-clés**

Mannequin numérique, Ergonomie, Inconfort, Simulation de posture, Automobile.



# **Developing biomechanical human models for ergonomic assessment of automotive controls – application to clutch pedal**

## **Abstract**

This thesis takes place in the context of the development of digital human models for ergonomic assessment of vehicle design, particularly automotive controls. It aims to develop biomechanical models that can take into account the dynamics of movement and the force exerted during a task to predict the movement and the associated discomfort. This work focused on the clutch pedal.

For the development of the discomfort criteria, the concept of neutral movement is explored. An approach, based on comparing imposed pedal configurations and less constrained pedal configurations movements, has been proposed. It allowed the identification of relevant biomechanical parameters and to propose indicators of discomfort for the design of the clutch pedal.

The relationships between posture and force exertion were studied experimentally by varying the level of force exerted on a static pedal. Our results show that the direction of force exertion and the postural adjustment follow the principle of minimization of joint torques. Furthermore, the use of a criterion for minimizing muscle activity showed an improvement in predicting the direction of effort for the low and intermediate force levels.

Discomfort indicators proposed in this study provide objective information that allows design engineers to compare design alternatives. Work on the control mechanisms of force exertion and posture is, in turn, a first step towards the simulation of posture/movement by taking into account force exertion.

## **Keywords**

Digital human model, Ergonomics, Discomfort, Simulation of posture, Automotive.



## Remerciements

Après trois années passées à travailler sur cette thèse, devenue « ma grande passion » comme le dirait si bien Omar Sharif, l'heure du bilan a sonné. Pour le bilan scientifique, je vais laisser aux courageux lecteurs la possibilité de se faire une idée. Je vais plutôt profiter de ces lignes pour remercier les personnes sans qui l'ouvrage que vous avez dans vos mains n'existerait pas.

Tout d'abord, je tiens à remercier Xuguang Wang pour tout ce qu'il m'a appris, pour son encadrement, pour sa confiance et son amitié au cours de ces trois années.

Je tiens aussi à remercier particulièrement messieurs Damien Chablat et Philippe Pudlo, pour le temps qu'ils ont consacré à la lecture critique de cet ouvrage. De même, je remercie madame Laurence Chèze et monsieur Christian Thiébaud pour leur participation au jury.

Je remercie également les personnes que j'ai pu côtoyer chez Renault, en particulier Jules Trasbot sans qui ce travail n'aurait pu exister. L'appel des joies de la vie de retraité ayant été trop fort pour Jules, je remercie également Thomas Chapuis puis Olivier Bailly et Antoine Delevoye pour avoir pris sa suite dans l'encadrement de ma thèse. Je n'oublie pas non plus tous les membres de mon comité de suivi de thèse : Anne Guillaume, Stéphane Bouillot, Xavier Chalandon et Christian Thiébaud pour le temps qu'ils m'ont consacré, pour leurs avis et conseils ainsi qu'Annie Picot pour sa gentillesse et sa bonne humeur.

Je pense aussi à toutes les personnes avec qui j'ai travaillé au cours du projet DHErgo : Fabienne Janin de l'ERT, Serge Van Sint Jan et Victor Sholucka de l'ULB, Fabian Guenzkofer et Florian Engstler du LfE-TUM, Juan Tomas Celigueta et Sergio Ausejo du CEIT, Hans-Joachim Wirsching de Human Solutions, Muriel Beaugonin d'ESI, Raphael Bichler de BMW et Lisa Denninger de PSA Peugeot Citroën.

De nombreuses personnes m'ont aidé et conseillé au cours de ces trois années. Je les en remercie et je m'excuse par avance auprès de ceux que je vais oublier. Je tiens en particulier à citer Yves et Richard pour leur disponibilité et leur aide sur la conception des dispositifs expérimentaux. Les moments passés avec vous à l'atelier resteront gravés dans ma mémoire.

Je ne peux pas oublier de remercier Julien N., spécialiste VICON et roi du tracking, sans qui je n'aurai pas pu avoir toutes ces belles données expérimentales. Je remercie également Thomas dit « TomTom » pour ses conseils en calcul d'optimisation et Elodie dit « Elo » pour ses dépannages en statistique.

Si ces trois années à l'INRETS puis à l'Ifsttar m'ont paru si courte et si enrichissante, c'est en particulier grâce à l'ensemble des personnes (chercheurs, techniciens et personnels administratifs) que j'ai côtoyé. Je pense en particulier à Sonia, Zohaib, Zhaopeng, Julien C (et son SciPhone), François, Caroline, Jeanne dit « Jeannette », Julien L. dit « Loulou » mon co-bureau préféré, Flo', Doris, Sophie, Anne-Laure, Cindy, Clem', Fabien, Xavier, Philippe et tous les autres que j'oublie. Votre contribution s'est plus souvent portée sur la bonne humeur et ambiance au laboratoire que sur l'avancement de ma thèse mais qu'importe, ces années n'en ont été que plus agréables.

Enfin je terminerai par remercier ma famille et mes amis pour leur soutien et leurs encouragements au cours de toutes ces années. Un grand merci aussi à Ninou qui m'a énormément soutenu dans le sprint final.

# Table of content

<b>GENERAL INTRODUCTION</b>	<b>1</b>
<b>1</b> <b><i>DIGITAL HUMAN MODELS (DHM) FOR ERGONOMICS IN AUTOMOTIVE INDUSTRY</i></b>	<b>3</b>
<b>2</b> <b><i>COLLABORATIONS BETWEEN RENAULT AND IFSTTAR</i></b>	<b>5</b>
<b>3</b> <b><i>OBJECTIVES OF THIS WORK</i></b>	<b>6</b>
<b>4</b> <b><i>STRUCTURE OF THE DOCUMENT</i></b>	<b>8</b>
<b>CHAPTER 1: LITERATURE REVIEW</b>	<b>9</b>
<b>1</b> <b><i>INTRODUCTION</i></b>	<b>11</b>
<b>2</b> <b><i>DISCOMFORT MODELING</i></b>	<b>12</b>
<b>3</b> <b><i>FORCE EXERTION ON CONTROLS</i></b>	<b>16</b>
<b>4</b> <b><i>POSTURE PREDICTION METHOD</i></b>	<b>19</b>
<b>5</b> <b><i>DISCUSSION AND WORK HYPOTHESES</i></b>	<b>24</b>
<b>CHAPTER 2: USING LESS-CONSTRAINED MOVEMENT TO IDENTIFY OBJECTIVE DISCOMFORT ASSESSMENT CRITERIA</b>	<b>27</b>
<b>1</b> <b><i>INTRODUCTION</i></b>	<b>29</b>
<b>2</b> <b><i>MATERIAL AND METHODS</i></b>	<b>30</b>
<b>3</b> <b><i>ANALYSIS OF THE DISCOMFORT PERCEPTION</i></b>	<b>46</b>
<b>4</b> <b><i>MOTION ANALYSIS OF THE CLUTCH PEDAL OPERATION</i></b>	<b>56</b>
<b>5</b> <b><i>DISCUSSION</i></b>	<b>65</b>
<b>6</b> <b><i>LIMITATIONS</i></b>	<b>73</b>
<b>7</b> <b><i>CONCLUSION</i></b>	<b>74</b>
<b>8</b> <b><i>APPENDIX</i></b>	<b>75</b>
<b>CHAPTER 3: MAXIMUM PEDAL FORCE, FORCE PERCEPTION AND CONTROL OF PEDAL FORCE DIRECTION</b>	<b>101</b>
<b>1</b> <b><i>INTRODUCTION</i></b>	<b>103</b>
<b>2</b> <b><i>MATERIAL AND METHODS</i></b>	<b>105</b>
<b>3</b> <b><i>EXPERIMENTAL OBSERVATIONS</i></b>	<b>113</b>
<b>4</b> <b><i>DISCUSSION</i></b>	<b>123</b>
<b>5</b> <b><i>PEDAL FORCE CONTROL SIMULATION</i></b>	<b>126</b>
<b>6</b> <b><i>CONCLUSION</i></b>	<b>140</b>
<b>7</b> <b><i>APPENDIX</i></b>	<b>141</b>

<b>CHAPTER 4: MUSCULOSKELETAL MODELING AND CONTROL OF THE PEDAL FORCE DIRECTION</b>	<b>157</b>
<b>1</b> <b><i>INTRODUCTION</i></b>	<b>159</b>
<b>2</b> <b><i>MUSCLE FORCE COMPUTATION</i></b>	<b>161</b>
<b>3</b> <b><i>PEDAL FORCE DIRECTION CONTROL BY MINIMIZING MUSCULAR ACTIVITIES</i></b>	<b>167</b>
<b>4</b> <b><i>RESULTS</i></b>	<b>171</b>
<b>5</b> <b><i>DISCUSSION AND CONCLUSION</i></b>	<b>177</b>
<b>6</b> <b><i>APPENDIX</i></b>	<b>180</b>
<b>GENERAL CONCLUSION AND PERSPECTIVES</b>	<b>185</b>
<b>1</b> <b><i>INTRODUCTION</i></b>	<b>187</b>
<b>2</b> <b><i>BIOMECHANICAL APPROACH FOR EVALUATING MOTION RELATED DISCOMFORT</i></b>	<b>187</b>
<b>3</b> <b><i>FORCE EXERTION-TASK CONTROL STRATEGY AND SIMULATION</i></b>	<b>189</b>
<b>4</b> <b><i>PERSPECTIVES FOR INTEGRATION IN AUTOMOTIVE DESIGN PROCESS</i></b>	<b>191</b>
<b>SYNTHESE</b>	<b>193</b>
<b>1</b> <b><i>INTRODUCTION</i></b>	<b>195</b>
<b>2</b> <b><i>IDENTIFICATION DE CRITERES OBJECTIFS D'INCONFORT A PARTIR DU MOUVEMENT « MOINS CONTRAIT »</i></b>	<b>198</b>
<b>3</b> <b><i>CAPACITE MAXIMUM, PERCEPTION ET CONTROLE DE LA DIRECTION DE L'EFFORT SUR PEDALE</i></b>	<b>207</b>
<b>4</b> <b><i>MODELE MUSCULO-SQUELETTIQUE ET CONTROLE DE LA DIRECTION D'EFFORT</i></b>	<b>215</b>
<b>5</b> <b><i>CONCLUSION GENERALE</i></b>	<b>217</b>
<b>REFERENCES</b>	<b>219</b>
<b>PERSONAL PUBLICATION</b>	<b>227</b>

## General introduction

<b>1</b>	<b><i>DIGITAL HUMAN MODELS (DHM) FOR ERGONOMICS IN AUTOMOTIVE INDUSTRY</i></b>	<b>3</b>
<b>2</b>	<b><i>COLLABORATIONS BETWEEN RENAULT AND IFSTTAR</i></b>	<b>5</b>
<b>3</b>	<b><i>OBJECTIVES OF THIS WORK</i></b>	<b>6</b>
<b>4</b>	<b><i>STRUCTURE OF THE DOCUMENT</i></b>	<b>8</b>



## 1 Digital Human Models (DHM) for ergonomics in automotive industry

In the automotive industry, the hypercompetitive market requires car manufacturers to develop their products better and faster. The vehicle development cycle is now between 3-5 years, from design studies to mass production. Thanks to the technologies of CAD (Computer Aided Design) and numerical simulation, it has become possible to assess the ergonomics of a vehicle design in the early stage of development using Digital Human Models (DHMs). Computer simulation using DHMs becomes a method to reduce the design cycle time and cost (Chaffin, 2008). Usually, the ergonomics issues are handled by experts late in the development cycle. DHMs can assist design engineers in considering ergonomic solutions in the very early design phase. In addition, it could also reduce the number of physical mock-ups and experiments.

Chaffin (2005) listed the main functionalities expected in a DHM by design engineers from a survey study by the SAE (Society of Automatic Engineering) G13 Committee. In particular for automotive design, Wang (2008a) identified four important functionalities critical to a DHM:

- Anthropometric modeling by sex, geographic origin, age ...,
- Realistic simulation of posture and movement,
- Prediction of discomfort for task-oriented movements,
- Simulation of a population to predict a percentage of accommodation to a task.

Wang (2008a) also stated that DHMs for ergonomic simulation must evolve into models capable of evaluating the dynamic and muscle parameters, in order, on the one hand, to better understand the mechanisms of movement control and discomfort, and the other hand, to develop ergonomic assessment tools for product design. This is particularly true for the ergonomic assessment of the automotive controls such as the clutch pedal, the hand brake or the gear stick. Indeed, the design of automotive controls concerns not only their reach but also hand or foot force exertion. Adjustment settings are usually available to improve their reach. For example, the users could adjust their seat to better reach the clutch pedal. But other pedal design parameters such as pedal resistance or pedal travel inclination are not adjustable by the user. Inappropriate automotive control design may contribute to muscle fatigue and cause discomfort for users. Thus, there is a need of DHMs capable of helping design engineers for assessing automotive controls.

Currently, only a few DHM software packages are used for ergonomics assessment of product or workplace in industries. More than 95% of the market of DHMs is hold by three software packages (Bubb and Fritzsche, 2008):

- Jack™ from Siemens (Figure 1a)
- Human Builder™ (ex-Safework) from Dassault systems (Figure 1b)
- Ramsis™ from Human solutions (Figure 1c)

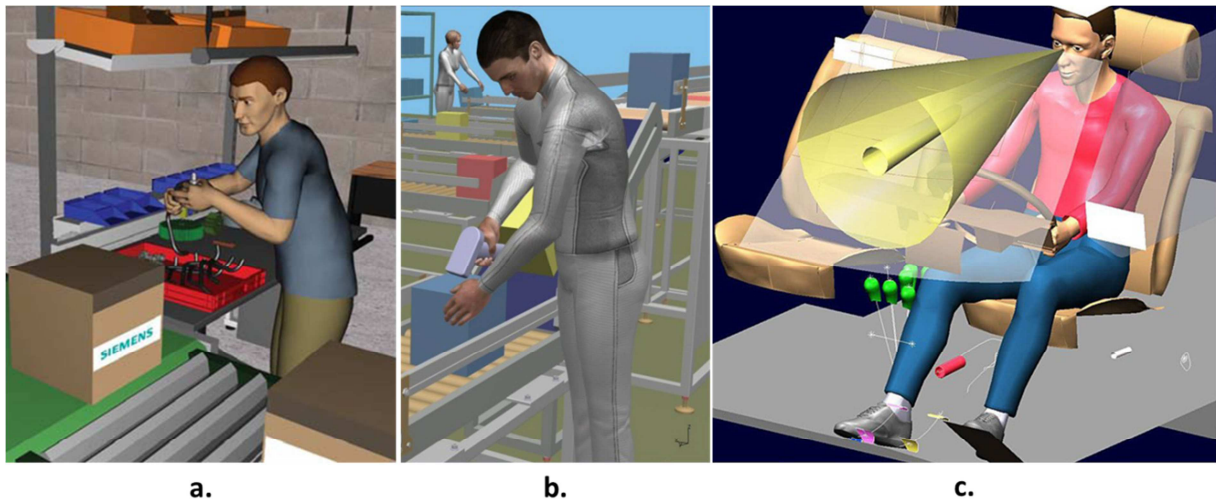


Figure 1: Digital Human Models used for ergonomics simulation in industry. a. Jack™ from Siemens, b. Human Builder™ from Dassault Systemes and c. Ramsis™ from Human solutions.

Jack™ and Human Builder™ claim to cover a large range of simulations from manual handling tasks for manufacturing chain to vehicle interior design. Both have developed specific tools for vehicle interior design: Occupant Packaging Toolkit for Jack™ and Vehicle Occupant Accommodation for Human Builder™. Ramsis™ is the result of cooperation between the German automotive industry, the software company Human solutions and the Institute of Ergonomics of TUM (Technical University of Munich). It was specially developed to aid in the ergonomic design of vehicle interior (Seidl, 1994). According to Bubb and Fritzsche (2008), Ramsis™ is used by over 75% of the world's major vehicle manufacturers.

These three manikins have specific functionalities for vehicle interior design such as reach envelops, vision and mirror analysis, belt analysis and integrated some of the SAE J-Standards such as the vehicle dimensions package (SAE J110) or the accommodation tool reference (J1516). Jack™ and Human Builder™ integrated the Cascade posture-prediction model developed by Reed et al. (2002) for predicting driving posture, which is mainly based

on statistical regression functions from experimental observations of driving postures. About discomfort analysis, working assessment methods such as OWAS (Karhu et al., 1977) or RULA (McAtamney and Corlett, 1993) are implemented. However, these methods were originally developed by ergonomics experts to assess working postures and/or tasks in industry (Dellman, 2004). In Ramsis™, a posture-prediction algorithm is based on the principle of maximizing the likelihood of joint angles relative to a database of driving postures (Seidl, 1994). More recently, the FOCOPP model (Seitz et al., 2005; Wirsching and Engstler, 2012) was proposed for predicting postures implying force exertion. Postures are predicted by minimizing joint load (sum of active joint torques, i.e. due to muscles, and passive joint torques) relative to joint strength (maximal voluntary joint torques, i.e. due to muscular strength and passive joint torques, i.e. due to the body parts' masses). The discomfort could be assessed at each joint from a linear correlation between joint load and joint discomfort (Zacher and Bubb, 2004). The posture prediction and discomfort modeling integrated in Ramsis™ have the advantage to take into account the force applied for predicting posture and discomfort. However, all external forces (magnitude and direction) have to be known and usually, only the useful component of the force to apply on the control is known. The force direction that a person may apply is not always known. In addition, relevant objective discomfort criteria are difficult to identify using this model.

## 2 Collaborations between Renault and IFSTTAR

This PhD thesis follows on a long history of collaborations between the car manufacturer Renault and IFSTTAR on the ergonomic assessment of vehicle interior design. Renault and IFSTTAR started working together on proposing digital tools for the evaluation of the ergonomic qualities of a car design in the late eighties with the development of the digital human model MAN3D (Verriest et al., 1994). This DHM allowed the three-dimensional geometric representation of individuals of any anthropometric dimensions and solved geometrical and static problems as reaching. However, like many DHMs, it did not guarantee a realistic representation of the gestural and postural behavior of a human being. Furthermore, the discomfort resulting from interactions with the environment and internal mechanical stresses affecting the musculoskeletal system was not considered. Then both Renault and IFSTTAR focused the development of tools for simulating realistic motion and for predicting discomfort. An important step was the European project REALMAN (2001-2004) in which

Renault and IFSTTAR participated. Following this project, Renault, IFSTTAR and Altran began the development of a motion simulation tool for ergonomic assessment of vehicle interior design called RPx and based on the concepts developed in REALMAN (Monnier et al., 2008). This methodology was successfully applied to movements related to vehicle conception such as car ingress/egress (Monnier et al., 2006) and driving controls reaching (Wang et al., 2006). The same approach was later extended to car ingress/egress by the elderly with the national project HANDIMAN (Chateauroux et al., 2007). However, the proposed motion simulation approach remained purely kinematic and the discomfort was evaluated only through the analysis of joint angles during motion, which might not be enough for assessing the force exertion-motions such as pedal clutching or handbrake pulling. To better understand the mechanisms of control of movement and discomfort during force exertion-task, IFSTTAR and Renault started a research project focused on force on automotive controls (FAC hereafter) in early 2008 for collecting data on drivers' capabilities and force perception on automotive controls (pedals, gear lever, and handbrake). From September 2008, a three-year European collaborative project called DHErgo (Digital Humans for Ergonomic design of products) coordinated by IFSTTAR was launched. The consortium composed of five academic partners (the Biomechanics and Ergonomics team from LBMC at IFSTTAR, the Institute of Ergonomics at the Technical University of Munich - LFE-TUM, the CEIT and the Université Libre de Bruxelles - ULB) , two software editors (Human Solutions and ESI) and three car manufacturers (BMW Group, PSA Peugeot Citroen and Renault SAS). The main objective of this project was to develop advanced DHM for ergonomic design that can, among other things, assess the discomfort and simulate a population including the effects of age, as well to simulate complex movements taking into account the dynamic constraints of a task (contacts, force exertion ...). This PhD thesis started at the end of the FAC project and was carried out during the whole DHErgo project.

### 3 Objectives of this work

This PhD thesis aims at developing biomechanical human models for ergonomic assessment of automotive controls and focused on two issues.

First research question is how to identify the most relevant parameters to assess the ergonomic qualities of a product objectively. Indeed, thanks to long experience in automotive engineering, currently existing automotive controls are generally well designed. From a

design engineers' point of view, it is more critical to choose the best solution among already well designed ones than to distinguish a well-designed product from bad ones. We believe that discomfort is induced by interactions with environment and internal biomechanical constraints affecting the musculoskeletal system. In this work, we propose a generic approach by comparing imposed and less-constrained movements for identifying relevant objective biomechanical indicators for evaluating a task.

Then second research question is how to predict realistic postures/movements when operating an automotive control. Despite recent progresses in motion simulation, current DHMs are mainly limited to geometric and kinematic representations of humans. We believe that the dynamic constraints (force requirements, contact forces ...) during an automotive control operation have to be considered for posture/movement prediction. For this, we need to understand how force (magnitude and direction) and posture are controlled during such a task. The two research questions were investigated separately but remained interdependent. As a matter of fact, to be used in the design cycle, an objective evaluation of discomfort requires a realistic motion simulation, and a realistic motion simulation has also to take into account discomfort criteria.

In this framework of developing DHM for ergonomic assessment of automotive controls, we focus particularly on one specific control: the clutch pedal. It is an important control in the European cars, which are mostly manual transmission cars. Besides, pedal could often restrict the posture of the user even more than hand controls and inappropriate pedal design may contribute to muscle fatigue and cause discomfort for users (Sanders and McCormick, 1993). Although, the approach developed in this work is applied to the pedal clutching task, the purpose is to propose a generic method that could be extended to other tasks.

### 4 Structure of the document

At first, existing studies will be reviewed in Chapter 1, focusing on three main items: discomfort modelling based on biomechanical parameters, experimental studies on automotive controls and especially on pedal control, and posture prediction methods. This chapter aims to have an overview of the current state of the art in the ergonomic assessment of the automotive controls in order to identify the working hypotheses.

Chapter 2 deals with the identification of objective discomfort assessment criteria for the clutching movement. It presents the first case study conducted in the DHErgo project. Based on the results of the motion analysis, a general methodology for developing biomechanical parameters based discomfort indicators is proposed and applied to the selected task.

Chapter 3 deals with the understanding of the control mechanism of force and posture during a clutching movement. Experimental data collected in the FAC project will be analysed. Based on the experimental observations, simulations using a biomechanical human model and optimization method were performed to explain separately, on the one hand, the control of the pedal force direction and on the other hand, the postural change in function of force exertion level.

Chapter 4 is an exploratory investigation on the potential contribution of the musculoskeletal models for a better understanding of the mechanism of force exertion control. The control of the pedal force direction was simulated using a custom musculoskeletal model and the results were compared to the one from Chapter 3.

Finally, the last section summarizes the main results of this PhD thesis and gives some perspectives for future researches.

# Chapter 1: Literature review

<b>1</b>	<b><i>INTRODUCTION</i></b>	<b>11</b>
<b>2</b>	<b><i>DISCOMFORT MODELING</i></b>	<b>12</b>
2.1	DEFINITION OF DISCOMFORT .....	12
2.2	DISCOMFORT MODELING AND BIOMECHANICS .....	13
<b>3</b>	<b><i>FORCE EXERTION ON CONTROLS</i></b>	<b>16</b>
3.1	GENERAL CONSIDERATIONS ON FORCE EXERTION.....	16
3.2	PEDAL FORCE EXERTION .....	17
<b>4</b>	<b><i>POSTURE PREDICTION METHOD</i></b>	<b>19</b>
4.1	KNOWLEDGE-BASED METHODS .....	19
4.2	DATA-BASED METHODS .....	21
<b>5</b>	<b><i>DISCUSSION AND WORK HYPOTHESES</i></b>	<b>24</b>



## 1 Introduction

In order to develop DHM tools for the ergonomic assessment of the automotive control, it seems important to consider the main characteristics of automotive control design and their effect on a person who manipulates it. From a technical point of view, an automotive control is a (electro-) mechanical device which has to be placed in a more or less predefined area for an efficient use. From the point of view of a user, an automotive control restricts the posture and requires some force level. Then these constraints affect the musculoskeletal system and may cause discomfort. Knowing the possible discomfort sources of a design, some changes can be proposed by the design engineer to improve the perception of the control.

Consequently, in order to improve the ergonomics of an automotive control, a design engineer needs:

- Objective discomfort criteria to understand which parameters should be changed to decrease the perceived discomfort
- Realistic force exertion data (magnitude and direction) on automotive controls
- Realistic posture when using a control

As a result, this literature review is divided in four sections. First general consideration on discomfort and discomfort modeling methods based on biomechanical parameters were reviewed. Then an overview of the factors influencing the force exertion was proposed. A focus on experimental studies on pedals was also done. The third section reviewed the posture prediction and optimization methods. Finally, this literature review was discussed to extract the work hypotheses of this PhD thesis.

## 2 Discomfort modeling

There are a large number of studies dealing with the discomfort in the literature. As the context of this study is the evaluation of discomfort of automotive design, the purpose of this part is not to make an exhaustive review of the discomfort models but rather a general idea of the different models using biomechanical parameters to assess discomfort perception.

### 2.1 Definition of discomfort

From a linguistic point of view, discomfort characterizes the lack of comfort, the prefix “dis-” being a negative sense. However, the concept of discomfort or comfort in itself is more complex to define. Nowadays it is omnipresent in the marketing discourse of consumer goods. It is also very active in the scientific literature. Indeed, Vink (2012) in an editorial in the journal *Applied Ergonomics* on the concept of comfort and discomfort has listed nearly 105,000 papers published between 1980 and June 2010 using the term "discomfort" in their title. However, only a few studies attempted to distinguish discomfort and comfort.

Zhang and his colleagues (Zhanget al., 1996; Helander et al., 1997) suggested that comfort and discomfort are not two opposing concepts on a continuous scale. Discomfort is primarily associated with biomechanical and physiological factors such as fatigue or pain, while comfort is associated with aesthetics and well-being (Figure 2a). The absence of discomfort does not automatically lead to the comfort and vice versa. One direct consequence of this conceptual distinction between comfort and discomfort is that it should be evaluated separately.

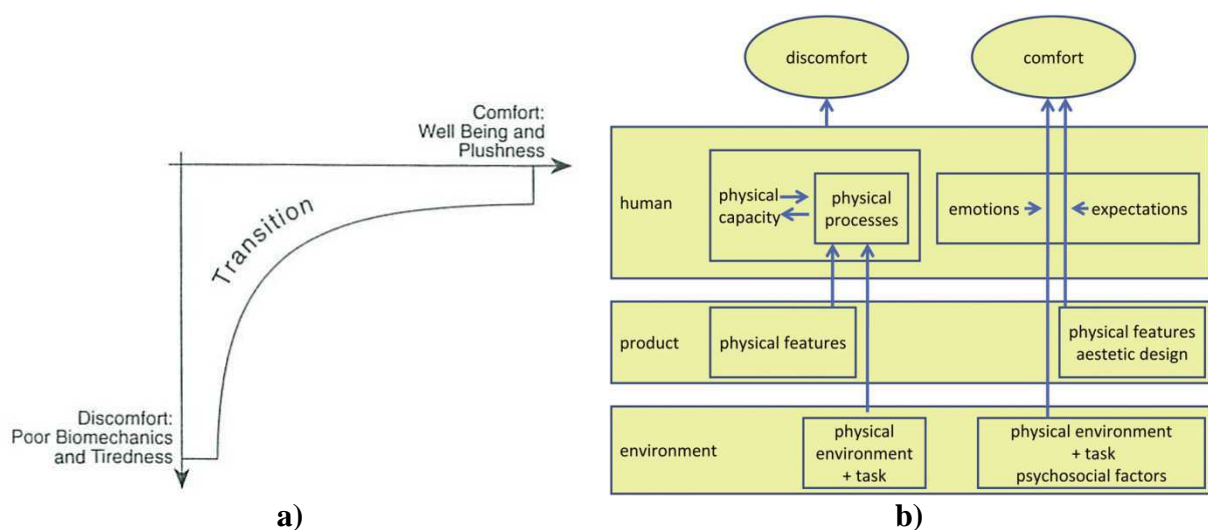


Figure 2: Conceptual model of sitting comfort and discomfort by a) Zhang et al. (1996) and b) De Looze (2003).

Following this same concept, De Looze (2003) proposed a model of comfort and discomfort in which he connects the physical environment to perceived discomfort (Figure 2b). This model assumes that the perceived discomfort matches a "dose-response" model used in the study of musculoskeletal disorders in the workplace (Winkel and Westgaard, 1992; Armstrong et al., 1993) (Figure 3). This model also considers that the external constraints generate an internal disturbance (dose) that triggers a cascade of reactions (response): chemical, physiological and biomechanical. Moreover, the model assumes that the amplitude of the "answers" is highly dependent on physical capacities of individuals.

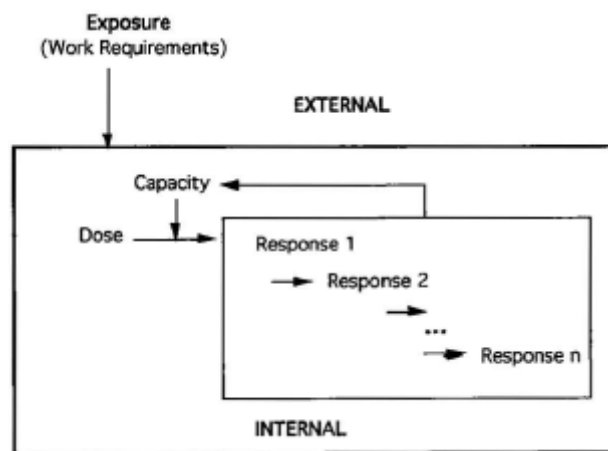


Figure 3: Conceptual "Dose-Response" model by Armstrong et al (1993)

## 2.2 Discomfort modeling and biomechanics

Currently, discomfort within DHM is usually assessed using body discomfort assessment methods such as OWAS (Karhu et al, 1977), RULA (McAtamney and Corlett, 1993), REBA (Highett and McAtamney, 2000) and OCRA (Occhipinti, 1998). But, most of these models are more oriented towards postural analysis and were developed initially for the ergonomic assessment of work postures in industry by a panel of experts in ergonomics. Only a rough estimation of posture is usually required from direct visual estimation or from recorded video. These methods can certainly be helpful for detecting main risk factor of a workplace. But they can hardly be used for ergonomic evaluation of a product such as a vehicle. Therefore, there is a need to develop discomfort predictive models to evaluate task-oriented motions.

From a general point of view, discomfort models have two main objectives. First, they are meant to understand the potential sources of discomfort in order to correct them, and secondly, they are meant to predict discomfort. The latter objective is particularly interesting

in the case of the implementation of a predictive method in a DHM. Discomfort models are usually built from data collected using questionnaire and/or rating scales, such as the CP50 scale recommended by Shen and Parson (1997).

Models based on biomechanical parameters are related to the hypothesis that discomfort is a sensation felt during the interaction of the body with the external environment. In general, biomechanical parameters considered are the joint angles, joint torques, muscle forces, etc ... There are many studies focused on biomechanical parameters for explaining discomfort perception. From a literature review on sitting comfort and discomfort, De Looze et al. (2003) argued that pressure distribution could be an objective measure with the clearest association to subjective ratings. In an experimental study on the automobile clutch pedal operation, Wang et al. (2004) studied the relationship between discomfort and 26 biomechanical parameters when depressing the clutch pedal. The most correlated biomechanical parameters to discomfort ratings were the knee joint work during pedal depression and the heel distance to the floor. Although no predictive models were proposed, the study showed the preference of not raising the leg in the approach phase, the preference of low joint work and moment especially at knee during the depression phase of the clutch pedal operation. Dickerson et al. (2006) investigated the relationship between shoulder torques and perception of muscular effort in loaded arm reaches. Individual subject torque profiles were significantly positively correlated with perceived effort scores rated using a modified Borg CR-10 Exertion Scale (Borg, 1982). Kuijt-Evers et al. (2007) studied the discomfort perceived when using hand tools according to EMG measures and palm pressure distribution and reported that the pressure-time integral was the best predictor of discomfort. More recently, Kee and Lee (2012) investigated the relationship between postural stresses and posture holding time, maximum holding time, torque at joints, lifting index and compressive forces at L5/S1. This study showed in particular a strong correlation between discomfort and compressive forces at L5/S1.

Some studies also proposed discomfort predictive models based on biomechanical parameters. For example, Jung and Choe (1996) developed a discomfort model for arm reaching posture based on joint angles. Based on experimental data, they defined a discomfort regression model in which the independent variables were the 7 joint angles of the upper limb and the weight of the object held with the hand. More recently, Wang et al. (2008) proposed a unified data based approach for DHM to predict both in-vehicle reach capacity and discomfort.

But most of these predictive models are specific and their application ranges are limited by the experimental conditions. However, some researchers attempted to propose generalized

biomechanical based discomfort models, considering that for any movement, the perceived discomfort may be a combination of discomfort feelings of all DoFs involved in the motion. Bubb and his colleagues (Bubb, 2003; Zacher and Bubb, 2004) attempted to identify joint angle and torque related discomfort functions for most of the joints of the human body. Kee and Karwowski (2001, 2003) defined joint angle based iso-comfort functions and proposed a ranking system for evaluation of joint motion discomfort. Using a similar approach, Chung et al. (2005) proposed a postural load assessment method for whole body manual tasks from postural classifications of body parts. However, these approaches are very dependent on the availability of data on the perception of discomfort in terms of joint angles and joint torques, and on the representativeness of the subjects' sample on which the model is based.

Finally, generalized discomfort models should be differentiated from generic approaches used to define task-related discomfort functions. Dufour and Wang (2005) proposed the concept of neutral movement for identifying discomfort function and applied it to the analysis of the discomfort of car ingress/egress movement (see also Wang, 2008b). The concept is based on the assumption that ideally, the neutral movement for a person should be the one which generates the least discomfort for a task and could therefore be considered as a motion reference. The basic idea is to define a corridor for each considered biomechanical parameter (joint angle for example, Figure 4), which reflects the intra- and inter-individual variability of the neutral movements. Any deviation from the neutral movement corridor due to environment constraints may reveal a possible discomfort perceived during a movement. Nevertheless the main limit of this concept is that the evaluation of discomfort depends greatly on the definition of the neutral movement.

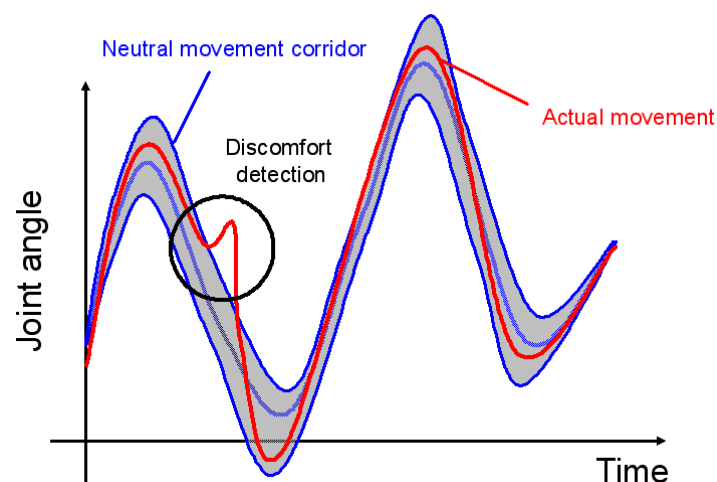


Figure 4: Concept of neutral movement (Wang, 2008)

### 3 Force exertion on controls

Understanding the force exertion characteristics can assist the ergonomist in developing and designing appropriate tools, products, workspaces and interventions to reduce musculoskeletal disorder risk (Daams, 1994 ; Mital et al., 1998 ; Das et al., 2004). The purpose of this section is to get an overview of the factors that can influence the exertion of force. In relation to the automotive control selected in this study, a non-exhaustive review of studies on force exertion on pedal is also presented.

#### 3.1 General considerations on force exertion

Force exertion capacity varies greatly depending on a high number of factors (Daams, 1994; Das et al., 2004; Kumar, 2004; Haslegrave, 2004). Figure 5 summarizes some of the factors that influence force exertion.

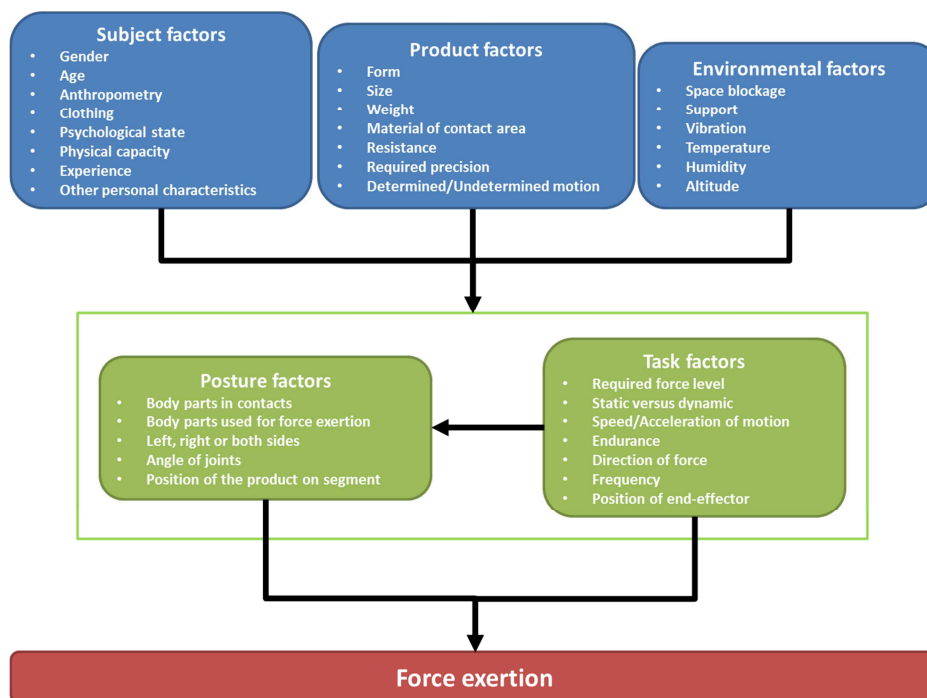


Figure 5: Factors influencing force exertion.

Strength varies with task, posture, subject and environmental conditions. Haslegrave (2004) stated that task factors (required force level, force direction ...) not only have a direct influence on strength but can also influence posture. Besides, she showed also that posture had a major influence on strength capability as it determines the mechanical advantage

offered to muscles to exert force. It is thus necessary to specify and control the body position if the corresponding strength values of the individuals are to be compared (Mital et al., 1998). In addition, many studies (Kroemer, 1970; Ayoub et al., 1981; Daams, 1994; Mital et al., 1998; Kumar, 2004) suggested that the assessment methods can also strongly affect muscle strength data. The following factors are generally mentioned:

- Type of force exertion: static isometric, isokinetic dynamic ... with an imposed or perceived by subjects force level
- Test conditions: measuring equipment, type of postural stress (straps, handles ...), instructions, posture of the subject, number of repetitions of a trial, motion speed ...
- Muscle fatigue: experimental duration, duration of rest, period in which the measurement was made (morning, afternoon ...)
- Subject: physical and psychological state at the time of the experiment

Thus, it is important of an extensive and detailed description of the experimental method focusing on all these factors to acquire muscle strength data. Moreover, the assessment of strength should be performed under conditions as close as possible as the specific task situations.

### 3.2 Pedal force exertion

First strength capability studies usually gave recommendations for the design of specific controls. For example, based on the maximum brake pedal force from the 5th percentile female group in terms of stature, Mortimer (1974) suggested the maximum braking from capability from a passenger car should not exceed 400N. Kroemer (1971) showed that maximum static forces of sitting operator depended on seat type, pedal type and position. His review showed that strong pedal force could be exerted when a suitable backrest is provided and when the pedal is placed almost at seat height and at a distance requiring low knee flexion angles (between 20° and 40° of flexion). A foot control position often restricts the posture but small variation in lower limb joint angle has also an impact on the force output. According to Lara-Lopez et al. (1999), changes in the knee angles affected maximum static forces exerted on a foot pedal by seated subjects. The smaller the knee flexion angle (from 20° to 80°) is, the greater the foot strength is. Mehta et al. (2007) agreed with this observation and stated that maximum leg strength was achieved when the leg was in almost elongated position (i.e. knee flexion angle between 35° and 45°).

The capability of the foot to create force can also be influenced by the direction of the applied force or moment (Das et al., 2004). Pheasant et al. (1982) showed, for example, that foot strength depended on foot thrust direction. For different pedal locations, the force in the direction of the hip (from the hip to the heel) was greater than the force in the direction of the knee (from the knee to the heel).

Subjects' characteristics and psychological parameters can influence the force exertion. Mortimer (1974) measured foot brake pedal force capability on a large sample of female and male drivers. Interestingly, verbal encouragement tended to increase the pedal force capability of the subjects. Besides, women were found significantly weaker than men. Pheasant et al. (1982) agreed with this observation reporting that average strength of the females was 81% of the average male strength. It was also reported that left and right legs had the same strength. In case of tractor pedal, Mehta et al. (2007) and Fathallah et al. (2008) showed that the recommendations on pedal force limits from the International Organization for Standardization were conflicting with the foot strength capability of specific tractor operator population, in particular Indian operators (Mehta et al, 2007) and under 17-year old aged operator (Fathallah et al., 2008).

Knowing the maximum strength is necessary but may not be sufficient for pedal design. Considering that pedals should have a low resistance to at least to overcome the effects of vibration and gravity (Southall, 1985), it may be interesting for pedal design to determine the minimum acceptable pedal resistance. This aspect may be particularly important for the clutch pedal operation according to Wang et al. (2000). However, few studies focused on automotive pedal force perception in the literature. Wang and Bullock (2004) reported a study by Mick (1995) on the relationship between the subjective sensation and the force applied to a pedal in order to determine the upper force limit for a force feedback-based active accelerator pedal. A minimum pedal resistance of 40 N was recommended for the accelerator based on the results of the experiment. However, only 12 subjects (6 females and 6 males) participated in this study. In addition, the recommendation is only relevant for pedal operation with the heel supported on the floor.

Another aspect of the pedal force exertion is how the force direction is controlled by the user. Few studies in the literature investigated the mechanism of the control of the force applied on a pedal. In case of clutch pedal operation, Wang et al. (2000) observed experimentally that the direction of the pedal force at the end of the pedal depression in the sagittal was highly dependent on the direction connecting the hip joint and the contact point. Using a 2D

biomechanical model, pedal force directions were predicted by minimizing the lower limb joint torques and were found in agreement with the experimental observation. A similar approach was used by Schmidt et al (2003) to understand the control of the foot force direction when pushing a fixed bicycle pedal. Pedal force direction was predicted using on the one hand, a 2D biomechanical model and joint torque minimization, and on the other hand, a musculoskeletal model and foot force maximization. Both approaches presented strong similarities and predicted force directions close to the hip-pedal direction were predicted as in experimental data. Schmidt et al. also showed that in case of bicycle pedal, the use of a musculoskeletal model was a better prediction of the force direction regarding the experimental data. Interestingly, even with different postures (seated on a bicycle and seated in a car) and thrust force directions (mainly vertical for bicycle and horizontal for car pedals), both studies suggested that the control of the foot force may follow the principle of reducing joint load.

## 4 Posture prediction method

Posture prediction is a key functionality of a DHM used in ergonomic assessment of a product or a workplace. Indeed, an unrealistic predicted posture may lead to wrong analysis and so, wrong ergonomic recommendations. Every DHM package used for ergonomics include an inverse kinematics (IK) solver which will compute a posture for the manikin to reach the goal from a given target position of a hand or foot. However, inverse kinematics alone produces a feasible posture, not necessarily a likely or realistic posture that a person may adopt. There exist a large variety of methods to simulate human-like postures and motions. The aim of this section is not to cover all the existing inverse kinematic solvers used to predict a posture or a motion but to focus on the methods that could be considered for a force-exertion posture prediction. Two main families of posture prediction methods were distinguished: knowledge-based methods and data-based methods (Wang, 2008a).

### 4.1 Knowledge-based methods

The knowledge-based methods assume that the motion control strategies are known as optimization criteria or heuristic rules. The general approach is to find the posture that

minimizes (or maximizes) an objective function while considering the task constraints and some physiological restrictions (joint limits for example).

Single-objective optimizations were widely used to predict a posture or a movement. Uno et al. (1989) proposed an arm reaching movement based on the minimization of the change in joint torques during motion. Soechting et al. (1995) showed that minimizing the amount of work to move the arm from its origin was successfully predicting the final reaching posture. Based on a discomfort predictive model using joint angle cost functions, Jung et al. (1996) predicted an arm reaching posture by minimizing the discomfort associated with a pointing task. Also for an arm reaching posture, Wang and Verriest (1998) proposed a geometric inverse kinematics algorithm based on the minimization of the norm of the joint angular velocities.

More recently, some multi-objective optimization (MOO) methods were proposed. The objective of the MOO methods is find a set of design variable  $q$  in order to minimize  $n$  objective functions  $f_i$  ( $i = 1, \dots, n$ ) simultaneously (Eq. 1) subject to equality and inequality constraints (Eq. 2):

$$\min_q F(q) = \begin{bmatrix} f_1(q) \\ \vdots \\ f_n(q) \end{bmatrix} \quad (\text{Eq. 1})$$

$$\begin{cases} g_j(q) \leq 0 & j = 1, \dots, m \\ h_k(q) = 0 & k = 1, \dots, p \end{cases} \quad (\text{Eq. 2})$$

With

$m$ , the number of inequality constraints

$p$ , the number of equality constraints

MOO was used by the VSR (Virtual Soldier Research) group using three objective terms of human performance measures: potential energy, joint displacement and joint discomfort (Yang et al., 2004). This approach was tested on many tasks such as reaching, climbing, walking, box lifting and seating (Abdel-Malek and Arora, 2008; Kim et al., 2009; Marler et al., 2011). Using a similar approach, Ma et al. (2009) predicted a drilling assembly operation posture considering the muscular fatigue and the discomfort as objective functions.

Knowledge-based methods have the advantage of being able to take into consideration as many objective functions as necessary to describe a motor control strategy. But one issue of these methods is that multiple objectives may conflict between them (e.g., what minimizes one function may increase another). One solution is to convert the MOO problem in a single-objective problem using a weighted sum of the different objective functions (Yang et al.,

2004; Ma et al., 2009; Marler et al., 2009). Then the issue lies in the estimation of the relative weights or priorities to assign to each objective. Maybe the weights depend on the preference of the individual. Finally, the major limitation of these posture prediction methods lies in the identification and validation of the objective functions.

## 4.2 Data-based methods

Unlike the knowledge-based approach, the data-based methods require little knowledge on motor control strategy. This approach uses existing posture data to predict a new posture. The realism of the simulation mostly depends on the richness of the database.

One method is to propose a statistical approach to predict posture from experimental data in a function of task and operator characteristics. Seidl (1994) proposed a posture-prediction algorithm currently implemented in Ramsis™. Based on postural constraints provided by the user, this algorithm maximizes the likelihood of joint angles relative to a database of human postures of a similar task. Although it is developed to analyze joint loads, The University of Michigan's 3D Static Strength Prediction Program (3DSSPP) has also a posture prediction module that uses a statistical model, combined with inverse kinematics (Chaffin, 1997). This algorithm defines whole-body postures by predicting body segment positions based on hand location and orientation (supine, neutral, or prone), and worker height and weight (Hoffman et al., 2007). Thus the effects of hand force on posture are not reflected in model predictions. Faraway (2000) developed a statistical functional regression model for prediction human reach motion. Based on a large set of reach motion data, the model aimed to predict the reach motion trajectories of a DHM based on the subject's characteristic (age, gender, stature ...) and on the target location. Reed et al. (2002) used a similar approach in the Cascade posture-prediction model to predict realistic driving posture. More recently, Hoffman (2008) developed a statistical posture-prediction model for standing hand force exertions (Figure 6). In this model, the magnitude and the direction of the force were considered as inputs with the subject's characteristics and the target location.

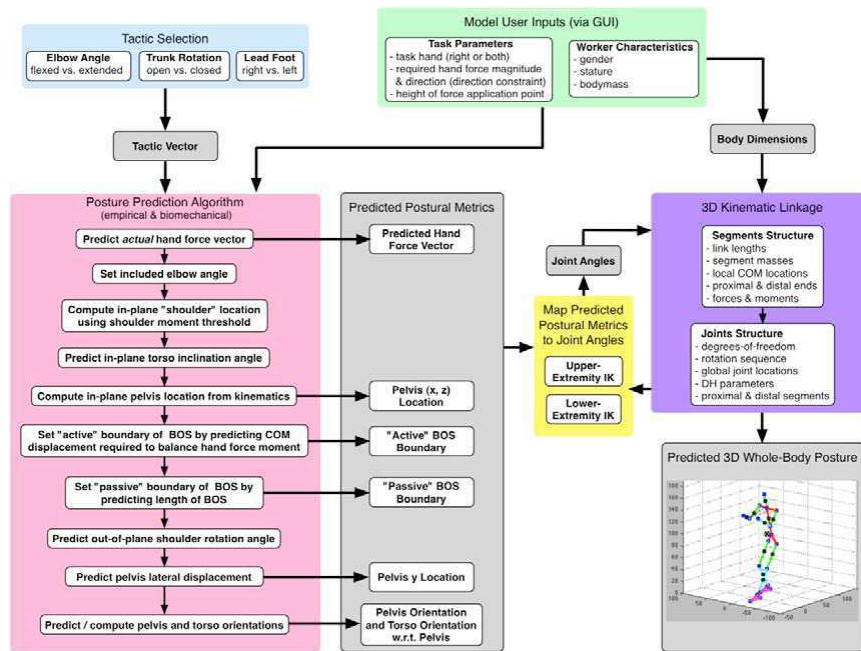


Figure 6: Main components and overall flow of the model proposed by Hoffman (2008).

Another approach proposed by Zhang and Chaffin (2000) predicted in-vehicle seated reaching movement using inverse kinematics in combination with experimental data. Based on weighted pseudo inverse, this method uses optimization to determine the weighting factors such that the predicting joint angular motion trajectories have minimum deviation from the joint angle trajectories of a real human reach motion. Seitz et al. (2005) also proposed an optimization-based approach for posture prediction called the FOCOPP model. This model is based on human posture and strength data and aims to predict the posture that minimizes the joint load due to a task. The FOCOPP model is presented as a generalized posture prediction model as it is not based on task-related data but on functional capacities data.

Finally, posture and motion prediction can also be accomplished by modifying motion-capture data to conform to the requirements of the task (Park et al. 2004; Monnier et al., 2006, 2008). This method has been implemented in the software RPx for the car manufacturer Renault. Globally, the process consists in three steps:

- Constitution of a structured motion database: each motion is stored according to the motion descriptors, i.e. motion performer's characteristics (gender, age, stature ...), environment parameters (vehicle geometry in this case), motion characteristics (motion strategies, key-frames ...) and reconstructed motion data (joint angle-time profiles, body segments position- and orientation-time profiles).

- Extraction of a referential motion, which is the closest to the new simulation scenario (new geometry, new subject, new set of end-effector position and orientation constraints ...) from the database.
- Modification of the selected referential motion: the selected referential motion is modified to match the constraints of the new scenario while preserving the shapes of the original motion trajectories and joint angle profiles.

An important database of motions has been established and integrated in RPx, from the simple act of pushing a button to the ingress/egress of a vehicle (Wang et al. 2006, Chateauroux et al. 2007) (Figure 7).

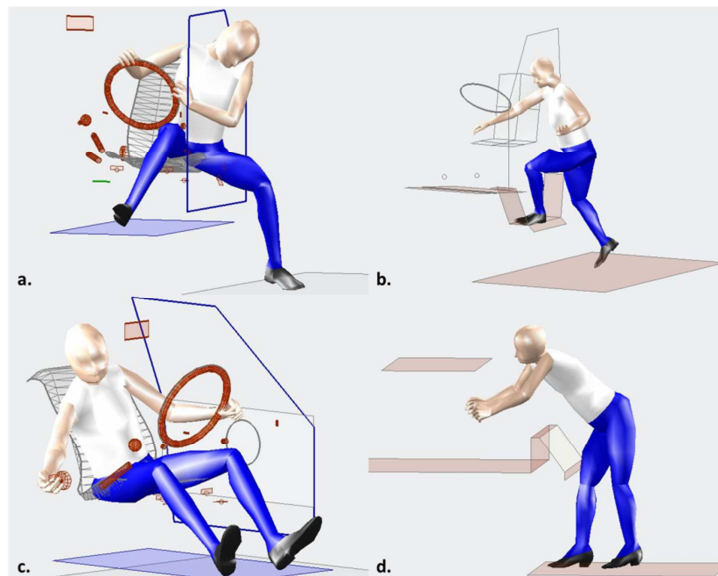


Figure 7: Examples of tasks in RPx motion database. a. Car egress, b. Light truck ingress, c. Glovebox reach and d. Trunk loading.

The motion database can be easily expanded without altering the structure of the entire motion simulation system. The main advantage of the data-based methods is the intrinsic realism of the reference motion, which could be conserved during the adaptation process.

However, main limitation of the data-based methods is that predicted postures or motions highly depend on the underlying dataset. The database must include tasks that are substantially similar to those to be simulated.

## 5 Discussion and work hypotheses

This literature review focused on the design engineer's expectations in terms of ergonomic assessment of the automotive controls. The main limitations of the current DHMs concern the discomfort modeling and the posture prediction, the two issues being closely related.

First, discomfort is a complex process which is primarily associated with physiological and biomechanical factors. The need of a design engineer in terms of discomfort modelling is not only to get a rating score but also to get insights about the sources of discomfort. But how to identify objective discomfort criteria remains to be one of challenging research issues. Any task oriented motion is more or less-constrained by the environment and thus require specific objective discomfort criteria. A generic approach to define the discomfort criteria should be considered so that it could be applicable to a large range of tasks. Based on these considerations, the concept of neutral movement proposed by Dufour and Wang (2005) is an interesting approach. Assuming that a better comfort may be obtained when people can make their own appropriate adjustments, these less-constrained motions can then be used as reference data for comparing a proposed solution and for identifying objective discomfort criterion based on biomechanical data. A five-step generic approach for the ergonomic assessment of a task-related motion is proposed (Wang et al., 2011). Based on the neutral movement concept, it consists in:

- 1) Identify the main critical design parameters
- 2) Plan an experimental design with motion and force measurements, discomfort evaluation and an experimental mock-up allowing the participants to easily choose their preferred adjustments
- 3) Conduct the experiment with voluntary participants
- 4) Process and analyze the data (subjective perception and motion analysis)
- 5) Identify relevant biomechanical parameters for discomfort assessment and define ergonomic criteria

In this study, the clutch pedal operation was chosen to investigate how the proposed approach could be helpful for improving the automotive control design when using a DHM tool. The data of the clutching movements collected in DHErgo project will be used for illustrating this approach.

Then the literature review clearly shows the dependency between force exertion and postural behavior. Tasks conditions (force requirements, force direction, type of control, control position ...) have a major influence on both force exertion and posture. As a result, the assessment of strength and posture when operating an automotive control should be performed under conditions as close as possible to the specific task. Maximum force exertions on a control are useful to provide force limit recommendations. But force perception may also be important to anticipate how the users would feel the control during its use. Besides, it can be assumed that according to the level of effort required for manipulating a control, postural adjustments are required in response to force solicitation. Then experimental investigations of the force exertion on control are necessary to understand the mechanism of control of force and posture. Understand the motor strategies that rule the behavior during a task is a necessary step to be able to predict realistic posture and force direction. Force control and posture prediction were rarely studied together in the literature. It was suggested that the motor strategy that controls the foot force may follow the minimization of the joint load. But, all these studies were performed in 2D whereas, as a clutch pedal is not fully aligned with the left hip joint, the force direction should be 3D, especially for high force exertion level. Few methods focused on force exertion-posture prediction. But only MOO methods have the advantage to be able to explain postural strategy, as they consider motion control strategies as optimization criteria to predict the posture. Interestingly, optimization methods seem to be suitable to explain both force control and postural behavior. In this study, the data from the FAC project are used to investigate the force exertion on automotive controls and especially on clutch pedal. All the aspects from force capability to the mechanisms of force and posture control of this task are going to be investigated in order to propose improvements for realistic force exertion-posture prediction using a DHM.



## Chapter 2: Using less-constrained movement to identify objective discomfort assessment criteria

<b>1</b>	<b>INTRODUCTION</b>	<b>29</b>
<b>2</b>	<b>MATERIAL AND METHODS</b>	<b>30</b>
2.1	SUBJECTS .....	30
2.2	EXPERIMENTAL SET-UP .....	32
2.3	EXPERIMENTAL CONDITIONS.....	34
2.4	EXPERIMENTAL PROCEDURE .....	36
2.5	DATA PROCESSING .....	37
2.6	EVALUATION OF THE MOTION RECONSTRUCTION.....	41
2.7	SUMMARY OF PROCESSED DATA.....	45
<b>3</b>	<b>ANALYSIS OF THE DISCOMFORT PERCEPTION</b>	<b>46</b>
3.1	QUESTIONNAIRE ANALYSIS .....	46
3.2	DISCOMFORT RATINGS ANALYSIS .....	52
<b>4</b>	<b>MOTION ANALYSIS OF THE CLUTCH PEDAL OPERATION</b>	<b>56</b>
4.1	COMPARISON OF CLUTCHING MOVEMENTS FOR IMPOSED AND LESS-CONSTRAINED PEDAL CONFIGURATIONS .....	56
4.2	ANALYSIS OF CLUTCH PEDAL FORCE EXERTION.....	58
<b>5</b>	<b>DISCUSSION</b>	<b>65</b>
5.1	PEDAL POSITION ADJUSTMENT AND DISCOMFORT PERCEPTION .....	65
5.2	PEDAL FORCE CONTROL AND DISCOMFORT PERCEPTION .....	66
5.3	TOWARDS A PROPOSAL FOR DEFINING OBJECTIVE DISCOMFORT INDICATORS .....	68
<b>6</b>	<b>LIMITATIONS</b>	<b>73</b>
<b>7</b>	<b>CONCLUSION</b>	<b>74</b>
<b>8</b>	<b>APPENDIX</b>	<b>75</b>
8.1	SELECTION OF THE TEST CLUTCH PEDAL CONFIGURATIONS.....	75
8.2	MEASUREMENT CHAIN FOR DHERGO EXPERIMENT .....	77
8.3	ANTHROPOMETRIC MEASUREMENTS.....	78
8.4	SUBJECTS' ANTHROPOMETRIC DIMENSIONS FOR THE DHERGO EXPERIMENT .....	81
8.5	CHARACTERIZATION DATA OF EACH GROUP OF SUBJECTS IN DHERGO EXPERIMENT .....	83
8.6	MARKERS' PLACEMENT ON SUBJECT FOR THE DHERGO EXPERIMENT .....	84
8.7	MARKERS' PLACEMENT ON MOCK-UP FOR THE DHERGO EXPERIMENT .....	85
8.8	DISCOMFORT QUESTIONNAIRE FOR THE DHERGO EXPERIMENT .....	86
8.9	EXPERIMENTAL SHEET OF THE DHERGO EXPERIMENT.....	88
8.10	RAMSIS™ DIGITAL HUMAN MODEL .....	90
8.11	QUESTIONNAIRE FREQUENCY TABLES .....	91
8.12	QUESTIONNAIRE REPRODUCIBILITY .....	94
8.13	IMPOSED VERSUS LESS-CONSTRAINED JOINT ANGLES.....	95
8.14	DISCOMFORT COST FUNCTION FOR KINEMATIC INDICATORS .....	96
8.15	DISCOMFORT MODELLING APPROACHES USING DISCOMFORT INDICATORS .....	97



## 1 Introduction

Thanks to recent progress in motion simulation, simulating a complex task oriented motion now becomes possible. But another challenging issue for DHM is how to assess motion related discomfort. Generally speaking from the design engineers' point of view, it is more critical to choose the best designed product among already well designed ones than to distinguish a well-designed product from badly ones. Because any task oriented motion is more or less constrained by the environment, a better comfort may be obtained when people can make their own appropriate adjustments. These less-constrained motions, also referred to "neutral" motions by Dufour and Wang (2005), can then be used as reference data for comparing a proposed solution and for identifying objective discomfort criterion based on biomechanical data. This biomechanical approach for evaluating motion related discomfort using the concept of less-constrained movement was adopted in the European project DHErgo. In this PhD thesis, the work was centered on the data from the case study on clutch pedal operation of DHErgo. As a case study, the aim of the experiment performed in the DHErgo project was not to investigate all the spectrum of pedal design parameters. Actually, the objective of this experiment was to investigate the concept of less-constrained movement introduced by Dufour and Wang (2005) and its effects on clutching movement and discomfort perception. Only a few studies of the comfort of pedal operation were reported in existing literature (see Haslegrave, 1995; Wang and Bullock, 2004). In past studies (Wang et al., 2000; Wang et al., 2004), four design parameters of the clutch pedal (seat height, pedal travel length, pedal travel inclination, pedal resistance) were investigated to understand their effects on lower limb movements and pedal discomfort. Although some design recommendations for pedal design were provided by Wang et al. (2004), ergonomic criteria for pedal design which can be easily used by design engineers are still missing. The purpose of this study is therefore to compare less-constrained clutching motions with normally constrained ones in order to identify objective discomfort assessment criteria for the clutch pedal operation that can be easily implemented in a DHM.

The study was organized in three parts. First the discomfort perceived during the clutch pedal operation experiment performed in DHErgo project was analyzed. Then the biomechanical analysis of the clutching movements collected was performed. Finally, the results of both analyses were discussed and some discomfort indicators for the clutch pedal operation were proposed.

## 2 Material and methods

The data used in this chapter were collected in the European project DHErgo. The detailed description of the data collecting protocol was given in D17 (2010) for the first case study on pedal clutching task.

### 2.1 Subjects

Twenty volunteer subjects took part in the experiment. They were divided in four anthropometric groups according to age and gender and stature. As the size of these samples was very small, homogeneous groups were recruited. Subject selection criteria were based on:

- **Age.** Two age groups were chosen:
  - Young subjects: between 20 and 35 years
  - Older subjects: between 65 and 80 years.
- **Stature.** Due to small sample size, only the 50th percentile value of the French population (IFTH, 2006) for each age-gender group in terms of stature was considered in order to get more information on age effects (Table 1).

**Table 1: Main characteristics of each group of subjects. Means and standard deviations are given.**

	Young male	Young female	Older male	Older female	All subjects
N	5	5	5	5	20
Age (years)	27 ± 5	26 ± 4	73 ± 5	69 ± 2	48 ± 23
Stature (mm)	1773 ± 49	1667 ± 30	1724 ± 22	1599 ± 46	1691 ± 75
Weight (kg)	70 ± 12	61 ± 3	81 ± 5	63 ± 6	69 ± 11

- **Physical conditions.** To recruit homogenous groups with functional capacities representative of the global population, the subject should not be athletics. Therefore, they should not be or have been high level sportsmen (or women), meaning that they should not be trained for national and international competitions. Then, people (young and older subjects) should not have had any history of trauma or serious disease, or particular known orthopedic (arthritis) or neurologic disorders. They should not undergo any medical treatment. With ageing, older people may have a reduction of their functional performance. As the experiments were physically demanding, the older subjects should be fit enough to produce all the maximal strength and ranges of motion measurements without any problem. The first condition was to recruit older

people who do not feel any difficulty during the activities of the daily life. A questionnaire was used to recruit the older subjects.

- **Driving experience.** All subjects were regular drivers with 2-year minimum driving experience.

The experimental protocol was approved by the ethical committee of Ifsttar. Informed consent was given before participating in the experiment.

Forty anthropometric dimensions were measured for all participants. They are described in Appendix. Functional tests were performed on each subject in order to characterize joint ranges of motion and maximum isometric joint torques. The tests were selected according to the relevancy to clutch pedal operation. Therefore, maximum isometric joint torques and ranges of motion were collected only for the left lower limb.

The active ranges of motion (ROM) were measured for the left hip, knee and ankle joints in flexion/extension, abduction/adduction (except knee) and axial rotation (except ankle). Except for hip flexion/extension and abduction/adduction ROMs performed standing; all ROMs were performed sitting on a stool (Figure 8).

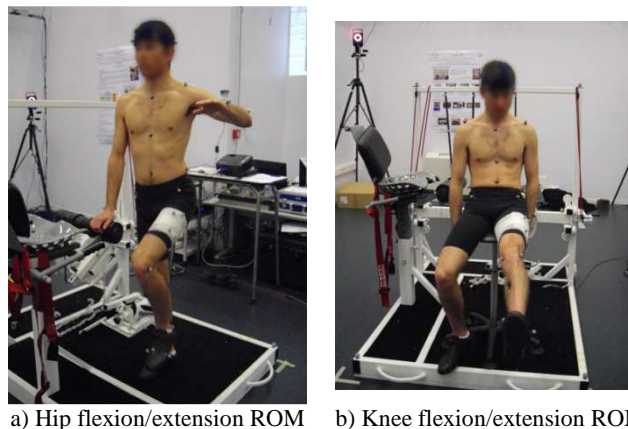


Figure 8: Active range of motion (ROM) measurements

Maximum isometric joint torques were performed for the three lower limb joints only in flexion/extension using a specifically designed ergometer. Each joint was tested randomly at different joint positions estimated with a goniometer (Figure 9). The angles were defined from the standing posture according to the recommendations by Gallagher et al. (1998) (see also Chaffin et al., 1999): ankle flexion of  $0^\circ$ , knee flexion of  $45^\circ$  and hip flexion of  $60^\circ$ . Hip measurements were taken with the subject standing and leaning on a back support. Knee and ankle measurements were taken with the subject sitting in a rigid seat. The means and

standard deviations of the ROMs and joint torques of each group of subjects are presented in Appendix.

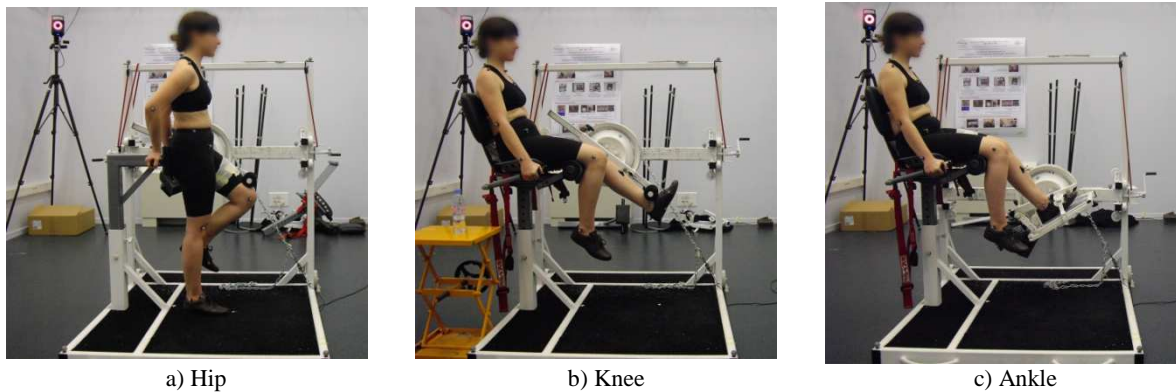


Figure 9: Maximum voluntary isometric joint torque measurements

## 2.2 Experimental set-up

### 2.2.i Mock-up

A multi-adjustable experimental vehicle package was used to define different driving configurations. It was composed of a seat, a steering wheel, an accelerator pedal, a clutch pedal and footrest (Figure 10). The device was similar to the one used by Wang et al (2000).

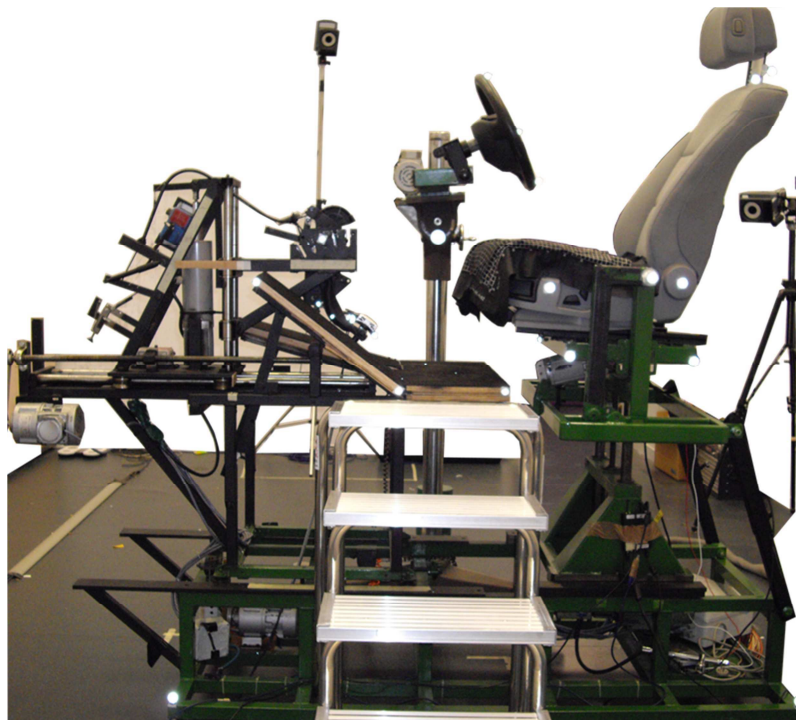


Figure 10: Experimental Mock-up used in DHErgo experiment

The seat and steering wheel adjustments in height were motorized as well as the clutch pedal adjustment both in depth and in height with respect to the accelerator pedal. The other

adjustments such as pedal travel length or the clutch pedal lateral position were done manually. Moreover, the lateral adjustment of the clutch pedal was not continuous but incremental. The range of adjustment was 60 mm with an increment of 10mm. The same linear spring device was used for all pedal configurations to generate pedal resistance during the pedal depression. However, in order to match the initial angle of the clutch pedal with horizontal plane, different pre-loadings were applied to the device. As a consequence, for a similar pedal travel length, the force needed to fully press the pedal may differ.

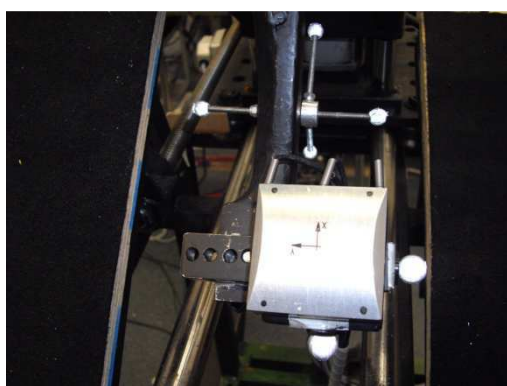
### 2.2.ii Motion capture

The movements of all participants were recorded using the opto-electronic motion capture system VICON with ten MX T40 cameras sampling at 100 Hz. The 3D trajectories of 40 reflective markers attached to participant were measured (location of the markers described in Appendix). In order to be able to recreate the mock-up geometry, 35 markers were put on it. Special attention was paid to the clutch pedal with 6 markers on the device to measure trajectories and pedal orientation during the depression.

### 2.2.iii Force and seat pressure measurement

A TME<sup>®</sup> uni-axis force sensor with a capacity of 2000 N was used to record the force applied by the subject on the ergometer. A TME 3-axis force sensor with a capacity of 1500 N on each axis was used to record the force applied by the subject on the clutch pedal during the clutching movement (Figure 11a). All force sensors were synchronized with VICON<sup>®</sup> system and sampling at 1kHz.

Two pressure maps (XSensor<sup>®</sup> X3Pro PX100) with pressure range 10-200 mmHg were also installed on the seat (one on the backrest, one on the seat) to qualitatively examine the pressure distribution during clutch pedal operation (Figure 11b).



a) Clutch pedal force sensor



b) Seat with pressure maps

Figure 11: Human/environment contact forces measurement devices

## 2.3 Experimental conditions

### 2.3.i Test configurations

For this case study of DHErgo project, the three end-users provided 11 clutch pedal configurations: 5 by BMW (BMW1 to BMW5), 3 by PSA Peugeot Citroën (PCA1 to PCA2) and 3 by Renault (REN1 to REN3). A common mock-up coordinate system was necessary, on one hand, to configure the experimental mock-up more easily and on the other hand, to compare different configurations. There is quite a consensus among the end-users on the direction of the different axis from the driver's point of view, i.e. x-axis towards back, y-axis from left to right and z-axis upwards. Therefore the main issue for the coordinate system is its origin. Generally, car manufacturers establish key reference points and dimension in vehicle's interior according to a H-point. This point is fixed to the vehicle seat and is usually defined using the SAE H-point machine (SAE J826). Globally, this point corresponds approximately to the middle of the two hip joint centers of a seated person. Car manufacturers have usually not a specific location H-point but a range depending on the seat horizontal and longitudinal adjustment. In this case study, a reference H-point for each configuration was defined. It was in the middle of the H-point travel path provided by the end-users (Figure 12).

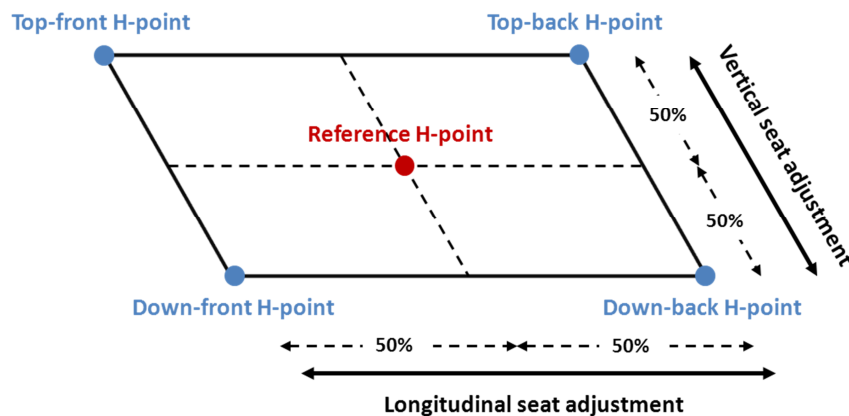


Figure 12: Definition of the reference H-point with the H-point range given by end-users

Among the eleven proposed pedal configurations, six were chosen in order to cover the large range of pedal design parameters from currently existing vehicles (Figure 13 and Table 2). The details of the selection of the test configurations can be found in Appendix.

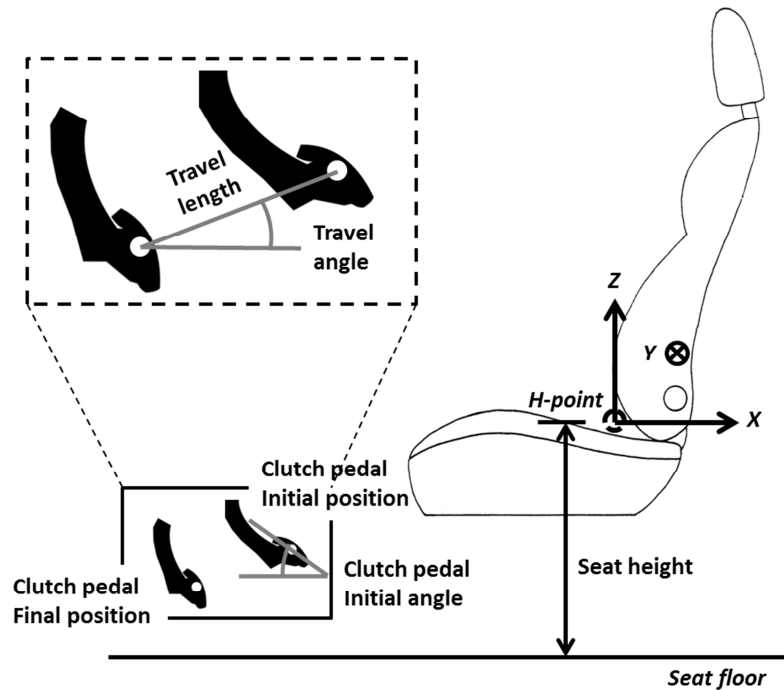


Figure 13: Mock-up coordinate system and pedal design parameters

Table 2: Definition of the six clutch pedal configurations tested. The pedal design parameters are defined in Figure 13

	Seat height (mm)	Travel length (mm)	Travel angle (deg.)	Clutch pedal initial position (mm)			Clutch pedal initial angle (deg.)
				X	Y	Z	
BMW1	256	131	0	-815	-60	-69	59
BMW2	247	163	0	-831	-110	-64	55
BMW4	174	149	0	-816	-120	17	58
PCA1	355	161	23	-770	-70	-199	33
PCA2	272	157	8	-766	-90	-130	49
REN3	360	137	15	-761	-70	-218	27

The configurations BMW1 to PCA1 and REN3 were selected as border configurations of the investigation space, whereas PCA2 was selected as central configuration. As a consequence, this last configuration was tested three times by the subjects to evaluate reproducibility. All configurations, repetitions included, were tested randomly by all subjects. In summary, each subject performed  $6 \times 2$  (imposed + less-constrained) +  $2 \times 2$  (repetitions of PCA2) = 16 trials. In order to limit the possible pedal adjustments and to have pedal parameters easily controllable by the subjects, the position of the clutch pedal was chosen as the adjustable parameter. Seat height, travel length, travel angle, pedal initial angle were fixed at the value provided by end-users. Finally, the pedal resistance was not adjusted by the subjects. Nevertheless between the pedal configurations, the pedal resistance may differ because of

different pre-loading applied to the spring device in order to match the initial angle of the clutch pedal with horizontal plane.

**2.3.ii Discomfort assessment**

Discomfort feelings when clutching were collected, for all trials, through a questionnaire, which was composed of two parts (see in Appendix). At first, multiple-choices questions were used for assessing the seat (Q1), the pedal design parameters (pedal position at beginning and end depression, travel length, travel angle – Q2 to Q5). Then, pedal force perception (Q6) and discomfort (Q7) were evaluated using two different rating scales. The perception of the clutch pedal force was assessed using the Borg’s CR-10 (Borg, 1998). Discomfort was evaluated using a modified CP-50 category partition scale (Chevalot and Wang 2004). In order to prevent from the misuse of the rating scale, three trials were tested by the subjects for training purpose (Table 3). They consisted of two extreme configurations a priori very uncomfortable (CAL1 and CAL2) and one average configuration considered as less uncomfortable (CAL3). Two extreme configurations were: one combined a high seat height, a small travel inclination angle and a long travel length and the other combined a low seat height, a high travel inclination angle and a long travel length. The average configuration had average pedal design parameter values.

**Table 3: Training clutch pedal configurations**

	Seat height	Clutch Pedal center of rotation			CP Travel angle	CP Travel length
	H30 (mm)	X (mm)	Y (mm)	Z (mm)	(°)	(mm)
CAL1	200	-900	-87	147	30	170
CAL2	400	-900	-87	147	0	170
CAL3	300	-900	-87	147	15	140

**2.4 Experimental procedure**

A typical experiment sheet of this experiment is presented in Appendix.

The experiment began with the measurement of the main subject anthropometric dimensions. Anatomical landmarks were palpated on pelvis and left lower limb according to the procedure described by Van Sint Jan et al (2007). In addition, reflective markers were put on these same points after manual palpation. Photos from two orthogonal views synchronized with a VICON motion capture were recorded in a calibrated environment.

Prior to the clutch pedal experiment, the data for characterizing subject’s individual physical capacity of the left lower limb were collected. For each joint ROM, the subject was asked to move slowly and to repeat the motion three times. For each joint torque, the subject was asked

to exert a maximum voluntary joint torque and to maintain it during 5s. Also, as recommended in the literature (Kumar, 2004), two trials will be recorded for each configuration. The highest effort value of the two trials will be taken as the maximum joint torque. Prior to the two trials the subject will be allowed to practice in order to get familiar with the task.

Then the subjects were invited to sit down in the experimental mock-up and to familiarize themselves with the available adjustments and with the discomfort rating scale. For each imposed pedal configuration, participants were asked first to adjust the horizontal seat position with respect to the accelerator pedal and then to adjust the steering wheel. An experimenter changed the pedal position, putting it out of reach of the subjects' foot. Then subjects were asked to choose their preferred pedal position while keeping all other parameters unchanged. Only the pedal position could be modified. In the longitudinal (x) and vertical (z) directions, the pedal adjustment was made by subjects themselves using a remote controller and the range of adjustment was superior to 100mm. In the lateral direction (y), the adjustment was made with the help of an experimenter in a range of 60 mm with a 10 mm-increment. The rest of the parameters such as travel angle or travel length for example remained the same between imposed and less-constrained configurations. This adjustment process continued until that a preferred clutch pedal position was found.

For all trials, before recording the clutching movement, the subjects were asked to fill in the discomfort questionnaire. Then, only one complete clutch pedal operation was recorded. The subjects were instructed to start motion with a standard driving posture (the left foot on the foot rest, the right foot on the acceleration pedal and the hands on the steering wheel), to press the clutch pedal with the left foot without changing the positions of the right foot and hands, then to maintain the clutch pedal fully pressed for about 3 seconds, finally to release the pedal and put the left foot back on the foot rest.

During the pedal position adjustment process, the subjects were able to perform as many times of pedal depression as necessary. The whole duration of the experiment lasted about four hours and a half. A pause of at least 10 minutes was imposed in the middle of the experiment during which drinks and biscuits were provided.

## 2.5 Data processing

At the end of an experimental session, following data types were available:

- Anthropometric measurements for each participant

- 3D markers trajectories of both subjects and mock-up
- Force exertion measurements
- Pressure map measurements
- Answers to the discomfort questionnaire

The answers to the discomfort questionnaire were collected. They were analyzed directly and no specific data pre-processing was needed. The global workflow of the data processing for inverse kinematic and inverse dynamic motion reconstruction, illustrated by Figure 14, is presented in the following parts.

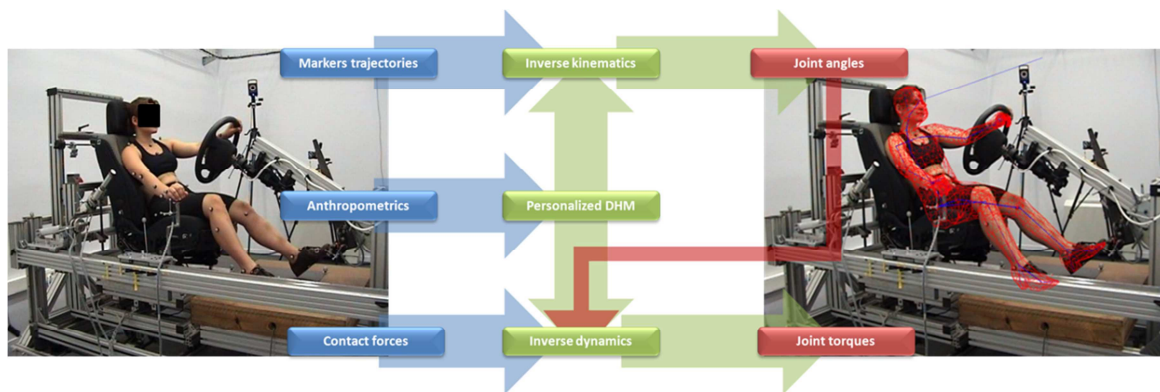


Figure 14: Motion reconstruction workflow

The data processing requires two main steps, a preparatory treatment of the data and the motion reconstruction.

### 2.5.i Preparatory treatment

#### Marker trajectories labeling and gap filling

The first data processing of the recorded movement is done with the VICON software. It consists of calculating the 3D marker positions and labelling the markers.

The major drawback of optical motion capture system is the loss of markers during movement. It occurs when the marker is not seen by at least 2 cameras. 3D position is then impossible to be calculated by the system.

To resolve the problem of missing markers, several solutions exist. First if the gap did not exceed 30 frames (Liu and McMillan, 2006), i.e. 0.3 second, it can be filled by the VICON software using a missing marker recovery tool, more or less based on various interpolation techniques and the use of kinematic information from the markers of the same segment or by Matlab using a spline interpolation. When this condition is not fulfilled, an algorithm based on the theories of rigid bodies' movements was applied (Veldpaus et al., 1988). This

algorithm can be only applied on a set of markers belonging to a same body segment when at least three markers attached to this same body are seen. Moreover, this algorithm assumes that the bodies are rigid and that no relative motions between markers exist. This assumption can be merely true in case of markers placed on human skin.

#### Personalized manikin editing

Ramsis™ (Human solutions GmbH, Kaiserslautern) manikin was used. A digital avatar of each participant was created using the measured anthropometric dimensions and the BodyBuilder module from Ramsis. This module allows the creation of a personalized manikin from 21 anthropometric dimensions measured on participants such as stature, weight, width between two shoulders, waist circumference and calf circumference etc... The dimensions which are not collected can be determined using statistical regression integrated in the module.

Then the manikins were superimposed on the calibrated photos using a DLT algorithm integrated in RPx software (Monnier, 2008). If the superimposition was not satisfying, the manikin's dimensions were adjustable manually directly in RPx (Figure 15).

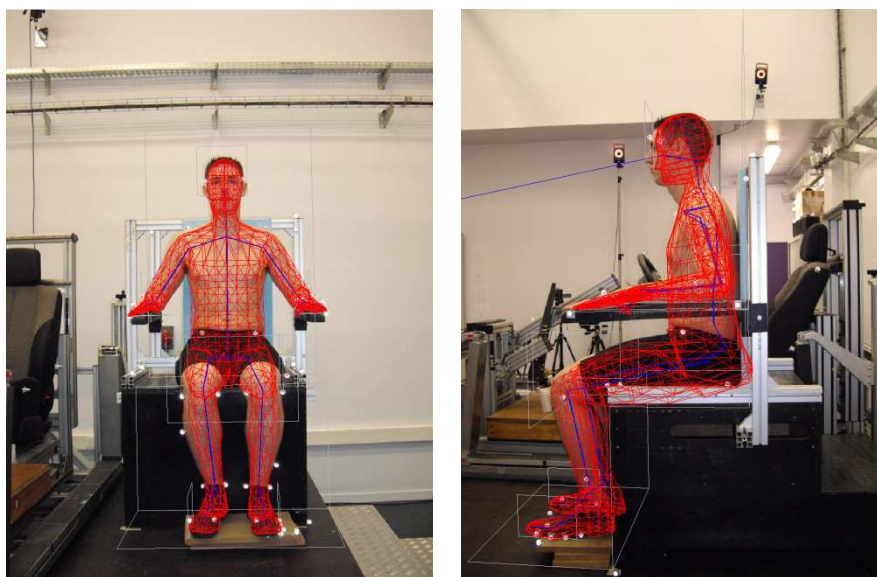


Figure 15: Manikin superimposition for subject 5 of FAC experiment on RPx

#### Markers attachment

The calibrated photos were taken synchronously with VICON motion captures. When personalized manikin is in the right posture and at the right dimensions, the motion captures are used to define markers coordinates in local body segment coordinate systems.

### 2.5.ii *Motion reconstruction*

#### Inverse kinematics motion reconstruction

The whole body motions were reconstructed using RPx by an inverse kinematic approach which calculates the joint angles from captured trajectories of skin markers by minimizing the distance between the captured and model-based markers positions (Ausejo and Wang 2008). The algorithm implemented in RPx is a global iterative method. The problem is constrained on the one hand, by the kinematic model of the DHM, i.e. Ramsis™ (see in Appendix for details on the kinematic model) in this case and, on the other hand, by the measured markers trajectories. The method is global because it reconstructs the motion of the whole body at once while guaranteeing joint constraints between the body segments. And the method is iterative because it reconstructs the posture considering successively the body segments as a hierarchical tree structure. The advantage is that it reduces a complex problem involving all segments into easier sub-problems. For lower and upper limbs, the motion reconstruction is often an over-guided problem because there is redundant information, i.e. more markers than strictly necessary, to define the posture of the kinematic chain at each instant. On the contrary, for the spine, it is hardly possible to estimate the spine motion using external markers and therefore the problem is under-guided. Monnier et al. (2007) implemented a coordination law between the joint angles of the spine in RPx to avoid unrealistic posture.

#### Inverse dynamics motion reconstruction

Joint forces and torques were computed from motion kinematics data, external forces and inertial properties of the body segments, using a 3D inverse dynamics method based Newton-Euler algorithm and homogeneous matrices (see for exemple, Doriot and Chèze 2004). The computation is done iteratively at each frame by isolating the body segments from the most distal to the most proximal. The computed joint torques are the sum of all torques acting on the segment, i.e. the torques due to gravity, to motion kinetics, to contact forces and to muscular forces. Body segment properties (mass, centre of mass, inertia) are calculated from subjects' anthropometric dimensions using the regression equations of Dumas et al. (Dumas et al. 2007). In case of DHErgo experiment, only the force applied on the clutch pedal was measured and it was decided to apply it to the left foot.

### 2.5.iii *Motion key-frames*

Two main key instants were identified for analyzing the clutching movement: the beginning of pedal depression, i.e. when the left foot start depressing the clutch pedal, and the end of

pedal depression, i.e. when pedal end travel is reached. The first one was defined as the first frame when the force recorded by the pedal sensor was above 5% of the maximal force recorded in the trial. The second one was defined as the first frame when the left foot velocity was below 5% of the maximum velocity recorded after the beginning of pedal depression in the trial. These specific instants or key-frames were determined for each recorded motion. Postures and forces were analyzed only at these key-frames.

#### **2.5.iv Pedal force and maximum isometric joint torque treatment**

The pedal force was analyzed without post treatment. However, two subjects (16\_ED and 18\_AC) were excluded from the dynamic part of the motion analysis because the force patterns were inconsistent. Indeed, the measurement channels were wrongly configured.

For the maximum isometric joint torque, the plateau method was used. The subject was asked to apply a required force level during 5 seconds. The average between 1.5 to 4.5 seconds was calculated. A counter-weight was added on the ergometer for each measurement so that the device remained in the determined angular position without external effort from the subject. The force transmitted by the cable was then put to zero. Therefore, only the muscular force applied by the subject was measured without body weight effect. The active muscle joint torque, called also net joint torque (NetJT), can be estimated by:

$$NetJT = \begin{cases} (F + F_R) \times R, & \text{when applied force direction is in the opposite direction of body weight} \\ (F - F_R) \times R, & \text{when applied force direction is in the same direction of body weight} \end{cases}$$

Where  $F$  is the measured external force,  $F_R$  is the measured resting force due to the body segment weight when the joint segment remains in the determined angular position without further muscle force activation and  $R$  is the radius of the ergometer's wheel (159.5 mm) used for angular positioning. In case that the body weight increases the cable force, then the body weight effect has to be removed for calculating the active joint torque NetJT. When required force direction is in opposite of body weight direction, then moment due to body weight has to be added.

## **2.6 Evaluation of the motion reconstruction**

In this part, the goal is to assess the quality of the motion reconstruction. For the kinematic reconstruction, a visual inspection of the reconstructed motions was first carried out. It allows

an inspection of visual quality of reconstructed motions. The largest error of motion reconstruction was related to the loss of the markers placed on the anatomical points of the pelvis. The manikin is positioned in space from these markers. So if they disappear, the algorithm has difficulty in positioning the manikin, resulting in jump or vibration of the pelvis. Then, the residues corresponding to the distance between the recorded marker position and the reconstructed one were calculated. For the dynamic reconstruction, the evaluation of the quality of the dynamic reconstruction was hardly possible. Indeed, all contact forces between the individual and the environment are required to verify the force and moment equilibriums at each instant. But the forces applied by the participants on the seat and on the floor with the right foot were not recorded. Moreover, the seat/thigh contact may affect the estimation of the left hip torque by the inverse dynamics procedure. The pressure map data were therefore analyzed visually and a raw estimation of the contact force between the seat and the left thigh as well as the resulting moment on the hip was done.

### *2.6.i Kinematic reconstruction evaluation*

The visual analysis of the reconstructed motions showed no major problem of marker losses. Indeed, four markers were placed on the pelvis (left and right anterior superior iliac spine, left and right crest tubercle) and they were all missed for only 1 trial. The labeling of the markers was presented in Appendix.

The mean residue for all markers and trials was  $11.7 \pm 3$  mm. The largest errors were obtained for a marker on the thigh (LTH3MK) and a marker on the left calcaneus (LFCCMK) with respective mean values of 16.7mm and 16.5mm (Figure 16). These errors were particularly due to relative motion between marker and body segment for LTH3MK (this marker was in contact with the seat during clutch pedal depression) and to marker displacement or loss for LFCCMK (this marker was often removed during motion and not exactly replaced the same. Moreover the obstructed environment made it hard to see by the cameras). However, it can be noted that the mean residues of this two markers were still reasonable. The other markers showed relatively reliable residue below 15 mm.

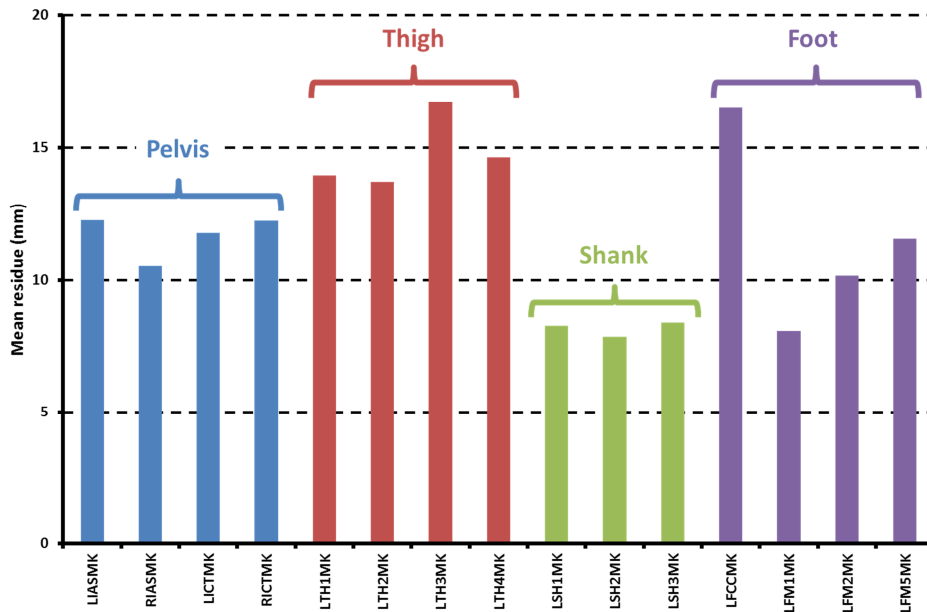


Figure 16: Mean values of markers' residues on all subjects and trials (DHergo experiment)

### 2.6.ii Dynamic reconstruction evaluation

The pressure map data were then extracted using XSensor<sup>®</sup> X3Pro software provided with the pressure maps and were visualized using Matlab<sup>®</sup>. The visual analysis of the data showed that the hypothesis of non-contact between the thigh and the seat during clutching movement could not be considered. Figure 17 showed the seat pressure for one of the younger male subjects for a low seat height (BMW4), an average seat height (PCA2) and a high seat height (REN3) at the beginning and the end of the clutch pedal depression.

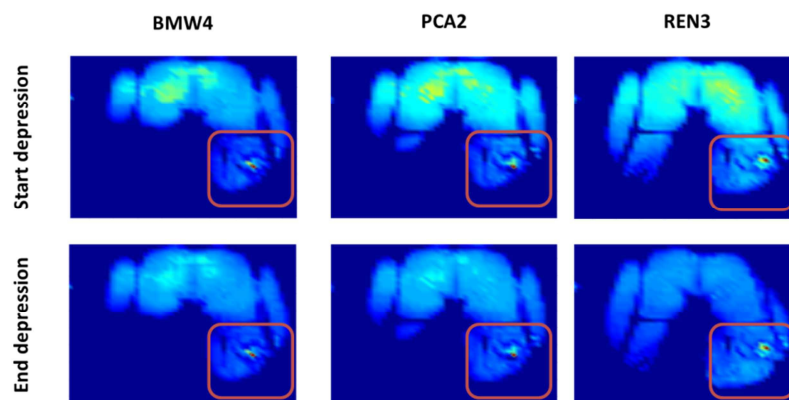


Figure 17: Seat pressure for one of the younger male subjects for a low seat (BMW4), an average seat height (PCA2) and a high seat (REN3) at the beginning and the end of the clutch pedal depression. The thigh is outlined in red on the pressure map images.

It can be observed that the contact between the seat and the left thigh was present for the three seat heights. Especially at the end of the pedal depression, buttocks and the thigh had quite the

same color, which means quite the same pressure. A raw estimation of the contact force and the resulting moment on hip was performed at the end of the pedal depression. That motion key-frame was selected because the left leg should be the most extended at the end of the pedal depression and so it should be the instant when the most contact between the thigh and the seat occurred. Then it should be considered that no reflective markers were put on the pressure maps. As a consequence, it was considered that the pressure maps were always in the same position between trials and subjects. The following considerations were done for the contact force and hip moment:

- Definition of a fixed contact zone: the pressure map used in the DHErgo experiment was a 48x48 grid of sensors. As a consequence, it was considered that the contact zone of the left hip should be limited to the bottom left quarter of the grid (row 25 to 48, column 25 to 48) as illustrated in Figure 17.
- Estimation of the contact force: it was considered that all the pressure map's sensors in contact with the thigh had the same orientation. As a result,  $F_{Thigh-Seat}$  was calculated as:

$$F_{Thigh-Seat} = \sum_{i=25}^{48} \sum_{j=25}^{48} P_{i,j} * S_{i,j} * \mu$$

With

*i*, a grid row,

*j*, a grid column,

$P_{i,j}$ , pressure recorded by the sensor (*i,j*) on the grid (in PSI, i.e. pound squared inch)

$S_{i,j}$ , surface of the sensor (*i,j*) in squared inch

$\mu$ , conversion parameter from pound to newton

- Estimation of the resulting hip moment: it was considered that the contact force was perpendicular to the thigh in the XZ plane of the mock-up reference frame. Besides, the force was applied at 1/2 of the thigh length from the hip joint. For each subject, the thigh length were based on the length of the thigh segment of the individualized RAMSIS™ manikin. As a result,  $T_{Thigh-Seat}$  was calculated as:

$$T_{Thigh-Seat} = F_{Thigh-Seat} * \frac{1}{2} * L_{Thigh}$$

Table 4 presents the estimation of  $F_{Thigh-Seat}$  and  $T_{Thigh-Seat}$  for the pedal configuration tested in the DHErgo experiment. Globally, it can be noticed that the contact force between the left hip

and the seat was 104 N on average and the resulting moment was 22 Nm on average. The contact force does not appear to be negligible. As a consequence, only the knee and ankle joint toques calculated by inverse dynamic reconstruction should be considered as reliable.

**Table 4: Estimation of the contact force between left thigh and the seat  $F_{Thigh-Seat}$  and the resulting hip moment  $T_{Thigh-Seat}$  for tested pedal configuration in DHErgo experiment using the seat pressure map data.**

		$F_{Thigh-Seat}$ (N)	$T_{Thigh-Seat}$ (Nm)
BMW1	Imposed	90 ± 48	19 ± 10
	Less constrained	102 ± 47	21 ± 10
BMW2	Imposed	98 ± 48	21 ± 9
	Less constrained	108 ± 49	23 ± 10
BMW4	Imposed	80 ± 41	15 ± 9
	Less constrained	82 ± 37	16 ± 8
PCA1	Imposed	132 ± 43	28 ± 9
	Less constrained	132 ± 49	28 ± 11
PCA2	Imposed	91 ± 44	19 ± 9
	Less constrained	110 ± 49	23 ± 10
REN3	Imposed	125 ± 45	27 ± 10
	Less constrained	128 ± 52	27 ± 11
All		104 ± 49	22 ± 10

## 2.7 Summary of processed data

<b>DHErgo experiment</b>		
<b>Number of participants</b>	20	
<b>Subject characterization trials</b>	<b>Anthropometry</b>	41
	<b>ROM</b>	7
	<b>Max. joint torque</b>	19
<b>Clutch pedal trials</b>	16 (clutch pedal operation)	
<b>Excluded participant</b>	0 (2 for dynamic analysis only)	
<b>Number of reconstructed trials for motion analysis</b>	16 x 20 = 320 (14 x 20 = 280 for dynamic analysis)	

### 3 Analysis of the discomfort perception

The discomfort perceived during the clutch pedal operation experiment performed in DHErgo project was assessed using a questionnaire (see in Appendix). The objective of such questionnaire was to collect a subjective global evaluation of the task using a discomfort rating scale, but also to get some insights on the effect of the pedal configuration parameters (seat, pedal positions at the start/end depression, pedal travel length/angle, pedal resistance) on the discomfort. Besides in the context of using the less-constrained movement concept, the analysis of the answers should identify the pedal adjustments made by the subjects as well as explain the effect of these adjustments on the perception of the task. In the following section, the answers to the questionnaire were analyzed. The answers were analyzed in terms of the following three independent variables:

- The group of subjects (SubjectGroup): young male, young female, old male and old female. Each group is constituted of 5 individuals of same age, gender and anthropometry.
- The configuration (Configuration): BMW1, BMW2, BMW4, PCA1, PCA2 and REN3.
- The type of configuration (ConfigType): imposed configuration and less constraint one.

For each question,  $(4 \times 5) \times (6 + 2) \times 2 = 320$  answers were considered. First, the multiple-choice questions Q1 to Q6 were considered and then discomfort ratings were analyzed.

#### 3.1 Questionnaire analysis

The multiple-choice questions focused on the subjective evaluation of the clutch pedal configuration and the effect of the seat on discomfort perception during the task:

- Question 1 (Q1) evaluated the effect of the seat on discomfort.
- Question 2 and 3 evaluated respectively the clutch pedal position at the beginning of the pedal depression and at the end:
  - The height of the pedal (Q2H/Q3H), i.e. the z-coordinate in the mock-up local coordinate system,
  - The distance from the seat (Q2D/Q3D) i.e. the x-coordinate,
  - The lateral position (Q2P/Q3P) i.e. the y-coordinate.

- Question 4 (Q4) evaluated the travel length.
- Question 5 (Q5) evaluated the travel inclination.
- Question 6 (Q6) evaluated the perception of the pedal resistance.

The effects of the three variables (Group of subjects, Configuration, Type of configuration) were analyzed using frequency tables. The Chi-square test was also performed to test the hypothesis that the row and column distributions are independent. This analysis focused particularly on the answers to the questions 2, 3 and 6. But the influence of the seat (Q1), the travel length (Q4) and travel inclination (Q5) were also assessed by the subjects. For more than 90% of the answers, the seat had no effect on the discomfort perception. The travel lengths of the clutch pedal were estimated too long or at good length at almost fifty-fifty. The travel inclinations of the clutch pedal were mostly estimated (72%) at good inclination. All results are presented in Appendix. Prior to the analysis, the reproducibility of the answers to the questionnaire was assessed in order to verify if the subjects were consistent in their evaluation of the pedal configuration.

### 3.1.i *Reproducibility*

For each subject, the central configuration PCA2 was tested three times for both imposed and less constraint types of configuration.

The questions Q1 to Q6 were multiple choices questions. In order to assess the reproducibility of each subject for these questions, answers were attributed to each question according to the number of similar answers on the three repetitions.

Condition	Description	Post treated value
<b>Cond1</b>	0 similar answer, i.e. the subject gave three different answers to the same question on the three repetitions	= 1
<b>Cond2</b>	2 similar answers, i.e. the subject gave two times the same answers to the same question on the three repetitions	= 2
<b>Cond3</b>	3 similar answers, i.e. the subject gave the same answers to the same question on the three repetitions	= 3

The reproducibility was defined for each subject and question as the frequency of each condition (Figure 18). The results are presented in Appendix. Globally, the subjects were able to give at least 2 similar answers to the same question in 98% of the cases. The same answers for the three repetitions was obtained in 61% of the cases. More specifically, the most reproducible question was the question on the seat Q1 (90% of Cond3) and the worst were the

question on the pedal distance at the end depression Q3D and the one on the pedal resistance Q6 (Cond3 < 50%). However, Cond1 was inferior to 10% for these two questions. Only three subjects (04\_VM, 13\_AT and 19\_JL) had a frequency for Cond3 inferior to 50%. But apart from the subject 19\_JL, all subjects had a combined frequency for Cond2 and Cond3 of at least 95%.

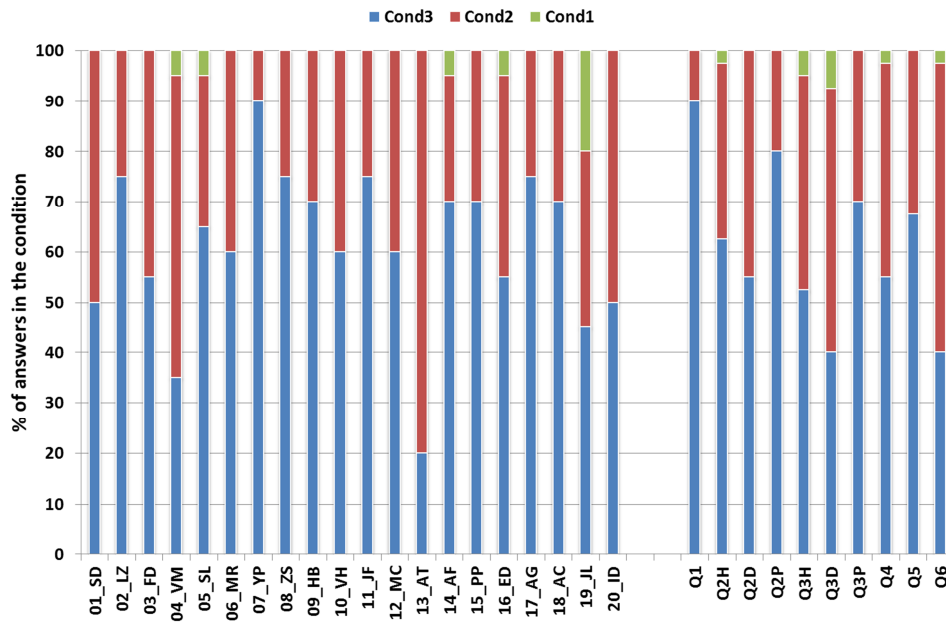


Figure 18: Reproducibility of the answers to the questionnaire by subjects and questions. Q1: effect of the seat, Q2H/Q3H: pedal height at the start/end depression, Q2D/Q3D: pedal distance at the start/end depression, Q2P/Q3P: pedal lateral position at the start/end depression, Q4: travel length, Q5: travel inclination, Q6: pedal resistance.

### 3.1.ii Evaluation of the pedal position

For the questions Q2 and Q3 of the questionnaire, the subjects were asked to judge the position of the clutch pedal at initial (or impressed) position and final (or fully pressed) position. The questions were divided in three sub-questions:

*The pedal in initial/final position is placed:*

Height (Q2H/Q3H)	Distance (Q2D/Q3D)	Position (Q2P/Q3P)
<input type="checkbox"/> Too high (1)	<input type="checkbox"/> Too far (1)	<input type="checkbox"/> Too left (1)
<input type="checkbox"/> At good height (2)	<input type="checkbox"/> At good distance (2)	<input type="checkbox"/> At good position (2)
<input type="checkbox"/> Too low (3)	<input type="checkbox"/> Too close (3)	<input type="checkbox"/> Too right (3)

Globally, the pedal was judged at good height or too high in initial position in respectively 63% and 32% of the answers to Q2. In final position, 69% of the answers to Q3 considered the pedal height as good and 19% as too low (Table 5). Then the distance from the seat was judged as good or too close in respectively 70% and 24% of the answers in initial position and

as good or too far in respectively 57% and 38% of the answers in final position. The clutch pedal was estimated at a good lateral position in most of the answers, respectively 64% and 67% for initial and final position. The rest of the answers, respectively 36% and 32% for initial and final position, considered the pedal as too on the right.

**Table 5: Assessment of the pedal position in x, y and z directions at the start and the end depression for imposed and less constrained configurations. Frequencies of the answers for each direction are shown.**

		Imposed	Less Constrained	Global	
Pedal start position (Q2)	Height*** (Q2H)	Too high (%)	55.6	8.8	32.2
		Good (%)	36.3	90.6	63.4
		Too low (%)	8.1	0.6	4.4
	Distance from seat*** (Q2D)	Too far (%)	11.3	0.6	5.9
		Good (%)	48.8	91.9	70.3
		Too close (%)	40	7.5	23.8
	Lateral position*** (Q2P)	Too leftward (%)	0.6	0	0.3
		Good (%)	35.6	91.8	63.5
		Too rightward (%)	63.8	8.2	36.2
Pedal end position (Q3)	Height*** (Q3H)	Too high (%)	18.9	4.4	11.6
		Good (%)	64.8	73.6	69.2
		Too low (%)	16.4	22	19.2
	Distance from seat*** (Q3D)	Too far (%)	32.7	42.8	37.7
		Good (%)	57.2	57.2	57.2
		Too close (%)	10.1	0	5
	Lateral position* (Q3P)	Too leftward (%)	0.6	0	0.3
		Good (%)	43.8	91.2	67.4
		Too rightward (%)	55.6	8.8	32.3

Chi-square test significance: \* p-value<0.05, \*\* p-value<0.01, \*\*\* p-value<0.001

More important is the effects of the type of configuration on the answers. Big differences were observed for the initial pedal position. More than 90% of the less constrained pedal configurations were considered “at good height, at good distance and at good lateral position” in the initial position. Imposed pedal configurations in the initial position were found too high in 55% of the answers to Q2, too close in 40% and too on the right in 64%. In the final position, the effects of the type of configuration were also significant but apart from lateral position evaluation, they were less strong. Indeed, the pedal were found much more frequently too low and too far in less constraint configurations compared to imposed ones: respectively 22% and 16% of the answers to Q3 for pedal height, 42% and 32% for pedal distance. Therefore the subjects tended to improve the beginning of the clutch pedal operation at the expense of the end. Figure 19 compares the distributions of the responses to Q2H, Q2P, Q3H and Q3P between freely adjusted and imposed pedal configurations.

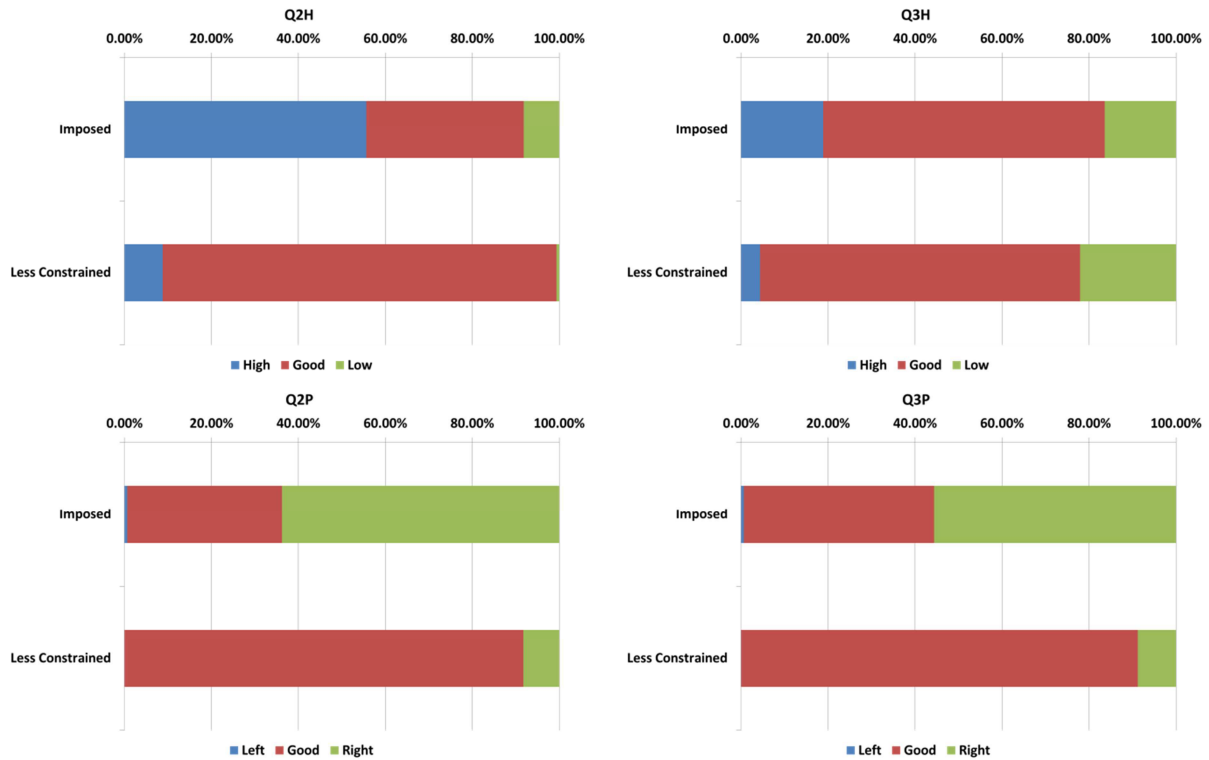


Figure 19: Distribution of the answers to Q2H, Q2P, Q3H and Q3P according to the type of configuration

The Chi-square test also revealed significant effects of the group of subjects and of the configuration (see in Appendix). Female subjects reported more frequently high clutch pedal in initial position, low clutch pedal in final position and pedal too on the right than the male subjects. PCA1 and REN3, two configurations with high seat, were more frequently judged too low whereas the configurations with low seat height were most of the time estimated as too high. In the same way, the configurations with a more leftward pedal, BMW2 and BMW4, were estimated good in lateral position more frequently than the others.

### 3.1.iii Evaluation of the pedal resistance

The question Q6 was about the perception of the pedal resistance by the subjects. The Borg's CR10 was used to assess the pedal force perceived by the subjects.

**Q6: During clutch pedal operation, the force to be applied is:**

- Very low (1)
- Low (2)
- Medium (3)
- High (4)
- Very high (5)

It is important to point out that no subject answered very high in the current experiment. Most of the clutch pedals (54%) were judged as medium level. 26% and 18% of the trials were

perceived as “low” or “high” (Table 6). No statistically significant effects of subject group and configuration type were found.

**Table 6: Assessment of the pedal resistance for the six clutch pedal configurations tested in the experiment. Frequencies of the answers for each configuration are shown.**

	BMW1	BMW2	BMW4	PCA1	PCA2	REN3	Total
Very Low (%)	0.00	0.00	5.00	0.00	4.17	2.50	2.50
Low (%)	30.00	40.00	55.00	12.50	20.00	12.50	26.25
Medium (%)	52.50	45.00	32.50	62.50	60.83	55.00	53.75
High (%)	17.50	15.00	7.50	25.00	15.00	30.00	17.50

The Chi-square test shows that there is a significant effect of the clutch pedal configuration on force perception (Figure 20). The pedal resistance of BMW4 was perceived as low for 55% of the answers and medium for 32.5%. The other pedal configurations had generally a pedal resistance perceived as medium (between 45% and 62.5%). It can also be observed that PCA1 and REN3 are the only pedal configurations with a frequency of pedal resistance higher than 20% for the “high” force level. The frequencies were respectively 25% and 30% for PCA1 and REN3.

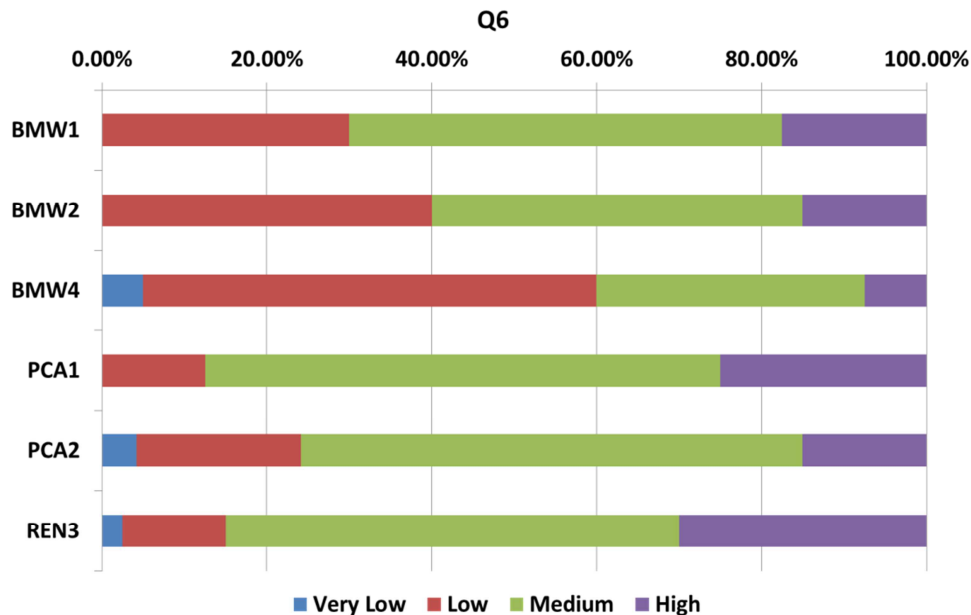


**Figure 20: Distribution of the answers to Q6 according to the configuration**

### 3.2 Discomfort ratings analysis

In the questionnaire, the subjects were only asked to rate the global discomfort of the clutching task. The effects of the same three variables (Group of subjects, Configuration, Type of configuration), as the ones considered in the questionnaire analysis, were assessed through ANOVA. Moreover, prior to analysis, the reproducibility of the subjects' ratings was assessed.

#### 3.2.i Reproducibility

For each subject, the configuration PCA2, the central configuration one of the experiment, was tested three times for both imposed and less constrained conditions, in order to evaluate the reproducibility of discomfort ratings. The maximum gap in discomfort rating between three repeated trials and their mean was calculated and shown in Figure 21. One can see that 13 out of 20 subjects had a mean maximum gap higher than 5, implying that the rating of a same target might change the discomfort category from trial to trial. In particular, the subjects 4, 6 and 14, who had an average value higher than 10, probably suggesting that they had difficulty in using the rating scale. In this experiment, the mean maximum gap value was 6.8.

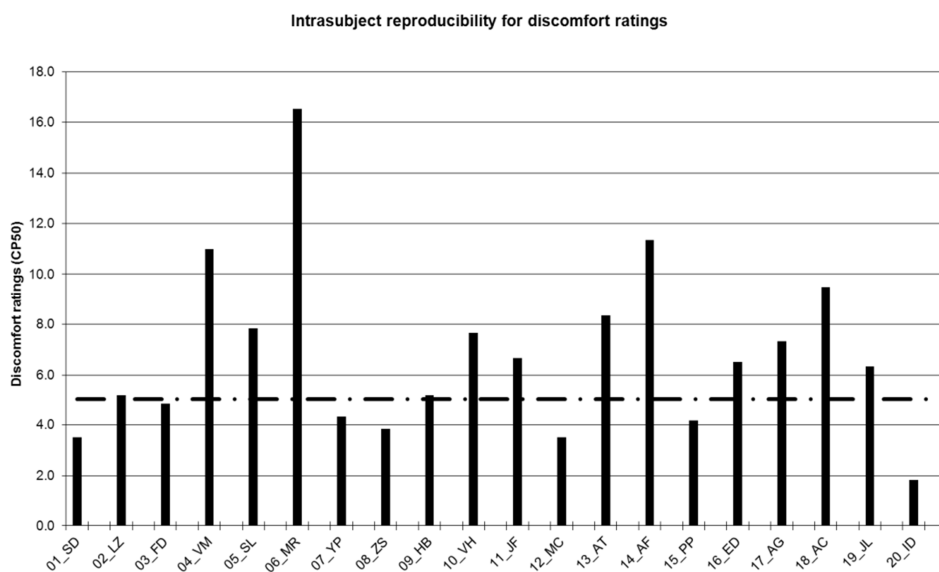


Figure 21: Reproducibility of discomfort ratings. Dotted line represents the reproducibility threshold at 5

#### 3.2.ii Effects of the controlled variables

The effects of the controlled parameters, i.e. pedal configuration, type of configuration, and group of subjects, were investigated. The results are summarized in Table 7 and showed that discomfort rating strongly depended on these three factors.

**Table 7: Means and standard deviations of the raw and centred CP50 scores according to the group of subjects (G), the test configuration (C) and the type of configuration (T)**

	CP50 raw scores	CP50 centred scores
Older Female	14.2 ± 9.3	
Older Male	18.0 ± 10.5	
Younger Female	20.3 ± 8.6	
Younger Male	16.9 ± 9.0	
BMW1	17.8 ± 10.3	0.48 ± 8.3
BMW2	16.8 ± 8.2	-0.55 ± 5.6
BMW4	13.6 ± 11.0	-3.77 ± 7.9
PCA1	20.7 ± 9.7	3.33 ± 8.1
PCA2	16.1 ± 8.9	-1.21 ± 6.8
REN3	21.5 ± 8.4	4.15 ± 8.9
Imposed	19.7 ± 9.6	2.32 ± 7.7
Less Constrained	15.0 ± 9.0	-2.32 ± 7.2
All	17.3 <sup>C***, G***, T***</sup> ± 9.6	0 <sup>C***, T***</sup> ± 7.79

\*p<0.05, \*\*p<0.01, \*\*\* p<0.001, C: configuration, G: group of subjects, T: type of configuration

However, although a significant effect of subject group on discomfort scores was observed, the average difference between subject groups were between 2.3 and 6.1, smaller than the average maximum gap of three repetitions, i.e. 6.8. In what follows, the analysis is therefore focused on the effects of pedal parameters, i.e. the configuration and the type of configuration, on discomfort ratings. According to Wang et al. (2004), one way to reduce subject effect was to centre the rating scores for a configuration at the average score of all configurations tested for each subject. Therefore centred rating scores rather than direct ones were used for studying the effects of pedal parameters on discomfort. The less constrained configurations were better rated than the imposed ones (Figure 22).

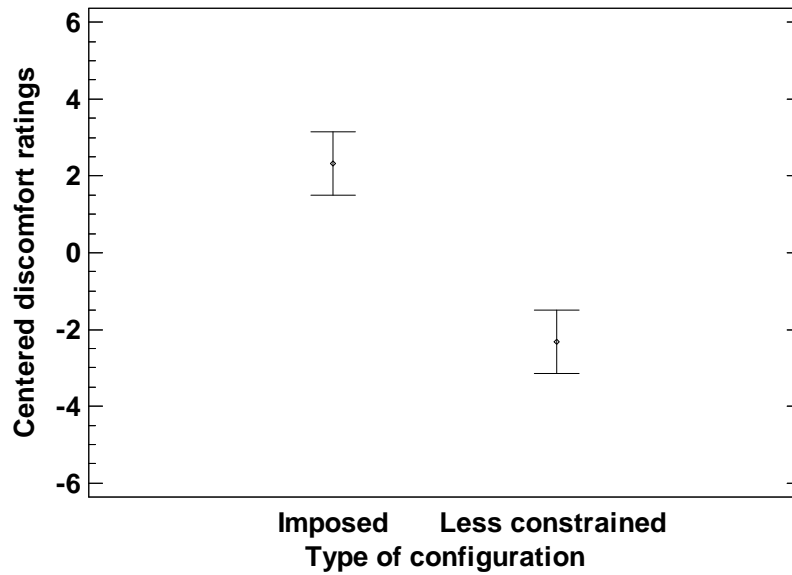


Figure 22: Discomfort ratings centered to each participant's mean value in terms of type of configuration

Then, pedal configuration had a strong effect on the discomfort ratings (Figure 23). BMW1 had the lowest discomfort score with a mean centered value of -3.78. PCA1 and REN3 had the highest discomfort ratings respectively of 3.33 and 4.15. BMW1, BMW2, PCA2 had average scores between 0.48 and 1.21.

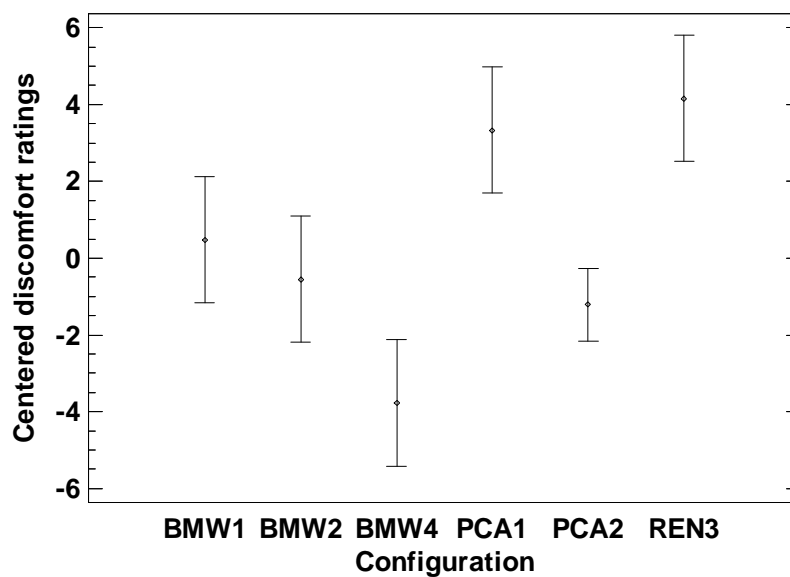


Figure 23: Discomfort ratings centered to each participant's mean value in terms of configuration

### 3.2.iii Discomfort/pedal resistance perception relation

In an earlier study by Wang et al. (2004), it was found that pedal resistance had a strong effect on discomfort perception. In this study, pedal resistance was not controlled but rather dependent on its initial position and travel length. The perception of the pedal resistance was

collected through the questionnaire using the Borg's CR10. A strong effect of the perceived pedal resistance on the discomfort ratings was found.

**Table 8: Means and standard deviations of the raw CP50 scores according to the perceived pedal resistance.**

	CP50 raw scores
Very low	7.9 ± 12.1
Low	11.4 ± 8.4
Medium	18.3 ± 7.7
High	24.7 ± 9.8
All	17.3 ± 9.6***

\*p<0.05, \*\*p<0.01, \*\*\* p<0.001

Figure 24 showed that discomfort ratings increased with the perceived level of pedal resistance.

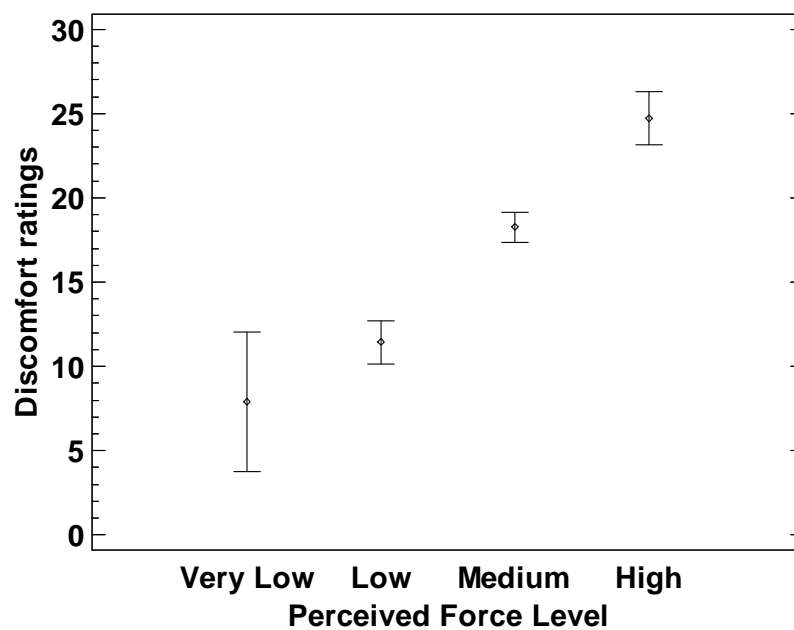


**Figure 24: Discomfort ratings in terms of perceived resistance levels (CP50 raw score)**

## **4 Motion analysis of the clutch pedal operation**

In this part, clutching movements were analyzed in order to understand the subjective evaluations made by the subjects. First, the motion kinematics was analyzed comparing the imposed and less-constrained configurations. Indeed, the analysis of subjective evaluations showed that less-constrained configurations led to an improvement of the clutch pedal position at the start depression at the expense of the end. But free pedal adjustment had no significant effects on pedal force perception. This kinematic analysis focused on the clutch pedal adjustments and their effects on joint angles to explain why the subjects preferred to improve the start depression than the end.

Second, the motion dynamics was analyzed focusing on the foot force applied on the pedal. The pedal resistance depended strongly of the configuration and could be considered a dominant factor for discomfort assessment in the analysis of discomfort ratings. Therefore the foot force applied to the pedal (amplitude and direction) was studied as well as its effect on joint torque.

### **4.1 Comparison of clutching movements for imposed and less-constrained pedal configurations**

#### **4.1.i Clutch pedal position adjustments**

The variation in pedal position between imposed and less-constrained configurations was estimated using the six markers fixed on the clutch pedal. For each pedal configuration, the positions of the clutch pedal markers of both imposed and less-constrained clutch pedal operation were collected at the first frame, i.e. before the start depression. The reproducibility of the adjustment in each axis (x-, y- and z-axis) was defined as the maximum gap between adjustment scores and their mean for each subject and was estimated from the three repetitions of the central configuration PCA2 in the experiment. The mean values were  $15 \pm 9$  mm in x-axis,  $10 \pm 8$  mm in y-axis and  $13 \pm 9$  mm in z-axis.

The pedal position change in x, y and z directions from imposed pedal positions to preferred ones were summarized in Table 9. On average, they were -8.8, -21 and -16.8 mm respectively in x, y and z directions. Globally the pedals were moved further away from the seat, lower and more leftward.

**Table 9: Means and standard deviations of the adjustments in x, y and z from an imposed pedal position to the preferred one for the six tested configurations**

	$\Delta x$ (mm)	$\Delta y$ (mm)	$\Delta z$ (mm)
Older Female	-1.9 ± 20.4	-21.2 ± 20.1	-21.1 ± 38.4
Older Male	-5.6 ± 28.1	-17.7 ± 22.2	-18.5 ± 36.7
Younger Female	-11.8 ± 13.8	-23.0 ± 20.8	-26.5 ± 30.1
Younger Male	-8.8 ± 22.5	-22.1 ± 19.9	-1.2 ± 36.6
BMW1	-3.0 ± 17.7	-41.0 ± 18.8	-45.5 ± 32.9
BMW2	-3.4 ± 20.6	-4.2 ± 12.7	-46.6 ± 24.8
BMW4	-1.4 ± 32.6	0.9 ± 4.0	-43.5 ± 30.8
PCA1	-3.9 ± 24.8	-31.0 ± 22.6	-4.4 ± 25.7
PCA2	-14.9 ± 18.0	-18.3 ± 14.0	0.2 ± 27.9
REN3	-13.8 ± 23.1	-37.9 ± 16.3	4.6 ± 36.4
Total	-8.8 <sup>C*, G*</sup> ± 22.5	-21.0 <sup>C***</sup> ± 20.6	-16.8 <sup>C***, G**</sup> ± 36.5

\*p<0.05, \*\*p<0.01, \*\*\* p<0.001, C: configuration, G: Group of subjects

Significant effects of the group of subjects were found for the adjustment on x-axis and z-axis. For the adjustment in the longitudinal direction (x-axis), the younger subjects put the pedal further from the seat than the older people. In the vertical direction (z-axis), only the adjustments of the younger males differed from the other subjects. Globally, all subjects tended to adjust the pedal in the same direction, i.e. further from the seat, lower and more on the left.

A significant effect of pedal configuration was observed, particularly strong for the adjustment in y-axis and z-axis. In y-axis, apart from BMW2 and BMW4, the pedals were moved more than 15 mm on left on average. The average lateral position of the less constrained configurations was therefore -109 mm from the central line of the seat. In z-axis, BMW1, BMW2 and BMW4 were lowered more than 40 mm on average whereas PCA1, PCA2 and REN3 presented little displacements.

#### 4.1.ii Joint angle analysis

The left lower limb had seven degrees of freedom (DOFs): three at the hip (flexion/extension, abduction/adduction and axial rotation), two at the knee (flexion/extension, axial rotation) and two at the ankle (flexion/extension or dorsiflexion/plantarflexion, inversion/eversion). The orientations of the joint axes from RAMSIS™ were kept to express the joint angles:

- GHUL-x, -y and -z respectively for hip axial rotation, abduction/adduction and flexion/extension
- GKNL-x and -y respectively for knee axial rotation, and flexion/extension
- GSPL-x and -z respectively for ankle inversion/eversion and inversion/eversion

The joint angles were examined at the beginning and the end of clutching movement. Paired t-tests were performed to estimate whether joint angles differed between imposed and less-

constrained configurations. The tests showed significant differences were found for the flexion-extension angles of all three joints as well as for the abduction/adduction angles of the hip (Figure 25). The mean values, standard deviations and the mean differences between the imposed and freely adjusted conditions are presented in Appendix.

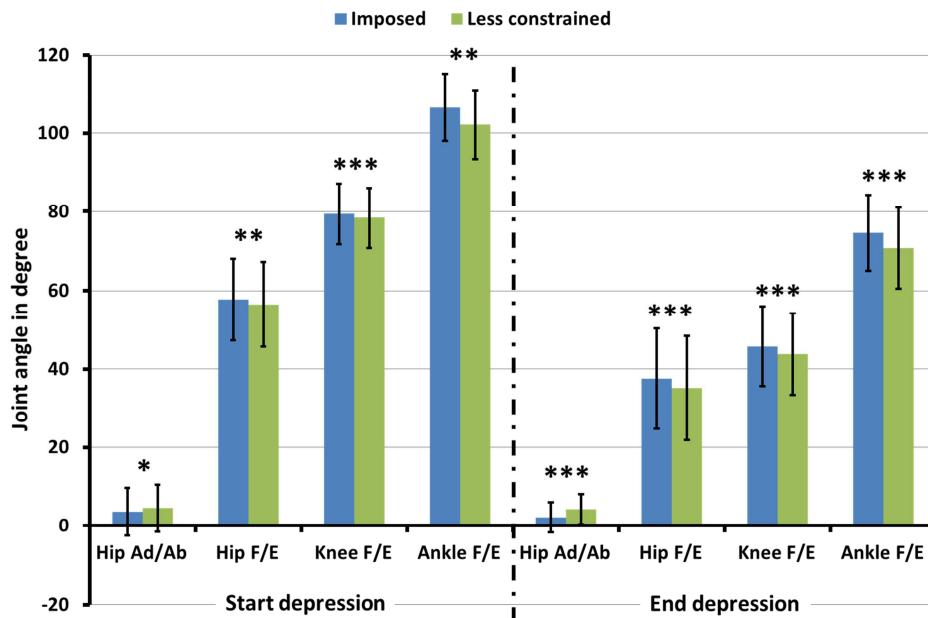


Figure 25: Mean joint angles for imposed and less-constrained configurations at start and end depression: hip adduction/abduction (Ad/Ab), hip flexion/extension (F/E), knee flexion/extension (F/E) and ankle flexion/extension (F/E) (\* $p < 0.05$ , \*\* $p < 0.01$ , \*\*\*  $p < 0.001$ )

First, the change of pedal position, especially in the longitudinal and vertical direction, led to a decrease in the flexion of the hip, knee and ankle joints at the beginning and an increase of the extension of these joints at the end of the pedal depression, especially for the ankle. The mean variations were  $1.2^\circ$ ,  $1^\circ$  and  $4.4^\circ$  respectively for hip, knee and ankle flexion/extension angle at the start depression and  $2.6^\circ$ ,  $1.9^\circ$  and  $3.9^\circ$  for the same angle at the end depression. The highest variation in the joint flexion-extension angle was found at the ankle at the beginning of the clutch pedal depression. Then, the lateral pedal adjustment caused an increase of the abduction, i.e. the thigh was further away from the median sagittal plane of the body between imposed and less constrained configurations:  $-0.9^\circ$  at the beginning of pedal depression and  $-2.1^\circ$  at the end.

#### 4.2 Analysis of clutch pedal force exertion

The clutch pedal device used in DHErgo experiment was a simple spring different from a diaphragm spring that can be found in a real car. The maximum force applied on the pedal

during the depression phase was at the end of the depression. As a consequence, the clutch pedal force exertion was only considered at the end of the depression.

#### 4.2.i Pedal force resultant and components

The foot force applied on the pedal was decomposed in three components according to the Figure 26.

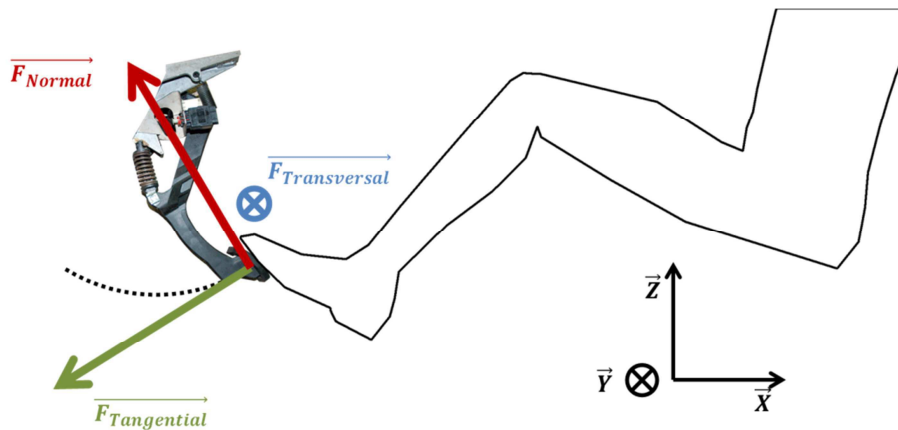


Figure 26: Clutch pedal force decomposition

The tangential and normal components were defined as being tangent and normal to the pedal path in the x-z plane. The transversal component was defined as orthogonal to the two previous components in order to get a direct trihedron. The mean values of the force resultant and the three components are presented in the Table 10. It can be noticed that the type of configuration had an effect on the transversal force only. Apart for PCA1 pedal configuration, the transversal component was small compared to the two other components. But interestingly, the mean values of the transversal force according to the group of subjects, the configuration or the type of configuration are negative, which means directed towards left in the driver's point-of-view. Then, it was decided to focus the analysis of the force components on the tangential and normal components.

Table 10: Mean values and standard deviations of force resultant, tangential force, normal and transversal force

	Resultant (N)	Tangential (N)	Normal (N)	Transversal (N)
Older Female	188 ± 23	183 ± 22	-30 ± 34	-8 ± 8
Older Male	184 ± 23	179 ± 22	-33 ± 29	-3 ± 9
Younger Female	177 ± 31	167 ± 25	-53 ± 33	-5 ± 9
Younger Male	171 ± 19	158 ± 16	-57 ± 32	-4 ± 10
BMW1	183 ± 27	172 ± 23	-56 ± 34	0 ± 9
BMW2	174 ± 25	164 ± 23	-53 ± 24	-6 ± 7
BMW4	166 ± 19	160 ± 18	-40 ± 24	-4 ± 7
PCA1	176 ± 28	171 ± 25	-14 ± 37	-12 ± 12
PCA2	183 ± 25	172 ± 24	-54 ± 32	-2 ± 8
REN3	185 ± 25	179 ± 22	-36 ± 29	-8 ± 8
Imposed	181 ± 24	172 ± 23	-45 ± 31	-2 ± 9
Less Constrained	178 ± 26	168 ± 24	-45 ± 36	-8 ± 8
Total	179 <sup>C**, G**</sup> ± 25	170 <sup>C**, G***</sup> ± 23	-45 <sup>C***, G***</sup> ± 34	-5 <sup>C***, G*, T***</sup> ± 9

\*p<0.05, \*\*p<0.01, \*\*\* p<0.001. C: configuration, G: group of subjects, T: Type of configuration

The resultant pedal force varied from 166N to 184N on average depending on pedal configuration. A strong effect of the pedal configuration on the pedal force resultant and its components was found. BMW4 had the lowest force resultant, whereas REN3 had the highest force resultant. The same observation can be made for the tangential component, which is the only component useful for moving the pedal. However, no significant effect of the type of configuration was observed on pedal force. Between imposed and less constrained configurations, the difference in the force resultant was only 4 N on average.

A strong effect of the group was also found, especially on the tangential and normal components. Indeed, the mean values of the normal and tangential components were respectively higher for younger subjects and older ones. Though older and younger subjects had quite similar the tangential force - displacement curves, the older participants tended to apply more force at the end of the depression (Figure 27). Moreover, the verticality of the curves of older subjects at the end of travel may suggest that the older subjects continued to increase the force applied on the pedal whereas it reached at its travel's end. For the normal component, the patterns of the curves are also quite similar between older and younger subjects (Figure 28). But the younger subjects had on average a higher the normal force component than the older subjects except for BMW2. The normal component increased quickly during the last third of the clutch pedal travel.

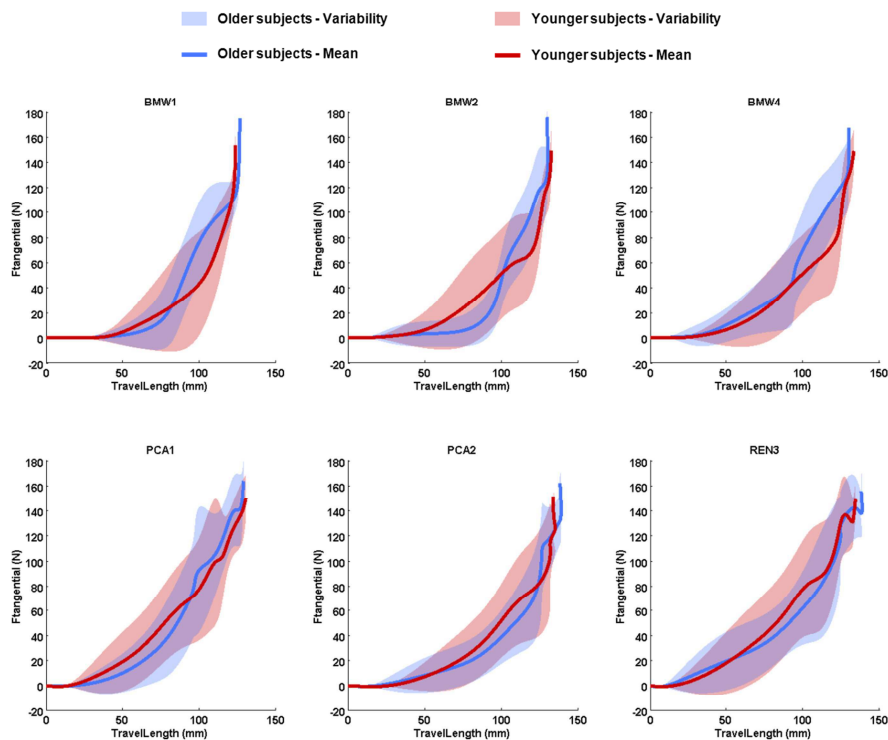


Figure 27: Mean tangential force according to mean travel length for older and younger subjects for each configuration. The variability was defined as the mean tangential force  $\pm$  tangential force standard deviation for older and younger subjects at each displacement of the pedal on its trajectory.

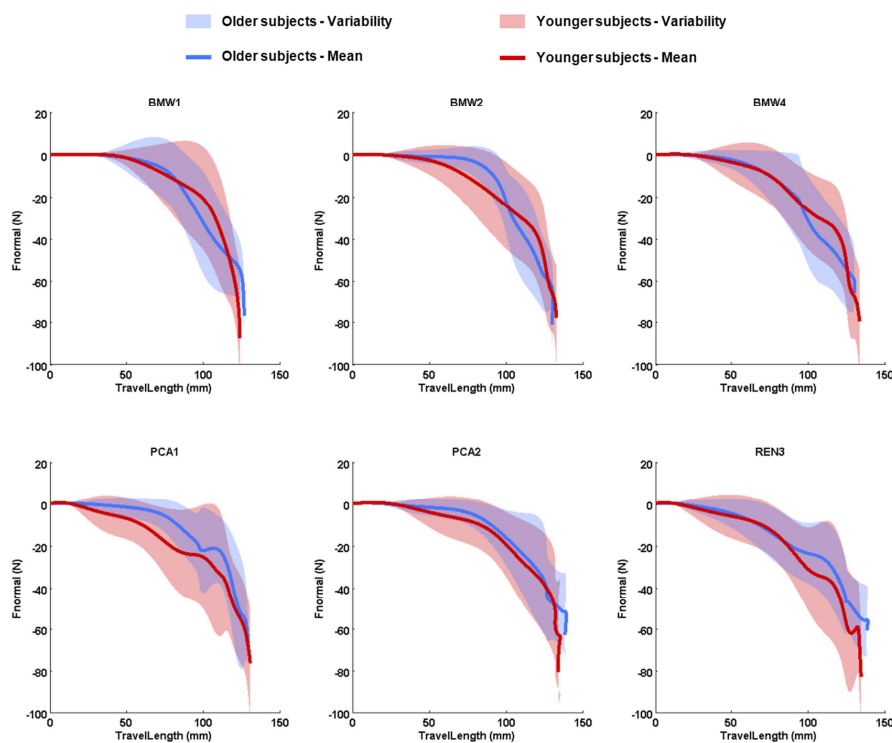


Figure 28: Mean normal force according to mean travel length for older and younger subjects for each configuration. The variability was defined as the mean tangential force  $\pm$  tangential force standard deviation for older and younger subjects at each displacement of the pedal on its trajectory.

#### 4.2.ii Pedal force direction

The force direction was analyzed at the end of pedal depression with respect to the direction from the hip joint center to the foot force application point on pedal. The force application point was approximated as the center of the pedal surface. First, the analysis of the force direction was made in the XZ plane of the mock-up reference frame. The angle was calculated using the scalar product of pedal force  $\vec{F}$  or  $\vec{F}'$  and the hip-foot force application point axis direction. The sign of the angle was attributed according to the counter-clockwise convention (Figure 29a). In the following section, the calculated angle was named  $\theta_{F_{Exp}}$  and the reference axis Hip-P<sub>App</sub>. Second, the effect of the lateral component on the pedal force direction was investigated in the XY plane of the mock-up reference frame. The deviation angles of the pedal force and the Hip-P<sub>App</sub> axis with respect to the x-axis, respectively  $\delta_{F_{Exp}}$  and  $\delta_{Hip/P_{App}}$ , were estimated (Figure 29b and Figure 29c).

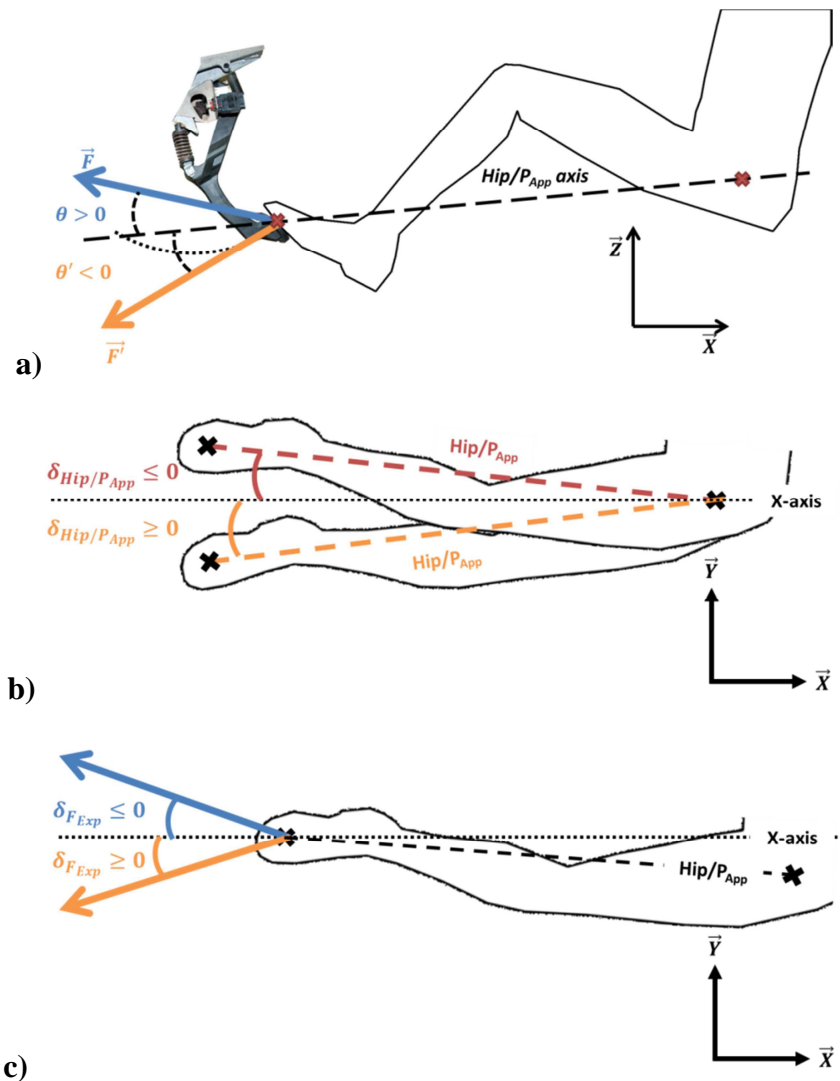


Figure 29: Definition of the angles used for the pedal direction analysis. a)  $\theta_{F_{Exp}}$ , angle between clutch pedal force and the Hip/P<sub>App</sub> axis in the XZ plane. b)  $\delta_{Hip/P_{App}}$ , deviation angle of the Hip-P<sub>App</sub> axis with respect to the x-axis in the XY plane. c)  $\delta_{F_{Exp}}$ , deviation angle of the pedal force with respect to the x-axis in the XY plane.

On average,  $\theta_{F_{Exp}}$  was  $-5.6^\circ$  (Table 11). As for the force resultant and components, it was affected by pedal configuration and group of subjects. About the pedal configurations, BMW4 had the force direction with the largest angle compared to Hip-P<sub>App</sub> axis with  $-9^\circ$  for mean value and REN3 had the narrowest angle with  $-1.6^\circ$  for mean value. It can also be observed that BMW1, BMW2 and PCA2 had close mean values of  $\theta_{F_{Exp}}$ , i.e. respectively  $-5.2^\circ$ ,  $-5.5^\circ$  and  $6.8^\circ$ . About the group of subjects, it can be noted that the older female had a mean value of  $\theta_{F_{Exp}}$  superior to 0. Globally, the younger subjects had largest mean angle than the older subjects, i.e.  $-6.1^\circ$  and  $-11.4^\circ$  for younger females and males versus  $0.8^\circ$  and  $-2.70$  for older ones.

Table 11: Means and standard deviations of  $\theta_{F_{Exp}}$ ,  $\delta_{F_{Exp}}$  and  $\delta_{Hip/P_{App}}$ .

	$\theta_{F_{Exp}}$ (deg)	$\delta_{F_{Exp}}$ (deg)	$\delta_{Hip/P_{App}}$ (deg)
Older Female	$0.8 \pm 8$	$2.4 \pm 2.6$	$-0.1 \pm 1.3$
Older Male	$-2.7 \pm 6.3$	$1 \pm 2.8$	$0.1 \pm 1.5$
Younger Female	$-6.1 \pm 8.1$	$1.7 \pm 2.9$	$-0.3 \pm 1.2$
Younger Male	$-11.4 \pm 8.5$	$1.6 \pm 3.9$	$-0.6 \pm 1.1$
BMW1	$-5.2 \pm 9.1$	$0 \pm 3.1$	$-1.3 \pm 1.5$
BMW2	$-5.5 \pm 6.7$	$2.1 \pm 2.3$	$0.4 \pm 0.9$
BMW4	$-9 \pm 7$	$1.6 \pm 2.3$	$0.5 \pm 0.9$
PCA1	$-3 \pm 10.1$	$4.2 \pm 4.5$	$-0.3 \pm 1.3$
PCA2	$-6.8 \pm 9.2$	$0.8 \pm 2.6$	$-0.2 \pm 1.1$
REN3	$-1.6 \pm 7.3$	$2.5 \pm 2.6$	$-0.7 \pm 1.4$
Imposed	$-6.1 \pm 8.4$	$0.6 \pm 3.3$	$-0.7 \pm 1.3$
Less Constrained	$-5.1 \pm 9.2$	$2.5 \pm 2.7$	$0.2 \pm 1.2$
Total	$-5.6^{C***, C***} \pm 8.8$	$1.6 \pm 3.1^{G*, C***, T***}$	$-0.2 \pm 1.3^{G*, C***, T***}$

\*p<0.05, \*\*p<0.01, \*\*\* p<0.001. C: configuration, G: group of subjects, T: type of configuration

About the lateral deviation, the configuration and the type of configuration had strong effects on  $\delta_{F_{Exp}}$  and  $\delta_{Hip/P_{App}}$ . The effect of the group of subjects was found weak. The Hip-P<sub>App</sub> axis with a mean lateral deviation of  $-0.2^\circ$  was close to be parallel to the x-axis and slightly directed rightward in the driver's point-of-view. On the contrary, the pedal force with a mean value of  $\delta_{F_{Exp}}$  of  $1.6^\circ$  was directed leftward on average. Interestingly, it can be noticed that the gap between the pedal force direction and the x-axis increased significantly with the less-constrained (from  $0.6^\circ$  to  $2.5^\circ$  on average) and that the lateral deviation of the Hip-P<sub>App</sub> axis changed from a rightward direction for imposed configurations ( $-0.7^\circ$  on average) to a leftward direction for less-constrained configurations ( $0.2^\circ$  on average). Finally, about the pedal configuration, the average values of  $\delta_{Hip/P_{App}}$  showed that the Hip-P<sub>App</sub> axis was oriented leftward for BMW2 and BMW4, respectively  $0.4^\circ$  and  $0.5^\circ$ , whereas it was oriented rightward for the other pedal configurations.

### 4.2.iii Joint torque analysis

Joint torques were projected onto the rotation axes of their respective joint. As for the inverse kinematics method, the orientations of the joint axes used were from RAMSIS™ kinematic model (see in Appendix). The joint torques were analyzed only at the end of pedal depression. As the contact forces between the thigh and the seat were not estimated, the hip joint torques were not considered. Only the joint torques on the flexion/extension axes were investigated because the clutch pedal operation was considered as a mainly flexion/extension operation. Knee and ankle flexion/extension torques were significantly affected by pedal configuration and group of subjects but not by configuration type (Table 12).

Table 12: Means and standard deviations of knee and ankle flexion/extension joint torque ([+] flexion and [-] extension)

	Knee (Nm)	Ankle (Nm)
Older Female	-24.5 ± 12.9	-8.9 ± 5.1
Older Male	-28.7 ± 11.1	-12.1 ± 4.6
Younger Female	-13.1 ± 11.7	-8.7 ± 5.6
Younger Male	-12.8 ± 9.1	-14.8 ± 5.3
BMW1	-18 ± 13	-13.3 ± 6
BMW2	-17.1 ± 9.6	-12.4 ± 5.1
BMW4	-12 ± 11.4	-12.5 ± 3.6
PCA1	-25.4 ± 14	-7.4 ± 5.7
PCA2	-17.6 ± 13	-12.2 ± 5.6
REN3	-27.4 ± 12.2	-9 ± 6
Imposed	-19 ± 12.9	-12 ± 5.2
Less Constrained	-19.2 ± 13.4	-10.8 ± 6.2
Total	-19.1 <sup>G***, C***</sup> ± 13.1	-11.4 <sup>G***, C***</sup> ± 5.7

\*p<0.05, \*\*p<0.01, \*\*\* p<0.001. C: configuration, G: group of subjects

BMW4 had the lowest joint torque average value, i.e. -12 Nm for knee. PCA1 and REN3 had the highest knee joint torque mean values, -25.4 Nm and -27.4 Nm. BMW1, BMW2 and PCA2 knee joint torque average values between -17 Nm and -18 Nm. About the ankle joint torques, it can be noticed that the two configurations with higher knee moments, i.e. PCA1 and REN3, are the ones with lower mean ankle moments, respectively -7.4 Nm and -9 Nm. The other configurations have quite the same mean value of moment, i.e. between -12 and -13 Nm.

As for the foot force on pedal, a strong effect of the group of subjects was found. Old subjects had higher knee torques than the young ones whereas for ankle, it was female subjects that had lower joint torques than the males.

## 5 Discussion

The main conclusions of the discomfort perception and motion analysis of the clutch pedal operation can be summarized as:

- Lower discomfort ratings were obtained for less constrained configurations,
- A clutch pedal position further away from the seat, lower and more on the left, from driver's point of view, was usually preferred,
- Freely adjusted pedal position improved the beginning of the clutch pedal operation at the expense of the end,
- Free pedal position adjustment led to a decrease of the flexion of the lower limb joints at the beginning and an increase of the extension of these joints at the end of the pedal depression, especially for the ankle,
- The pedal resistance perception was highly dependent on pedal configuration and correlated with discomfort ratings.
- The foot force on pedal and the joint torques were highly dependent on the pedal configuration,
- The group of subjects had significant effects on the foot force on pedal and on the knee torques.

The analysis of the discomfort ratings showed that discomfort was decreased by adjusting the position of the clutch pedal. However, the results should be interpreted with caution. Indeed the average difference in raw CP50 scores between imposed and less constrained configurations was 5.1, whereas the reproducibility in rating score was 6.8.

### 5.1 Pedal position adjustment and discomfort perception

The analysis of the clutch pedal position adjustments showed on average that the subjects moved the pedal further away from the seat and also lowered it for the less-constrained configurations. The pedal adjustment led to a decrease in the flexion of the hip, knee and ankle joints at the beginning and an increase of the extension of these joints at the end of the pedal depression as the travel length was kept unchanged. The difference in the joint flexion extension angle between freely adjusted and imposed configurations was the highest for the ankle. Compared to the joint ROM values collected, the ankle angle was very close to its dorsiflexion limit at the beginning of pedal depression (Table 13) for the imposed configurations.

Table 13: Means and standard deviations of range of motion (ROM) in flexion/extension (hip, knee and ankle)

			All subjects
ROM (deg)	Hip	Extension	$-15 \pm 10$
		Flexion	$87 \pm 14$
	Knee	Extension	$12 \pm 7$
		Flexion	$130 \pm 8$
	Ankle	Plantarflexion	$46 \pm 8$
		Dorsiflexion	$122 \pm 5$

The subjects might adjust the pedal position so as to reduce the ankle dorsiflexion angle away from its limit when depressing the pedal. This may explain the decrease in discomfort rating for preferred pedal configurations. Hip abduction was also increased at the beginning and the end of pedal depression, which is related to lateral adjustment of pedal position. There may be two explanations. It could be explained by the minimisation of the distance from rest position to the pedal at the beginning of the depression, according to the hypothesis of minimum work suggested by Wang et al. (2004). Another explanation could be that the participants may have preferred a pedal aligned with the hip in the plane passing through left hip centre and parallel to sagittal plane. Indeed, it was found that the transversal component of the pedal force was oriented leftward in driver's point of view in the plane XY of the mock-up reference frame. Therefore, it could suggest that the pedal lateral adjustments were made in order to align the pedal force direction and the Hip-P<sub>App</sub> axis in the XY plane. However the data suggested that the gap between pedal force direction and the Hip-P<sub>App</sub> axis in the XY plane increased with the pedal adjustments, from 1.3° to 2.3°. Besides it was found that the absolute value of the transversal component increased on average from imposed to less-constrained configuration. But the data also showed that the orientation of the Hip-P<sub>App</sub> axis changed from a rightward direction for imposed configurations to a leftward direction for less-constrained configurations. As a consequence, the lateral pedal adjustments may due to a preference of the subjects to have a leftward deviation of the pedal force.

## 5.2 Pedal force control and discomfort perception

It was observed that pedal configuration had strong effects on clutch pedal force (resultant, components and direction) and joint torques (knee and ankle). From the analysis of the discomfort perception, it was found pedal configuration had also strong effects on pedal resistance perception and discomfort ratings. Besides, a strong effect of the perceived pedal resistance on the discomfort ratings was found. Therefore the correlations between clutch

pedal tangential and normal forces, pedal force direction, joint torques (knee and ankle) and the CP50 raw scores were investigated (Table 14).

**Table 14: Coefficients of correlation between CP50 raw scores, normal and tangential pedal forces, pedal force direction in the XZ plane ( $\theta_{F_{Exp}}$ ) and knee and ankle joint torques.**

	Normal force	Tangential Force	$\theta_{F_{Exp}}$	Knee torque	Ankle torque	CP50 raw scores
Normal force	1	<b>-0.1327*</b>	<b>0.8286***</b>	<b>-0.7848***</b>	<b>0.7137***</b>	0.0723
Tangential force		1	0.093	<b>-0.236***</b>	<b>-0.2493***</b>	-0.0611
$\theta_{F_{Exp}}$			1	<b>-0.8364***</b>	<b>0.6541***</b>	-0.0062
Knee torque				1	<b>-0.5564***</b>	<b>-0.1489*</b>
Ankle torque					1	<b>0.1205*</b>
CP50 raw scores						1

\*p<0.05, \*\*p<0.01, \*\*\* p<0.001.

It can be observed that only the joint torques were significantly correlated with the discomfort ratings but the correlation was also weak. This observation is in agreement with Wang et al. (2004) who had also found correlation between discomfort ratings and joint torques, especially knee torques. Interestingly, the correlations of knee and ankle torques with the CP50 scores were opposite. This was expected because geometrically, in order to decrease the pedal force lever arm on the knee joint, the one on the ankle joint need to be increased. This explains also the negative correlation coefficient between knee and ankle torque. Moreover, it can be noted that considering the correlation coefficient, the knee torque decreased when the discomfort ratings increased. Because knee torques were negative, it means that higher discomfort was perceived with higher knee torque in absolute. Indeed, BMW4 configuration was the least uncomfortable pedal configuration according to discomfort questionnaire and also had the lowest mean knee torque value, i.e. -12 Nm; whereas PCA1 and REN3 were the most uncomfortable pedal configurations and had the highest mean knee torques, i.e. respectively -25.4 Nm and -27.4 Nm. On the contrary, considering that ankle torques were also negative, higher perceived discomfort were correlated with lower ankle torques.

As expected, the knee torques were also significantly correlated with tangential and normal components of pedal force as well as the pedal force direction. Yet the correlation was especially strong with normal pedal force and pedal force direction. The strong correlation, 0.83, between pedal force direction and normal pedal force suggested that the pedal force direction and so the knee torque were controlled by the normal component of the pedal, which

is by definition non-useful to move the pedal on its trajectory. So, for each configuration, there may exist an optimal force direction that minimize joint torques, especially knee, and, as a consequence, minimize discomfort. The use of the normal component to decrease the knee torque may also explain the effect of the group of subjects on pedal force (resultant, tangential, normal and direction) and knee torques. Indeed, the analysis of the clutch pedal force showed that young subjects more have more solicited the normal component of the clutch pedal force than the elderly, about -50 Nm for the younger subjects and -30 Nm for the older one. As the consequence, the younger subjects had higher  $\theta_{F_{Exp}}$  angle than the older subjects, i.e.  $-6.1^\circ$  and  $-11.4^\circ$  for younger female and male versus  $0.8^\circ$  and  $-2.70$  for older female and male (Figure 30). And the resulting knee torques were lower for the younger subjects, i.e. about -13 Nm, than for the older ones, i.e. between -24 Nm and -29 Nm.

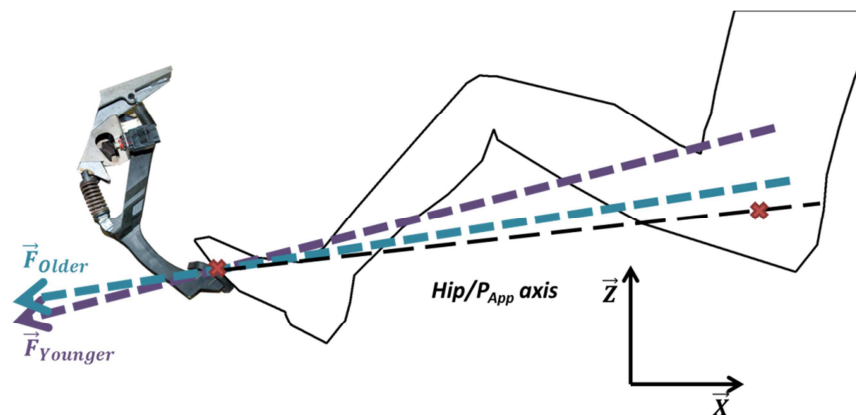


Figure 30: Pedal force direction for older ( $F_{Older}$ ) and younger ( $F_{Younger}$ ) subjects

### 5.3 Towards a proposal for defining objective discomfort indicators

The effects of free pedal adjustments on the discomfort perception and on the motion were analyzed and led to the conclusion that pedal position adjustment is an iterative trial-error process in which a subject generally carries out a large number of trials before finding a preferred pedal position and that this process may result from the principle of minimum work and minimum discomfort, in agreement with an earlier suggestion from Wang et al (2000). Indeed the pedal was positioned neither too high, thus avoiding unnecessary work raising the leg, nor too low, which helped to avoid an uncomfortably large ankle extension at the end of pedal travel. It was also adjusted to be neither too close, thus reducing ankle dorsiflexion, nor too far, avoiding too large a joint extension at the end of travel. Interestingly, the results of the present study seem to show that the comfort at the beginning of depression was more

privileged than the comfort at the end of travel. Moreover, the results also showed, in agreement with Wang et al (2004) that discomfort rating was strongly dependent on pedal resistance and that discomfort was significantly correlated to joint torques at the end of pedal depression, especially to the knee joint torque.

Taking all these observations into account, this section of the study aimed at using kinematic and dynamic parameters of leg depression movements for building discomfort indicators. Kinematic indicators are based on leg position during the task. Dynamic indicators represent the joint loads due to external force exertion.

### 5.3.i Discomfort indicators for clutch pedal operation

For the clutching task investigated in the current study, kinematic parameters could be three joint flexion extension angles at the beginning and end of depression. In order to consider lateral position adjustment, there could be several candidate parameters, such as hip abduction-adduction angle, the travel distance from the foot rest position to that at beginning of depression or the lateral position of the left foot at beginning of depression. Due to a small change of pedal lateral position, the variation of hip abduction/adduction angle between imposed and less-constrained configurations was very small. As the foot position on the foot rest before depression was not strictly controlled, a part of variability could be introduced to any parameters that are dependent on foot rest position. Therefore, the foot lateral position was used here for constructing a discomfort indicator. The following discomfort indicators are therefore proposed from the suggested kinematic and dynamic parameters:

- Seven kinematic indicators:
  - Two hip flexion angles (IndHipStart and IndHipEnd) respectively at the start and end depression,
  - Two knee flexion angles (IndKneeStart and IndKneeEnd)
  - Two ankle flexion angles (IndAnkleStart and IndAnkleEnd),
  - The left foot position which is characterized by the ball of foot lateral position ( $y_{BoF}$ ) at the beginning of the depression normalized by half of the subject's pelvis width (IndLPos). Pelvis width is defined as the distance between the two iliac crests:

$$IndLPos = \left| 1 - \frac{|y_{BoF}|}{0.5 * Width_{pelvis}} \right|$$

- Two dynamic indicators:

- Knee torques at the end of depression normalized for each subject by their maximum knee strength (IndKneeJT),
- Ankle torques at the end of depression normalized for each subject by their maximum ankle strength (IndAnkleJT),

The kinematic discomfort indicators based on joint angles were defined using joint angle related discomfort functions similar to those by Kee and Karwowski (2002) and by Cruse et al. (1990) (Figure 31 for the ankle and in Appendix for hip and knee). Based on the joint limits either measured in the current experiment or from literature (e.g. Chaffin et al., 1999; Kapandji, 1994), the suggested cost functions, varying from 0 to 1, are characterized by 3 zones: the zero discomfort zone, the transition zone and the full discomfort zone. The zero discomfort zones were based on the review of preferred driving postures by Wang and Bullock (2004). The full discomfort zones were defined for a joint angle value beyond joint limits collected in the DHErgo experiment during the subject's characterization trials (see in Appendix). The transition zone is a linear transition between zero and full discomfort zones.

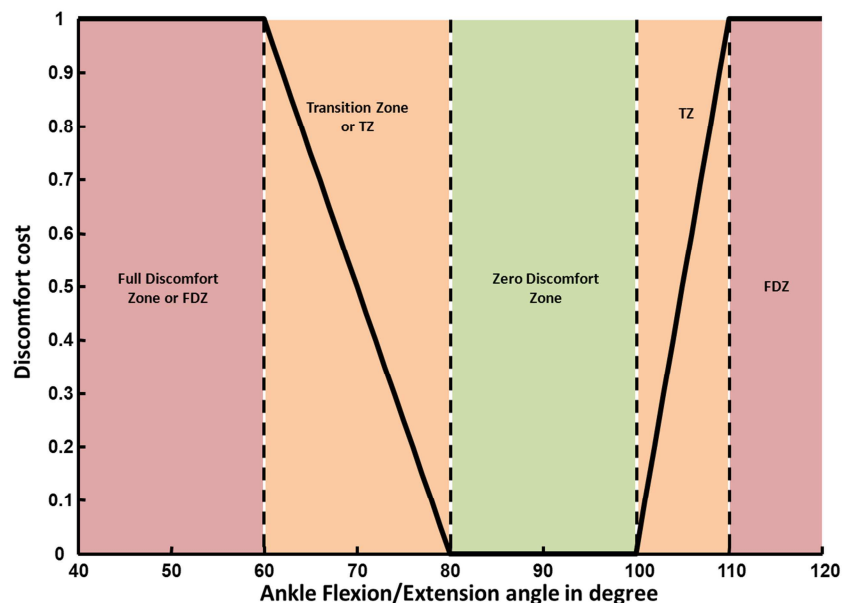


Figure 31: Discomfort cost function for ankle flexion/extension angle

Then the indicator IndLPoS was defined as a V-function with zero discomfort at the half of pelvis width. Pelvis width was defined as the distance between the iliac crests and was provided for each subject by the anthropometric measurements. Nevertheless, it should be noted that in practice, the lateral clutch pedal position is restricted by the brake pedal at the

right and the doorframe at the left. Finally knee and ankle flexion/extension torques were standardized using the maximum voluntary isometric joint torque values of each subject. Only knee and ankle dynamic indicators were considered because the contact forces between thigh and seat were not considered in the motion reconstruction of the clutch pedal operation. As a consequence, dynamic indicator was not estimated for hip.

Among the proposed indicators, IndHipEnd, IndKneeEnd, IndAnkleStart and IndKneeJT were significantly correlated with raw CP50 scores, and IndLPos with the centred CP50 scores (Table 15). IndHipEnd, IndKneeEnd, IndAnkleStart and IndKneeJT as the raw CP50 scores depend on the subject's characteristics (anthropometry, physical capacity, perception ...), whereas IndLPos and centred CP50 scores do not. This may explain the correlation with either the raw or the centred CP50 scores. Note the negative correlations with IndHipEnd and IndKneeEnd. This is expected as the less-constrained configurations caused an increase in lower limb joint extension at the end of depression, and thus an increase in discomfort according to the cost functions. IndHipEnd, IndKneeEnd, IndAnkleStart and IndKneeJT are significantly correlated each other.

**Table 15: Table of coefficients of correlation between CP50 raw scores, CP50 centered scores and the proposed discomfort indicators. The significant coefficients of correlation (i.e. p-value < 0.05) are noted in red.**

	Ind HipStart	Ind HipEnd	Ind KneeStart	Ind KneeEnd	Ind AnkleStart	Ind AnkleEnd	Ind KneeJT	Ind AnkleJT	Ind LPos	CP50 Raw	CP50 Cent.
IndHipStart	1,000	<b>0,872</b>	<b>0,235</b>	<b>0,277</b>	0,088	<b>0,305</b>	-0,012	<b>-0,354</b>	0,086	-0,038	0,090
IndHipEnd		1,000	<b>0,249</b>	<b>0,456</b>	<b>-0,204</b>	<b>0,393</b>	<b>-0,223</b>	<b>-0,296</b>	<b>0,145</b>	<b>-0,222</b>	0,029
IndKneeStart			1,000	<b>0,725</b>	-0,084	<b>0,589</b>	-0,123	<b>-0,411</b>	0,004	-0,046	-0,029
IndKneeEnd				1,000	<b>-0,290</b>	<b>0,641</b>	<b>-0,229</b>	<b>-0,344</b>	0,019	<b>-0,258</b>	-0,091
IndAnkleStart					1,000	<b>-0,402</b>	<b>0,249</b>	0,045	-0,112	<b>0,281</b>	0,058
IndAnkleEnd						1,000	<b>-0,127</b>	<b>-0,601</b>	0,083	-0,064	-0,025
IndKneeJT							1,000	-0,080	0,004	<b>0,215</b>	0,079
IndAnkleJT								1,000	<b>-0,137</b>	-0,115	-0,060
IndLPos									1,000	0,063	<b>0,204</b>
CP50 Raw										1,000	<b>0,809</b>
CP50 Cent.											1,000

Figure 32 shows the mean and standard deviation values of four selected indicators and the normalized discomfort for imposed and less-constrained configurations of BMW4, PCA2 and REN3. It can be noticed that discomfort predicted by IndKneeJT and IndLPos agree quite well with the perceived discomfort when comparing the three configurations BMW4, PCA2 and REN3. IndAnkleStart, IndLPos and IndKneeEnd give a good indication of pedal assessment when comparing imposed and less-constrained configurations. InAnkleStart and

IndKneeEnd show especially the preference of the subjects to improve the beginning of the pedal depression at the expense of the end in the case of less-constrained configurations.

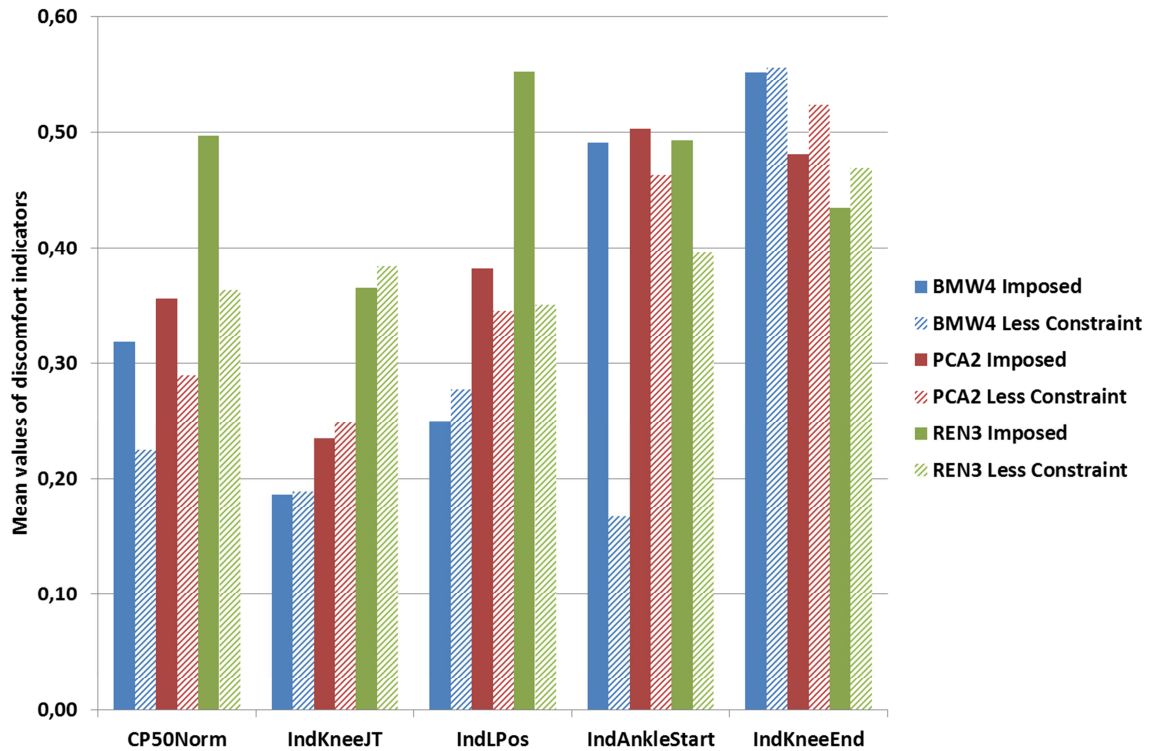


Figure 32: Comparison between imposed and less constraint configurations of BMW4, PCA2 and REN3 using discomfort indicators. CP50Norm indicates normalized CP50 scores, varying from 0 to 1.

### 5.3.ii Discomfort indicators and discomfort modelling

The open issue is how to combine the proposed indicators to meet the design engineers expectations (see in Appendix for more details). A linear regression was performed on the CP50 raw scores using the discomfort indicators. A regression model selection procedure was carried out to evaluate the behaviour of the fitted model according to the number of indicators considered. The model was found statistically significant although its adjusted  $R^2$  was weak. Five from the seven considered indicators had significant effects on the regression: IndHipStart, IndHipEnd, IndKneeEnd, IndAnkleStart and IndAnkleJT. The equation of the model was:

$$\begin{aligned}
 \text{CP50 raw score} = & 25.2 + 26 * \text{IndHipStart} - 27.2 * \text{IndHipEnd} \\
 & -9.0 * \text{IndKneeEnd} + 3.3 * \text{IndAnkleStart} + 1.8 * \text{IndAnkleEnd} \\
 & -13.7 * \text{IndAnkleJT} + 5.2 * \text{IndLPos}
 \end{aligned}$$

## 6 Limitations

There are several limitations of the present approach that can be pointed out.

Firstly, defining objective discomfort indicators from biomechanical parameters is very challenging. Many biomechanical parameters can be considered. In this study, relevant parameters were selected by comparing imposed and less-constrained configurations. As only the pedal position could be adjusted for less-constrained configurations, the proposed discomfort indicators may not be applicable to other situations where other pedal design parameters are adjustable. However, we believe that the proposed approach could be used for identifying relevant discomfort criteria.

Secondly, individual discomfort indicators which allowed the assessment of the pedal starting and end positions as well as its resistance as well as two approaches on how to combine these indicators were proposed. About the discomfort model the linear regression based on CP50 scores had poor results. This may be explained by the poor reproducibility of the subject's ratings using the CP50 scale. Besides, each subject may not use the same interval of the CP50 scale to estimate a similar discomfort perception. Actually, how to combine these indicators into one global discomfort indicator requires deep expertise in product design. These indicators could provide objective elements for an expert to form a global assessment of different design solutions. But global ratings and the proposed indicators are not opposed to each other and should be considered as complementary tools for the ergonomic assessment of products.

Thirdly, the proposed discomfort indicators are based on kinematic and dynamic parameters of a movement under investigation, implying that motion simulation should be experimentally validated. The definition of dynamic and kinematic indicators is quite generic. However, the definition of the dynamic indicators could be an issue. Indeed, their definition is based on the knowledge of maximum isometric joint torque and these types of data are hard to get. Some data exist in the literature but the variability of joint strength according to age, gender, anthropometry or posture is unknown. Currently, the most reliable way to get these data is experimentally. Therefore, the integration of such discomfort modelling in DHM is difficult.

Finally, by definition, clutch pedal depression is not a very uncomfortable task. Discomfort would be caused rather by the long repetition of clutching movements, in a traffic jam or during an urban journey. Under the current experimental conditions, subjects were asked to assess a pedal configuration without any real task associated. Only the discomfort related to

the clutching movement was investigated, not the task associated with the movement. More realistic experimental conditions should be encouraged in future.

## 7 Conclusion

By comparing six existing pedal configurations and corresponding freely adjusted ones, results showed that pedal position was adjusted in all three directions to ensure a good starting pedal position at expense of its end position. Low joint torque at the end of depression was associated with the tested pedal configurations with a low discomfort rating, confirming earlier findings by Wang et al (2004) that the pedal resistance is a dominant factor in discomfort evaluation of the automotive clutch pedal. By comparing the movements of the imposed and freely adjusted pedal configurations, relevant biomechanical parameters were identified for proposing 9 discomfort indicators.

The present work illustrates that the less-constrained motion concept was useful for identifying motion-related biomechanical discomfort indicators. The method presented in this study lies within the scope of industrial needs for product design assessment. The proposed discomfort indicators provide objective information helpful for design engineers to compare alternative designs.

Finally, the study confirmed the importance to take into account the dynamic parameters (joint torques, muscle forces ...) of a motion for discomfort assessment. the proposed discomfort indicators are based on kinematic and dynamic parameters of a movement under investigation, implying that motion simulation should take into account kinematic and dynamic constraints and should also be experimentally validated when using a DHM..

## 8 Appendix

### 8.1 Selection of the test clutch pedal configurations

A principal components analysis is done to define a plan of comparison of the different configurations in order to select a space of experimentation. For this case study of DHErgo project, end-users provided 11 clutch pedal configurations: 5 by BMW (BMW1 to BMW5), 3 by PSA Peugeot Citroën (PCA1 to PCA2) and 3 by Renault (REN1 to REN3) (Table 16). According to the study of Wang et al (2000), 6 parameters have been considered important to configure a clutch pedal:

- Seat height or H30
- Clutch pedal travel length
- Clutch pedal travel angle
- Clutch pedal initial position (x-, y- and z-coordinates)

**Table 16: Eleven initial clutch pedal configurations provided by end-users in DHErgo project for the first case study.**

	Seat Height (mm)	Travel Length (mm)	Travel Angle (in degree)	Clutch pedal initial position		
				CPx (mm)	CPy (mm)	CPz (mm)
BMW1	256	131	0	-814.5	-60	-69
BMW2	247	163	0	-831	-110	-64
BMW3	314	151	8	-777	-120	-136
BMW4	174	149	0	-816	-120	17
BMW5	253	150	0	-816	-100	-77
PCA1	355	161	23	-770	-70	-199
PCA2	272	157	8	-766	-80	-130
PCA3	254	158	15	-799	-90	-96
REN1	240	139	8	-799	-70	-68
REN2	300	139	8	-776	-70	-140
REN3	360	137	15	-761	-70	-218
All	275 ± 54	149 ± 11	8 ± 7.5	793 ± 24	-87 ± 22	-107 ± 67

First the correlation matrix of the design parameters was calculated. The R coefficient of Bravais Pearson was used (Table 17). This coefficient considers two parameters as correlated if its value is superior to 0.6.

Table 17: Correlation matrix of the clutch pedal parameters

	Seat Height	CPTravelLength	CPTravelAngle	CPx	CPy	CPz
SeatHeight	1.000	-0.015	0.728	0.775	0.433	-0.981
CPTravelLength		1.000	0.227	-0.059	-0.504	-0.014
CPTravelAngle			1.000	0.733	0.409	-0.778
CPx				1.000	0.400	-0.843
CPy					1.000	-0.481
CPz						1.000

The analysis was therefore performed on the three less correlated pedal design parameters (seat height, travel length and clutch pedal initial position y-coordinate) and the travel angle parameter was also kept. This decision was made because this parameter is usually considered as one of the main pedal design parameters by the end-users. The principal components analysis showed that more than 85% variance of 11 configurations can be explained by the 2 main principal components:

	1 <sup>st</sup> component	2 <sup>nd</sup> component	3 <sup>rd</sup> component	4 <sup>th</sup> component
% of variance	51.9	34.5	9.1	4.5

The projection of the clutch pedal configurations in the plane defined by the 1st and the 2nd principal components showed that the area of experiment could be reduced to 6 configurations: BMW1, BMW2, BMW4, PCA1 and REN3 as border configurations; PCA2 as central configuration (Figure 33).

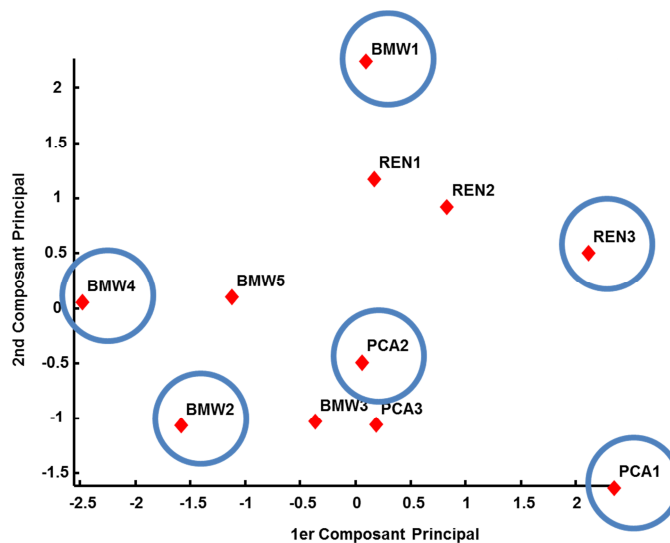


Figure 33: Projection of the eleven clutch pedal configuration in the plane defined the 1st and the second principal components. The selected configurations are circled in blue.

## 8.2 Measurement chain for DHErgo experiment

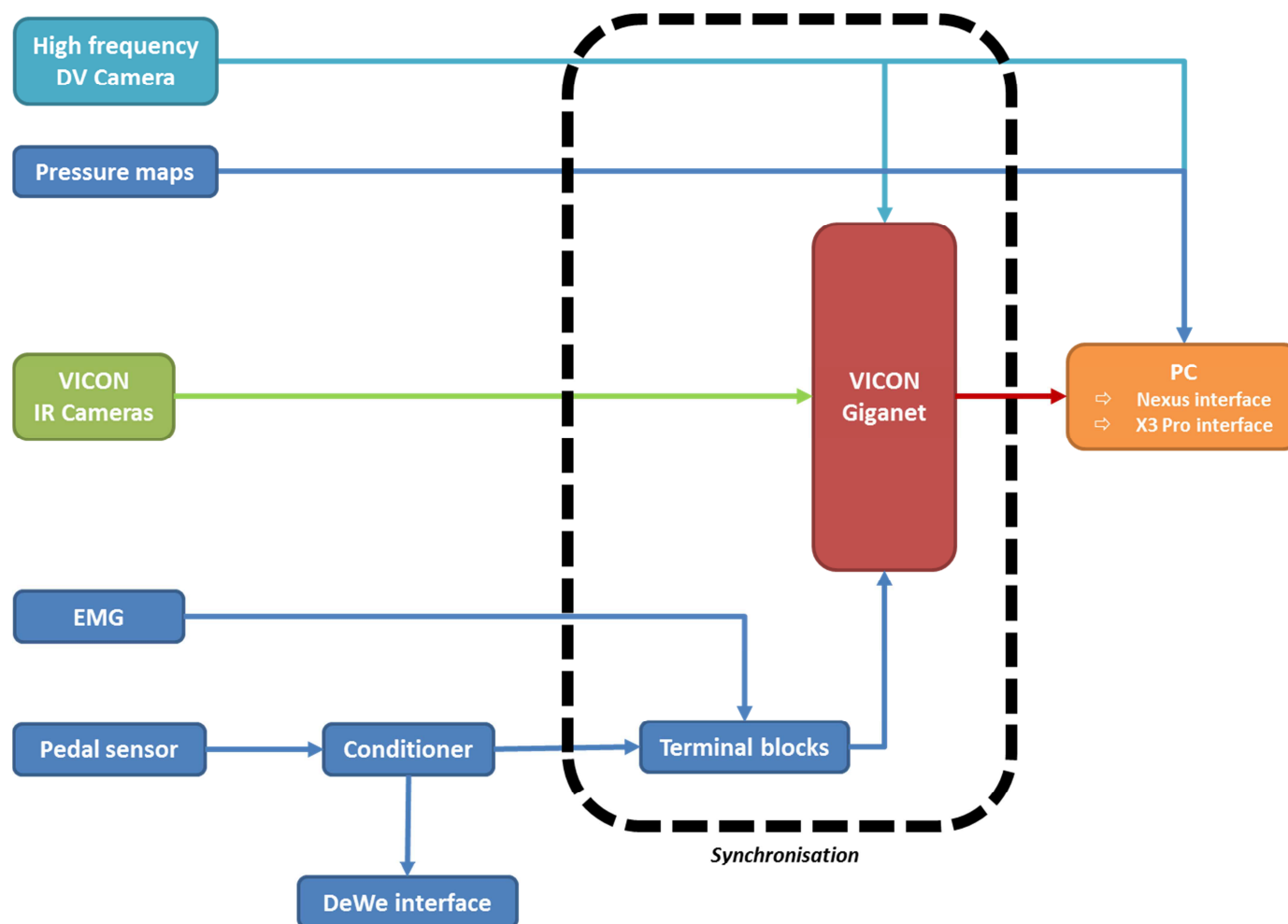
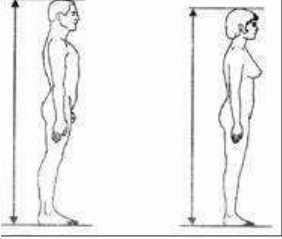
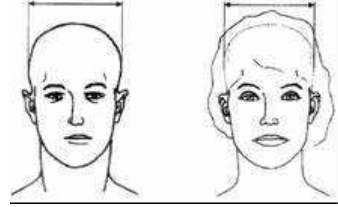
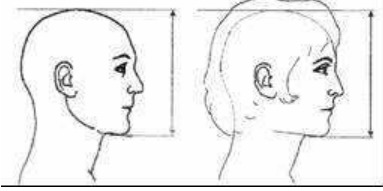
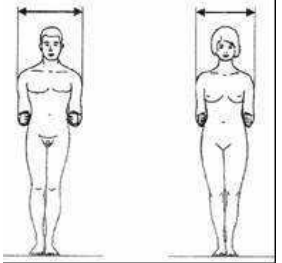
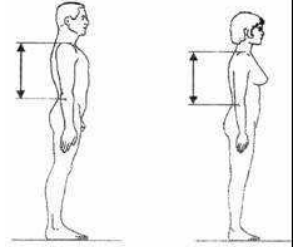
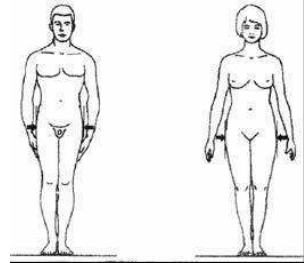
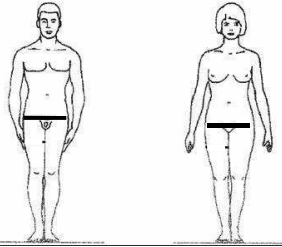
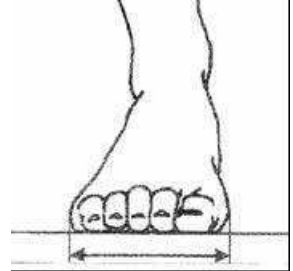
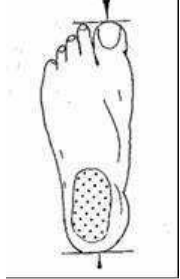
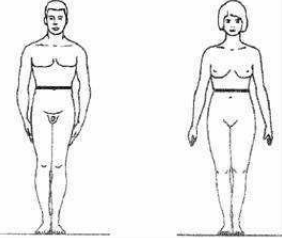
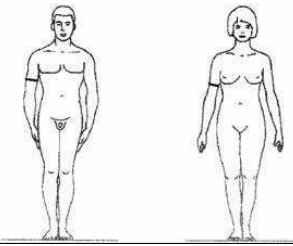
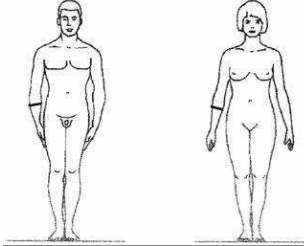
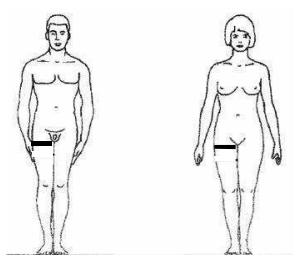


Figure 34: Measurement chain for DHErgo experiment.

8.3 Anthropometric measurements

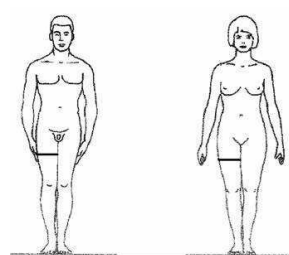
<p>M1</p>  <p>Stature</p>	<p>M2</p>  <p>Head width</p>	<p>M3</p>  <p>Head height</p>
<p>M4</p>  <p>Bideltoid shoulder width</p>	<p>M5</p>  <p>Upper arm length</p>	<p>M6</p>  <p>Maximum Hip width</p>
<p>M7</p>  <p>Circumference at hip level</p>	<p>M8</p>  <p>Foot breadth</p>	<p>M9</p>  <p>Foot length</p>
<p>M10</p>  <p>Minimum Waist circumference</p>	<p>M11</p>  <p>Maximum Upper arm circumference</p>	<p>M12</p>  <p>Maximum Forearm circumference</p>

M13



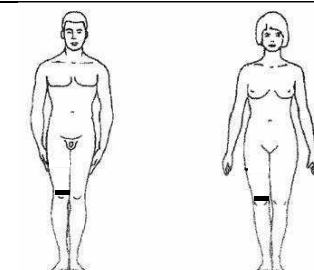
Section Upper Leg at Crotch Level

M14



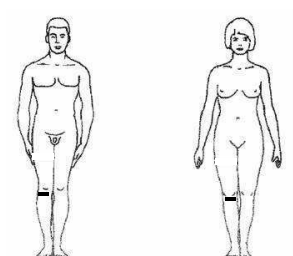
Maximum Thigh circumference

M15



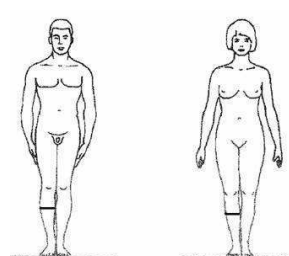
Inferior Section of Upper leg at Femoral condyles level

M16



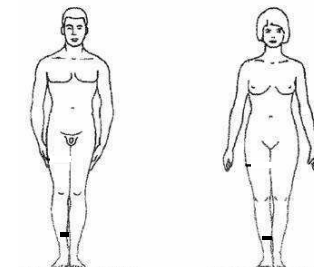
Superior Section for lower leg at frontal tuberosity of tibial proximal epiphysis

M17



Maximum Lower leg circumference

M18



Inferior Section for lower leg at tibial epiphysis tuberosity

M19



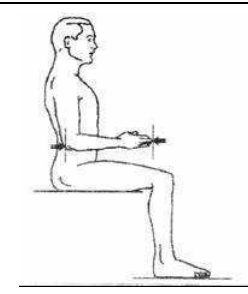
Sitting height

M20

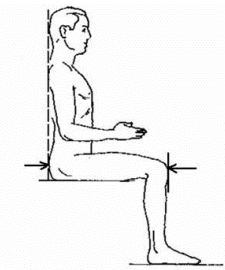
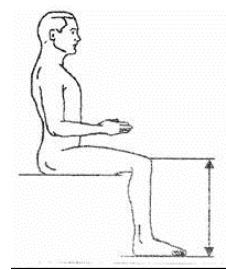
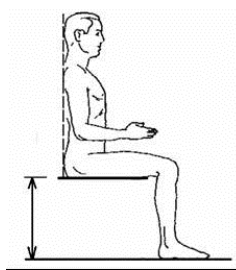
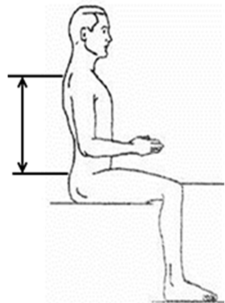
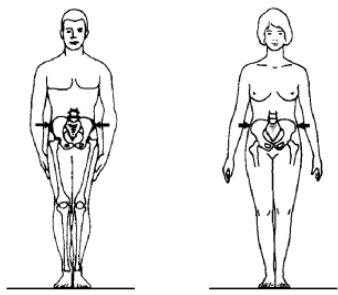
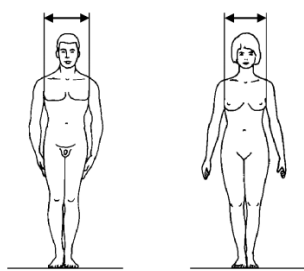
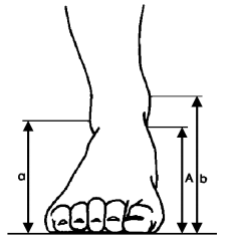
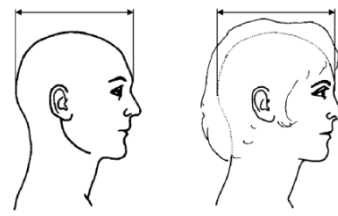


Chest depth

M21



Forearm length

M22		M23		M24	
	<b>Buttock-knee length</b>		<b>Knee height sitting</b>		<b>Seat height</b>
M25	<b>Weight</b>	M26	<b>Body fat %</b>	M27	<b>Skeletal Muscle %</b>
M28	<b>BMI</b>	M29	<b>Stature with shoes on</b>	M30	<b>Trunk height (calculated)</b>
M31		M32		M33	
	<b>C7 to Sacrum middle bony tip</b>		<b>Pelvis width</b>		<b>Chest width</b>
M34		M35			
	measure A to be measured <b>Foot height</b>		<b>Head length</b>		
M36	<b>Age</b>	M37	<b>Gender</b>	M38	<b>Foot breath with shoes</b>
M39	<b>Foot length with shoes</b>	M40	<b>Shoe size</b>		

## 8.4 Subjects' anthropometric dimensions for the DHErgo experiment

Subject	M1	M2	M3	M4	M5	M6	M7	M8	M9	M10	M11	M12	M13	M14	M15	M16	M17	M18	M19	M20	M21	M22	M23	M24
01_SD	1684	145	216	394	300	345	975	90	234	665	252	231	592	592	428	322	358	220	1276	196	446	591	500	394
02_LZ	1699	146	209	421	327	354	990	91	250	731	288	245	621	621	440	376	392	233	1303	203	448	613	512	395
03_FD	1813	148	233	478	349	362	1006	98	278	813	310	280	623	623	426	556	395	234	1413	201	502	595	523	426
04_VM	1639	149	216	421	298	364	1061	91	245	738	270	246	641	641	404	339	360	209	1264	221	429	607	489	392
05_SL	1756	147	232	437	340	297	871	94	255	697	272	252	516	516	346	302	325	202	1328	172	457	588	514	412
06_MR	1700	171	225	436	343	306	866	93	252	713	256	250	490	490	371	314	343	221	1270	210	478	590	498	395
07_YP	1775	147	225	467	358	362	1055	97	272	814	307	281	626	626	431	385	412	247	1372	208	480	617	522	412
08_ZS	1682	147	206	410	314	339	945	91	242	671	246	225	551	551	379	321	356	216	1283	200	436	571	495	385
09_HB	1823	163	224	479	349	340	1020	98	283	909	298	276	611	611	418	348	383	242	1391	229	501	509	537	445
10_VH	1632	150	205	409	291	334	958	89	234	728	283	248	625	625	425	359	386	242	1232	200	434	578	483	361
11_JF	1708	168	228	475	345	373	1039	101	262	938	291	276	583	583	450	368	376	238	1302	212	484	581	543	392
12_MC	1610	154	209	417	304	347	961	93	236	886	263	238	554	554	388	323	337	210	1211	230	448	585	495	399
13_AT	1730	156	229	442	348	342	1000	95	259	1032	306	273	572	572	396	352	363	235	1299	270	468	632	541	425
14_AF	1630	149	211	420	335	356	1019	89	243	777	282	245	609	609	421	345	348	216	1221	255	435	582	480	358
15_PP	1695	168	220	441	368	357	1000	100	262	1064	284	279	561	561	435	372	375	237	1268	280	472	628	555	430
16_ED	1530	159	219	423	285	335	1010	90	236	876	272	245	571	571	411	319	345	205	1165	290	412	538	446	335
17_AG	1743	166	212	500	369	372	1029	95	273	1019	309	286	581	581	415	352	401	245	1302	250	485	615	533	406
18_AC	1645	152	210	420	329	377	1085	88	232	932	268	240	612	612	438	351	358	224	1243	213	456	612	505	408
19_JL	1745	169	239	484	360	360	1032	96	262	996	319	294	578	578	423	372	406	249	1319	275	474	619	533	400
20_DN	1580	148	207	404	275	336	998	87	237	845	259	231	530	530	339	299	327	203	1195	210	417	534	470	355

 Young subjects

 Older subjects

Subject	M25	M26	M27	M28	M29	M30	M31	M32	M33	M34	M35	M36	M37	M38	M39	M40
01_SD	58.6	21.6	74.4	20.7	1705	882	674	278	264	81	189	30	FEMALE	91	258	39
02_LZ	64.8	25.8	70.5	22.5	1725	908	693	258	269	93	179	29	FEMALE	94	270	40
03_FD	80.3	17.3	78.6	24.4	1830	987	752	270	303	81	199	29	MALE	101	305	48
04_VM	63.7	30.6	65.8	23.7	1660	872	692	290	266	72	200	23	FEMALE	92	267	40
05_SL	58.3	9.4	85.9	18.9	1776	916	652	258	288	80	196	23	MALE	96	285	42
06_MR	55.6	8.5	86.9	19.2	1718	875	664	254	271	75	183	24	MALE	94	274	41
07_YP	79.3	16.0	79.8	25.2	1800	960	742	281	276	85	197	21	MALE	106	300	45
08_ZS	57.2	20.7	75.2	20.2	1700	898	707	271	262	81	189	21	FEMALE	91	269	40
09_HB	78.7	16.9	79.0	23.7	1850	946	733	307	313	96	206	34	MALE	103	305	45
10_VH	62.4	26.2	70.0	23.4	1650	871	662	283	270	84	199	22	FEMALE	90	259	39
11_JF	76.8	26.5	69.9	26.3	1730	910	706	311	320	93	199	72	MALE	103	289	43
12_MC	58.2	30.2	66.3	22.5	1630	812	663	293	269	74	187	66	FEMALE	91	267	40
13_AT	77.0	26.3	70.0	25.7	1752	874	682	326	300	92	188	78	MALE	99	287	43
14_AF	62.4	35.9	60.7	23.5	1647	863	693	296	266	80	184	67	FEMALE	90	269	40
15_PP	79.0	25.9	70.4	27.5	1715	838	685	340	301	99	195	76	MALE	103	287	43
16_ED	66.0	35.5	61.2	28.2	1550	830	660	318	290	85	195	68	FEMALE	95	257	39
17_AG	84.5	28.1	68.3	27.8	1768	896	713	329	349	72	194	67	MALE	99	296	44
18_AC	72.0	35.0	61.3	26.6	1670	835	650	296	297	86	185	72	FEMALE	94	261	40
19_JL	87.5	26.0	70.3	28.7	1770	919	732	309	331	92	207	66	MALE	100	286	43
20_DN	56.1	31.5	65.1	22.5	1600	840	638	305	268	85	176	69	FEMALE	92	258	39

Young subjects  
 Older subjects

## 8.5 Characterization data of each group of subjects in DHErgo experiment

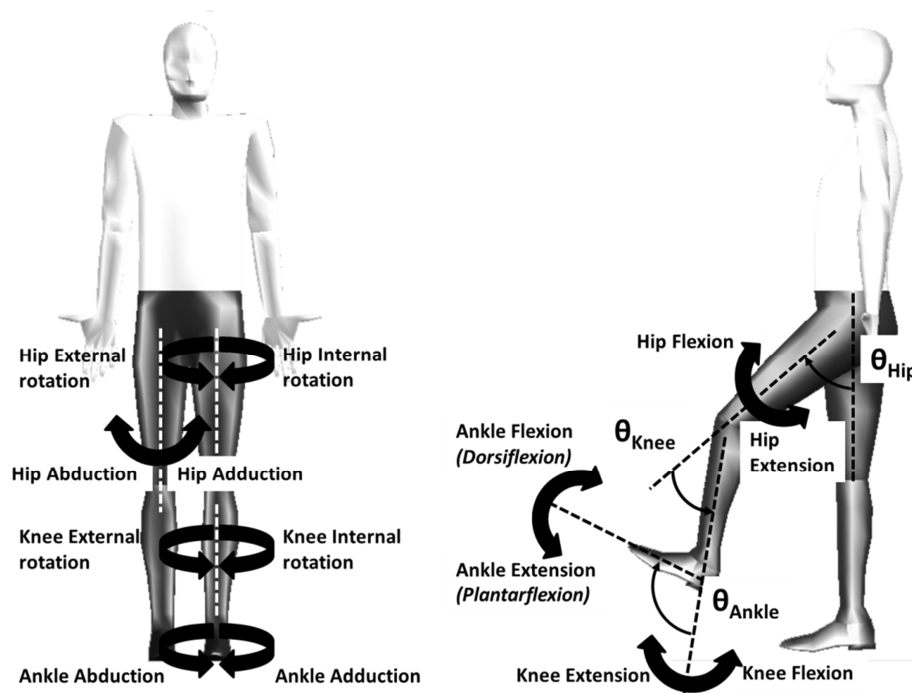
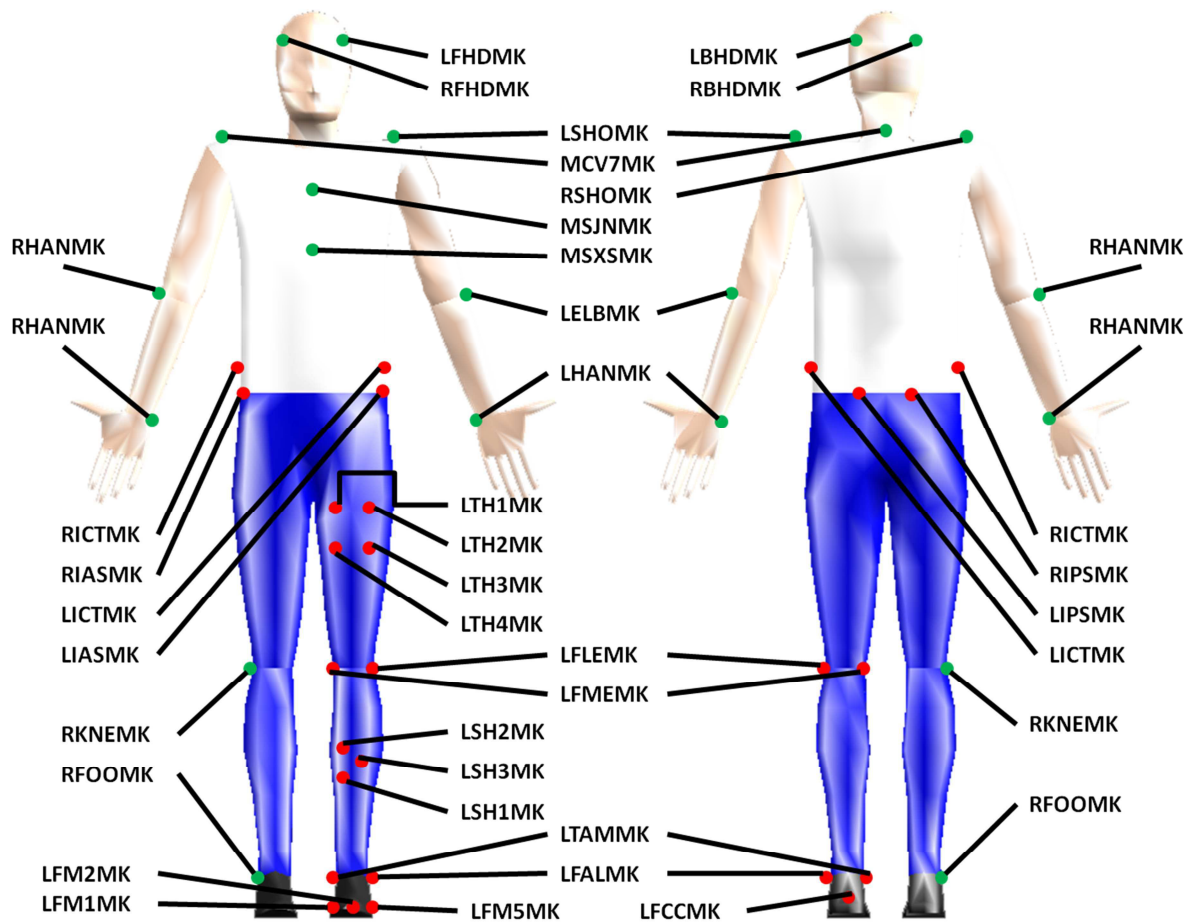


Figure 35: Definition of the motion tested in the characterization of the subjects' ROM.

Table 18: ROM and joint torques data for each group of subjects. Means and standard deviations are presented.

			Young male	Young female	Older male	Older female	All subjects
ROM (°)	Hip	Extension	-13 ± 9	-22 ± 5	-6 ± 12	-18 ± 4	-15 ± 10
		Flexion	87 ± 5	91 ± 3	88 ± 27	81 ± 11	87 ± 14
		Abduction	37 ± 4	50 ± 2	25 ± 15	40 ± 4	37 ± 12
		Adduction	-14 ± 3	-18 ± 4	-16 ± 6	-20 ± 6	-17 ± 5
		External rot.	-30 ± 5	-32 ± 6	-46 ± 24	-28 ± 6	-34 ± 14
		Internal rot.	31 ± 14	40 ± 6	22 ± 9	25 ± 9	29 ± 11
	Knee	Extension	9 ± 6	12 ± 6	13 ± 7	14 ± 8	12 ± 7
		Flexion	133 ± 6	138 ± 5	122 ± 7	125 ± 5	130 ± 8
		External rot.	-38 ± 7	-54 ± 13	-40 ± 6	-43 ± 6	-44 ± 10
		Internal rot.	17 ± 12	22 ± 7	24 ± 13	22 ± 12	21 ± 11
	Ankle	Plantarflexion	46 ± 6	39 ± 8	56 ± 3	44 ± 2	46 ± 8
		Dorsiflexion	121 ± 7	124 ± 5	123 ± 4	119 ± 6	122 ± 5
		Abduction	-34 ± 13	-47 ± 4	-39 ± 11	-41 ± 12	-40 ± 11
		Adduction	12 ± 7	17 ± 5	1 ± 12	14 ± 8	11 ± 10
Joint strength (Nm)	Hip	Extension	106 ± 30	67 ± 9	91 ± 23	49 ± 17	78 ± 30
		Flexion	112 ± 17	83 ± 8	98 ± 19	71 ± 11	91 ± 21
	Knee	Extension	105 ± 17	69 ± 23	75 ± 9	66 ± 12	79 ± 22
		Flexion	49 ± 19	34 ± 9	36 ± 8	22 ± 9	35 ± 15
	Ankle	Plantarflexion	91 ± 32	88 ± 33	55 ± 14	49 ± 38	71 ± 34
		Dorsiflexion	34 ± 4	18 ± 4	36 ± 9	22 ± 10	27 ± 10

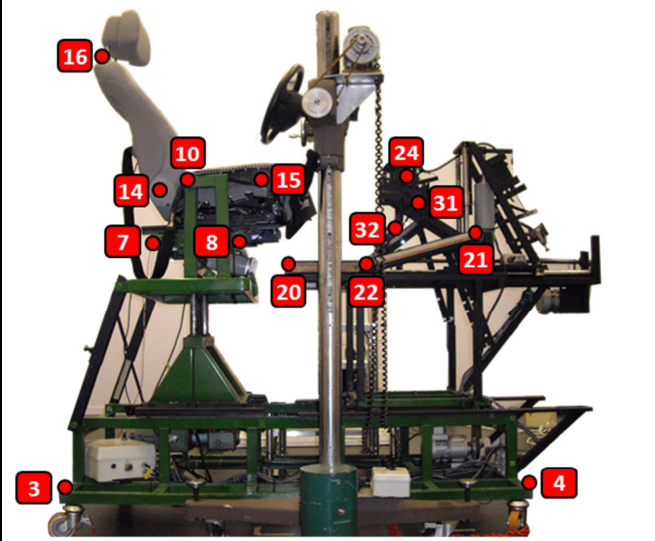
8.6 Markers' placement on subject for the DHErgo experiment



<b>LFHDMK</b>	Left temple	<b>RFHDMK</b>	Right temple
<b>LBHDMK</b>	Left back head	<b>RBHDMK</b>	Right back head
<b>MCV7MK</b>	7 <sup>th</sup> cervical vertebrae	<b>MSXSМК</b>	Xiphoid process (Sternum)
<b>MSJNMK</b>	Jugular Notch (Sternum)		
<b>LIASMK</b>	Left anterior superior iliac spine	<b>RIASMK</b>	Right anterior superior iliac spine
<b>LIPSMK</b>	Left posterior superior iliac spine	<b>RIPSMK</b>	Right posterior superior iliac spine
<b>LICTMK</b>	Left iliac crest tubercle	<b>RICTMK</b>	Right iliac crest tubercle
<b>LFLEMK</b>	Left femoral lateral epicondyle	<b>LFMEMK</b>	Left femoral medial epicondyle
<b>LTH1MK</b>	Thigh technical cluster marker 1	<b>LTH2MK</b>	Thigh technical cluster marker 2
<b>LTH3MK</b>	Thigh technical cluster marker 3	<b>LTH4MK</b>	Thigh technical cluster marker 4
<b>LFALMK</b>	Left lateral malleolus	<b>LTAMMK</b>	Left medial malleolus
<b>LSH1MK</b>	Shank technical cluster marker 1	<b>LSH2MK</b>	Shank technical cluster marker 2
<b>LSH3MK</b>	Shank technical cluster marker 3		
<b>LFCCMK</b>	Left foot calcaneous	<b>LFM1MK</b>	Left foot 1 <sup>st</sup> metatarsus
<b>LFM2MK</b>	Left foot 2 <sup>nd</sup> metatarsus	<b>LFM5MK</b>	Left foot 5 <sup>th</sup> metatarsus
<b>LSHOMK</b>	Left shoulder	<b>RSHOMK</b>	Right shoulder
<b>LELBMK</b>	Left elbow	<b>RELBMK</b>	Right elbow
<b>LHANMK</b>	Left hand	<b>RHANMK</b>	Right hand
<b>RKNEMK</b>	Right external knee	<b>RFOOMK</b>	Right foot

<b>Number of markers</b>	36
--------------------------	----

## 8.7 Markers' placement on mock-up for the DHErgo experiment

	N°	Name	Description (orientation according to driver's point of view)
	1	FRA_BL	Back left of mock-up frame
	2	FRA_BR	Front left of mock-up frame
	3	FRA_FL	Back right of mock-up frame
	4	FRA_FR	Front right of mock-up frame
	5	SBA_BL	Back left of seat base
	6	SBA_BR	Front left of seat base
	7	SBA_FL	Back right of seat base
	8	SBA_FR	Front right of seat base
	9	PHX_BK	H-point reference point left
	10	PHX_FT	H-point reference point right
	11	SEA_BL	Back left of seat
	12	SEA_BR	Front left of seat
	13	SEA_BU	Up left of backrest of seat
	14	SEA_FL	Back right of seat
	15	SEA_FR	Front right of seat
	16	SEA_FU	Up right of backrest of seat
	17	FLO_BL	Back left of floor (horizontal plane)
	18	FLO_BR	Front left of floor (inclined plane)
	19	FLO_BM	Middle left of floor (horizontal plane)
	20	FLO_FL	Back right of floor (horizontal plane)
	21	FLO_FR	Front right of floor (inclined plane)
	22	FLO_FM	Middle right of floor (horizontal plane)
	23	CPD_BU	Centre of rotation left
	24	CPD_FU	Centre of rotation right
	25	CPD_YB	Y-axis sensor (+)
	26	CPD_YF	Y-axis sensor (-)
	27	CPD_YM	Y-axis sensor (-)
	28	CPD_XP	X-axis sensor (+)
	29	CPD_XM	X-axis sensor (-)
	30	CPD_ZP	Z-axis sensor (+)
	31	GPD_UP	Accelerator pedal axis
	32	GPD_DN	Accelerator pedal up
	33	WHE_UW	Steering wheel up
	34	WHE_MW	Steering wheel middle
	35	WHE_DW	Steering wheel down

### 8.8 Discomfort questionnaire for the DHErgo experiment

Sujet :

Date :

Nom de la configuration (à remplir par l'expérimentateur) :

*Q1 : Ressentez-vous une gêne due à l'assise du siège ?*

Oui

Non

Remarques :

*Q2 : La position de la pédale en début de course est :*

Trop haute

A bonne hauteur

Trop basse

Trop loin

A bonne distance

Trop près

Trop à gauche

A bonne distance

Trop à droite

Remarques :

*Q3 : La position de la pédale en fin de course est :*

Trop haute

A bonne hauteur

Trop basse

Trop loin

A bonne distance

Trop près

Trop à gauche

A bonne distance

Trop à droite

Remarques :

*Q4 : La longueur de la course de la pédale est :*

Trop longue

A bonne longueur

Trop courte

Remarques :

*Q5 : L'inclinaison de la course de la pédale est :*

Peu inclinée

A bonne inclinaison

Trop inclinée

Remarques :

**Q6 : Lors du débrayage, l'effort à appliquer sur la pédale est :**

- Très faible       Faible       Moyen       Fort       Maximum

**Remarques :**

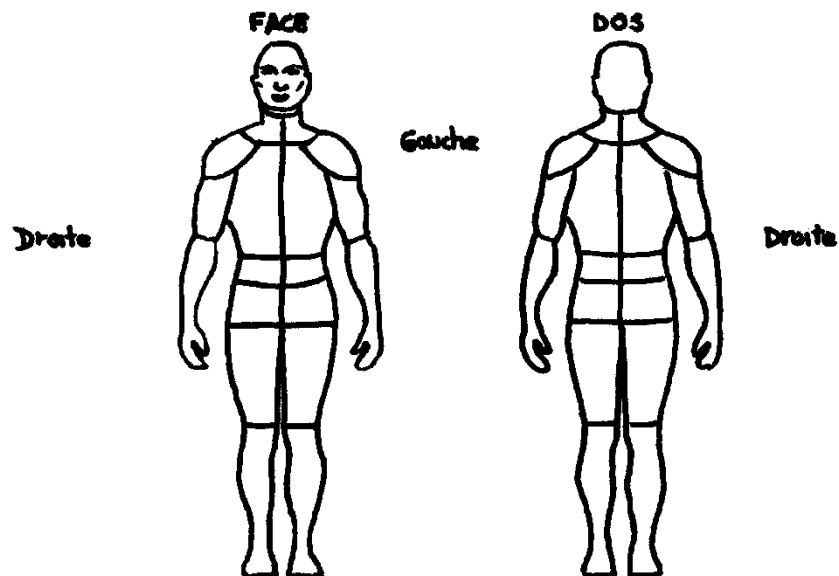
**Q7 : L'inconfort ressenti durant le débrayage était :**

- |  |                                      |                                 |                                |                                |                                     |  |
|--|--------------------------------------|---------------------------------|--------------------------------|--------------------------------|-------------------------------------|--|
| <input type="checkbox"/> Imperceptible | <input type="checkbox"/> Très faible | <input type="checkbox"/> Faible | <input type="checkbox"/> Moyen | <input type="checkbox"/> Elevé | <input type="checkbox"/> Très élevé | <input type="checkbox"/> Extrêmement élevé |
|  | 1 2 3 4 5 6 7 8 9 10                 | 1 2 3 4 5 6 7 8 9 10            | 1 2 3 4 5 6 7 8 9 10           | 1 2 3 4 5 6 7 8 9 10           | 1 2 3 4 5 6 7 8 9 10                | 11 12 13 ...                               |

**Remarques :**

**Q8 : Quelles sont les parties du corps où vous ressentez le plus d'inconfort ?**

**Entourez-les sur la figure ci-dessous.**



**Indiquez l'intensité de la gêne ressentie selon l'échelle suivante**

- |  |                                      |                                 |                                |                                |                                     |  |
|--|--------------------------------------|---------------------------------|--------------------------------|--------------------------------|-------------------------------------|--|
| <input type="checkbox"/> Imperceptible | <input type="checkbox"/> Très faible | <input type="checkbox"/> Faible | <input type="checkbox"/> Moyen | <input type="checkbox"/> Elevé | <input type="checkbox"/> Très élevé | <input type="checkbox"/> Extrêmement élevé |
|--|--------------------------------------|---------------------------------|--------------------------------|--------------------------------|-------------------------------------|--|

## 8.9 Experimental sheet of the DHErgo experiment

N° trial	Filename	Configuration	Comments
<b>Calibration plate</b>			
1	CALIB_TAR1_1	Target 1	
2	CALIB_TAR2_1	Target 2	
3	CALIB_TAR3_1	Target 3	
<b>Palpation</b>			
4	xx_XX_LIAS_1	Left Anterior Superior Iliac Spine (LIAS)	
5	xx_XX_RIAS_1	Right Anterior Superior Iliac Spine (RIAS)	
6	xx_XX_LIPS_1	Left Posterior Superior Iliac Spine (LIPS)	
7	xx_XX_RIPS_1	Right Posterior Superior Iliac Spine (RIPS)	
8	xx_XX_LICT_1	Left Ilium Crest Tubercle (LICT)	
9	xx_XX_RICT_1	Right Ilium Crest Tubercle (RICT)	
10	xx_XX_LFTC_1	Left Greater Trochanter (FTC)	
11	xx_XX_LFME_1	Left Medial Femoral Epicondyles (FME)	
12	xx_XX_LFLE_1	Left Lateral Femoral Epicondyles (FLE)	
13	xx_XX_LTTC_1	Left Tibial Anterior Tuberosity (TTC)	
14	xx_XX_LTAM_1	Left Medial Malleoli (TAM)	
15	xx_XX_LFAL_1	Left Lateral Malleoli (FAL)	
16	xx_XX_LFNE_1	Left Fibula's Neck (FNE)	
<b>Static Posture</b>			
17	xx_XX_STND_1	Static Standing	
18	xx_XX_SEAT_1	Static Seated	
<b>Movement</b>			
19	xx_XX_HPCR_1	Hip Circumduction	
<b>Range of Motion</b>			
20	xx_XX_H_FE_ROM_1	Hip Flexion-Extension ROM	
21	xx_XX_H_AA_ROM_1	Hip Abduction-Adduction ROM	
22	xx_XX_H_AR_ROM_1	Hip Axial Rotation ROM	
23	xx_XX_K_FE_ROM_1	Knee Flexion-Extension ROM	
24	xx_XX_K_AR_ROM_1	Knee Axial Rotation ROM	
25	xx_XX_A_FE_ROM_1	Ankle Flexion-Extension ROM	
26	xx_XX_A_AA_ROM_1	Ankle Abduction-Adduction ROM	

N° trial	Filename	Joint	Angle	Direction	Force Level	Comments	Effort Value	% Difference
<b>Joint Torque Measurement</b>								
27	xx_XX_H060_F_MX_1	Hip	90°	Flexion	Maximum			
28	xx_XX_H060_F_MX_2	Hip	90°	Flexion	Maximum			
29	xx_XX_H060_REST_1	Hip	90°	Extension	Rest			
30	xx_XX_H060_E_MX_1	Hip	90°	Extension	Maximum			
31	xx_XX_H090_E_MX_2	Hip	90°	Extension	Maximum			
32	xx_XX_K045_REST_1	Knee	45°	Flexion	Rest			
33	xx_XX_K045_F_MX_1	Knee	45°	Flexion	Maximum			
34	xx_XX_K045_F_MX_2	Knee	45°	Flexion	Maximum			
35	xx_XX_K045_E_MX_1	Knee	45°	Extension	Maximum			
36	xx_XX_K045_E_MX_2	Knee	45°	Extension	Maximum			
37	xx_XX_A090_F_MX_1	Ankle	90°	Flexion	Maximum			
38	xx_XX_A090_F_MX_2	Ankle	90°	Flexion	Maximum			
39	xx_XX_A090_REST_1	Ankle	90°	Extension	Rest			
40	xx_XX_A090_E_MX_1	Ankle	90°	Extension	Maximum			
41	xx_XX_A090_E_MX_2	Ankle	90°	Extension	Maximum			

N° Trial	Filename	Configuration	TravelLength	Discomfort ratings	Effort ratings	Comments
<b>Discomfort perception</b>						
42		CAL1	170			
43		CAL2	170			
44		CAL3	140			
45	xx_XX_BMW1_MOTION1	BMW1	131			
46	xx_XX_BMW1_NTMVT01	BMW1	131			
47	xx_XX_BMW2_MOTION1	BMW2	163			
48	xx_XX_BMW2_NTMVT01	BMW2	163			
49	xx_XX_BMW4_MOTION1	BMW4	149			
50	xx_XX_BMW4_NTMVT01	BMW4	149			
51	xx_XX_PCA1_MOTION1	PCA1	161			
52	xx_XX_PCA1_NTMVT01	PCA1	161			
53	xx_XX_PCA2_MOTION1	PCA2	157			
54	xx_XX_PCA2_NTMVT01	PCA2	157			
55	xx_XX_REN3_MOTION1	REN3	137			
56	xx_XX_REN3_NTMVT01	REN3	137			

### 8.10 Ramsis™ digital human model

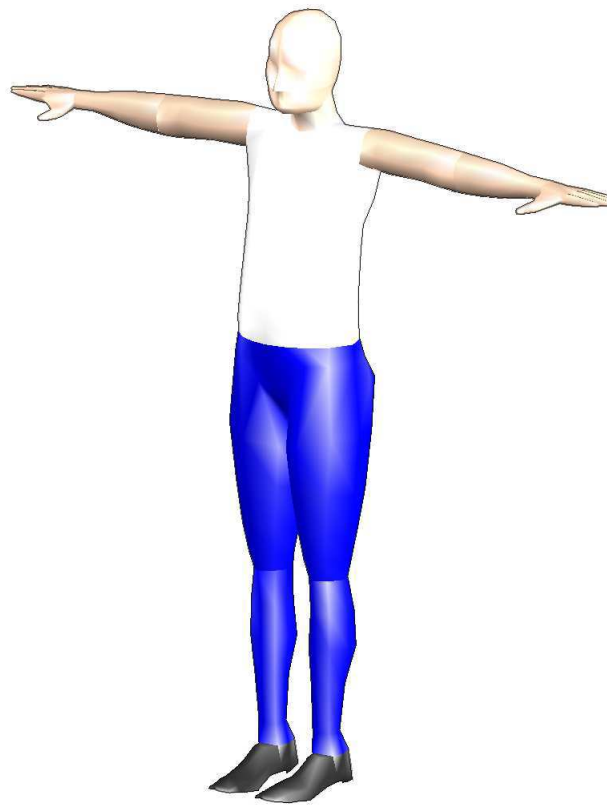


Figure 36: Ramsis™ manikin - Skin model.

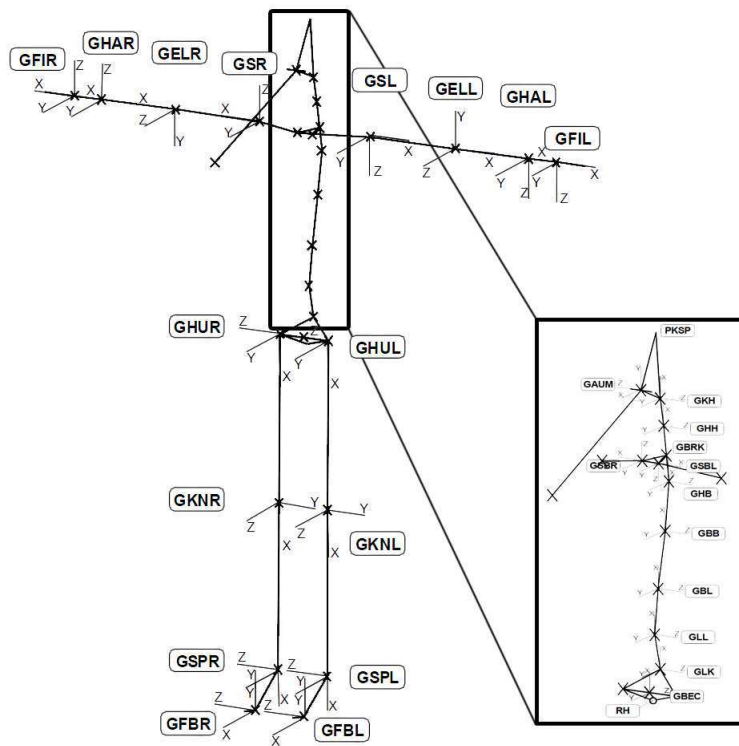


Figure 37: Ramsis™ manikin - Kinematic model.

## 8.11 Questionnaire frequency tables

Table 19: Frequency table for Question 1

	Q1 <sup>G**</sup>	
	Yes (%)	No (%)
Older Female	10.00	90.00
Older Male	2.50	97.50
Younger Female	11.25	88.75
Younger Male	0.00	100.00
BMW1	5.00	95.00
BMW2	7.50	92.50
BMW4	12.50	87.50
PCA1	10.00	90.00
PCA2	1.67	98.33
REN3	7.50	92.50
Imposed	6.88	93.13
Less Constrained	5.00	95.00
Total	5.94	94.06

Chi-square test significance: \* p-value<0.05, \*\* p-value<0.01, \*\*\* p-value<0.001  
G: Group of subjects, C: Configuration, T: Type of configuration

Table 20: Frequency table for Question 2

	Q2H <sup>G***, T***</sup>			Q2D <sup>T***</sup>			Q2P <sup>G**, C*, T***</sup>		
	Too high (%)	Good (%)	Too low (%)	Too far (%)	Good (%)	Too close (%)	Too leftward (%)	Good (%)	Too rightward (%)
Older Female	48.75	48.75	2.50	6.25	62.50	31.25	0.00	51.90	48.10
Older Male	23.75	72.50	3.75	3.75	76.25	20.00	0.00	80.00	20.00
Younger Female	40.00	57.50	2.50	7.50	70.00	22.50	0.00	55.00	45.00
Younger Male	16.25	75.00	8.75	6.25	72.50	21.25	1.27	67.09	31.65
BMW1	42.50	57.50	0.00	12.50	57.50	30.00	0.00	52.50	47.50
BMW2	40.00	57.50	2.50	7.50	75.00	17.50	0.00	80.00	20.00
BMW4	40.00	60.00	0.00	2.50	67.50	30.00	2.50	75.00	22.50
PCA1	27.50	62.50	10.00	10.00	72.50	17.50	0.00	55.00	45.00
PCA2	28.33	65.83	5.83	1.67	73.33	25.00	0.00	62.71	37.29
REN3	22.50	72.50	5.00	10.00	70.00	20.00	0.00	57.50	42.50
Imposed	55.63	36.25	8.13	11.25	48.75	40.00	0.63	35.63	63.75
Less Constrained	8.75	90.63	0.63	0.63	91.88	7.50	0.00	91.77	8.23
Total	32.19	63.44	4.38	5.94	70.31	23.75	0.31	63.52	36.16

Chi-square test significance: \* p-value<0.05, \*\* p-value<0.01, \*\*\* p-value<0.001  
G: Group of subjects, C: Configuration, T: Type of configuration

Table 21: Frequency table for Question 3

	Q3H <sup>G*, C***, T***</sup>			Q3D <sup>C*, T***</sup>			Q3P <sup>C***, T*</sup>		
	Too high (%)	Good (%)	Too low (%)	Too far (%)	Good (%)	Too close (%)	Too leftward (%)	Good (%)	Too rightward (%)
Older Female	10.13	62.03	27.85	39.24	59.49	1.27	0.00	51.25	48.75
Older Male	11.39	77.22	11.39	28.75	62.50	8.75	0.00	85.00	15.00
Younger Female	16.25	60.00	23.75	45.00	47.50	7.50	0.00	63.75	36.25
Younger Male	8.75	77.50	13.75	37.97	59.49	2.53	1.27	69.62	29.11
BMW1	22.50	72.50	5.00	30.00	65.00	5.00	0.00	55.00	45.00
BMW2	22.50	65.00	12.50	50.00	45.00	5.00	0.00	82.50	17.50
BMW4	15.00	75.00	10.00	25.00	72.50	2.50	2.50	85.00	12.50
PCA1	5.00	55.00	40.00	57.50	35.00	7.50	0.00	57.50	42.50
PCA2	5.88	75.63	18.49	29.66	66.10	4.24	0.00	65.55	34.45
REN3	10.26	58.97	30.77	50.00	42.50	7.50	0.00	62.50	37.50
Imposed	18.87	64.78	16.35	32.70	57.23	10.06	0.63	43.75	55.63
Less Constrained	4.40	73.58	22.01	42.77	57.23	0.00	0.00	91.19	8.81
Total	11.64	69.18	19.18	37.74	57.23	5.03	0.31	67.40	32.29

Chi-square test significance: \* p-value<0.05, \*\* p-value<0.01, \*\*\* p-value<0.001  
G: Group of subjects, C: Configuration, T: Type of configuration

Table 22: Frequency table for Question 4

	Q4 <sup>G*, T*</sup>		
	Too long (%)	Good (%)	Too short (%)
Older Female	56.25	42.50	1.25
Older Male	47.50	50.00	2.50
Younger Female	45.00	45.00	10.00
Younger Male	46.25	53.75	0.00
BMW1	45.00	52.50	2.50
BMW2	62.50	32.50	5.00
BMW4	30.00	67.50	2.50
PCA1	50.00	45.00	5.00
PCA2	50.00	47.50	2.50
REN3	52.50	42.50	5.00
Imposed	43.75	50.63	5.63
Less Constrained	53.75	45.00	1.25
Total	48.75	47.81	3.44

Chi-square test significance: \* p-value<0.05, \*\* p-value<0.01, \*\*\* p-value<0.001  
G: Group of subjects, C: Configuration, T: Type of configuration

Table 23: Frequency table for Question 5

	Q5 <sup>G**</sup>		
	Little inclined (%)	Good (%)	Too inclined (%)
Older Female	6.25	72.50	21.25
Older Male	18.75	72.50	8.75
Younger Female	5.00	66.25	28.75
Younger Male	10.00	77.50	12.50
BMW1	10.00	77.50	12.50
BMW2	17.50	65.00	17.50
BMW4	10.00	75.00	15.00
PCA1	10.00	62.50	27.50
PCA2	6.67	79.17	14.17
REN3	12.50	60.00	27.50
Imposed	11.88	66.88	21.25
Less Constrained	8.13	77.50	14.38
Total	10.00	72.19	17.81

Chi-square test significance: \* p-value<0.05, \*\* p-value<0.01, \*\*\* p-value<0.001  
G: Group of subjects, C: Configuration, T: Type of configuration

Table 24: Frequency table for Question 6

	Q6 <sup>C***</sup>			
	Very Low (%)	Low (%)	Medium (%)	High (%)
Older Female	5.00	20.00	55.00	20.00
Older Male	2.50	25.00	60.00	12.50
Younger Female	1.25	25.00	51.25	22.50
Younger Male	1.25	35.00	48.75	15.00
BMW1	0.00	30.00	52.50	17.50
BMW2	0.00	40.00	45.00	15.00
BMW4	5.00	55.00	32.50	7.50
PCA1	0.00	12.50	62.50	25.00
PCA2	4.17	20.00	60.83	15.00
REN3	2.50	12.50	55.00	30.00
Imposed	2.50	21.88	54.38	21.25
Less Constrained	2.50	30.63	53.13	13.75
Total	2.50	26.25	53.75	17.50

Chi-square test significance: \* p-value<0.05, \*\* p-value<0.01, \*\*\* p-value<0.001  
G: Group of subjects, C: Configuration, T: Type of configuration

## 8.12 Questionnaire reproducibility

Table 25: Frequency table of the conditions of the reproducibility for each subject and each question. For each subject, the reproducibility was evaluated on all questions. For each question, it was estimated on all subjects.

	Cond1 (%) i.e. 0 similar answer	Cond2 (%) i.e. 2 similar answers	Cond3 (%) i.e. 3 similar answers
Subjects	01_SD	0	50
	02_LZ	0	25
	03_FD	0	45
	04_VM	5	60
	05_SL	5	30
	06_MR	0	40
	07_YP	0	10
	08_ZS	0	25
	09_HB	0	30
	10_VH	0	40
	11_JF	0	25
	12_MC	0	40
	13_AT	0	80
	14_AF	5	25
	15_PP	0	30
	16_ED	5	40
	17_AG	0	25
	18_AC	0	30
	19_JL	20	35
	20_ID	0	50
Questions	Q1	0	10
	Q2H	2,5	35
	Q2D	0	45
	Q2P	0	20
	Q3H	5	42,5
	Q3D	7,5	52,5
	Q3P	0	30
	Q4	2,5	42,5
	Q5	0	32,5
	Q6	2,5	57,5

### 8.13 Imposed versus less-constrained joint angles

Table 26: Means, standard deviations and the mean differences of the lower limb joint angles at beginning and end of pedal depression.

Joint	DoF		Beginning of pedal depression (deg.)	End of pedal depression (deg.)
Hip	Flexion/Extension	Imposed	57.7 ± 10.4	37.6 ± 12.8
		Free	56.5 ± 10.7	35.1 ± 13.3
		$\Delta$ HipFE	1.2** ± 5.0	2.6*** ± 6.6
	Abduction/Adduction	Imposed	3.6 ± 6.1	2.1 ± 3.8
		Free	4.5 ± 6.0	4.2 ± 3.9
		$\Delta$ HipAA	-0.9* ± 3.9	-2.1*** ± 3.4
Knee	Flexion/Extension	Imposed	79.5 ± 7.7	45.8 ± 10.2
		Free	78.4 ± 7.6	43.8 ± 10.4
		$\Delta$ KneeFE	1.0** ± 4.6	1.9*** ± 6.4
Ankle	Flexion/Extension	Imposed	106.6 ± 8.6	74.6 ± 9.6
		Free	102.2 ± 8.8	70.8 ± 10.3
		$\Delta$ AnkleFE	4.4*** ± 8.0	3.9*** ± 6.3

\*p<0.05, \*\*p<0.01, \*\*\* p<0.001

8.14 Discomfort cost function for kinematic indicators

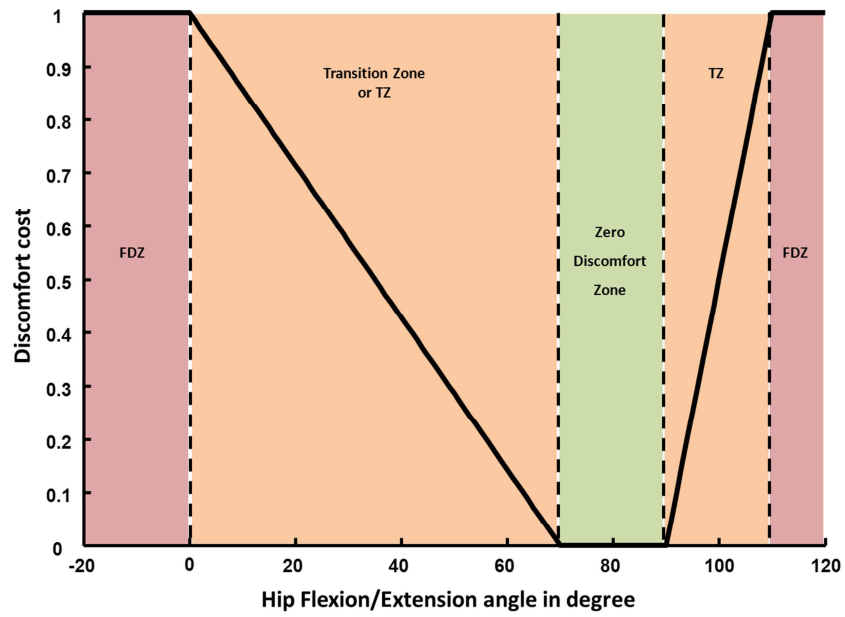


Figure 38: Discomfort cost function for hip flexion/extension angle

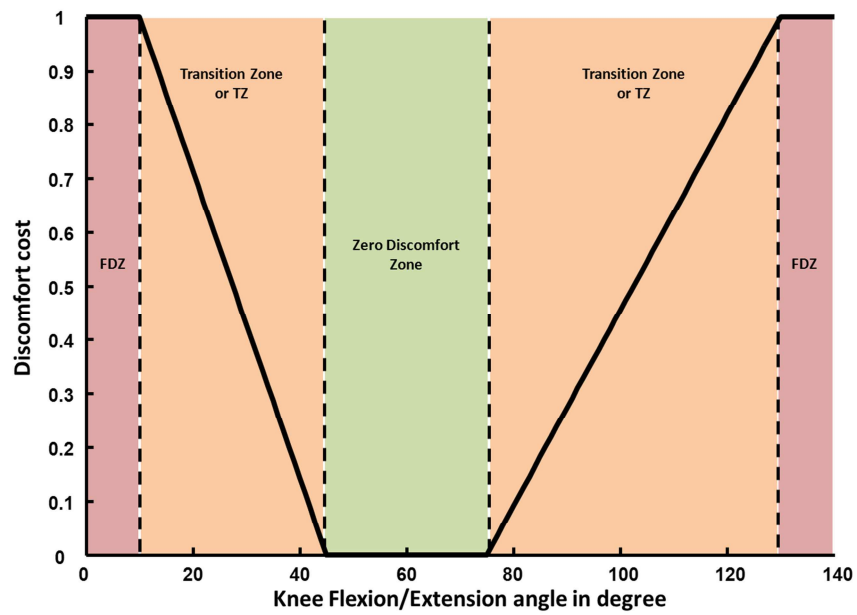


Figure 39: Discomfort cost function for knee flexion/extension angle

## 8.15 Discomfort modelling approaches using discomfort indicators

### 8.15.i CP50 linear regression

The Table 27 presents the coefficients of the indicators in the fitted model with their respective p-values, the coefficients of determination  $R^2$  and adjusted  $R^2$ . By definition, the  $R^2$  measures the percentage of the variability in Y, i.e. the dependent variable that has been explained by the fitted model. Adjusted  $R^2$  measures also this percentage of variability but compensates for the number of variables in the model.

Table 27: Coefficients of the fitted model from linear regression

	Coefficient value
Constant	21.8***
IndHipStart	26.5*
IndHipEnd	-27.4**
IndKneeStart	5.3
IndKneeEnd	-6.5
IndAnkleStart	3.4*
IndAnkleEnd	3.1
IndKneeJT	1.5
IndAnkleJT	-11.1
IndLPos	7.1
$R^2 = 20.2\%$	
Adjusted $R^2 = 17.2\%$	

A regression model selection procedure was also performed to evaluate the behaviour of the fitted model according to the number of indicators considered. The Table 28 presents the best n-variable models with n from 0 to 9 according to adjusted  $R^2$  and their classification.

Table 28: Results of the regression model selection procedure

$R^2$	Adjusted $R^2$	Included variables	
20.0	17.7	ABDEFHI	A=IndHipStart
19.6	17.6	ABDEHI	B=IndHipEnd
20.1	17.5	ABCDEFHI	C=IndKneeStart
20.2	17.2	ABCDEFGHI	D=IndKneeEnd
18.7	17.1	ABDHI	E=IndAnkleStart
17.9	16.6	ABDH	F=IndAnkleEnd
16.6	15.6	ABH	G=IndKneeJT
15.0	14.3	AB	H=IndAnkleJT
7.9	7.5	E	I=IndLPos
0.0	0.0		

It showed that the best model in terms of adjusted  $R^2$  was a 7 variables-model and the best compromise was a 4 variables-model. Between these two models, the adjusted  $R^2$  improved of only 1%. None of these two models included the IndKneeJT whereas it was found to be the more significant to differentiate clutch pedal configuration. Besides, this indicator is included in only one model, the one including all the indicators.

### *8.15.ii Linear discriminant analysis model*

Three distinct discomfort categories of the modified CP50 rating scale used in the experiment were considered: imperceptible (0 on CP50), low (11 to 20) and high (31 to 40). The categories were composed of 16, 97 and 17 trials respectively. In order to maximize the robustness of the model, sets of 15 trials were randomly selected in each category. The general idea was to perform the discriminant analysis with trial samples of the same size in each category. One of the issues was the limited data available in the two extreme categories. It was decided to select almost all available trials in these two categories. As a consequence, the cross-validation of the model was mostly performed on the unselected data of the “low” category.

For each selected trials, all discomfort indicators were considered. Then a linear discriminant analysis (LDA) was performed using XLSTAT software. This method is used to find a linear combination of parameters which characterizes or separates two or more classes of variables. Compared to regression analysis, the LDA considers categorical dependent variables and not numerical quantitative dependent variable. In this case, the LDA provided three linear discriminant functions, one for each category. The Table 29 and Table 30 presented the three linear discriminant functions of each model: F1, F2 and F3 corresponding respectively to imperceptible, low and high discomfort categories.

Table 29: Linear discriminant functions F1, F2 and F3 for Model1 to Model8

	Fonction	Constant	IndHipStart	IndHipEnd	IndKneeStart	IndKneeEnd	IndAnkleStart	IndAnkleEnd	IndKneeJT	IndAnkleJT	IndLPos
Model1	F1	-61.7	-98.4	125.0	60.8	73.0	9.2	11.5	57.7	80.5	26.1
	F2	-45.8	-98.0	111.7	57.9	46.8	11.9	19.9	42.8	63.5	24.9
	F3	-49.5	-102.1	114.1	56.4	45.8	13.1	21.6	46.3	61.5	30.1
Model2	F1	-51.8	-73.4	96.9	33.3	27.4	11.0	19.0	49.9	87.1	24.7
	F2	-44.0	-99.9	106.1	32.9	13.7	11.7	23.0	44.7	63.8	24.8
	F3	-45.3	-81.3	94.2	42.9	17.3	12.6	21.5	46.0	66.1	28.6
Model3	F1	-60.9	-140.1	150.2	51.4	45.3	15.0	14.8	50.1	77.6	26.4
	F2	-52.2	-139.0	144.9	55.2	33.8	15.3	19.3	35.7	61.5	29.7
	F3	-51.8	-135.5	139.7	57.4	35.4	16.4	18.4	39.8	58.3	31.0
Model4	F1	-49.3	-83.2	100.5	32.7	26.4	12.5	15.3	45.8	80.6	20.8
	F2	-43.7	-93.0	103.3	40.2	19.5	12.0	18.9	37.6	63.7	22.4
	F3	-42.1	-84.2	94.6	39.9	20.8	13.2	17.1	38.7	60.0	26.1
Model5	F1	-53.6	-78.9	97.5	25.2	26.2	14.1	20.2	55.4	104.8	13.7
	F2	-43.4	-87.9	99.2	36.6	22.5	14.5	23.0	34.4	70.2	17.3
	F3	-42.0	-75.6	87.1	32.1	19.3	14.2	22.4	45.4	82.6	15.7
Model6	F1	-48.7	-42.5	88.1	51.8	29.4	7.0	15.8	38.5	85.8	9.0
	F2	-38.7	-56.7	81.4	40.7	12.9	6.9	24.8	32.9	76.8	9.2
	F3	-39.7	-38.5	74.5	56.0	18.6	8.4	20.3	30.8	72.6	13.2
Model7	F1	-45.8	-54.0	86.9	42.5	28.3	7.8	11.3	37.4	75.2	19.3
	F2	-43.4	-86.9	95.9	40.5	6.8	5.9	26.2	35.1	66.3	19.8
	F3	-38.4	-55.0	77.2	46.2	15.1	9.3	17.4	31.4	61.4	23.6
Model8	F1	-45.2	-33.6	72.7	67.1	37.7	2.3	16.4	29.3	78.2	20.6
	F2	-42.7	-28.8	64.4	75.1	25.8	1.6	26.8	22.4	81.3	19.5
	F3	-39.0	-29.4	61.9	74.1	29.2	3.1	21.1	23.7	67.9	23.9

Table 30: Linear discriminant functions F1, F2 and F3 for Model9 to Model10

	Fonction	Constant	IndHipStart	IndHipEnd	IndKneeStart	IndKneeEnd	IndAnkleStart	IndAnkleEnd	IndKneeJT	IndAnkleJT	IndLPos
Model9	F1	-46.9	-61.8	79.8	28.9	38.5	10.0	6.5	51.6	92.0	14.2
	F2	-30.4	-50.1	62.1	38.3	21.2	8.7	12.2	31.9	66.3	17.5
	F3	-35.7	-52.7	65.6	36.5	19.0	10.3	15.7	38.5	75.4	16.0
Model10	F1	-48.6	-26.7	73.0	34.0	46.4	14.3	5.7	41.6	95.0	8.4
	F2	-33.6	-35.1	62.7	44.9	28.9	9.5	15.6	28.2	71.0	8.4
	F3	-37.0	-31.7	64.4	40.6	33.2	14.0	10.6	31.2	71.9	13.9

Then the principle is to calculate the results of each function with the indicators of a trial. The function which gives the higher score determines the category in which the trial belongs. The Table 31 showed the percentage of right prediction for the data selected to build each model. The cross-validation was performed using the unselected trials of the three considered discomfort categories.

Table 31: Global and discomfort category prediction rates of the LDA models on the selected samples of trials

		Model1	Model2	Model3	Model4	Model5	Model6	Model7	Model8	Model9	Model10
Global		78%	78%	71%	69%	82%	84%	84%	71%	71%	82%
By Discomfort category	Imperceptible	87%	80%	80%	80%	87%	87%	80%	73%	80%	80%
	Low	80%	73%	80%	67%	80%	87%	87%	67%	73%	93%
	High	67%	80%	53%	60%	80%	80%	87%	73%	60%	73%

## Chapter 3: Maximum pedal force, force perception and control of pedal force direction

<b>1</b>	<b>INTRODUCTION</b>	<b>103</b>
<b>2</b>	<b>MATERIAL AND METHODS</b>	<b>105</b>
2.1	SUBJECTS .....	105
2.2	EXPERIMENTAL SET-UP .....	105
2.3	TEST CONDITIONS .....	107
2.4	EXPERIMENTAL PROCEDURE .....	108
2.5	DATA PROCESSING .....	109
2.6	EVALUATION OF RECONSTRUCTED MOTIONS .....	110
2.7	SUMMARY OF PROCESSED DATA .....	112
<b>3</b>	<b>EXPERIMENTAL OBSERVATIONS</b>	<b>113</b>
3.1	MAXIMUM PEDAL FORCE EXERTION ( <i>ExpMax</i> ) .....	113
3.2	INTERMEDIATE LEVELS OF PEDAL FORCE EXERTION AND FORCE PERCEPTION ( <i>ExpPcp</i> ) ...	117
<b>4</b>	<b>DISCUSSION</b>	<b>123</b>
<b>5</b>	<b>PEDAL FORCE CONTROL SIMULATION</b>	<b>126</b>
5.1	SIMULATION OF THE PEDAL FORCE DIRECTION [SIM1] .....	128
5.2	SIMULATION OF THE POSTURAL ADJUSTMENT [SIM2] .....	131
5.3	DISCUSSIONS OF THE TWO SIMULATION METHODS .....	135
<b>6</b>	<b>CONCLUSION</b>	<b>140</b>
<b>7</b>	<b>APPENDIX</b>	<b>141</b>
7.1	MEASUREMENT CHAIN FOR FAC PROJECT .....	141
7.2	ANTHROPOMETRIC MEASUREMENTS .....	142
7.3	SUBJECTS' ANTHROPOMETRIC DIMENSION FOR THE FAC PROJECT .....	144
7.4	MARKERS' PLACEMENT ON SUBJECT FOR THE FAC PROJECT .....	146
7.5	MARKERS' PLACEMENT ON MOCK-UP FOR THE FAC PROJECT .....	147
7.6	EXTRACT FROM EXPERIMENTAL SHEET OF THE FAC PROJECT .....	148
7.7	TANGENTIAL, NORMAL AND TRANSVERSAL PEDAL FORCE COMPONENTS ACCORDING TO THE FORCE LEVEL .....	149
7.8	PELVIS DISPLACEMENT FOR SHORT WOMEN, AVERAGE MEN AND TALL MEN ACCORDING TO THE FORCE LEVEL .....	150
7.9	VARIATION OF JOINT ANGLES FOR SHORT WOMEN, AVERAGE MEN AND TALL MEN ACCORDING TO THE FORCE LEVEL .....	151
7.10	HIP, KNEE AND ANKLE FLEXION/EXTENSION ANGLES ACCORDING TO THE PEDAL POSITION AND THE GROUP OF SUBJECTS .....	152
7.11	FUNCTIONAL MAXIMUM DATA USED IN THE SIMULATION .....	154
7.12	COMPARISON OF SIMULATED AND EXPERIMENTAL PEDAL FORCE DIRECTIONS .....	155
7.13	COMPARISON OF SIMULATED AND EXPERIMENTAL NORMAL AND TRANSVERSAL FORCES. 156	



## 1 Introduction

Accurate representation of task-oriented postures is critical when digital human models are used for ergonomic assessments. For force exertion tasks such as automotive control tasks, the posture is not only adapted to geometrical restrictions but also to the force requirements of the task. Besides, posture has a major influence on strength capability as it determines the mechanical advantage offered to muscles to exert force (Haslegrave, 2004).

Force exertion capacity can vary greatly depending on a high number of factors (Daams, 1994; Kumar, 2004; Haslegrave, 2004). In case of automotive pedals, some studies investigated lower limb maximum strength (Kroemer, 1971; Mortimer, 1974; Pheasant et al., 1982; Metha et al, 2007) but few focused on the force perception (Wang and Bullock, 2004). The experimental conditions varied a lot from a study to another on for example the type of pedals (accelerator, brake or clutch pedal), the range of end effector positions (align or not with hip joint center) or the type of vehicles. Besides, postures of force exertion are usually only succinctly described. Only a few studies in the literature investigated the mechanism of the control of the force applied on a pedal (Wang et al, 2000; Schmidt et al., 2003). Both studies suggested that the control of the foot force may follow the principle of reducing joint load, but were performed in 2D whereas, as a pedal may not be fully aligned with the left or right hip joint, the force direction should be 3D, especially for high force exertion level.

Most of the existing DHM packages used in the automotive industry for ergonomic assessment of a product or workplace have a kinematic approach of the human motion without considering the dynamics. The simulation of force exertion postures usually requires manual manipulation of the manikin and so some expertise. More recently, some optimization-based methods were suggested (Seitz et al., 2005; Abdel-Malek and Arora, 2008). These simulation methods have the advantage to be able to explain postural strategy, as they consider motion control strategies as optimization criteria to predict the posture. But they have not been validated.

The data used in this study were collected in a collaborative project between IFSTTAR and the car manufacturer Renault (called '*FAC project*' afterwards) on the muscular capacity of the upper and lower limb when operating on automotive controls. The aim of this collaborative project was to collect data on the force exertion capacity of the upper and lower limbs to define ergonomic criteria for the improvement of the ergonomics of automotive controls. Only the part on the clutch pedal was investigated and presented. A complete presentation of the whole experimental protocol and the preliminary results can be found in the report by Wang et al. (2009).

The purpose of the study presented in this section was to better understand the mechanisms of the pedal force exertion when changing the level of force exertion and pedal position. In particular, the force and posture control strategies were investigated in order to propose improvements of DHMs in automotive control tasks simulation. The study was organized in three parts. First maximum pedal force exertion on different pedal positions were investigated. Then the effects of pedal force level on force perception, posture and force direction were analyzed. Finally, optimization-based methods were used to explain both force and posture controls during pedal force exertion. The results from simulations were compared with experimental observations.

## 2 Material and methods

### 2.1 Subjects

Thirty voluntary male and female subjects participated in the experiment (Table 32). They were aged from 20 to 44 and had neither musculoskeletal abnormalities nor any history of trauma. All of them had driving experience of more than one year. They were divided into three groups according to stature and gender of French driver population (IFTH, 2006):

- 10 short females: <1625 mm (5<sup>th</sup> percentile of the French driver population)
- 10 average height males: 1705 - 1810 mm (50<sup>th</sup> percentile of the French driver population)
- 10 tall males: >1810 mm (95<sup>th</sup> percentile of the French driver population)

Table 32: Main characteristics of the participants

Group	Age (years)	Stature (mm)	Weight (kg)
Short females	30.8 ± 6.8	1582 ± 38	54.3 ± 10
Average males	28.5 ± 8.7	1763 ± 40	73.1 ± 11.4
Tall males	31.6 ± 7.2	1854 ± 29	82.4 ± 10.3

The experimental protocol was approved by the ethical committee of Ifsttar. Informed consent was given before participating in the experiment.

Twenty one anthropometric dimensions were measured for all participants (see in Appendix).

### 2.2 Experimental set-up

#### 2.2.i Mock-up

A multi-adjustable experimental vehicle package was used to define different driving configurations (Figure 40). It was composed of a seat, a steering wheel, a floor, a clutch pedal, a gear stick and one hand brake. The location of all of these elements could be adjusted according to the configurations to be tested. They were defined in a specific mock-up coordinate system centered at a reference seat H-point located with help of SAE H-point machine (SAE J826) and a FARO arm digitizer. The x-axis was directed backwards, y-axis laterally to the right and z-axis upward. The seat slide angle was fixed at 4°. Then for each pedal configuration, the gear stick was fixed at an average position ([-307 mm; 337 mm; 145 mm] in the mock-up coordinate system). The hand brake was not used for the experiment on clutch pedal.

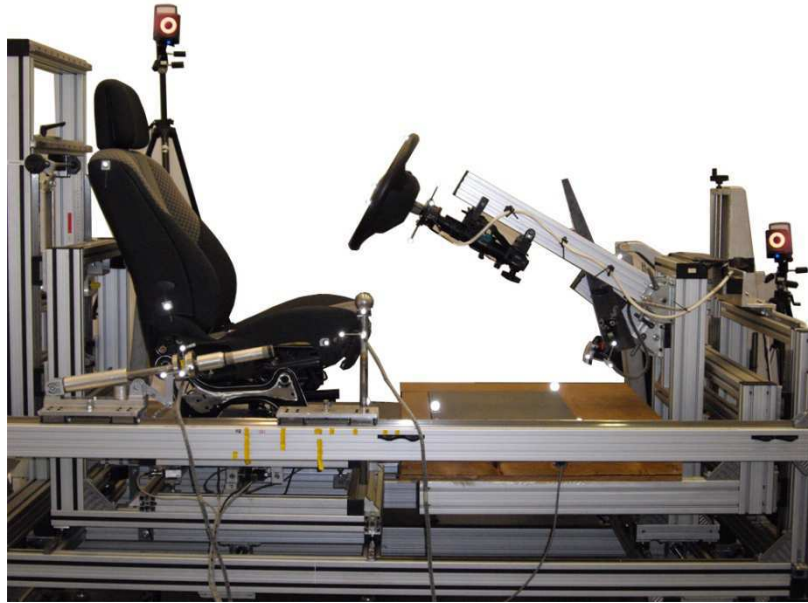


Figure 40: Experimental mock-up for static pedal force exertion experiment

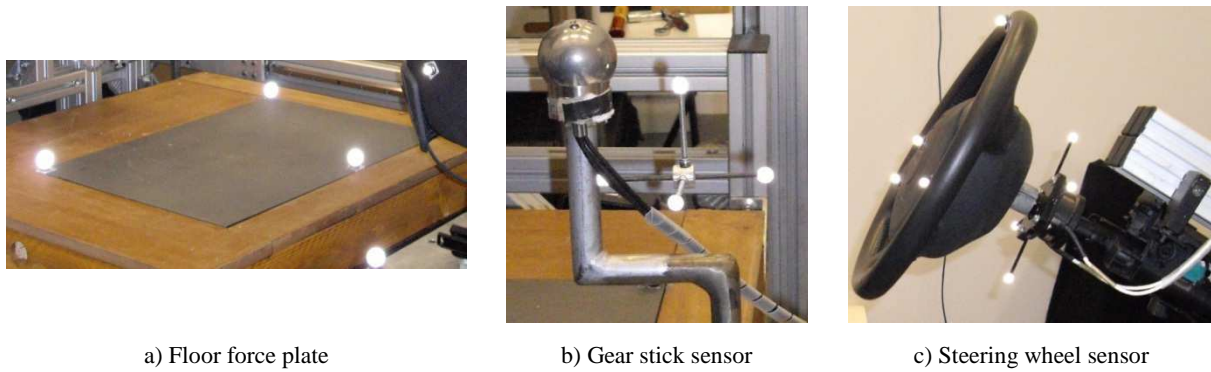
### 2.2.ii Motion capture

The same motion capture system as the one for DHErgo experiment was used (VICON system with ten MX T40 cameras sampling at 100 Hz). Forty two reflective markers were put on the subject. Thirty-five markers were placed on the multi-adjustable mock-up to characterize the geometry, the position of the car elements (seat, steering wheel, clutch pedal, floor ...) and the orientation of the force sensors. The locations of the markers described in Appendix.

### 2.2.iii Force measurements

About the force sensors, the mock-up was equipped with the same pedal force sensor as the one used for the DHErgo experiment to measure the force exertion on the clutch pedal, i.e. a TME 3-axis force sensor with a capacity of 1500 N on each axis. Three other force sensors were also used during force exertion on the pedal:

- A BERTEC force plate on the floor (Figure 41a)
- A gear stick handle shaped TME 3-axis force sensor with a capacity of 1000 N on each axis (Figure 41b)
- A 6-axis force sensor (Denton 2554) between the steering wheel and the steering column (Figure 41c)



a) Floor force plate

b) Gear stick sensor

c) Steering wheel sensor

Figure 41: Sensors for postural adjustment study

All force sensors were synchronized with VICON system and sampling at 1 kHz.

### 2.3 Test conditions

Three clutch pedal configuration were selected by Renault for this study: one for a vehicle with a low seat height (i.e. sports cars or small cars), one for a vehicle with an average seat height (i.e. sedan cars) and a last one for a vehicle with a high seat height (i.e. minivan). For each selected configuration, two positions were tested: the middle of the travel position and end of the travel position. As a consequence, six configurations were considered (Figure 42):

- P1M and P1F were pedal positions respectively at mid-travel and end-travel for a vehicle with a low seat height,
- P2M (mid-travel) and P2F (end-travel) for a vehicle with an average seat height,
- P3M (mid-travel) and P3F (end-travel) for a vehicle with a high seat height.

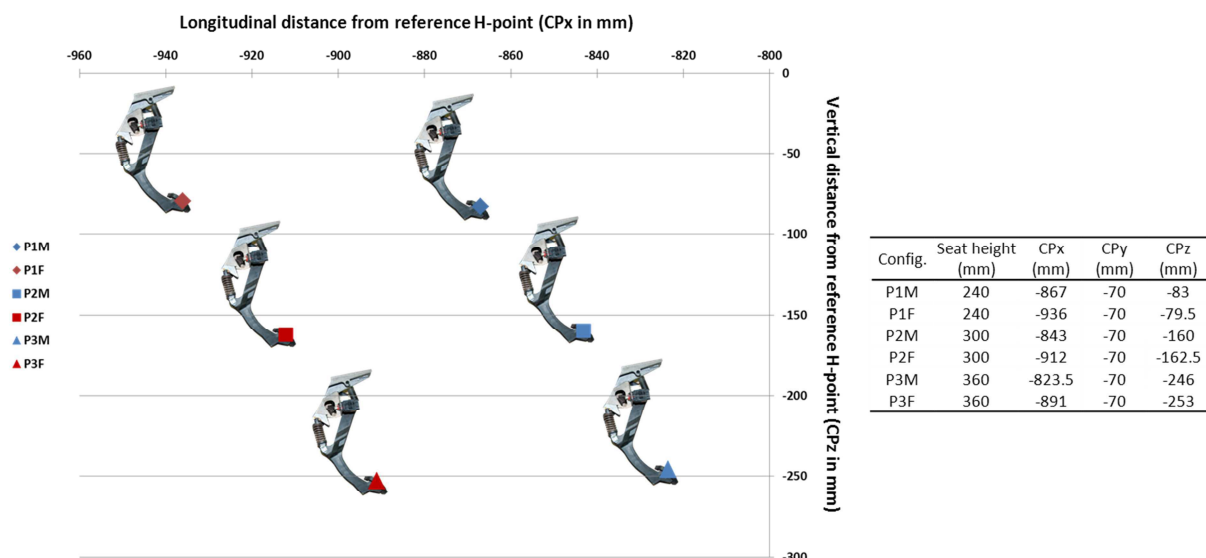


Figure 42: Configuration selected for the static force exertion experiment

The experiment on the clutch pedal was divided in two parts.

- **Maximum force exertion on static clutch pedal (called “ExpMax” in the rest of this study).** In this part of the experiment, the six configurations were tested randomly. For each configuration, a rest trial and then a maximum trial were performed.
- **Force perception on static clutch pedal (called “ExpPcp” in the rest of this study).** For this part of the experiment, only one configuration was tested (P2F) depending on five modalities of force level: very low, low, medium, high, and maximum. The levels were chosen considering the Borg’s CR-10 (Borg, 1998). A rest posture was also measured prior to force perception trials. Each subject performed first two maximum force exertions. A third one was measured if the relative gap between the two trials exceeded 10% of the maximum. Then the four other force level exertions were randomized.

As a result, each subject performed  $6 \times 2 = 12$  trials in ExpMax and 6 (+1 if necessary) trials in ExpPcp, i.e. 18 (+1) trials in total.

## 2.4 Experimental procedure

The experiment began with the measurement of the main subject anthropometric dimensions and the placement of the reflective markers. Photos from two orthogonal views synchronized with a VICON motion capture were recorded on a calibrated throne.

Prior to experimentation, each subject was asked to adjust the seat position longitudinally in a standard driving configuration with respect to the clutch pedal end position corresponding to the position P2F and to the steering wheel but with a seat height fixed at 286 mm. The seat adjustment should be in a specific range defined by Renault. The formula provided gives the position of the seat relative to the reference H-point according to the length of the lower limbs, with a confidence interval of 80%.

$$\Delta H_{ref} = 0.62982 \times L_{MI} - 0.62141 \times D_{HtoBeg} - 58.59$$

With

$L_{MI} = L_{Thigh} + h_{Knee} - 100$ , the length of the lower limb (in mm)

$L_{Thigh}$ , buttock-knee length (see anthropometric measurements in Appendix)

$h_{Knee}$ , knee height sitting (see anthropometric measurements in Appendix)

$D_{HtoBeg} = \|\overrightarrow{(H_{ref}CP_{end})}\|$ , distance from the reference H-point ( $H_{ref}$ ) to the clutch pedal position at end-travel ( $CP_{end}$ ).

Based on the recommendation for measuring muscle strength by Gallagher et al (1998), the subjects were instructed to exert their maximum force (or an intermediate force level) as fast as possible once a red light turning on and to maintain the maximum force until to the light turning off. The force exertion duration was 5 seconds for each trial. Non-verbal encouragement was given during the force exertion. At least two trials were repeated for maximum force measurement. If more than 10% difference between the two repetitions, third measurement was performed. The trial with maximum force level was retained. At least two minutes of rest were imposed between two maximum force trials. For intermediate force levels, at least 40 seconds were proposed. For the left foot pedal operation, the subject was asked to place the left hand on the top left of the steering wheel, the right hand on the gear stick handle, the right foot on the floor and the left foot on the clutch pedal. A special caution was taken on the left heel which should not be in contact with the floor during pedal force exertion. The whole duration of the experiment lasted about four hours and a half. But this duration was for the whole experiment including maximum force exertion and force perception of handbrake and gear stick. The clutch pedal part represented in terms of trials about 20% of the whole experiment.

## 2.5 Data processing

From the FAC project, following data types were available:

- Anthropometric measurements for each participant
- 3D markers trajectories attached on both subjects and mock-up
- Force exertion measurements on the force plate (right foot), the gear stick sensor (right arm), the steering wheel sensor (left arm) and the pedal sensor (left foot).

As this study focused on the pedal force exertion, only the force data from the pedal sensor were considered.

The global workflow of the data processing for inverse kinematic and inverse dynamic motion reconstruction was the same as the one used on the DHErgo experiment data. Please refer to the “data processing” section of the DHErgo experiment for more details. Only the validation of the motion reconstruction and the treatment of the pedal force specific to the FAC project are described in the following parts.

### 2.5.i Pedal force treatment (*ExpMax* and *ExpPcp*)

In the FAC project, the static pedal force was determined using the plateau method. The instruction to participants was to apply a required level of pedal force as rapidly as possible and to maintain it for 5 seconds. The mean value of each trial was calculated from 1.5s to 4.5s. This range was chosen to avoid the loading phase at the beginning of the force exertion and the slackness at the end. An exclusion threshold was defined on the value of the standard deviation of each trial. It was fixed at 70N, which represented 8 trials, i.e. 1.5% of the trials.

### 2.5.ii Pedal force perception (*ExpPcp* only)

In the *ExpPcp* of the FAC project, the force levels were chosen considering the Borg's CR-10 (Borg, 1998). This scale is a category (C) ratio (R) scale in 10 points developed for studying perceived exertion. A power law between the perception level, i.e. the category, and the stimuli, i.e. the magnitude of pedal force, was implicitly assumed. The CR10 also assigns a scalar, i.e. the ratio, to each force level verbal term, which linearizes the power law. Table 33 shows the force level used in the *ExpPcp* with the corresponding scalar. In this study, the linear relation was considered to analyze the pedal force perception law.

Table 33: Categories of the Borg's CR10 for the perceived exertion with the corresponding ratio scalars.

Force level (Category)	Force level (Ratio)
Very low	1
Low	2
Medium	3
High	5
Maximum	10

In order to compare different subjects, the pedal force resultants of each level were also normalized for each subject by his/her maximum force. These normalized pedal forces were used to analyze the pedal force perception of the *ExpPcp*.

## 2.6 Evaluation of reconstructed motions

As for DHErgo experiment, the forces applied by the participants on the seat were not recorded. Moreover, in this experiment, there were no pressure maps to indicate a raw estimation of the contact force between the left thigh and the seat. That's why, only the quality of the kinematic motion reconstruction was assessed.

The visual analysis showed large instabilities of the pelvis for two subjects (09\_RA and 17\_AB). These were due to the complete loss of the markers on the pelvis. Contrary to DHErgo experiment, only two markers were placed on the right and left anterior superior iliac spine. They were missed because of the corpulence of the subjects. Therefore the two subjects were excluded from the analysis.

The mean distance between the recorded marker positions and the reconstructed ones, for all markers and trials was  $9 \pm 3$  mm. The largest differences between the model-based markers' positions and those captured by VICON<sup>®</sup> were obtained for the marker on the left elbow with a mean value of 15.6mm (Figure 43). This error may certainly be due to marker displacement relative to the underlying bone. For instance, the calibration posture for the markers' attachment corresponded to the forearms flexed at 90° whereas the left forearm was almost fully extended in the clutch pedal trials. The other markers showed relatively small residue ( $< 15$  mm on average).

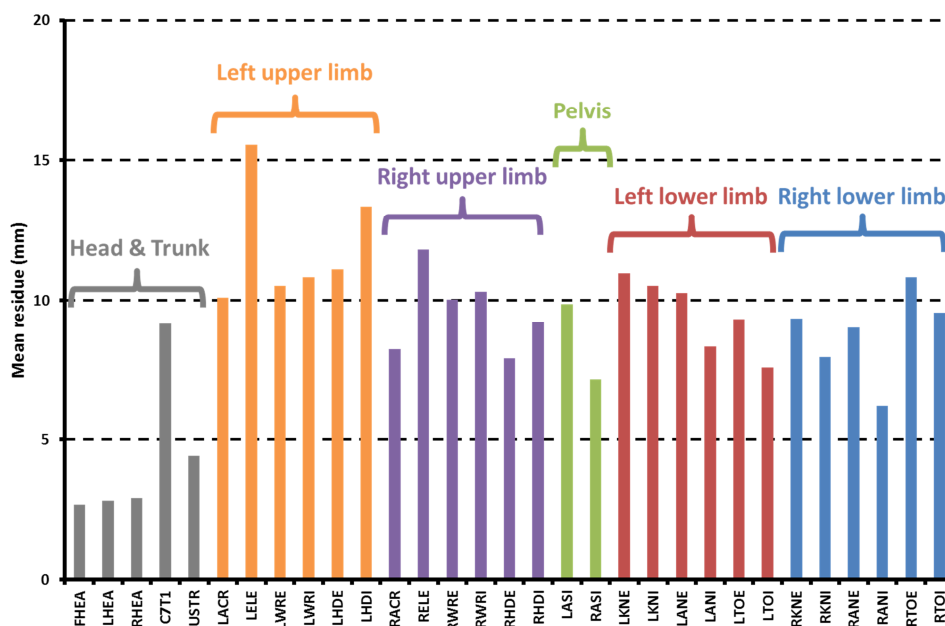


Figure 43: Mean values of markers' residues on all subjects and trials (FAC project). The labeling of the markers was presented in Appendix.

**2.7 Summary of processed data**

<b>FAC project</b>	
<b>Number of participants</b>	30
<b>Anthropometry measurements</b>	21
<b>Clutch pedal trials</b>	12 (maximum pedal force) + 7 (pedal force perception)
<b>Excluded participant</b>	2
<b>Number of reconstructed trials for motion analysis</b>	$28 \times 19 + 8 \times 1$ (3 <sup>rd</sup> maximum) - 8 = 532

### 3 Experimental observations

#### 3.1 Maximum pedal force exertion (*ExpMax*)

In this part of the study, the maximum foot force applied on the pedal at the six pedal positions (P1M, P1F, P2M, P2F, P3M, and P3F) was analyzed. The force resultants, three components (normal, tangential and lateral) and force directions were considered.

##### 3.1.i Pedal force resultant and components

The pedal force resultant was decomposed in three components: tangential, normal and transversal components (Figure 44).

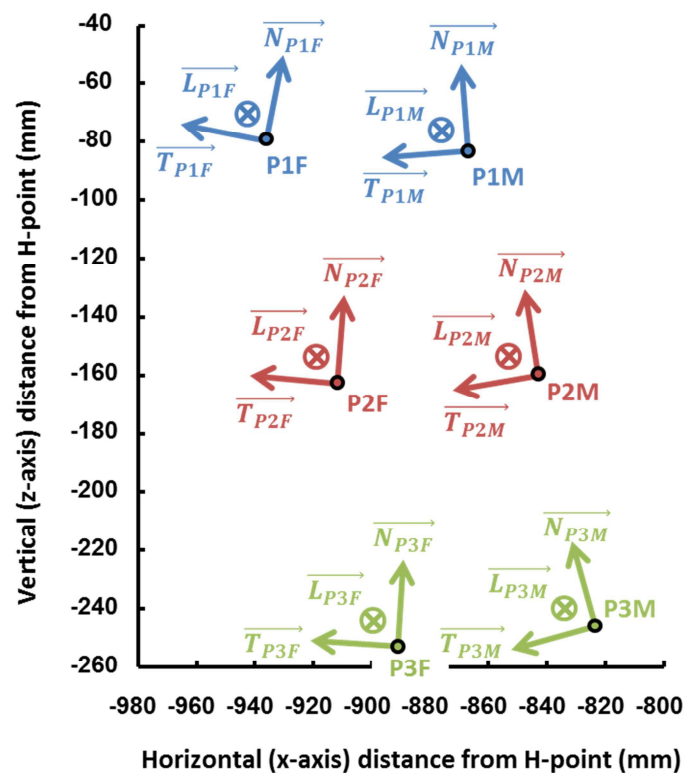


Figure 44: Normal (N), tangential (T) and transversal (L) force components for each pedal position. Pedal positions and force components were defined in the mock-up coordinate system. Z-axis was upward, X-axis was backward and Y-axis was rightward.

The three force components were defined as being tangential, normal and perpendicular to the pedal trajectory. The results are presented in Table 34.

**Table 34: Means and standard deviations of the force resultants and the three components according to pedal position and group of subjects.**

	Resultant (N)	Normal (N)	Tangential (N)	Transversal (N)
P1F	616 ± 269	-279 ± 150	540 ± 237	-49 ± 27
P1M	779 ± 346	-218 ± 114	740 ± 336	-71 ± 40
P2F	631 ± 296	-277 ± 155	560 ± 261	-55 ± 30
P2M	749 ± 314	-185 ± 97	718 ± 305	-70 ± 38
P3F	543 ± 256	-284 ± 159	455 ± 211	-44 ± 34
P3M	677 ± 295	-176 ± 106	646 ± 281	-71 ± 40
Tall men	773 ± 236	-287 ± 103	706 ± 242	-58 ± 37
Average men	729 ± 322	-257 ± 163	669 ± 297	-72 ± 37
Short women	446 ± 254	-145 ± 103	411 ± 244	-49 ± 32
Total	666 <sup>G***, P*</sup> ± 304	-237 <sup>G***, P**</sup> ± 138	610 <sup>G***, P***</sup> ± 289	-60 <sup>G**, P**</sup> ± 37

\*p<0.05, \*\*p<0.01, \*\*\* p<0.001. G: group of subjects; P: pedal position

First, the normal and tangential forces are the main force components. On average, normal, tangential and transversal components were respectively -237 N, 610 N and -60 N. Significant effects of both the group of subjects and the pedal position were found on the force resultant and the three force components. Regarding the effects of pedal position, a lower force resultant was found at the end-travel than at mid travel (Figure 45a). This difference between the end-travel and mid-travel positions can also be observed for tangential and transversal forces. However, the normal components (absolute values) were higher at the end than at mid-travel (Figure 45b), i.e. from -279 N to -284 N for the end-travel positions versus from -176 N to -218 N for the mid-travel positions.

As expected, short women had a force capacity significantly lower than the 2 male groups (Figure 45c). The maximum force resultants were 421 N, 764 N and 772 N on average respectively for short women, average men and tall men. Short women had also significantly lower maximum forces in all three components than the men. Two male groups had almost same force exertion capacity.

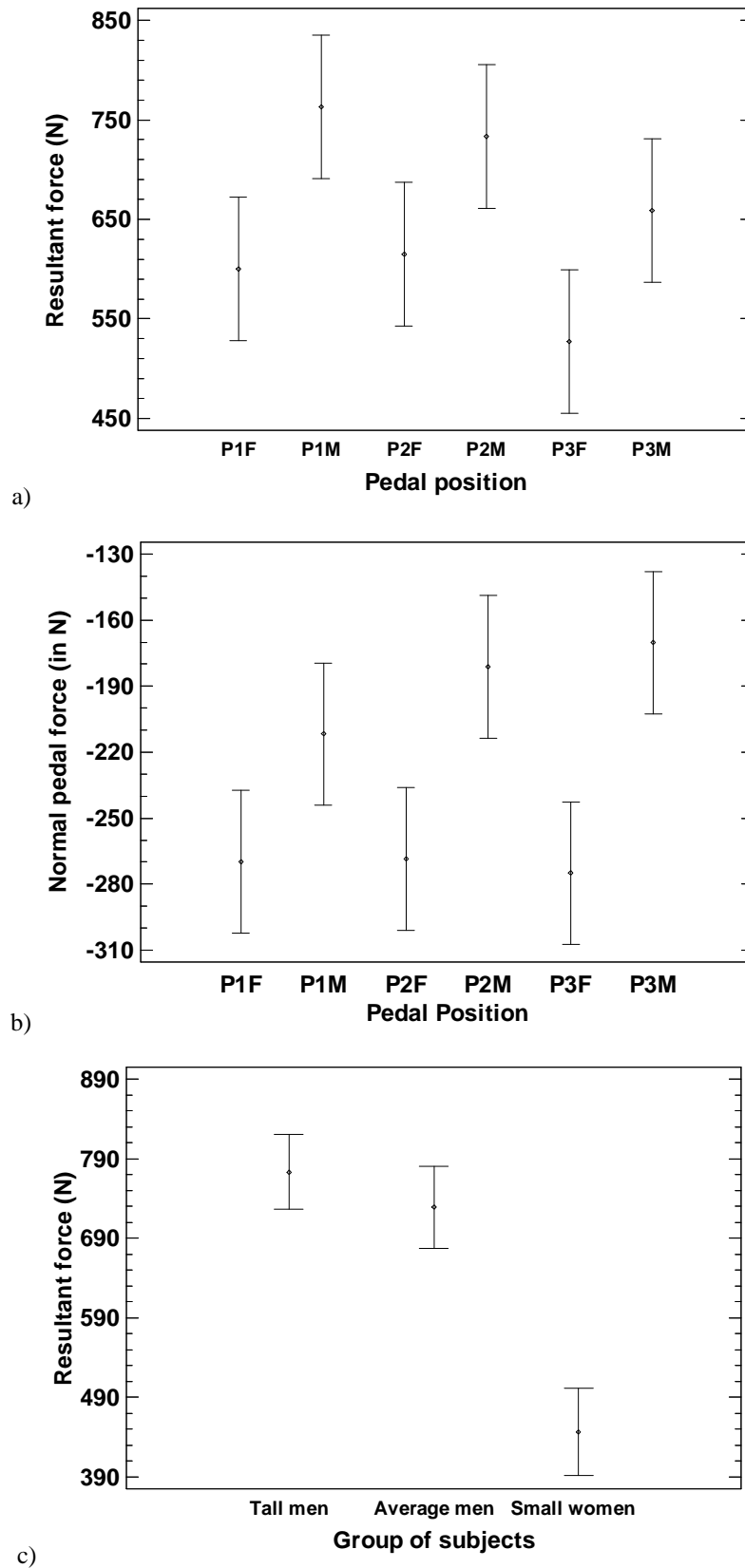


Figure 45: Resultant force mean values in terms of pedal position (a) and of group of subjects (b). Normal force mean values in terms of pedal position (c).

### 3.1.ii Pedal force direction

As for the DHErgo experiment, the pedal force direction was investigated in two ways. First, the direction of the pedal force was analyzed in the XZ plane with respect to the hip-force application point axis. Second, the effect of the lateral component on the pedal force direction was investigated in the plane XY.  $\theta_{F_{Exp}}$ , the pedal force direction in the plane XZ,  $\delta_{F_{Exp}}$  and  $\delta_{Hip/P_{App}}$ , the lateral deviation of respectively the pedal force direction and the Hip- $P_{App}$  axis in the plane XY were defined as for the DHErgo experiment. The results are presented in Table 35.

Table 35: Means and standard deviations of  $\theta_{F_{Exp}}$ ,  $\delta_{F_{Exp}}$  and  $\delta_{Hip/P_{App}}$  for maximum pedal force exertion.

	$\theta_{F_{Exp}}$ (deg)	$\delta_{F_{Exp}}$ (deg)	$\delta_{Hip/P_{App}}$ (deg)
P1F	$-5.8 \pm 7.5$	$4.7 \pm 1.6$	$-1.1 \pm 1$
P1M	$-10.8 \pm 6.4$	$5.5 \pm 1.7$	$-1.5 \pm 0.9$
P2F	$-5.9 \pm 6.8$	$5.4 \pm 2$	$-1.3 \pm 1.1$
P2M	$-11.1 \pm 5.4$	$5.9 \pm 1.9$	$-1.7 \pm 0.9$
P3F	$-5.9 \pm 6.4$	$5 \pm 2.6$	$-1.6 \pm 1.1$
P3M	$-10.8 \pm 5.3$	$6.9 \pm 2.2$	$-1.7 \pm 1.1$
Short women	$-5.9 \pm 7.2$	$6.6 \pm 1.5$	$-2.2 \pm 1.2$
Average men	$-7.4 \pm 5.9$	$6 \pm 1.7$	$-1 \pm 0.9$
Tall men	$-11 \pm 6.1$	$4.4 \pm 2.3$	$-1.4 \pm 0.7$
Total	$-8.4 \pm 6.7^{G***, P***}$	$5.6 \pm 2.1^{G***, P***}$	$-1.5 \pm 1^{G***}$

\* $p < 0.05$ , \*\* $p < 0.01$ , \*\*\*  $p < 0.001$ . G: group of subjects; P: pedal position

$\theta_{F_{Exp}}$  had an average value of  $-8.4^\circ$ . Significant effects of both pedal position and subject group were found. A post-hoc test showed two homogenous groups for the pedal positions: the mid-travel positions (P1M, P2M, and P3M) with an average angle around  $-11^\circ$ , the end-travel positions (P1F, P2F and P3F) with an average angle around  $-6^\circ$ . Short women and average men had similar mean values of  $\theta_{F_{Exp}}$ , respectively  $-5.9^\circ$  and  $-7.4^\circ$ , whereas the tall men had larger average angle, around  $-11^\circ$ .

About the transversal deviation of the pedal force, the main observation is that the subjects did not exert force in the same direction as the Hip- $P_{App}$  axis in the XY plane. Indeed, on average,  $\delta_{F_{Exp}}$  and  $\delta_{Hip/P_{App}}$  were  $5.6^\circ$  and  $-1.5^\circ$ . The hip-force application point axis was oriented slightly rightward whereas the pedal force was oriented leftward (from the driver's point of view). There was significant effect of the group of subjects on  $\delta_{F_{Exp}}$  and  $\delta_{Hip/P_{App}}$ . But the maximum differences between the groups were small. They were respectively  $2.2^\circ$  between short women and tall men for  $\delta_{F_{Exp}}$  and  $1.2^\circ$  between short women and average men

for  $\delta_{Hip/P_{App}}$ . A significant effect of the pedal position was also found on  $\delta_{F_{Exp}}$ . The average maximum difference between the six pedal positions was also small, about  $2^\circ$ .

### 3.2 Intermediate levels of pedal force exertion and force perception (*ExpPcp*)

The pedal force perception was only performed on the pedal position P2F, which was at the end travel position from an average seat height. The subjects were asked to apply a pedal according to five force level terms from the Borg's CR10 scale: very low, low, medium, high and maximum. In the following section, the pedal force resultants and directions were investigated. The values of the pedal force components (tangential, normal and transversal) according to the force level were presented in Appendix. Moreover, the postural adjustment of the subjects according to force level was also investigated.

#### 3.2.i Pedal force resultant

Table 36 shows the means and standard deviations of the force resultant according to the force level for each group of subjects. As expected, the force resultant increased significantly with the force level. Besides, it can be noticed that, as in *ExpMax*, the short women had lower pedal force values for each force level compared to the men. On average, the pedal forces at each force level for the male subjects were two times as high as the short females.

**Table 36: Means and standard deviations of the pedal force resultant according to the force level for the three groups of subjects.**

	Force resultant (N)		
	Short women	Average men	Tall men
Very low	45 ± 21	98 ± 46	90 ± 32
Low	77 ± 57	149 ± 82	141 ± 48
Medium	110 ± 40	255 ± 135	273 ± 126
High	244 ± 134	410 ± 290	462 ± 173
Maximum	407 ± 217	754 ± 319	826 ± 224
All	215 ± 204 <sup>F***</sup>	403 ± 349 <sup>F***</sup>	437 ± 339 <sup>F***</sup>

\*p<0.05, \*\*p<0.01, \*\*\* p<0.001. F: force level

The normalized pedal forces are shown in Table 37 and Figure 46. As expected, the normalized force increased with the force level. No significant effect of the group of subjects was found on for each force level. It suggests that the pedal force perception law based on normalized forces was the same for all subjects.

Table 37: Means and standard deviations of the normalized pedal force (Fnorm).

Fnorm	
Very low	0.13 ± 0.08
Low	0.19 ± 0.11
Medium	0.32 ± 0.13
High	0.53 ± 0.15
Maximum	0.95 ± 0.08
Total	0.51 <sup>F***</sup> ± 0.35

\*p<0.05, \*\*p<0.01, \*\*\* p<0.001. F: force level

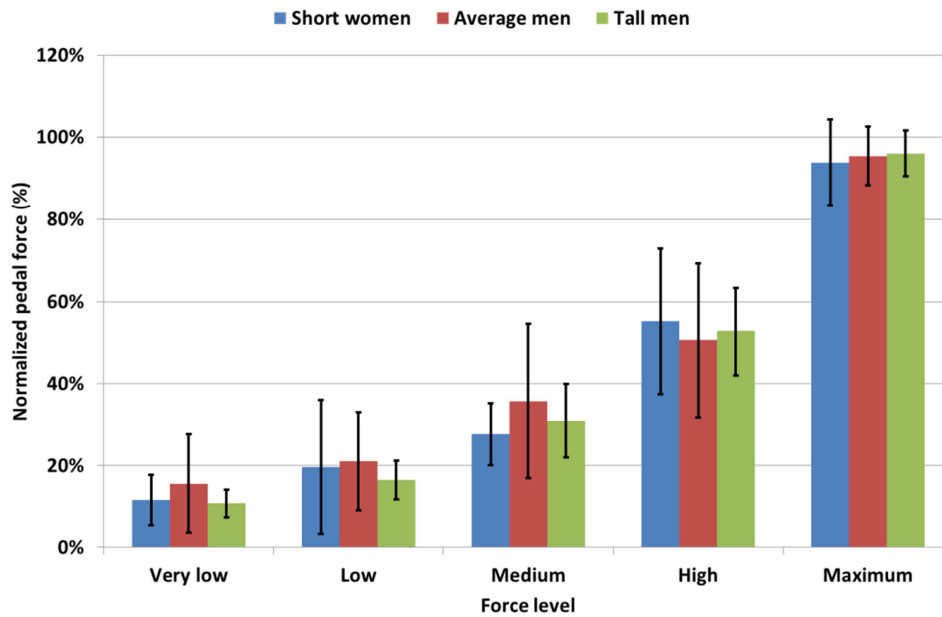


Figure 46: Evolution of the normalized pedal force according to force level for short women, average men and tall men.

By definition, Borg’s CR10 scale assigns a scalar to each force level verbal term so that a numerical relationship between force amplitude and perception. A linear regression of the normalized pedal force according to the CR10’s scalars was performed. The result showed an adjusted R<sup>2</sup> of 91% (Figure 47).

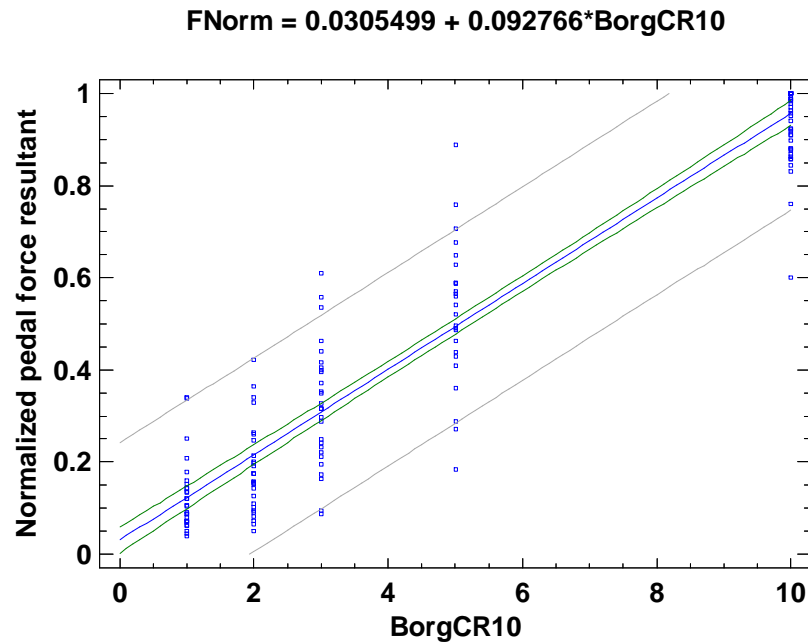


Figure 47: Plot of the fitted model using linear regression ( $R^2=91\%$ ). BorgCR10 correspond to the scalars assigned to force levels in Borg's CR10 scale: Very low=1, Low=2, Medium=3, High=5, Maximum=10.

### 3.2.ii Pedal force direction

As for the analysis of the maximum pedal force exertion,  $\theta_{F_{Exp}}$ , the pedal force direction in the XZ plane was investigated as well as the deviation angles  $\delta_{F_{Exp}}$  and  $\delta_{Hip/P_{App}}$  in the plane XY. The means and standard deviations of  $\theta_{F_{Exp}}$ ,  $\delta_{F_{Exp}}$  and  $\delta_{Hip/P_{App}}$  are presented in Table 38.

Table 38: Means and standard deviations of the Force/hip-ankle axis angle for maximum pedal force exertion.

	$\theta_{F_{Exp}}$ (deg)	$\delta_{F_{Exp}}$	$\delta_{Hip/P_{App}}$
Very low	$-15.1 \pm 8$	$3.3 \pm 3$	$-1.1 \pm 1$
Low	$-12.2 \pm 6.4$	$4 \pm 2.7$	$-1.5 \pm 0.9$
Medium	$-9.5 \pm 6.9$	$4.4 \pm 2.7$	$-1.3 \pm 1.1$
High	$-6.9 \pm 5.5$	$5 \pm 1.9$	$-1.7 \pm 0.9$
Maximum	$-6.7 \pm 5.7$	$5.6 \pm 3$	$-1.6 \pm 1.1$
Short women	$-7.1 \pm 6.6$	$6 \pm 2.3$	$-2.5 \pm 0.9$
Average men	$-8.5 \pm 7.1$	$4.7 \pm 2.1$	$-1.5 \pm 0.9$
Tall men	$-12.1 \pm 6.7$	$3.6 \pm 2.6$	$-1.6 \pm 0.8$
Total	$-9.5 \pm 7.1^{G***, F***}$	$4.7 \pm 2.6^{G***, F***}$	$-1.8 \pm 1^{G***, F***}$

\* $p < 0.05$ , \*\* $p < 0.01$ , \*\*\*  $p < 0.001$ . G: group of subjects; F: force level

Significant effects of both the force level and the group of subjects were found on  $\theta_{F_{Exp}}$ ,  $\delta_{F_{Exp}}$  and  $\delta_{Hip/P_{App}}$ . It can be observed that absolute value of  $\theta_{F_{Exp}}$  decreased with the level of force, from  $-15.1^\circ$  on average for very low force level to  $-6.7^\circ$  on average for maximum

force level. This means that the pedal force direction got closer to the Hip-P<sub>App</sub> axis when increasing force level. On average, short women had also pedal force direction closer to the Hip-P<sub>App</sub> axis than the men with an average angle of  $-7^\circ$  versus  $-8.5^\circ$  and  $-12.1^\circ$  for respectively average and tall men.

About the transversal deviation of the pedal force, the subjects did not exert force in the same direction as the Hip-P<sub>App</sub> axis in the XY plane. On average  $\delta_{F_{Exp}}$  and  $\delta_{Hip/P_{App}}$  were  $4.7^\circ$  (leftward direction in driver's point of view) and  $-1.8^\circ$  (rightward direction in driver's point of view) for respectively. This observation is the same as in the analysis of maximum pedal force exertion. Moreover  $\delta_{F_{Exp}}$  increased with the force level but the maximum difference was only  $2.3^\circ$ . For  $\delta_{Hip/P_{App}}$ , the effect of force level was also significant but the maximum difference between the mean values was only  $0.6^\circ$ .

### **3.2.iii Postural adjustment**

The aim of this part of the analysis of pedal force perception was to look at how posture changed according to force level. As in DHErgo experiment analysis, whole body motions were reconstructed by an inverse kinematic procedure using the kinematic model of RAMSIS™ manikin. Postures of a digital human model (DHM) are fully described by a set of joint angles. Thanks to visual inspection, it was observed that the subjects tended to rise up from the seat when increasing force level. Consequently, the postural adjustment was estimated first by considering the displacement of the pelvis joint GHZ of RAMSIS™ manikin according to the force level, and then by considering the lower joint angles.

#### **Pelvis displacement**

The displacement of the pelvis on x-, y- and z-axis of the mock-up coordinate system was calculated for each subject and each force level with respect to a rest posture recorded prior to the session of the force perception trials.

The means and standard deviations of the pelvis displacement on x-, y- and z-axis for each group of subjects according to the force level are summarized in Appendix. Both force level and group of subjects had significant effects on the postural adjustment. Table 39 shows the pelvis displacements for all subjects for each force level.

Table 39: Means standard deviations of pelvis displacement on x-, y- and z-axis according to force level for all subjects.

	X-axis (mm)	Y-axis (mm)	Z-axis (mm)
Very Low	$-0.6 \pm 5.1$	$-0.2 \pm 8.8$	$3.6 \pm 7.5$
Low	$2.5 \pm 8.7$	$-0.9 \pm 8.1$	$5.1 \pm 8.2$
Medium	$5.2 \pm 8.5$	$0.3 \pm 8.9$	$8.2 \pm 8.5$
High	$11.2 \pm 11.7$	$3 \pm 10.1$	$14.4 \pm 11.1$
Maximum	$15.8 \pm 14.5$	$7.1 \pm 11.1$	$27.4 \pm 12.7$

Globally, it can be noticed that the subjects mainly adjusted their posture by moving the pelvis back and up. A small lateral displacement, less than 10 mm on average, on the right can also be observed. Figure 48 illustrates the pelvis displacement on each axis for the three groups of subjects. The same tendency can be observed, especially for the pelvis displacement on z-axis. On x-axis, short women tended to less move backward than the men. Moreover, they also tended to move forward for very low and low force level with respective average displacements on x-axis of -2.5 mm and -2 mm.

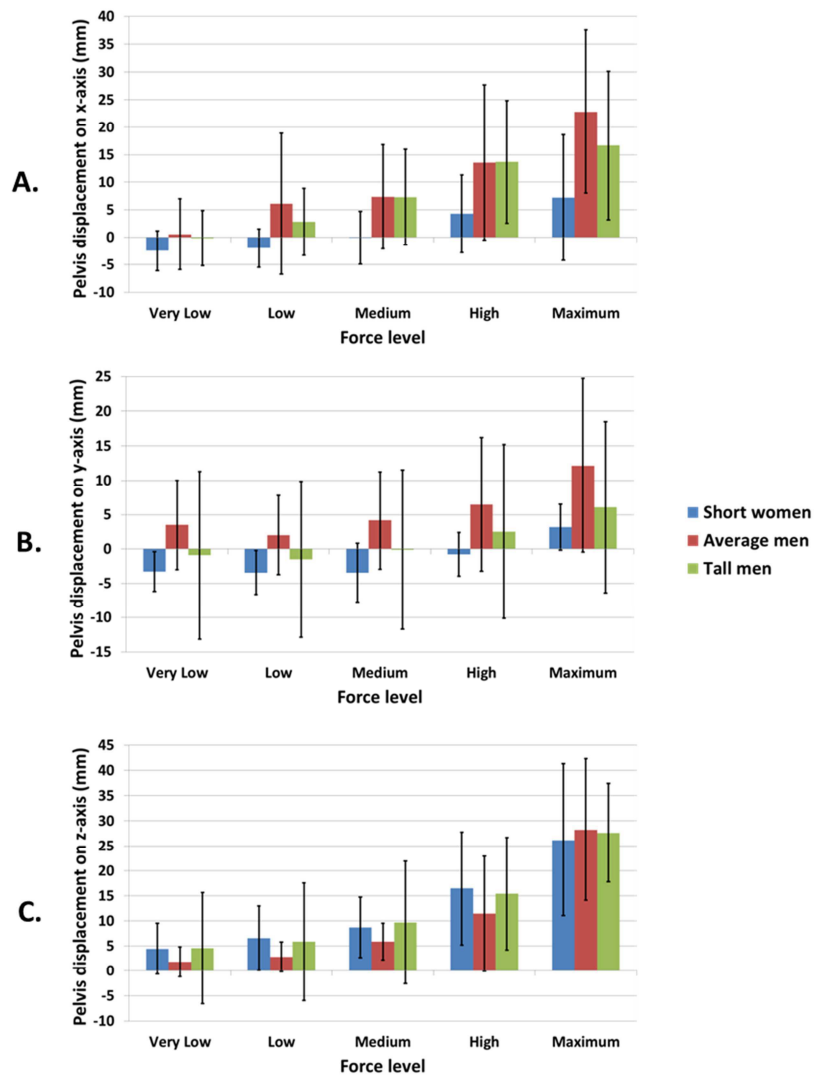


Figure 48: Pelvis displacement on x-axis (A.), y-axis (B.) and z-axis (C.) according to the force levels for short women, average men and tall men.

## Joint angle variations

The variations in joint angles of the left lower limb were then analyzed. As the subjects adjusted their posture by moving the hip backward, upward and rightward, four joint angles were considered:

- Hip, knee and ankle flexion/extension angles which should explain backward and upward postural adjustment,
- Hip adduction/abduction angle which should explain rightward adjustment.

The means and standard deviations of these four joint angles for each group of subjects according to the force level are summarized in Appendix (Table 51 to Table 54). The force level affected significantly these four joint angles, especially for the knee flexion/extension angles. The group of subjects had only an effect on hip and knee flexion/extension angles. Table 40 shows the means and standard deviations of hip abduction/adduction angle, hip, knee and ankle flexion/extension angles for all subjects according to the force level.

**Table 40: Means and standard deviations of hip abduction/adduction angle, hip, knee and ankle flexion/extension angles for all subjects according to the force level. Ab/Ad = Abduction/Adduction, F/E = Flexion/Extension.**

	Hip Ab/Ad (deg.)	Hip F/E (deg.)	Knee F/E (deg.)	Ankle F/E (deg.)
Rest	5.2 ± 5.7	58.3 ± 13.9	48 ± 8.3	65.7 ± 5.4
Very Low	4.9 ± 5.5	57.9 ± 11.5	46.7 ± 8.4	67 ± 5.6
Low	5.5 ± 5.6	55.9 ± 14.1	46 ± 8.7	65.4 ± 6.9
Medium	5.6 ± 5	55.6 ± 11.9	43.5 ± 9.1	64.6 ± 5.9
High	6.2 ± 5.3	52.9 ± 11.7	41.1 ± 9.6	63.4 ± 6.9
Maximum	8.5 ± 6.3	48.8 ± 11.1	35.8 ± 10	62.7 ± 5.6

First, it can be observed that the hip adduction increased significantly only at the maximum force level. For the intermediate force levels, the mean value of the abduction/adduction angle is between 5-6°, whereas it increased at 8.5° when at the maximum force level. Nevertheless the variation of this angle in function of force level is small with a maximum gap about 3.6° on average. The flexion/extension angles of the hip, knee and ankle joints decreased with force level. Their changes were -9.5°, -12.2° and -3° respectively for hip, knee and ankle from the rest to maximum force postures, showing that the subjects extended their left leg with the increase of force level. Among the three joints of the lower limb, high angle variations were observed for hip and knee. The ankle flexion/extension angle did not vary much with the increase of force level. Concerning the effects of subject group, it can also be noticed that the hip and knee flexion/extension angles of short women were significantly smaller than the men (Figure 49). It means that short women had their left leg significantly more extended than the men.

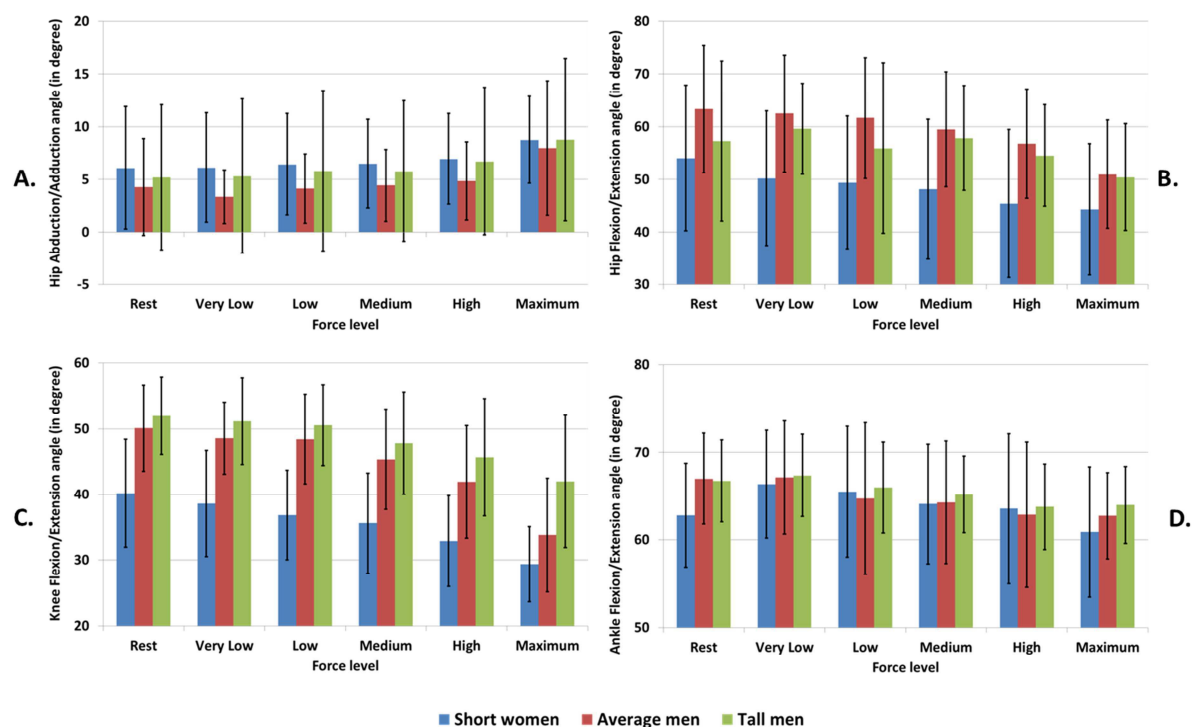


Figure 49: Hip abduction/adduction (A.), hip flexion/extension (B.), knee flexion/extension (C.) and ankle flexion/extension (D.) angles according to force level for short women, average men and tall men.

## 4 Discussion

The main observations of the analysis of the maximum pedal force exertion and the pedal force perception can be summarized as:

- Maximum pedal force exertion had higher mean values for mid-travel pedal positions than for end-travel pedal positions. Pedal force direction was closer to the Hip-Force application point axis (Hip- $P_{App}$  axis) for end-travel pedal positions than for mid-travel pedal positions.
- Short women had on average less force capacity than the men as expected. They had an average force direction closer to the Hip- $P_{App}$  axis.
- The pedal force perception law depended only on the normalized pedal force but not on group of subjects in agreement the CR10 model of perceived force exertion of Borg,
- Pedal force direction tended to get closer to the Hip- $P_{App}$  axis when the force level increased,
- Maximum and intermediate pedal force exertion were directed leftward from the driver's point of view whereas the Hip- $P_{App}$  axis were directed little rightward,

- Subjects adjusted their posture by moving the pelvis backward, upward and slightly rightward with the increase of the force level,
- Postural adjustment process when changing force exertion level mainly involved the change in hip and knee flexion/extension angles.

The analysis of the maximum pedal force exertion showed that globally the force exerted on the mid-travel pedal positions were higher than the force exerted on the end-travel position. This may be explained by the muscle force depends on the muscle length and therefore on the angle of the joint it acts on (Kroemer, 1999). Active muscle force or muscle tension, i.e. muscle force due to muscle contraction, is maximal when the muscle is at its resting length or optimal length (Figure 50). The active muscle force decreases when the muscle is shorten or elongated. Then the muscles cannot provide maximal force when a joint get in a position close to the upper or lower limit of its ROM. Thus, the joint strength decreases.

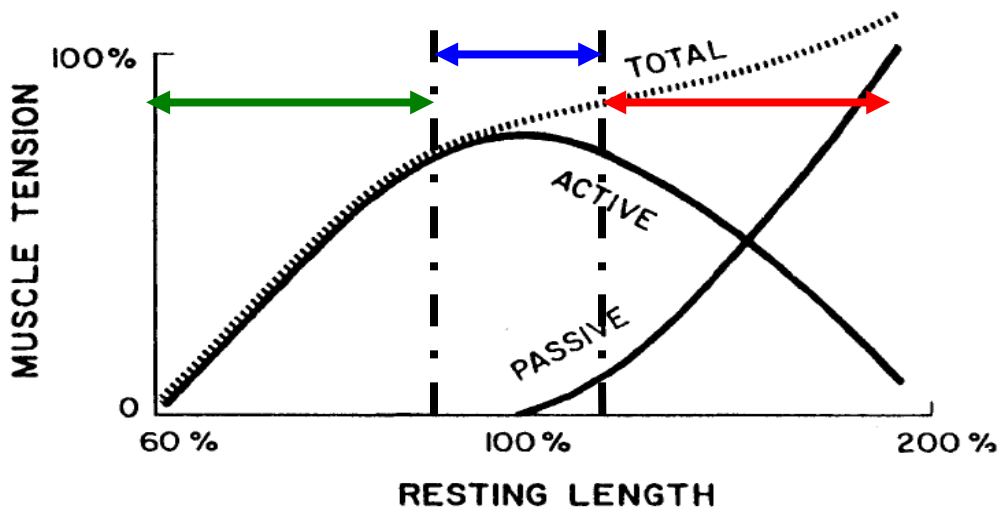


Figure 50: Active, passive and total tension within a muscle at different lengths (Kroemer, 1999).

As a consequence, in case of pedal force exertion, the subjects had globally a more flexed leg for the mid-travel position and therefore had higher force capacity (see in Appendix for hip, knee and ankle flexion/extension angles). This may also explain the significant difference of pedal force direction between mid-travel and end-travel positions. Indeed, Figure 51 shows an average pedal force direction and left lower limb posture in the XZ plane for a pedal positioned at mid-travel (plain) and end-travel (transparent).

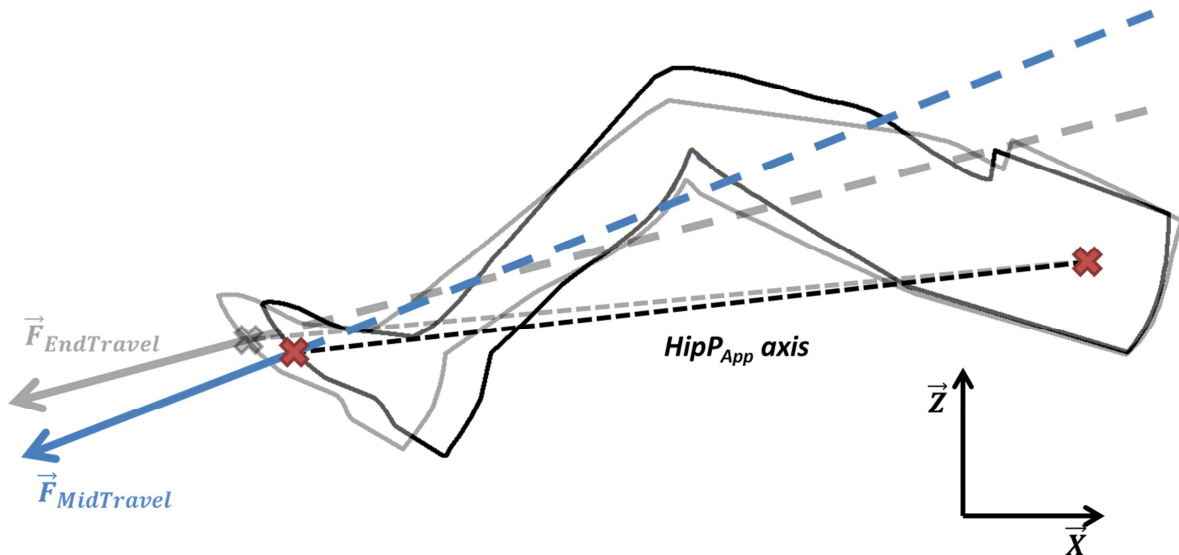


Figure 51: Comparison of pedal force direction for a pedal at mid-travel position (plain) and at end-travel position (transparent).

The mid-travel posture was mainly characterized by a higher flexion of the hip and knee joints than the end-travel posture. Ankle flexion/extension angle stayed rather the same. As a consequence, the knee was further from the Hip- $P_{App}$  axis for mid-travel pedal position than for end-travel position. Therefore in order to decrease the knee torque, the pedal force direction had to move towards the knee joint. Therefore, this explains a larger average angle  $\theta_{F_{Exp}}$  at mid-travel pedal position. This relation between posture and force direction may also explain the effect of the group of subjects, and thus effects of the anthropometry. Indeed, the tall men had globally a more flexed lower limb than the other subject groups. This could explain at least partly why they also had the highest flexion/extension angles for hip and knee. On the opposite, the short women had a less flexed lower limb and so smallest angles values flexion/extension angle mean values for hip and knee (see in Appendix for hip, knee and ankle flexion/extension angles).

It was found that the pedal force direction tended to get closer to the Hip $P_{app}$  axis when the force level increased. Two explanations could be suggested. First a postural adjustment was found with the increase of the force level and the subjects tended to extend the left leg, especially by extension of the hip and the knee. Therefore, the knee joint was closer to the hip-force application point axis, thus reducing the angle between the force direction and the hip- $P_{app}$  axis. Another explanation could be that people more tended to reduce the joint load as the force level increased.

About the postural adjustment, the subjects tended to move the hip backward, upward and slightly rightward when increasing force level in agreement with the variation in joint angles.

The postural adjustment could be explained by the need of reducing the joint load when increasing force exertion level, because the moment arms of the pedal force at the knee and hip were reduced by extending the leg.

Finally, for all force levels, pedal force exertion was directed leftward whereas the Hip-P<sub>app</sub> axis was oriented rightward. For the Hip-P<sub>app</sub> axis, it can be noticed that the mean angle  $\delta_{Hip/P_{app}}$  between  $-1^\circ$  and  $-2^\circ$ , which means that this axis was on average almost parallel to the x-axis of the mock-up reference frame. The orientation of the pedal force on the left was in agreement with the orientation observed in the DHErgo experiment. Moreover the leftward deviation of the pedal force increased with the force level. Results from both FAC and DHErgo experiments suggested that there may be a preferred pedal force direction directed leftward. This could be resulted from the small displacement of the pelvis on the right when increasing the force level.

In summary, the hypothesis of minimizing joint loads seems to explain not only the pedal force exertion control as already suggested by Wang et al. (2000), but also the postural adjustment.

## 5 Pedal force control simulation

In what follows, we'll verify if this hypothesis is valid for different anthropometric dimensions, pedal positions and force levels. Moreover, the biomechanical model proposed by Wang et al. (2000) analyzed the pedal direction in 2D whereas a 3D approach should be used in the present study as the transversal forces being hardly negligible. It should also be interesting to see whether or not the lateral deviation of the pedal force could also be explained by minimizing joint torques. As the postural adjustment and the force direction control seem to be strongly connected, two simulation problems were defined:

- Simulation of the force direction with a given posture for a given pedal (imposed tangential force) [Sim1]
- Simulation of the posture with an imposed pedal force (both force resultant and direction are imposed) [Sim2]

For both simulation problems, the minimization of joint torques as objective function can be formulated as:

$$\text{Minimize } G = \sum_{Joint} \sum_{DoF} \left( \frac{T_{Joint}^{DoF}}{(T_{Joint}^{DoF})_{Max}} \right)^2 \quad (\text{Eq. 3})$$

With

$$Joint = \{Hip, Knee, Ankle\}$$

$$DoF = \{Abduction/Adduction (AA), Flexion/Extension (FE), Axial rotation (R)\}$$

$T_{Joint}^{DoF}$  is the moment projected on a joint rotation axis (DOF) for a joint. The three lower limb joints (hip, knee and ankle) were considered in the optimization. The kinematic model of the lower limb has 7 DoFs. However, two joint torques were not considered in the objective function:  $T_{Knee}^{AA}$  the knee moment in abduction/adduction and  $T_{Ankle}^R$  the ankle moment in axial rotation, because they were not supposed to contribute to the motion and the force exertion. The joint torque can be computed as:

$$\overrightarrow{T}_{Joint} = \begin{bmatrix} T_{Joint}^{AA} \\ T_{Joint}^{FE} \\ T_{Joint}^R \end{bmatrix} = \overrightarrow{O}_{Joint} P_{App} \times \overrightarrow{F}_{Pedal} - \overrightarrow{O}_{Joint} P_{App} \times \overrightarrow{F}_{Rest} \quad (\text{Eq. 4})$$

With

$O_{Joint}$ , joint center

$P_{App}$ , force application point

$F_{Pedal}$ , pedal force vector

$F_{Rest}$ , pedal force in the rest posture, i.e. the contribution of the weight of the leg on the pedal

In the joint torque calculation (Eq. 4), the pedal force recorded at rest position was considered as the action of the body weight on the pedal. Consequently, its contribution to the joint torque, considered as passive, was removed in order to keep only the active contribution of the force exerted on the pedal. The computed joint torques were normalized in the objective function (Eq. 3) using maximum joint torque values  $(T_{Joint}^{DoF})_{Max}$  from the literature (see in Appendix).

As a result, the objective function G can be expressed as (Eq. 5):

$$G = \sum_{Joint} \sum_{DoF} \left( \frac{T_{Joint}^{DoF}}{(T_{Joint}^{DoF})_{Max}} \right)^2 = \left( \frac{T_{Hip}^{AA}}{(T_{Hip}^{AA})_{Max}} \right)^2 + \left( \frac{T_{Hip}^{FE}}{(T_{Hip}^{FE})_{Max}} \right)^2 + \left( \frac{T_{Hip}^R}{(T_{Hip}^R)_{Max}} \right)^2 + \dots$$

$$\left( \frac{T_{Knee}^{FE}}{(T_{Knee}^{FE})_{Max}} \right)^2 + \left( \frac{T_{Knee}^R}{(T_{Knee}^R)_{Max}} \right)^2 + \left( \frac{T_{Ankle}^{AA}}{(T_{Ankle}^{AA})_{Max}} \right)^2 + \dots$$

$$\left( \frac{T_{Ankle}^{FE}}{(T_{Ankle}^{FE})_{Max}} \right)^2 \quad (\text{Eq.5})$$

### 5.1 Simulation of the pedal force direction [Sim1]

The goal in Sim1 is to find the force direction that minimizes the joint torques caused by the pedal force. In this problem, observed postures for a pedal position as well as the pedal force in the rest posture were used as inputs for simulation. Therefore,  $\overrightarrow{O_{Joint}P_{App}}$  and  $\overrightarrow{F_{Rest}}$  in Eq. 4 were constants. The unknown in Sim1 is the pedal force  $\overrightarrow{F_{Sim}}$  and is constrained as:

$$\overrightarrow{F_{Pedal}} = \overrightarrow{F_{Sim}} = \begin{bmatrix} F_{Sim}^{Normal} \\ F_{Sim}^{Transversal} \\ F_{Sim}^{Tangential} \end{bmatrix} \text{ so that } F_{Sim}^{Tangential} = F_{Exp}^{Tangential}$$

The problem in Sim1 can be summarized as:

$$\text{Find } F_{Sim}^{Normal} \text{ and } F_{Sim}^{Transversal} \text{ so as to minimize } G \text{ (Eq.5)}$$

The simulation was performed using the Matlab<sup>®</sup> function *fmincon*. Simulated and experimental force directions were compared in Figure 52 and Figure 53 for both ExpMax and ExpPcp. The values of simulated pedal force directions, normal and transversal forces are presented in Appendix (Table 58 and Table 59).

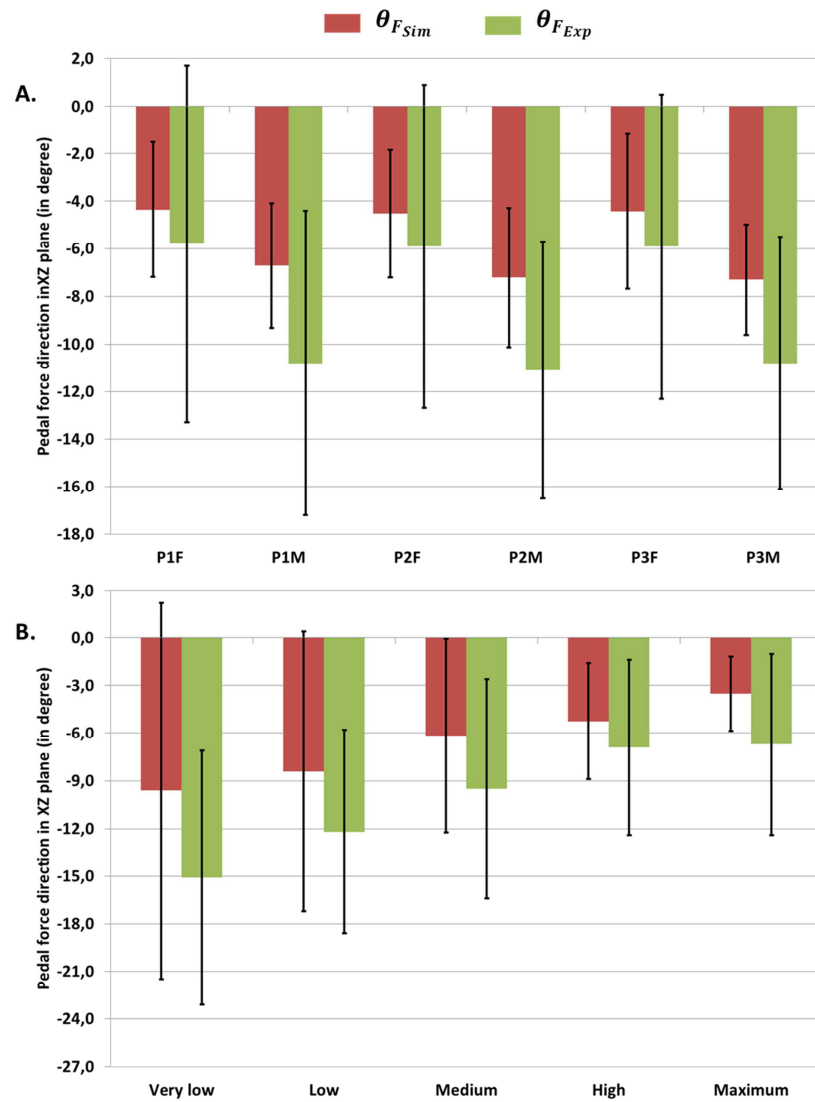


Figure 52: Means and standard deviations of experimental and simulated pedal force direction in XZ plane (respectively  $\theta_{F_{Exp}}$  and  $\theta_{F_{Sim}}$ ) for (A) maximum pedal force exertion experiment and (B) pedal force perception experiment.

Regarding the pedal force direction in the XZ plane, experimental observations  $\theta_{F_{Exp}}$  and simulations  $\theta_{F_{Sim}}$  had the same tendencies. For ExpMax trials, simulated pedal force direction ( $\theta_{F_{Sim}}$ ) was closer to the Hip-P<sub>app</sub> axis at mid-travel positions than at end-travel positions. Short women had an average force direction closer to the Hip-P<sub>app</sub> axis. For ExpPcp trials, pedal force direction tended to get closer to the HipP<sub>app</sub> axis when the force level increased. Globally, the simulated pedal directions were closer to the Hip-P<sub>App</sub> than the experimental ones. The gaps between simulated and experimental force directions were from 5.5° for very low force level to between 1° and 2° for the end-travel pedal positions. Note that the gap between simulated and experimental force directions was larger for the short women and the tall men, between 3° and 5°, than for the average men, about 1°.

Regarding the lateral deviation in XY plane, the simulation predicted a rightward (in the driver's point of view) lateral deviation whereas the experimental data showed a leftward lateral deviation. This is particularly obvious in case of maximum pedal force exertion. For the pedal force perception experiment, the simulation and experimental data agreed for very low and low force levels as well as for the average lateral deviation of short women.

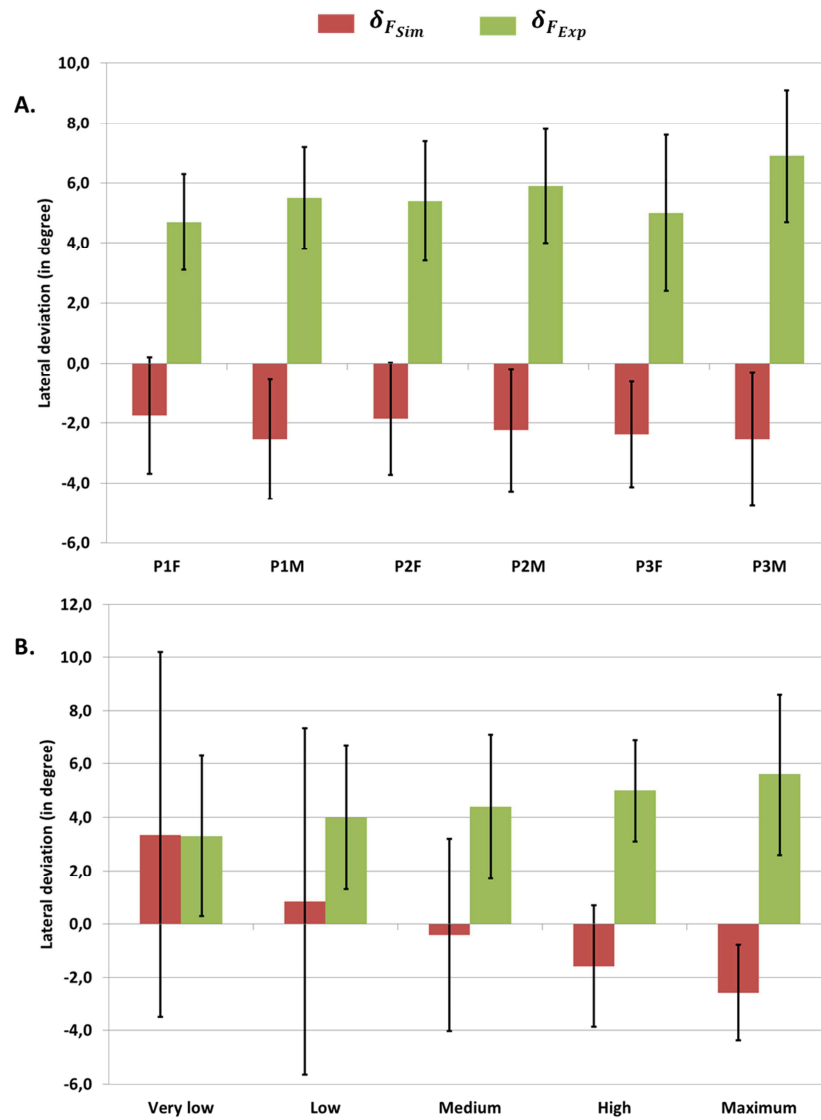


Figure 53: Means and standard deviations of experimental and simulated pedal force lateral deviation in XY plane (respectively  $\delta_{F_{Exp}}$  and  $\delta_{F_{Sim}}$ ) for (A) maximum pedal force exertion experiment and (B) pedal force perception experiment.

## 5.2 Simulation of the postural adjustment [Sim2]

The goal of the algorithm Sim2 is to find the postural adjustment that minimizes the joint torques generated by an imposed pedal force. Compared to the problem of Sim1, the pedal force, the pedal position and the pedal force in the rest posture were constants in Sim2 and the unknown variable was the posture. From experimental data, it was found that the subjects adjusted their postures according to the force level by moving the pelvis backward and upward. The main simulation issue is to manage the contacts between the seat and the subject, especially the contacts trunk/backrest and thigh/seat. Ideally, a surface-surface contact model should be used. But such data were not available in the FAC project. Some simplifying hypotheses were therefore made:

- Hyp. 1 – Displacement in the sagittal plane: Experimentally, the rightward displacement of the pelvis was found weaker than the back- and up-displacements. It was decided to consider only the back- and up displacement in the sagittal plane in the simulation.
- Hyp. 2 – Constraints on the displacement: In order to consider the contact between the seat backrest and the subject's trunk, it was hypothesized that the displacement was following a line in the sagittal plane. The ratio  $\frac{\Delta x}{\Delta z}$  in the simulation was estimated using the mean value of the same ratio from experimental data, i.e.  $\frac{\Delta x}{\Delta z} = \tan 35^\circ$ . Besides  $\Delta x$  and  $\Delta z$  were constrained as positive in order to avoid displacement into the seat.
- Hyp 3 – Displacement of the hip joint: in order to limit the number of DoFs in the simulation, it was considered that the pelvis was translating without any rotation and so that the displacement of the left hip joint in the sagittal plane was close to the pelvis's one.
- Hyp. 4 – Minimization of the hip displacement: by definition, the minimization of the joint torques aims at adjusting the posture in order to get a Hip- $P_{App}$  axis as close as possible to the pedal force direction regardless to the pedal force magnitude. Consequently, a term regarding the minimization of the hip displacement was added to the objective function in order to consider the need of reducing the pressure between body and seat when moving the pelvis.

The problem in Sim2 can be summarized as Eq. 6:

$$Find \overrightarrow{\Delta Hip} = \begin{bmatrix} \|\overrightarrow{\Delta Hip}\| * \sin 35^\circ \\ 0 \\ \|\overrightarrow{\Delta Hip}\| * \cos 35^\circ \end{bmatrix} \text{ such that}$$

$$\min H(\overrightarrow{\Delta Hip}) = \min \left( \omega_{JT} * \sum_{Joint} \sum_{DoF} \left( \frac{T_{Joint}^{DoF}(\overrightarrow{\Delta Hip})}{(T_{Joint}^{DoF})_{Max}} \right)^2 + \omega_{Dis} * \left( \frac{\|\overrightarrow{\Delta Hip}\|}{(\|\overrightarrow{\Delta Hip}\|)_{Max}} \right)^2 \right)$$

$\omega_{JT}$  and  $\omega_{Dis}$  are the weight coefficients attributed respectively to the minimization of the joint torques and to the minimization of the hip displacement in the objective function H. In this study, it was considered that the minimization of the joint torques had priority on the minimization of the displacement and the following values for the weights were chosen:  $\omega_{JT} = 1$  and  $\omega_{Dis} = 1/2$ . Moreover it was decided to limit the displacement of the hip joint as:  $(\|\overrightarrow{\Delta Hip}\|)_{Max} = 100$  mm. Actually, the maximum displacement observed experimentally was around 85 mm. The limit value in the simulation was fixed at 100mm in order not to constrain the results.

As for Sim1, Matlab<sup>®</sup> function *fmincon* was used. But contrary to Sim1, Sim2 required another optimization to solve the minimization problem. Indeed, the displacement of the left hip joint induces necessarily a change in the hip, knee and ankle joint angles in order to keep the contact foot/pedal. It also causes a change in the position of the hip, knee and ankle joint centers, which are necessary to compute the joint torques in Eq. 6. This is a typical inverse kinematics problem. 7 DoFs were considered in the kinematic model as in Sim1 and the position of the target was considered in 3D. The inverse kinematics problem was therefore under-constrained (more variables than unknowns) and was solved using a classic iterative resolution based on the Jacobian pseudo-inverse. At each iteration, the joint limits were verified. If a joint angle was at its limit, the corresponding DoF was blocked, i.e. the value of the joint angle was fixed at its limit values. Then the column of the Jacobian matrix corresponding to the blocked DoF is nullified and the Jacobian pseudo-inverse is recomputed. The joint angles are then computed and the distance between the target and the end-effector is updated. The joint limits values from RAMSIS<sup>™</sup> were considered, which were based according to Kapandji (1994) (see in Appendix).

The inverse kinematics problem can be formalized as:

For a given  $\overrightarrow{\Delta Hip}$  (from minimization of joint torques),

*Initialization*

$$\overrightarrow{O_{Hip}} = (\overrightarrow{O_{Hip}})_{Rest} + \overrightarrow{\Delta Hip}, \quad \overrightarrow{O_{Knee}} = (\overrightarrow{O_{Knee}})_{Rest} + \overrightarrow{\Delta Hip},$$

$$\overrightarrow{O_{Ankle}} = (\overrightarrow{O_{Ankle}})_{Rest} + \overrightarrow{\Delta Hip},$$

$$\{\theta_{Joint}^{DoF}\} = \{\theta_{Joint}^{DoF}\}_{Rest} = \{\theta_{Hip}^{AA}, \theta_{Hip}^R, \theta_{Hip}^{FE}, \theta_{Knee}^R, \theta_{Knee}^{FE}, \theta_{Ankle}^{AA}, \theta_{Ankle}^{FE}\}_{Rest},$$

$$\varepsilon = \|\overrightarrow{P_{Foot}P_{App}}\| \text{ (Distance between the foot point } P_{Foot} \text{ and the pedal application point } P_{App}\text{)}$$

If  $\|\overrightarrow{O_{Hip}P_{App}}\| \leq L_{Thigh} + L_{Shank} + L_{Foot}$  (sum of the lengths of thigh, shank and foot)

While  $\varepsilon_i > 1 \text{ mm}$ ,

Compute the jacobian matrix  $J(\{\theta_{Joint}^{DoF}\}_i)$

Compute the pseudo-inverse jacobian matrix  $J^+$

Check the joint limits

Compute  $\{\theta_{Joint}^{DoF}\}_{i+1}$  as  $\{\theta_{Joint}^{DoF}\}_{i+1} = \{\theta_{Joint}^{DoF}\}_i + J^+ \varepsilon_i$

Compute  $\varepsilon_{i+1}$

End while

Therefore the double optimization of Sim2 can be illustrated as in Figure 54.

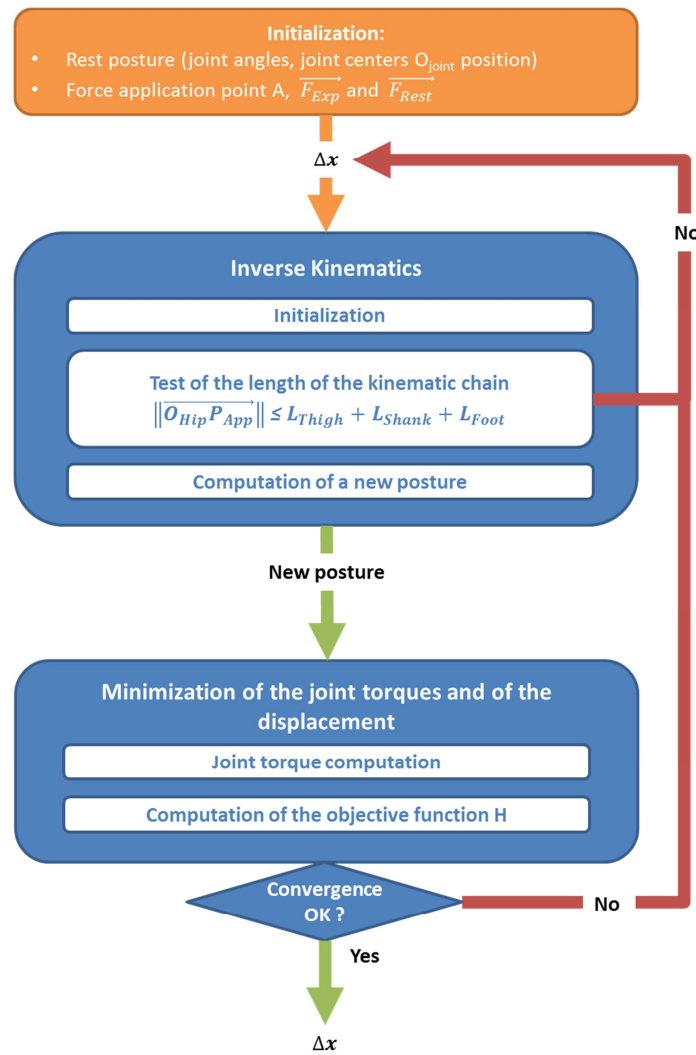


Figure 54: Structure of the double optimization algorithm for the simulation of the postural adjustment.

Globally, the same magnitudes of hip displacement were found by simulation when compared to experimental data (Table 41). In x-axis, the displacement mean value was 8.1 mm in the simulation versus 7.1 mm in the experiment. In z-axis, the mean values were 11.5 mm and 12.2 mm respectively in the simulation and in the experiment. Interestingly, simulation correctly predicted that hip displacement increased with force level.

Table 41: Comparison of the postural adjustments on x- and z- axis for experiment and simulation. Means and standard deviations are presented.

	$\Delta_{Exp}^z$ (mm)	$\Delta_{Exp}^x$ (mm)	$\Delta_{Optim}^z$ (mm)	$\Delta_{Optim}^x$ (mm)
Very low	3.6 ± 7.5	-0.6 ± 5.1	0.6 ± 0.4	0.4 ± 0.3
Low	5.1 ± 8.2	2.5 ± 8.7	0.7 ± 0.7	0.5 ± 0.5
Medium	8.2 ± 8.5	5.2 ± 8.5	3.6 ± 8.4	2.5 ± 6
High	14.4 ± 11.1	11.2 ± 11.7	11.7 ± 16.3	8.2 ± 11.4
Maximum	27.4 ± 12.7	15.8 ± 14.5	26.3 ± 23.3	18.4 ± 16.3
All	12.2 <sup>1***</sup> ± 14	7.1 <sup>1***</sup> ± 12	11.5 <sup>1***</sup> ± 18.9	8.1 <sup>1***</sup> ± 13.2

\*p<0.05, \*\*p<0.01, \*\*\* p<0.001. F: force level

Table 42 shows the simulated and the experimental flexion/extension joint angles according to the force level. The simulation gives quite good prediction of the three main joint angles.

**Table 42: Means and standard deviations of hip, knee and ankle flexion/extension angles for all subjects according to the force level in the simulation of postural adjustment (Sim2) and in the pedal force perception experiment (ExpPcp). F/E = Flexion/Extension.**

	ExpPcp (deg.)			Sim2 (deg.)		
	Hip F/E	Knee F/E	Ankle F/E	Hip F/E	Knee F/E	Ankle F/E
Very low	58 ± 12	47 ± 8	67 ± 6	58 ± 14	48 ± 8	66 ± 5
Low	56 ± 14	46 ± 9	65 ± 7	58 ± 14	48 ± 8	66 ± 5
Medium	56 ± 12	44 ± 9	65 ± 6	58 ± 14	47 ± 9	65 ± 5
High	53 ± 12	41 ± 10	63 ± 7	56 ± 15	44 ± 11	65 ± 5
Maximum	49 ± 11	36 ± 10	63 ± 6	53 ± 15	39 ± 11	63 ± 5

Other joint angles (hip abduction/adduction and axial rotation, knee axial rotation and ankle abduction/adduction) were almost kept unchanged as expected (Table 43), because the displacement of the hip joint was constrained on line in the sagittal plane.

**Table 43: Means and standard deviations of hip abduction/adduction and axial rotation, knee axial rotation and ankle abduction/adduction angles for all subjects according to the force level in the simulation of postural adjustment (Sim2). R = axial rotation, A/A = Abduction/Adduction.**

	Hip R (deg.)	Hip A/A (deg.)	Knee R (deg.)	Ankle A/A (deg.)
Very low	-13,2 ± 8,5	5,1 ± 5,7	0 ± 6,7	-1,6 ± 4,1
Low	-13,2 ± 8,5	5,1 ± 5,7	0 ± 6,7	-1,6 ± 4,1
Medium	-13,2 ± 8,5	5 ± 5,8	-0,1 ± 6,7	-1,5 ± 4,1
High	-13,5 ± 8,4	4,6 ± 5,8	0,2 ± 6,5	-1,3 ± 4
Maximum	-13,2 ± 8,5	5 ± 5,8	-0,1 ± 6,7	-1,5 ± 4,1

### 5.3 Discussions of the two simulation methods

In summary, the results of Sim1 and Sim2 confirm the hypothesis of minimization of joint torque for pedal force direction control and postural adjustment when changing force level. However, Sim1 predicted a rightward (in the driver's point of view) lateral deviation whereas the experimental data showed a leftward lateral deviation.

The analysis of the results of both simulation problems (pedal force direction control and postural change with force level) showed some limitations.

First the simulation of the pedal force direction in the XZ plane showed a mean difference of about 3° between the simulated and the experimental directions. This difference resulted from the underestimation of the normal component of the pedal force (see in Appendix). Although

the normal component is not useful to move the pedal, it can control the force direction in order to minimize the joint torques. This underestimation of the normal component might be a consequence of the objective function of the optimization, which aimed to minimize the joint moments generated by the pedal force. The pedal force at rest position was considered as the contribution of the lower limb weight and was thus not considered in the calculation of the moments. But the seat-thigh contact forces were unknown in the FAC project. The video recordings suggested that this contact existed. In fact, the seat-thigh contact forces were partly considered in the computation of the joint torques in the simulations. Figure 55 shows respectively the forces exerted by the left lower limb at rest position (Figure 55a) and when pressing the pedal (Figure 55b).

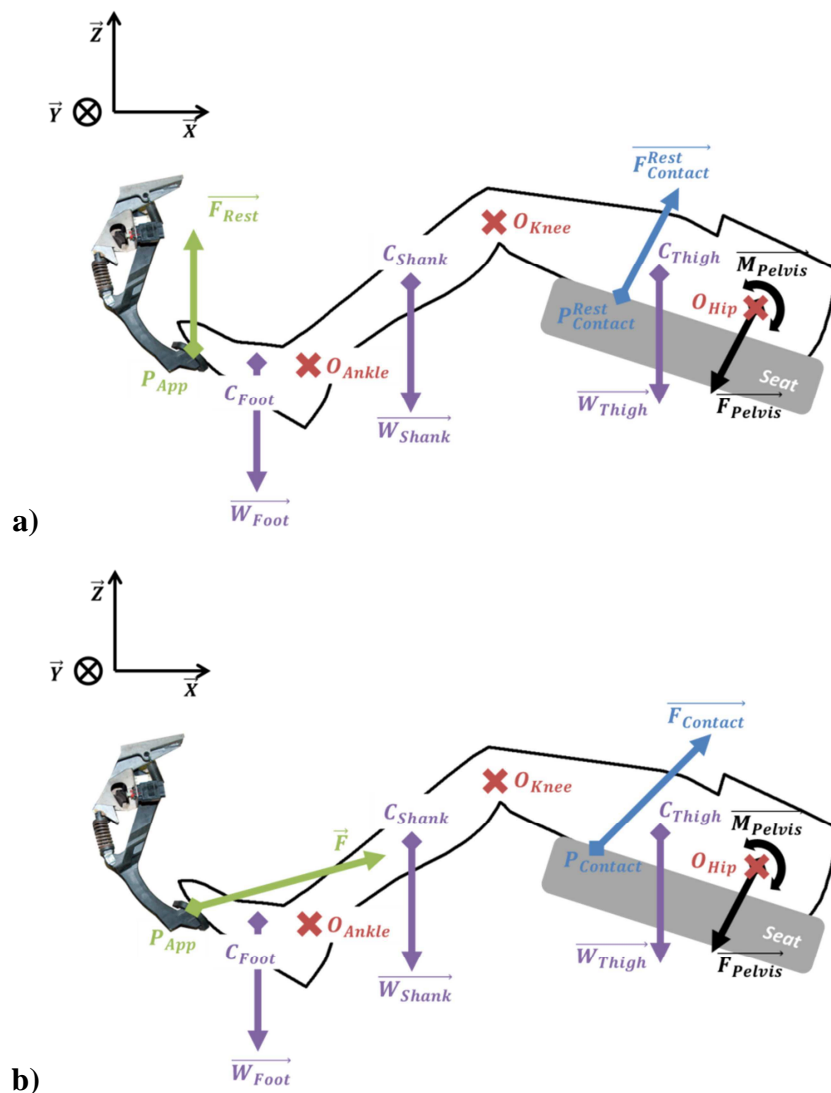


Figure 55: Forces exerted on the left lower limb at rest position (a) and when pressing the pedal (b).  $\vec{W}_{Foot}$ ,  $\vec{W}_{Shank}$  and  $\vec{W}_{Thigh}$  represent respectively the weights of the foot, the shank and the thigh.  $C_{Hip}$ ,  $C_{Knee}$  and  $C_{Ankle}$  represent the centers of mass of their respective body segments.  $O_{Hip}$ ,  $O_{Knee}$  and  $O_{Ankle}$  represent the joint centers.  $\vec{F}_{Rest}$  and  $\vec{F}$  represent the pedal force respectively at rest position and when pressing the pedal applied at  $P_{App}$ .  $\vec{F}_{Contact}^{Rest}$  and  $\vec{F}_{Contact}$  represent the seat/thigh contact force at rest position and when pressing the pedal. These contact forces are respectively applied at the points  $P_{Contact}^{Rest}$  and  $P_{Contact}$ .  $M_{Pelvis}$  and  $\vec{F}_{Pelvis}$  represent the moment and force applied on the pelvis.

For hip, knee and ankle joints, the joint moments  $\overrightarrow{M_{Joint}^{Rest}}$  and  $\overrightarrow{M_{Joint}}$  respectively at rest position and when pressing the pedal can be formalized as:

For hip,

$$\begin{aligned}\overrightarrow{M_{Hip}^{Rest}} &= \overrightarrow{O_{Hip}P_{App}} \times \overrightarrow{F^{Rest}} + \overrightarrow{O_{Hip}C_{Foot}} \times \overrightarrow{W_{Foot}} + \overrightarrow{O_{Hip}C_{Shank}} \times \overrightarrow{W_{Shank}} \\ &\quad + \overrightarrow{O_{Hip}C_{Thigh}} \times \overrightarrow{W_{Thigh}} + \overrightarrow{O_{Hip}P_{Contact}^{Rest}} \times \overrightarrow{F_{Contact}^{Rest}} \\ \overrightarrow{M_{Hip}} &= \overrightarrow{O_{Hip}P_{App}} \times \vec{F} + \overrightarrow{O_{Hip}C_{Foot}} \times \overrightarrow{W_{Foot}} + \overrightarrow{O_{Hip}C_{Shank}} \times \overrightarrow{W_{Shank}} + \overrightarrow{O_{Hip}C_{Thigh}} \\ &\quad \times \overrightarrow{W_{Thigh}} + \overrightarrow{O_{Hip}P_{Contact}} \times \overrightarrow{F_{Contact}}\end{aligned}$$

For knee,

$$\begin{aligned}\overrightarrow{M_{Knee}^{Rest}} &= \overrightarrow{O_{Knee}P_{App}} \times \overrightarrow{F^{Rest}} + \overrightarrow{O_{Knee}C_{Foot}} \times \overrightarrow{W_{Foot}} + \overrightarrow{O_{Knee}C_{Shank}} \times \overrightarrow{W_{Shank}} \\ \overrightarrow{M_{Knee}} &= \overrightarrow{O_{Knee}P_{App}} \times \vec{F} + \overrightarrow{O_{Knee}C_{Foot}} \times \overrightarrow{W_{Foot}} + \overrightarrow{O_{Knee}C_{Shank}} \times \overrightarrow{W_{Shank}}\end{aligned}$$

For ankle,

$$\begin{aligned}\overrightarrow{M_{Ankle}^{Rest}} &= \overrightarrow{O_{Ankle}P_{App}} \times \overrightarrow{F^{Rest}} + \overrightarrow{O_{Ankle}C_{Foot}} \times \overrightarrow{P_{Foot}} \\ \overrightarrow{M_{Ankle}} &= \overrightarrow{O_{Ankle}P_{App}} \times \vec{F} + \overrightarrow{O_{Ankle}C_{Foot}} \times \overrightarrow{P_{Foot}}\end{aligned}$$

Then, the joint torques computed  $\overrightarrow{T_{Hip}}$ ,  $\overrightarrow{T_{Knee}}$  and  $\overrightarrow{T_{Ankle}}$  in the simulation can be expressed as:

$$\begin{aligned}\overrightarrow{T_{Hip}} &= \overrightarrow{O_{Hip}P_{App}} \times \vec{F} - \overrightarrow{O_{Hip}P_{App}} \times \overrightarrow{F^{Rest}} \\ &= \overrightarrow{M_{Hip}} - \overrightarrow{M_{Hip}^{Rest}} - \left( \overrightarrow{O_{Hip}P_{Contact}} \times \overrightarrow{F_{Contact}} - \overrightarrow{O_{Hip}P_{Contact}^{Rest}} \times \overrightarrow{F_{Contact}^{Rest}} \right) \\ \overrightarrow{T_{Knee}} &= \overrightarrow{O_{Knee}P_{App}} \times \vec{F} - \overrightarrow{O_{Knee}P_{App}} \times \overrightarrow{F^{Rest}} = \overrightarrow{M_{Hip}} - \overrightarrow{M_{Hip}^{Rest}} \\ \overrightarrow{T_{Ankle}} &= \overrightarrow{O_{Ankle}P_{App}} \times \vec{F} - \overrightarrow{O_{Ankle}P_{App}} \times \overrightarrow{F^{Rest}} = \overrightarrow{M_{Hip}} - \overrightarrow{M_{Hip}^{Rest}}\end{aligned}$$

As a consequence, by removing  $F_{Rest}$ , the effect of the contact between the seat and the thigh was partly removed. However, the computation of hip joint torque in the simulation did not take into account the possible increase of the contact forces with the force level. Therefore this increase would have an effect on the hip moment calculation.

Secondly, then the simulation of pedal direction for average men showed better results than the other groups. This could be due to the fact that the maximum isometric joint torque values used in the algorithm were average values based on Chaffin et al. (1999) for the flexion/extension torques, on Delp (1990) for the other degrees of freedom. The data from Chaffin et al. (1999) were average values from experimental data collection whereas the data from Delp (1990) were based the performance of his musculoskeletal model of an average

man. Globally, the data used did not take into account the gender, the age or the anthropometry of the subjects. It could explain why the results are better for the average men. Thirdly, the differences in the lateral deviation in the XY were found between the simulation and the experiment. Indeed, the simulation predicted a rightward (in the driver's point of view) lateral deviation whereas the experimental data showed a leftward lateral deviation. To evaluate the behavior of the simulation, the distance of the left knee to the vertical plane containing the Hip-P<sub>App</sub> axis was computed (Table 44).

**Table 44: Means and standard deviations of the distance of the left knee to the vertical plane containing the HipP<sub>App</sub> axis for maximum pedal force exertion trials (a) and pedal force perception trials (b). Negative distance means that the knee was positioned leftward compared to the HipP<sub>App</sub> axis. Positive distance means that the knee was positioned rightward compared to the HipP<sub>App</sub> axis.**

a)	Distance Knee/HipP <sub>App</sub> axis (mm)	b)	Distance Knee/HipP <sub>App</sub> axis (mm)
P1F	-24,8 ± 29,3	Very low	-22,5 ± 25,7
P1M	-40,5 ± 36,0	Low	-24,2 ± 25,9
P2F	-24,9 ± 26,2	Medium	-24,5 ± 23,6
P2M	-33,9 ± 31,9	High	-25,2 ± 26,7
P3F	-26,8 ± 25,2	Maximum	-20,4 ± 23,1
P3M	-31,4 ± 29,1	Short women	-36,9 ± 27,0
Short women	-50,2 ± 28,3	Average men	-22,1 ± 16,8
Average men	-29,0 ± 24,2	Tall men	-4,1 ± 13,0
Tall men	-4,6 ± 13,2	Total	-22,9 ± 24,5
Total	-30,4 ± 29,9		

For both maximum pedal force exertion and pedal force perception trials, the average knee distance was negative, meaning that the knee was positioned leftward compared to the HipP<sub>App</sub> axis. In order to minimize the hip abduction/adduction and axial rotation torques, the pedal reaction force had also to be directed leftward compared to the HipP<sub>App</sub> axis. As a consequence, the force applied on the pedal was directed rightward in the simulation (Figure 56). The results of the simulation were therefore consistent with the posture and the criterion of optimization, i.e. minimization of the joint torques.

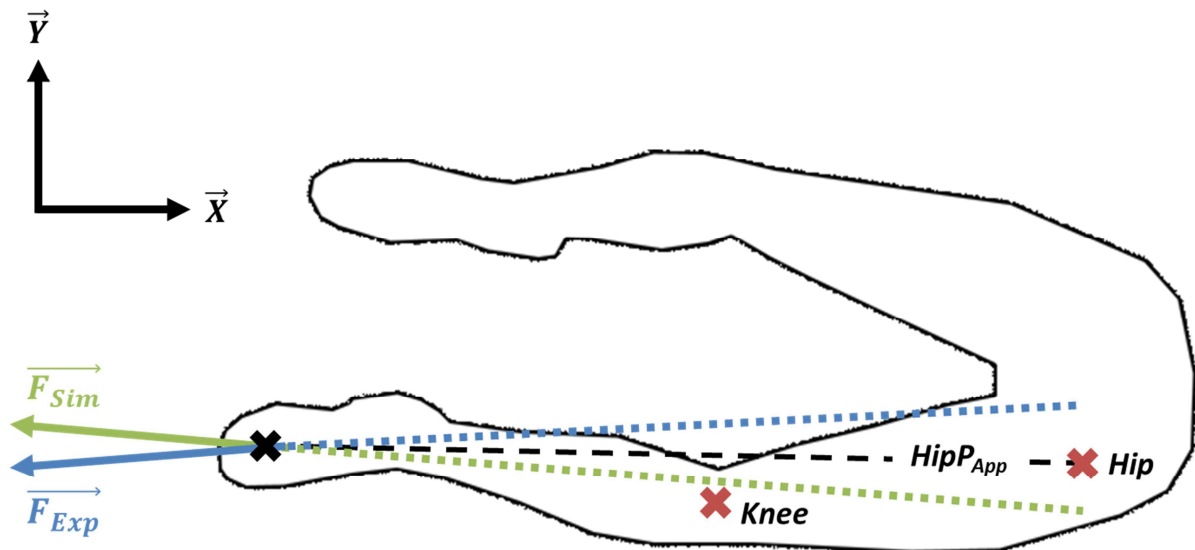


Figure 56: Pedal force direction in the XY plane for FAC project (blue) and simulation (green).

This suggests that the minimization of the joint torques cannot explain the lateral deviation of the pedal force but only the force direction in the XZ plane. This is also in agreement with the hypothesis of a preferred pedal force direction, considered in the previous analysis of the lateral deviation of pedal force in the FAC project data. An explanation of this preferred pedal force direction could be anatomical. Indeed, the anatomy of the hip joint may suggest that a pedal force applied rightward could generate more stresses on the femur neck than a force applied leftward. However, this hypothesis could not be verified with a rigid body model.

Finally the simulation of the postural adjustment showed mean values of the hip joint displacement in x-axis and z-axis of the same magnitude as in experimental data, especially for “high” and “maximum” force level. For the force level from “very low” to “medium”, the simulated hip displacement was smaller than experimental observation. To simulate the postural adjustment according to the force level, the terms corresponding to the minimization of joint torques and to the minimization of the displacement in the objective function were weighted and the same values were used for every force levels. The fact that the magnitude of the simulated displacements close to the experimental one for “high” and “maximum” force level but inferior to the experiment for “very low” to “medium” force level may suggest that the weighting coefficients between minimization of the joint torques and minimization of the hip displacement might depend on force level. A more realistic modeling of the contact forces between body and seat should be considered in future.

## 6 Conclusion

The analysis of maximum pedal force exertions showed that higher forces were exerted for mid-travel pedal positions than for en-travel pedal positions. The more extended the leg is, the closer to the Hip- $P_{App}$  axis the pedal force direction. Pedal force capacities were also found dependent on the gender. On the opposite, pedal force perception law did not depend on the group of subjects but only on normalized force level. With the increase of the force level, all subjects adjusted their posture by moving the pelvis backward, upward and slightly rightward and the pedal force direction tended to get closer to the Hip $P_{app}$  axis. Maximum and intermediate force levels pedal force exertion were directed leftward in the driver's point of view whereas the Hip $P_{app}$  axis were directed little rightward.

The present work illustrates that the hypothesis of minimization of the joint torques suggested by Wang et al. (2000) was able to explain the contribution of the normal force component to control the pedal force direction. The simulation of the pedal force direction also showed that the lateral deviation of the pedal force was not explained by this criterion of minimization. This preferred pedal force direction in the XY plane has to be controlled by other mechanisms and needs further investigation. Then the simulation of the postural adjustment showed that the minimization of the joint torques explained the displacements observed experimentally. This simulation also showed that the postural adjustment was the result of a compromise between reducing the joint load and displacing the pelvis, especially for the intermediate force levels. The multi-objective function used in the simulation suggested that the need of reducing the joint load may increase with the force exertion level.

Finally, this study demonstrates the strong relationship between, posture, force capacity and force direction. This study also shows the need of a more realistic modeling the contacts with seat (seat-thigh contact and back-backrest contact).

## 7 Appendix

### 7.1 Measurement chain for FAC project

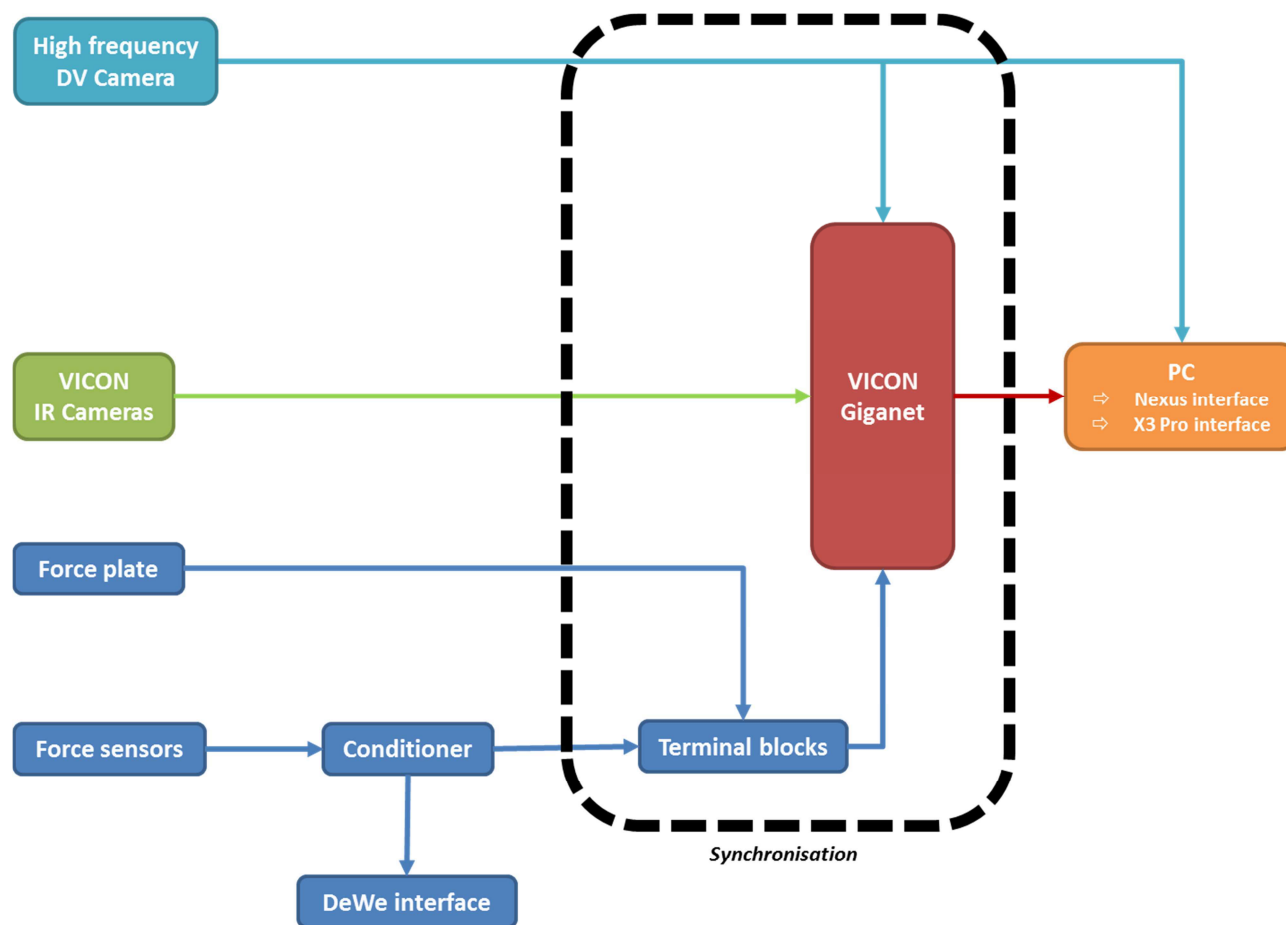
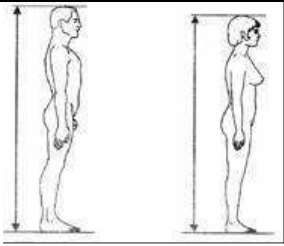
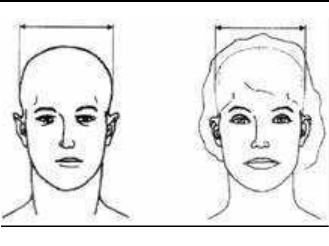
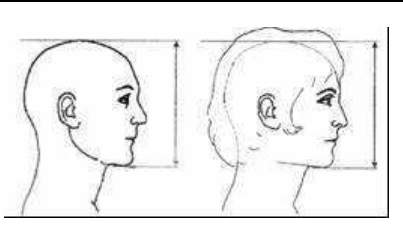
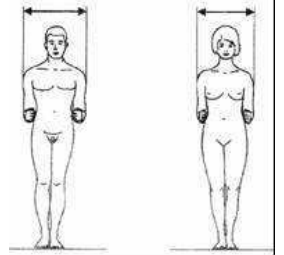
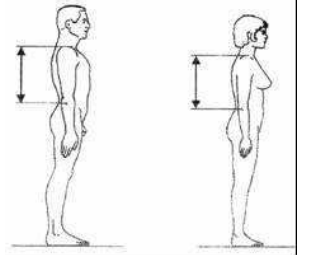
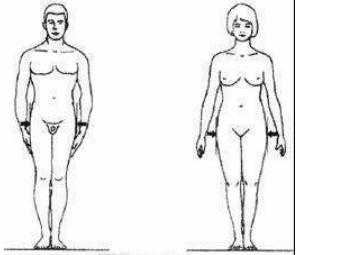
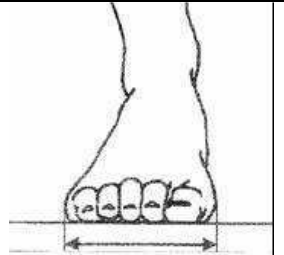
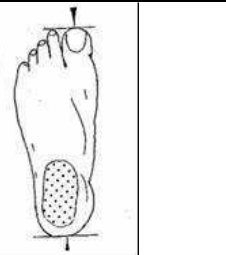
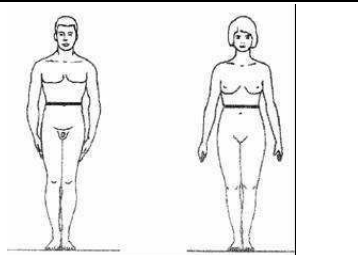
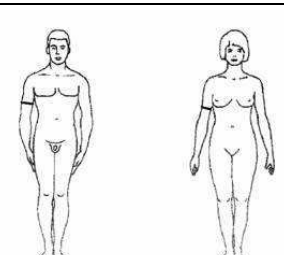
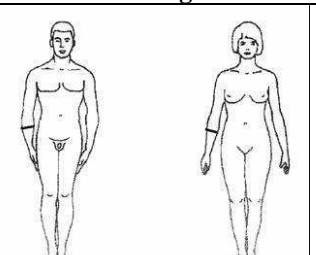
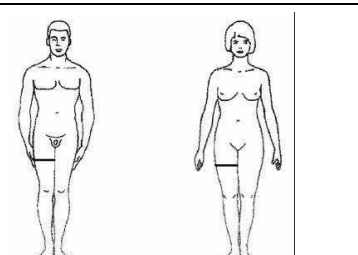
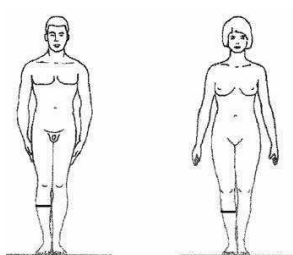


Figure 57: Measurement chain for FAC project.

7.2 Anthropometric measurements

<p>M1</p> 	<p>M2</p> 	<p>M3</p> 
<p>Stature</p>	<p>Head width</p>	<p>Head height</p>
<p>M4</p> 	<p>M5</p> 	<p>M6</p> 
<p>Bideltoid shoulder width</p>	<p>Upper arm length</p>	<p>Maximum Hip width</p>
<p>M8</p> 	<p>M9</p> 	<p>M10</p> 
<p>Foot breadth</p>	<p>Foot length</p>	<p>Minimum Waist circumference</p>
<p>M11</p> 	<p>M12</p> 	<p>M14</p> 
<p>Maximum Upper arm circumference</p>	<p>Maximum Forearm circumference</p>	<p>Maximum Thigh circumference</p>

M17



Maximum Lower leg circumference

M19



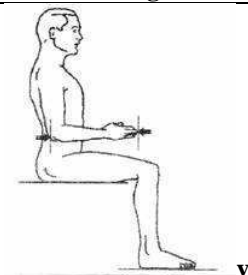
Sitting height

M20



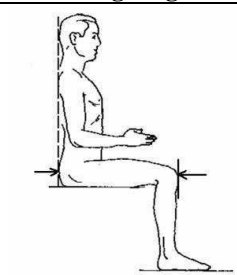
Chest depth

M21



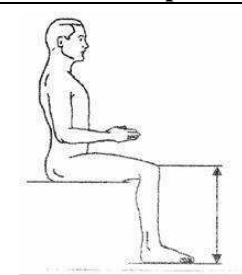
Forearm length

M22



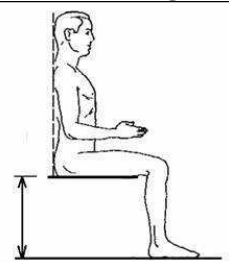
Buttock-knee length

M23



Knee height sitting

M24



Seat height

M25

Weight

M29

Stature with shoes on

M30

Trunk height (calculated)

M36

Age

M37

Gender

7.3 Subjects' anthropometric dimension for the FAC project

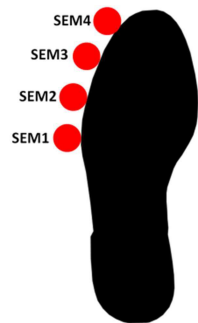
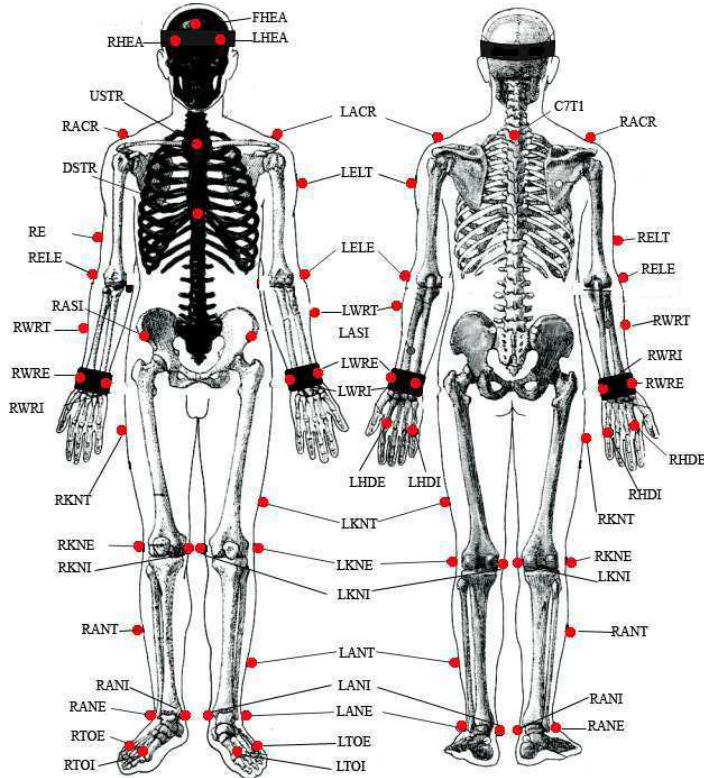
Subject	M1	M2	M3	M4	M5	M6	M8	M9	M10	M11	M12	M14	M17	M19	M20	M21	M22
02_SM	1625	154	205	424	324	357	82	230	760	285	245	555	345	1330	212	410	555
03_NC	1570	151	214	401	319	295	85	222	680	246	220	485	336	1230	220	437	545
04_DD	1849	160	229	504	340	377	95	270	925	315	265	545	380	1372	235	490	690
05_YP	1775	148	228	466	341	351	103	275	852	310	277	610	425	1350	220	480	626
06_JC	1800	158	223	481	350	332	85	260	805	280	252	515	355	1375	240	480	602
07_RZ	1835	158	246	465	355	370	103	281	912	340	285	605	425	1365	240	495	660
08_CB	1660	150	235	431	298	318	92	256	800	285	255	525	350	1320	215	430	554
09_RA	1754	149	228	482	361	346	92	263	995	325	280	550	391	1300	260	485	635
10_LG	1894	155	245	515	376	372	101	287	1025	355	305	610	430	1442	250	517	660
11_GM	1825	147	251	470	374	360	96	262	925	310	270	560	390	1335	264	500	654
12_SM	1565	111	212	406	294	344	89	234	720	266	228	524	353	1200	230	439	578
13_SN	1822	142	219	481	351	351	94	264	922	313	264	548	366	1356	256	587	610
14_RT	1882	140	230	460	361	344	105	279	805	285	280	496	355	1422	222	525	623
15_DM	1828	151	223	461	355	355	91	270	845	268	254	527	365	1370	219	587	635
16_SR	1768	155	221	424	339	315	94	259	770	245	241	456	338	1338	236	477	585
17_AB	1607	137	212	451	325	355	89	237	1000	334	260	601	393	1212	330	442	600
18_AA	1777	150	216	440	344	300	96	260	686	253	244	483	322	1363	205	468	570
19_AM	1860	150	234	480	368	347	103	280	848	302	285	580	390	1354	278	503	645
20_EB	1524	140	218	396	271	300	76	211	700	248	213	478	320	1184	210	392	561
21_GL	1864	154	240	491	372	346	101	292	819	283	276	534	368	1384	232	522	643
22_FM	1830	150	231	474	364	348	102	270	831	300	295	585	423	1403	208	484	614
23_LT	1788	163	235	497	366	357	98	256	921	335	291	578	387	1370	253	460	604
24_JT	1905	145	231	502	369	385	114	285	882	342	300	644	440	1430	255	544	677
25_ED	1800	146	236	468	350	330	92	283	844	275	250	518	390	1352	214	507	627
26_RP	1752	161	231	501	362	360	92	273	984	329	303	591	395	1300	220	483	627
27_RR	1755	162	235	508	350	338	97	252	912	316	277	570	384	1315	257	475	610
28_LM	1515	147	211	416	294	302	90	228	708	274	238	534	341	1164	230	410	515
29_CH	1598	153	220	415	290	336	83	235	758	277	230	553	352	1237	205	447	553
30_CM	1610	138	215	388	315	322	80	227	722	246	213	495	346	1250	205	418	563
31_NM	1618	148	232	412	318	310	85	242	790	267	223	517	350	1234	234	424	585

Small female  
 Average male  
 Tall male

Subject	M23	M24	M25	M29	M30	M36	M37	Group	Seat adjustment		Laterality
									Chosen	Used	
02_SM	480	420	57.4	1640	910	38	Female	Small	-55	-55	Right-handed
03_NC	482	405	46.3	1590	825	37	Female	Small	-80	-80	Right-handed
04_DD	565	425	80.4	1870	947	30	Male	Tall	85	85	Left-handed
05_YP	534	408	79.2	1799	942	20	Male	Average	0	10	Right-handed
06_JC	535	410	71	1815	965	25	Male	Average	-20	0	Right-handed
07_RZ	535	414	89.1	1860	951	35	Male	Tall	65	65	Right-handed
08_CB	480	395	63.7	1684	925	38	Male	Average	-80	-68	Right-handed
09_RA	525	398	83	1779	902	33	Male	Average	-78	2.3	Right-handed
10_LG	560	444	100.9	1908	998	36	Male	Tall	95	80	Left-handed
11_GM	552	407	81.4	1848	928	34	Male	Tall	55	55	Right-handed
12_SM	490	396	52.1	1584	804	32	Female	Small	-80	-50	Right-handed
13_SN	570	400	81.2	1844	956	35	Male	Tall	80	60	Right-handed
14_RT	570	430	70.6	1907	992	33	Male	Tall	50	50	Right-handed
15_DM	568	419	67.7	1838	951	37	Male	Tall	40	40	Ambidextrous
16_SR	532	419	54.9	1885	919	37	Male	Average	-20	-20	Right-handed
17_AB	513	380	79.6	1630	832	42	Female	Small	30	-10	Right-handed
18_AA	542	423	57.2	1800	940	23	Male	Average	-50	-20	Right-handed
19_AM	573	410	82.2	1880	944	43	Male	Tall	70	70	Left-handed
20_EB	435	342	46.8	1545	842	26	Female	Small	-80	-80	Left-handed
21_GL	594	443	75.2	1884	941	24	Male	Tall	30	60	Right-handed
22_FM	550	424	79.4	1843	979	20	Male	Tall	0	20	Right-handed
23_LT	518	386	85.9	1802	984	21	Male	Average	20	20	Right-handed
24_JT	687	430	98.1	1918	1000	21	Male	Tall	60	93	Right-handed
25_ED	558	430	70.7	1823	922	24	Male	Average	-40	20	Right-handed
26_RP	510	380	83.5	1773	920	20	Male	Average	-40	-10	Right-handed
27_RR	548	390	82.1	1774	925	44	Male	Average	-12	10	Left-handed
28_LM	554	330	52.7	1537	834	23	Female	Small	-80	-50	Left-handed
29_CH	458	357	55	1618	880	32	Female	Small	-80	-80	Right-handed
30_CM	468	372	51.7	1636	878	22	Female	Small	-80	-70	Right-handed
31_NM	490	340	57.6	1640	894	31	Female	Small	-80	-50	Right-handed

	Small female
	Average male
	Tall male

7.4 Markers' placement on subject for the FAC project

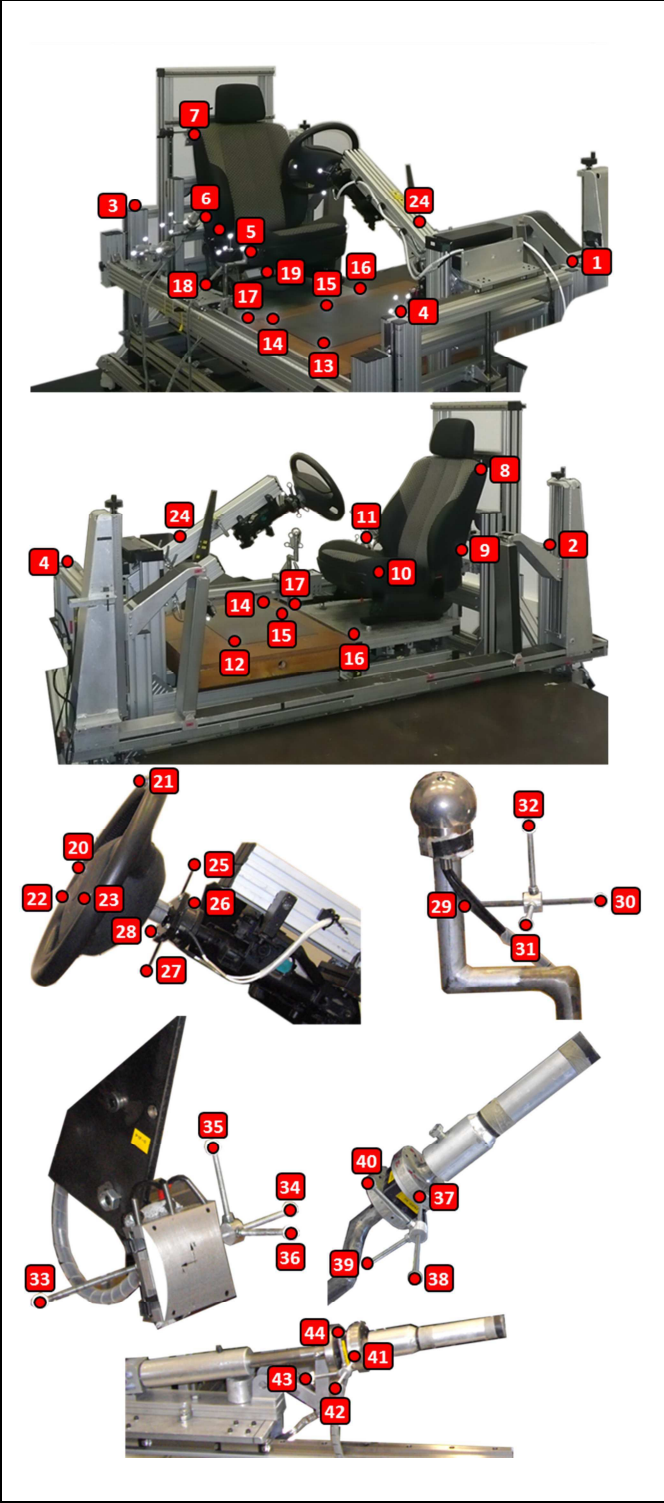


<b>RHEA</b>	Right temple
<b>LHEA</b>	Left temple
<b>FHEA</b>	Forehead middle
<b>C7T1</b>	7 <sup>th</sup> cervical vertebrae
<b>USTR</b>	Upper sternum
<b>DSTR</b>	Lower sternum
<b>RACR</b>	Right acromio-clavicular joint
<b>LACR</b>	Left acromio-clavicular joint
<b>RELT</b>	Right upper arm technical marker
<b>LELT</b>	Left upper arm technical marker
<b>RELE</b>	Right external elbow
<b>LELE</b>	Left external elbow
<b>RWRT</b>	Right lower arm technical marker
<b>LWRT</b>	Left lower arm technical marker
<b>RWRE</b>	Right external wrist
<b>LWRE</b>	Left external wrist
<b>RWRI</b>	Right internal wrist
<b>LWRI</b>	Left internal wrist
<b>RHDE</b>	Right external hand (carpus)
<b>LHDE</b>	Left external hand (carpus)
<b>RHDI</b>	Right internal hand (carpus)
<b>LHDI</b>	Left internal hand (carpus)
<b>RASI</b>	Right anterior superior iliac spine
<b>LASI</b>	Left anterior superior iliac spine
<b>RKNT</b>	Right thigh technical marker
<b>LKNT</b>	Left thigh technical marker
<b>RKNE</b>	Right external knee
<b>LKNE</b>	Left external knee
<b>RKNI</b>	Right internal knee
<b>LKNI</b>	Left internal knee
<b>RANT</b>	Right shank technical marker
<b>LANT</b>	Left shank technical marker
<b>RANE</b>	Right external malleolus
<b>LANE</b>	Left external malleolus
<b>RANI</b>	Right internal malleolus
<b>LANI</b>	Left internal malleolus
<b>RTOE</b>	Right external tarsus
<b>LTOE</b>	Left external tarsus
<b>RTOI</b>	Right internal tarsus
<b>LTOI</b>	Left internal tarsus
<b>SEM1</b>	Shoe (sole) 1
<b>SEM2</b>	Shoe (sole) 2
<b>SEM3</b>	Shoe (sole) 3
<b>SEM4</b>	Shoe (sole) 4

Number of markers

44

7.5 Markers' placement on mock-up for the FAC project

	N°	Name	Description (orientation according to driver's point of view)
	1	MAC1	Front left of mock-up frame
	2	MAC2	Back left of mock-up frame
	3	MAC3	Back right of mock-up frame
	4	MAC4	Front right of mock-up frame
	5	SIE1	Front right of seat
	6	SIE2	Back right of seat
	7	SIE3	Up right of seat
	8	SIE4	Up left of seat
	9	SIE5	Back left of seat
	10	SIE6	Front left of seat
	11	SIEH	Reference H-point
	12	UPF1	Front left of floor force plate
	13	UPF2	Front right of floor force plate
	14	UPF3	Back right of floor force plate
	15	UPF4	Back left of floor force plate
	16	PFS1	Front left of seat base
	17	PFS2	Front right of seat base
	18	PFS3	Back right of seat base
	19	PFS4	Back left of seat base
	20	VOL1	Steering wheel middle
	21	VOL2	Steering wheel up
	22	VOL3	Steering wheel left
	23	VOL4	Steering wheel right
	24	VOL5	Steering column
	25	CVO1	X-axis steering wheel sensor (+)
	26	CVO2	Y-axis steering wheel sensor (+)
	27	CVO3	X-axis steering wheel sensor (-)
	28	CVO4	Y-axis steering wheel sensor (-)
	29	LVI1	Y-axis gear stick sensor (-)
	30	LVI2	Y-axis gear stick sensor (+)
	31	LVI3	X-axis gear stick sensor (+)
	32	LVI4	Z-axis gear stick sensor (+)
	33	PED1	Y-axis pedal sensor (+)
	34	PED2	Y-axis pedal sensor (-)
	35	PED3	X-axis pedal sensor (+)
	36	PED4	Z-axis pedal sensor (+)
	37	FMS1	Y-axis static handbrakesensor (+)
	38	FMS2	Y-axis static handbrake sensor (-)
	39	FMS3	Z-axis static handbrake sensor (+)
	40	FMS4	X-axis static handbrake sensor (+)
	41	FMD1	Y-axis dynamic handbrake sensor (+)
	42	FMD2	Y-axis dynamic handbrake sensor (-)
	43	FMD3	Z-axis dynamic handbrake sensor (+)
	44	FMD4	X-axis dynamic handbrake sensor (+)

## 7.6 Extract from experimental sheet of the FAC project

N	Cmd	NomFichier	H	X	Y	Z	TypeEff	DirEff	NivEff	Note	Commentaire		
<b>Perception de l'effort</b>													
I	OOO	xx_XX_TroneC	Trone de Calibration								X		
ii	OOO	xx_XX_EnvirD	Environnement LV1 P2F 286								X		
iii	OOO	xx_XX_PosRef	286	Pieds sur plancher et mains sur volant								X	
1	LV	xx_XX_L00_O1	286	-307	337	145	Stat	O	Repos				
...	...	...	...	...	...	...	...	...	...	...	...		
37	LV	xx_XX_LFA_L1	286	-307	337	145	Stat	Gauche	Faible	X			
38	PED	xx_XX_P00_O1	300	-912	-70	-163	Stat	O	Repos				
39	PED	xx_XX_PMA_O1	300	-912	-70	-163	Stat	O	Max	X			
40	PED	xx_XX_PMA_O2	300	-912	-70	-163	Stat	O	Max	X			
41	PED	xx_XX_PFA_O1	300	-912	-70	-163	Stat	O	Faible	X			
42	PED	xx_XX_PFO_O1	300	-912	-70	-163	Stat	O	Fort	X			
43	PED	xx_XX_PTF_O1	300	-912	-70	-163	Stat	O	T Fable	X			
44	PED	xx_XX_PMO_O1	300	-912	-70	-163	Stat	O	Moyen	X			
45	FAM	xx_XX_F00_O1	286	-130	350	75	Stat	O	Repos				
...	...	...	...	...	...	...	...	...	...	...	...		
51	FAM	xx_XX_FFA_O1	286	-130	350	75	Stat	O	Faible	X			
Iv	OOO	xx_XX_EnvirM	Environnement dernière config								X		
N	Cmd	NomFichier	H	X	Y	Z	TypeEff	DirEff	NivEff	Note	Commentaire		
<b>Effort maximum statique</b>													
52	FAM_A	xx_XX_FA5_O1	286	-40	400	200	Stat	O	Repos				
...	...	...	...	...	...	...	...	...	...	...	...		
61	FAM_A	xx_XX_FA3_M1	286	-220	400	-50	Stat	O	Max	X			
62	FAM	xx_XX_F12_O1	286	-220	300	200	Stat	O	Repos				
...	...	...	...	...	...	...	...	...	...	...	...		
81	FAM	xx_XX_F11_M1	286	-130	300	75	Stat	O	Max	X			
82	PED	xx_XX_P1F_O1	240	-936	-70	-79.5	Stat	O	Repos				
83	PED	xx_XX_P1F_M1	240	-936	-70	-79.5	Stat	O	Max	X			
84	PED	xx_XX_P2F_O1	300	-912	-70	-163	Stat	O	Repos				
85	PED	xx_XX_P2F_M1	300	-912	-70	-163	Stat	O	Max	X			
86	PED	xx_XX_P2M_O1	300	-843	-70	-160	Stat	O	Repos				
87	PED	xx_XX_P2M_M1	300	-843	-70	-160	Stat	O	Max	X			
88	PED	xx_XX_P3F_O1	360	-891	-70	-253	Stat	O	Repos				
89	PED	xx_XX_P3F_M1	360	-891	-70	-253	Stat	O	Max	X			
90	PED	xx_XX_P1M_O1	240	-867	-70	-83	Stat	O	Repos				
91	PED	xx_XX_P1M_M1	240	-867	-70	-83	Stat	O	Max	X			
92	PED	xx_XX_P3M_O1	360	-824	-70	-246	Stat	O	Repos				
93	PED	xx_XX_P3M_M1	360	-824	-70	-246	Stat	O	Max	X			
94	LV	xx_XX_L40_O1	286	-212	396	119	Stat	O	Repos				
...	...	...	...	...	...	...	...	...	...	...	...		
121	LV	xx_XX_L2U_M1	286	-410	268	218	Stat	Haut	Max	X			
<b>Effort maximum Dynamique</b>													
122	FAM	xx_XX_FS5_D1	286	-40	400	200	Dyna	O	Max	X			
123	FAM	xx_XX_FS2_D1	286	-220	400	200	Dyna	O	Max	X			
124	FAM_A	xx_XX_FA2_D1	286	-220	400	200	Dyna	O	Max	X			
125	FAM_A	xx_XX_FA5_D1	286	-40	400	200	Dyna	O	Max	X			
v	OOO	xx_XX_EnvirF	Environnement dernière config								X		

## 7.7 Tangential, normal and transversal pedal force components according to the force level

**Table 45: Means and standard deviations of the tangential component of the pedal force according to the force level. The results are presented for each group of subjects.**

	Tangential force (N)		
	Short women	Average men	Tall men
Very low	38 ± 18	82 ± 41	71 ± 27
Low	60 ± 39	130 ± 75	119 ± 44
Medium	105 ± 43	227 ± 126	240 ± 117
High	219 ± 118	372 ± 265	411 ± 162
Maximum	363 ± 203	672 ± 283	728 ± 215
All	191 ± 186	359 ± 313	383 ± 306

**Table 46: Means and standard deviations of the normal component of the pedal force according to the force level. The results are presented for each group of subjects.**

	Normal force (N)		
	Short women	Average men	Tall men
Very low	-22 ± 13	-52 ± 22	-54 ± 20
Low	-31 ± 19	-71 ± 34	-75 ± 21
Medium	-54 ± 23	-112 ± 52	-128 ± 52
High	-104 ± 63	-169 ± 119	-205 ± 68
Maximum	-174 ± 85	-326 ± 161	-378 ± 96
All	-93 ± 84	-176 ± 155	-203 ± 149

**Table 47: Means and standard deviations of the transversal component of the pedal force according to the force level. The results are presented for each group of subjects.**

	Transversal force (N)		
	Short women	Average men	Tall men
Very low	-4 ± 2	-6 ± 5	-3 ± 5
Low	-6 ± 6	-12 ± 9	-7 ± 6
Medium	-10 ± 4	-19 ± 13	-18 ± 14
High	-26 ± 15	-30 ± 20	-38 ± 25
Maximum	-43 ± 26	-75 ± 30	-65 ± 36
All	-22 ± 23	-36 ± 35	-33 ± 35

## 7.8 Pelvis displacement for short women, average men and tall men according to the force level

**Table 48: Means and standard deviations of pelvis displacement on x-axis according to the force level and the group of subjects. Results presented are in millimeter.**

Group of subjects ***	Force level ***				
	Very Low	Low	Medium	High	Maximum
Tall men	-0.2 ± 5	2.8 ± 6.1	7.3 ± 8.7	13.7 ± 11.1	16.7 ± 13.5
Average men	0.5 ± 6.4	6.1 ± 12.8	7.4 ± 9.5	13.6 ± 14.1	22.8 ± 14.8
Short women	-2.5 ± 3.6	-2 ± 3.5	-0.1 ± 4.8	4.3 ± 7.1	7.2 ± 11.4
All	-0.6 ± 5.1	2.5 ± 8.7	5.2 ± 8.5	11.2 ± 11.7	15.8 ± 14.5

\*p<0.05, \*\*p<0.01, \*\*\* p<0.001

**Table 49: Means and standard deviations of pelvis displacement on y-axis according to the force level and the group of subjects. Results presented are in millimeter.**

Group of subjects ***	Force level ***				
	Very Low	Low	Medium	High	Maximum
Tall men	-0.9 ± 12.2	-1.5 ± 11.	-0.1 ± 11.6	2.5 ± 12.7	6.0 ± 12.5
Average men	3.5 ± 6.5	2.0 ± 5.8	4.1 ± 7.1	6.5 ± 9.7	12.1 ± 12.6
Short women	-3.3 ± 2.9	-3.5 ± 3.2	-3.5 ± 4.3	-0.8 ± 3.2	3.2 ± 3.4
All	-0.2 ± 8.8	-0.9 ± 8.1	0.3 ± 8.9	3.0 ± 10.1	7.1 ± 11.1

\*p<0.05, \*\*p<0.01, \*\*\* p<0.001

**Table 50: Means and standard deviations of pelvis displacement on z-axis according to the force level and the group of subjects. Results presented are in millimeter.**

Group of subjects ***	Force level ***				
	Very Low	Low	Medium	High	Maximum
Tall men	4.6 ± 11.1	5.8 ± 11.8	9.7 ± 12.3	15.4 ± 11.3	27.6 ± 9.8
Average men	1.8 ± 3.0	2.8 ± 3.0	5.9 ± 3.7	11.4 ± 11.5	28.2 ± 14.1
Short women	4.4 ± 5.1	6.5 ± 6.5	8.7 ± 6.1	16.5 ± 11.3	26.2 ± 15.2
All	3.6 ± 7.5	5.1 ± 8.2	8.2 ± 8.5	14.4 ± 11.1	27.4 ± 12.7

\*p<0.05, \*\*p<0.01, \*\*\* p<0.001

## 7.9 Variation of joint angles for short women, average men and tall men according to the force level

**Table 51: Means and standard deviations of hip abduction/adduction angle according to the group of subjects and the force level. Result presented are in degree.**

Group of subjects	Force level *					
	Rest	Very Low	Low	Medium	High	Maximum
Tall men	5,2 ± 6,9	5,3 ± 7,3	5,8 ± 7,6	5,8 ± 6,7	6,7 ± 7,0	8,8 ± 7,7
Average men	4,3 ± 4,6	3,4 ± 2,6	4,1 ± 3,3	4,4 ± 3,4	4,9 ± 3,7	8,0 ± 6,4
Short women	6,1 ± 5,8	6,1 ± 5,2	6,4 ± 4,8	6,5 ± 4,2	7,0 ± 4,3	8,8 ± 4,1
All	5,2 ± 5,7	4,9 ± 5,5	5,5 ± 5,6	5,6 ± 5,0	6,2 ± 5,3	8,5 ± 6,3

\*p<0.05, \*\*p<0.01, \*\*\* p<0.001

**Table 52: Means and standard deviations of hip flexion/extension angle according to the group of subjects and the force level. Result presented are in degree.**

Group of subjects ***	Force level ***					
	Rest	Very Low	Low	Medium	High	Maximum
Tall men	57,3 ± 15,2	59,6 ± 8,6	55,9 ± 16,2	57,8 ± 9,9	54,5 ± 9,6	50,4 ± 10,1
Average men	63,4 ± 12,1	62,5 ± 11,1	61,6 ± 11,4	59,5 ± 10,9	56,8 ± 10,3	51 ± 10,2
Short women	54 ± 13,8	50,2 ± 12,8	49,4 ± 12,6	48,1 ± 13,3	45,4 ± 14,1	44,3 ± 12,5
All	58,3 ± 13,9	57,9 ± 11,5	55,9 ± 14,1	55,6 ± 11,9	52,9 ± 11,7	48,8 ± 11,1

\*p<0.05, \*\*p<0.01, \*\*\* p<0.001

**Table 53: Means and standard deviations of knee flexion/extension angle according to the group of subjects and the force level. Result presented are in degree.**

Group of subjects ***	Force level ***					
	Rest	Very Low	Low	Medium	High	Maximum
Tall men	52 ± 5,9	51,2 ± 6,6	50,5 ± 6,2	47,8 ± 7,8	45,7 ± 9	42 ± 10,1
Average men	50,1 ± 6,6	48,6 ± 5,5	48,4 ± 6,8	45,4 ± 7,7	41,9 ± 8,6	33,8 ± 8,7
Short women	40,2 ± 8,3	38,6 ± 8,1	36,8 ± 6,8	35,6 ± 7,6	32,9 ± 6,9	29,4 ± 5,7
All	48 ± 8,3	46,7 ± 8,4	46 ± 8,7	43,5 ± 9,1	41,1 ± 9,6	35,8 ± 10

\*p<0.05, \*\*p<0.01, \*\*\* p<0.001

**Table 54: Means and standard deviations of ankle flexion/extension angle according to the group of subjects and the force level. Result presented are in degree.**

Group of subjects	Force level *					
	Rest	Very Low	Low	Medium	High	Maximum
Tall men	66,7 ± 4,7	67,4 ± 4,7	66 ± 5,2	65,2 ± 4,4	63,8 ± 4,9	64 ± 4,4
Average men	67 ± 5,2	67,1 ± 6,5	64,7 ± 8,7	64,3 ± 7	62,9 ± 8,3	62,7 ± 4,9
Short women	62,8 ± 6	66,4 ± 6,2	65,5 ± 7,5	64,1 ± 6,9	63,5 ± 8,6	60,9 ± 7,5
All	65,7 ± 5,4	67 ± 5,6	65,4 ± 6,9	64,6 ± 5,9	63,4 ± 6,9	62,7 ± 5,6

\*p<0.05, \*\*p<0.01, \*\*\* p<0.001

7.10 Hip, knee and ankle flexion/extension angles according to the pedal position and the group of subjects

Table 55: Means and standard deviations of hip, knee and ankle flexion/extension angle for each group of subjects and pedal position in case of maximum pedal force exertion

		Hip Flexion/Extension (deg)	Knee Flexion/Extension (deg)	Ankle Flexion/Extension (deg)
Tall men	P1F	55 ± 9	44 ± 9	64 ± 5
	P1M	63 ± 9	57 ± 7	70 ± 3
	P2F	52 ± 10	45 ± 9	63 ± 6
	P2M	61 ± 9	60 ± 5	70 ± 5
	P3F	48 ± 11	47 ± 11	60 ± 5
	P3M	56 ± 9	60 ± 8	68 ± 4
Average men	P1F	58 ± 11	37 ± 10	61 ± 7
	P1M	66 ± 10	52 ± 12	70 ± 8
	P2F	53 ± 11	37 ± 12	60 ± 7
	P2M	63 ± 13	55 ± 12	71 ± 8
	P3F	48 ± 12	40 ± 10	57 ± 8
	P3M	58 ± 10	56 ± 10	67 ± 7
Short women	P1F	47 ± 12	23 ± 6	59 ± 11
	P1M	59 ± 13	38 ± 8	70 ± 11
	P2F	44 ± 13	29 ± 8	58 ± 12
	P2M	54 ± 13	42 ± 8	72 ± 8
	P3F	39 ± 14	33 ± 10	57 ± 11
	P3M	48 ± 12	48 ± 9	69 ± 11

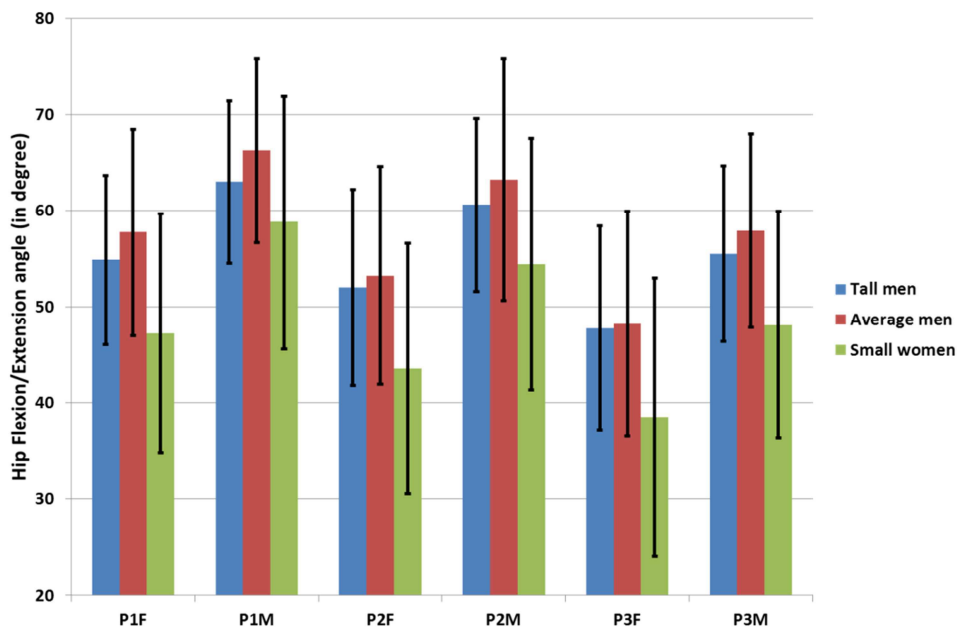


Figure 58: Hip flexion/extension angle mean values for each group of subjects in relation to the pedal position

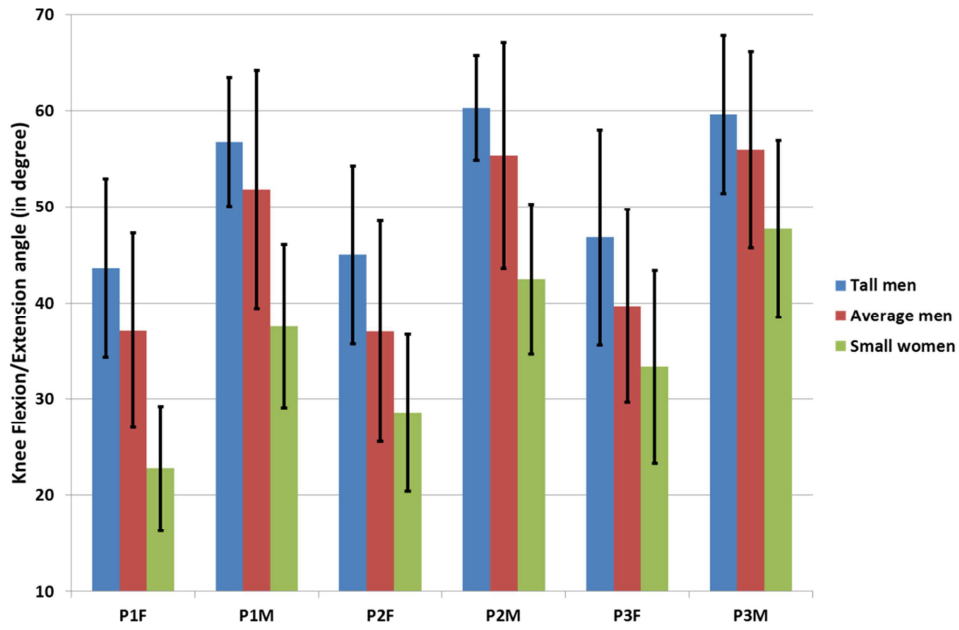


Figure 59: Knee flexion/extension angle mean values for each group of subjects in relation to the pedal position

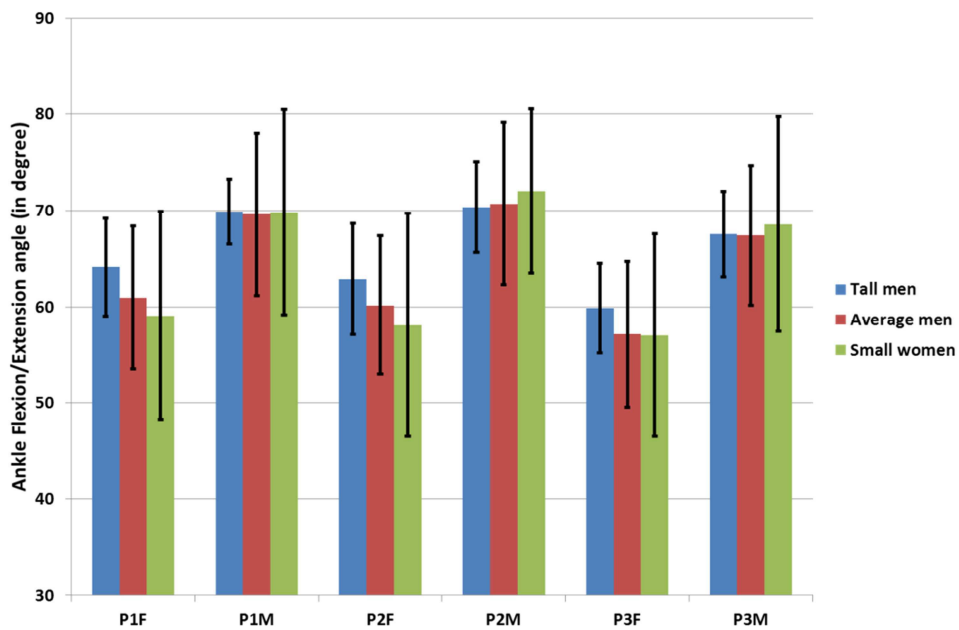


Figure 60: Ankle flexion/extension angle mean values for each group of subjects in relation to the pedal position

### 7.11 Functional maximum data used in the simulation

**Table 56: Maximum torques for the different degrees of freedom considered for the lower limb model in the simulation of the pedal force direction.**

Joint	Motion	Maximum torque value (N.m)	Source
Hip	Flexion	185	Chaffin et al. (1999)
	Extension	190	Chaffin et al. (1999)
	Abduction	190	Delp et al. (1990)
	Adduction	190	Delp et al. (1990)
	Internal rotation	60	Delp et al. (1990)
	External rotation	60	Delp et al. (1990)
Knee	Flexion	100	Chaffin et al. (1999)
	Extension	168	Chaffin et al. (1999)
	Internal rotation	20	Arbitrary
	External rotation	20	Arbitrary
Ankle	Dorsiflexion	126	Chaffin et al. (1999)
	Plantarflexion	126	Chaffin et al. (1999)
	Inversion	20	Arbitrary
	Eversion	20	Arbitrary

**Table 57: Joint ranges of motion (ROM) for the different degrees of freedom of the considered for the lower limb model in the simulation of the postural adjustment. The data are based on Kapandji (1994).**

Joint	Motion	Joint limit angle (in deg.)
Hip	Flexion	120
	Extension	-20
	Abduction	45
	Adduction	-30
	Internal rotation	-60
	External rotation	40
Knee	Flexion	140
	Extension	0
	Internal rotation	20
	External rotation	-40
Ankle	Dorsiflexion	120
	Plantarflexion	40
	Abduction	20
	Adduction	-20

## 7.12 Comparison of simulated and experimental pedal force directions

Table 58: Means and standard deviations of experimental and simulated pedal force direction in XZ plane (respectively  $\theta_{F_{Exp}}$  and  $\theta_{F_{Sim}}$ ) and lateral deviation in XY plane (respectively  $\delta_{F_{Exp}}$  and  $\delta_{F_{Sim}}$ ) for a) maximum pedal force exertion experiment and b) pedal force perception experiment.

a)	$\theta_{F_{Sim}}$	$\theta_{F_{Exp}}$	$\delta_{F_{Sim}}$	$\delta_{F_{Exp}}$
P1F	$-4.3 \pm 2.8$	$-5.8 \pm 7.5$	$-1.7 \pm 1.9$	$4.7 \pm 1.6$
P1M	$-6.7 \pm 2.6$	$-10.8 \pm 6.4$	$-2.5 \pm 2.0$	$5.5 \pm 1.7$
P2F	$-4.5 \pm 2.7$	$-5.9 \pm 6.8$	$-1.9 \pm 1.9$	$5.4 \pm 2$
P2M	$-7.2 \pm 2.9$	$-11.1 \pm 5.4$	$-2.2 \pm 2.0$	$5.9 \pm 1.9$
P3F	$-4.4 \pm 3.2$	$-5.9 \pm 6.4$	$-2.4 \pm 1.8$	$5 \pm 2.6$
P3M	$-7.3 \pm 2.3$	$-10.8 \pm 5.3$	$-2.5 \pm 2.2$	$6.9 \pm 2.2$
Short women	$-3.3 \pm 2.7$	$-5.9 \pm 7.2$	$-1.4 \pm 2.2$	$6.6 \pm 1.5$
Average men	$-6.3 \pm 2.9$	$-7.4 \pm 5.9$	$-1.9 \pm 1.9$	$6 \pm 1.7$
Tall men	$-7.1 \pm 2.2$	$-11 \pm 6.1$	$-3.1 \pm 1.5$	$4.4 \pm 2.3$
All	$-5.8 \pm 3.1^{G***, P***}$	$-8.4 \pm 6.7^{G***, P***}$	$-2.2 \pm 2.0^{G***}$	$5.6 \pm 2.1^{G***, P***}$
b)	$\theta_{F_{Sim}}$	$\theta_{F_{Exp}}$	$\delta_{F_{Sim}}$	$\delta_{F_{Exp}}$
Very low	$-9.6 \pm 11.9$	$-15.1 \pm 8$	$3.3 \pm 6.8$	$3.3 \pm 3$
Low	$-8.4 \pm 8.8$	$-12.2 \pm 6.4$	$0.8 \pm 6.5$	$4 \pm 2.7$
Medium	$-6.2 \pm 6.1$	$-9.5 \pm 6.9$	$-0.4 \pm 3.6$	$4.4 \pm 2.7$
High	$-5.3 \pm 3.7$	$-6.9 \pm 5.5$	$-1.6 \pm 2.3$	$5 \pm 1.9$
Maximum	$-3.5 \pm 2.3$	$-6.7 \pm 5.7$	$-2.6 \pm 1.8$	$5.6 \pm 3$
Short women	$-2.0 \pm 4.6$	$-7.1 \pm 6.6$	$1.4 \pm 7.3$	$6 \pm 2.3$
Average men	$-7.7 \pm 7.5$	$-8.5 \pm 7.1$	$-0.2 \pm 2.8$	$4.7 \pm 2.1$
Tall men	$-7.7 \pm 7.2$	$-12.1 \pm 6.7$	$-2.0 \pm 3.2$	$3.6 \pm 2.6$
All	$-6.1 \pm 7.1^{G***, P***}$	$-9.5 \pm 7.1^{G***, P***}$	$-0.5 \pm 4.8^{G***, P***}$	$4.7 \pm 2.6^{G***, P***}$

\*p<0.05, \*\*p<0.01, \*\*\* p<0.001. G: group of subjects; P: Pedal position; F: force level

## 7.13 Comparison of simulated and experimental normal and transversal forces

Table 59: Means and standard deviations of simulated and experimental normal and transversal forces for a) maximum pedal force exertion and b) pedal force perception experiments.

a)	Normal force (N)		Transversal force (N)	
	Simulation	Experiment	Simulation	Experiment
P1F	-260 ± 119	-279 ± 150	16 ± 23	-49 ± 27
P1M	-166 ± 82	-218 ± 114	34 ± 32	-71 ± 40
P2F	-254 ± 123	-277 ± 155	20 ± 22	-55 ± 30
P2M	-141 ± 72	-185 ± 97	28 ± 27	-70 ± 38
P3F	-261 ± 133	-284 ± 159	20 ± 18	-44 ± 34
P3M	-136 ± 79	-176 ± 106	27 ± 26	-71 ± 40
Short women	-125 ± 87	-145 ± 103	8 ± 16	-49 ± 32
Average men	-232 ± 124	-257 ± 163	20 ± 24	-72 ± 37
Tall men	-236 ± 105	-287 ± 103	40 ± 24	-58 ± 37
All	-203 <sup>G***, P***</sup> ± 117	-237 <sup>G***, P**</sup> ± 138	24 <sup>G***</sup> ± 25	-60 <sup>G**, P**</sup> ± 37
b)	Normal force (N)		Transversal force (N)	
	Simulation	Experiment	Simulation	Experiment
Very low	-38 ± 27	-44 ± 23	-3 ± 6	-4 ± 5
Low	-57 ± 35	-63 ± 32	1 ± 7	-8 ± 7
Medium	-93 ± 58	-100 ± 55	5 ± 12	-16 ± 12
High	-156 ± 86	-167 ± 93	13 ± 16	-32 ± 21
Maximum	-266 ± 123	-303 ± 144	30 ± 27	-62 ± 34
Short women	-81 ± 86	-93 ± 85	3 ± 11	-22 ± 23
Average men	-170 ± 134	-176 ± 155	8 ± 16	-36 ± 35
Tall men	-173 ± 126	-203 ± 149	23 ± 28	-33 ± 35
All	-146 <sup>G***, F***</sup> ± 125	-163 <sup>G***, F***</sup> ± 143	13 <sup>G***, F***</sup> ± 22	-31 ± 32 <sup>G*, F***</sup>

\*p&lt;0.05, \*\*p&lt;0.01, \*\*\* p&lt;0.001. G: group of subjects; P: Pedal position; F: force level

## Chapter 4: Musculoskeletal modeling and control of the pedal force direction

<b>1</b>	<b>INTRODUCTION</b>	<b>159</b>
<b>2</b>	<b>MUSCLE FORCE COMPUTATION</b>	<b>161</b>
2.1	MODELING OF THE MUSCULOSKELETAL SYSTEM OF THE HUMAN BODY .....	161
2.2	MODELING OF THE PHYSIOLOGICAL BEHAVIOR OF THE MUSCLE .....	161
2.3	DEFINITION OF THE MUSCLE FORCE .....	163
2.4	COMPUTATION OF THE MUSCLE FORCES .....	165
<b>3</b>	<b>PEDAL FORCE DIRECTION CONTROL BY MINIMIZING MUSCULAR ACTIVITIES</b>	<b>167</b>
3.1	DESCRIPTION OF THE MUSCULOSKELETAL MODEL USED .....	167
3.2	OPTIMIZATION PROBLEM .....	170
<b>4</b>	<b>RESULTS</b>	<b>171</b>
4.1	FORCE FORCE DIRECTION .....	171
4.2	MUSCLE FORCE PATTERNS.....	173
<b>5</b>	<b>DISCUSSION AND CONCLUSION</b>	<b>177</b>
<b>6</b>	<b>APPENDIX</b>	<b>180</b>
6.1	COMPARISON OF SIMULATED AND EXPERIMENTAL PEDAL FORCE DIRECTIONS .....	180
6.2	COMPARISON OF SIMULATED AND EXPERIMENTAL NORMAL AND TRANSVERSAL FORCES. ....	182



## 1 Introduction

Most of the existing DHMs, especially the ones used in automotive industry, only allow a kinematical approach of the movement. A task-related motion simulation is therefore based mostly on controlling kinematical parameters such as joint angles. However, it became obvious that the dynamic parameters such as joint torques are key parameters to be considered for understanding the perceived discomfort especially for forceful tasks, such as clutching pedal operation investigated in this PhD thesis. But the analysis of the dynamics of a motion is not limited to the joint forces and torques. Many existing studies focused on the musculoskeletal modeling mainly in the clinical applications field (Erdemir, 2007). But with the recent development of DHM packages including musculoskeletal modeling (Anybody Modeling System™, SIMM™/OpenSim™, LifeMOD™ for example), the application field of these models extended to automotive industry (Frayse et al., 2007, estimated muscle forces of the lower limb during a clutch pedal operation).

The analysis of the pedal force control showed that the minimization of joint torque could globally explain the pedal force direction in the XZ plane but not the lateral deviation of the pedal force. In chapter 3, it was showed that the criteria of minimization of joint torques applied better for the “high” and “maximum” force levels than for intermediate levels. Schmidt et al. (2003) showed in case of a fixed bicycle pedal that the use of a musculoskeletal model and the maximization of pedal force could be more effective to predict pedal force direction. The direction of the maximum feasible foot force was determined from a force feasible space (FFS) that represented the range of possible forces the lower limb could theoretically produce. In this study, we are going to explore a musculoskeletal model and to evaluate the minimization of the muscular activity as a potential pedal force control law. This criteria was preferred because of the interpretation regarding the minimization of joint torques may be easier.

The aim of this section was to perform an exploratory investigation of musculoskeletal models in comparison with multi-body model without muscles for a better understanding of the mechanism of force exertion control. This chapter is divided in two parts. First, an introduction to musculoskeletal modeling and muscle force computation was briefly presented. Then the criterion of minimization of the muscular activity was examined for predicting pedal force direction. The results from this criterion were compared with those by minimizing joint torques as well as with experimental observations. Besides, muscular activation patterns were analyzed in order to understand the effect of the proposed muscular optimization criteria.

## 2 Muscle force computation

### 2.1 Modeling of the musculoskeletal system of the human body

For most of existing digital human models used for ergonomic applications, such as AnyBody™, SIMM™ or LifeMod™, the human body is usually modeled as a set of rigid bodies, i.e. the skeleton, connected by the joints. Body movement is powered by "motors", i.e. the muscles. Of all the muscles of the human body, the skeletal muscles are of the most interest as they act to move the segments of the human body by contracting and thereby generate forces on the external environment. Muscles are usually modeled by their line(s) of action. It consists in defining a muscle as a straight line from its point of origin to its point of insertion. Some via-points can be introduced to take into account the deviation of the muscular lines of action by the bony structures. Similarly, the large muscles (the gluteus muscles for example) are modeled by multiple lines of action. The enveloping of deflection surfaces also called wrapping is increasingly used recently. Instead of via-points, the muscles are deflected by virtual surfaces of simple geometric shapes, including cylinders and spheres (Dickerson, 2006; Desailly, 2008). This allows a better approximation of the deviations of muscle lines of action.

### 2.2 Modeling of the physiological behavior of the muscle

In engineering terms, the muscle has a behavior that could be described as viscoelastic: *visco* because its behavior depends on the strain rate and *elastic* as it recovers its original shape and length at the end of a load (Kroemer, 1999).

The muscle strength, also referred as muscle tension, represents the maximal force that a muscle can produce and depends on muscle length (Figure 61). The muscle strength  $F_i^{Total}$  at a given muscle length  $l_i$  is composed of an active component  $f_i^{Active}$  due to the muscular contraction and a passive component  $\sigma_i^{Passive}$  due to the mechanical characteristics of the muscle-tendon unit structure:

For a muscle  $i$ ,

$$F_i^{Total}(l_i) = f_i^{Active}(l_i) + \sigma_i^{Passive}(l_i)$$

The active component of the muscle strength is maximal when the muscle is at its resting length, also called optimal length in the literature. When the muscle shortens, the muscle

strength decreases with the muscular contraction as unique contributor. When the muscle is elongated, the active component of the muscle strength decreases while the passive component increases to the structural limits of the muscle-tendon unit.

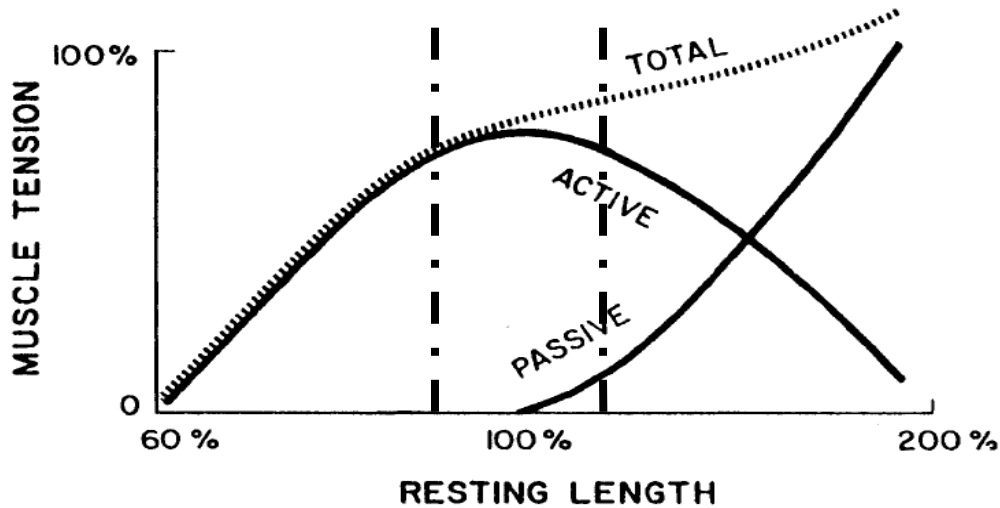


Figure 61: Active, passive and total tension within a muscle at different lengths (Kroemer, 1999).

In the context of the ergonomic assessment of products, the most interesting component is the active component of the muscle strength because this component corresponds to the muscle's physiological behavior as a force actuator. Consequently, the passive component of the muscle strength was not considered in the present study.

The modeling of the physiological behavior of muscles requires the theory of muscle dynamics. Usually the muscle dynamics includes two parts, activation and contraction dynamics. First, the muscle receives a nervous signal also called excitation. From this excitation there is a time delay before the muscle is in its active state and contraction is enabled. Muscle relaxation is also subjected to a time delay. This process is called activation dynamics and can be modeled as a first-order linear differential equation (Manal and Buchanan, 2003; Lloyd and Besier, 2003). Then the contraction dynamics is the dynamical process from the active state of the muscle to force generation to the segments. The most prevalent muscle model used in the literature is the model of Hill (Zajac, 1989). In this phenomenological model, the muscle is considered as a contractile element combined with one or more elastic elements in parallel and/or in series. There are three levels of model definition:

- Model with one contractile element (Figure 62a) in which only the isometric maximum capacity is defined, i.e.  $f_i^{Max} = f_i^{Active}(l_i^{Optimal}) = K_{PCSA} * PCSA_i$ , with

$f_i^{Max}$  the ability of the muscle maximum isometric muscle  $i$  (N),  $K_{PCSA}$  a proportionality factor that can be found in the literature in the literature (in  $N.m^{-2}$ ),  $PCSA_i$  the physiological cross section area (PCSA) of the muscle  $i$  and  $l_i^{Optimal}$  the optimal length of muscle  $i$ .

- Model with two elements in series (a contractile, i.e. muscle and elastic, i.e. tendon) (Figure 62b) which defines the active component of muscle performance, i.e.  $f_i^{Max}$  proportional to the length and contraction speed.
- Full-model with three elements (a non-linear elastic element is added in parallel with the muscle contractile element, i.e. taking into account of the elasticity of the muscle during passive stretching) (Figure 62c).

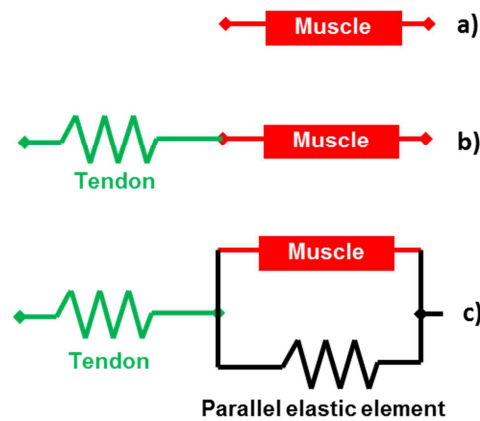


Figure 62: Three levels of definition of Hill's muscle model.

With a Hill-model with two or three elements, the muscle forces exerted on a body segment depend on a dynamic mechanical system which can be described by a first order differential equation. With a Hill-model with only the contractile element, the muscle is considered as a simple force actuator that can produce any force between zero and maximum force.

### 2.3 Definition of the muscle force

The muscle force represents the force generated by muscular contraction to bring closer to each other its origin and insertion point. It is transmitted to the bones by tendons, and thus exerts a torque to the joint connecting the two adjacent segments to which is attached the muscle. Geometrically, joint torque therefore depends on both the muscle force but also on the lever-arm of the muscle (Figure 63).

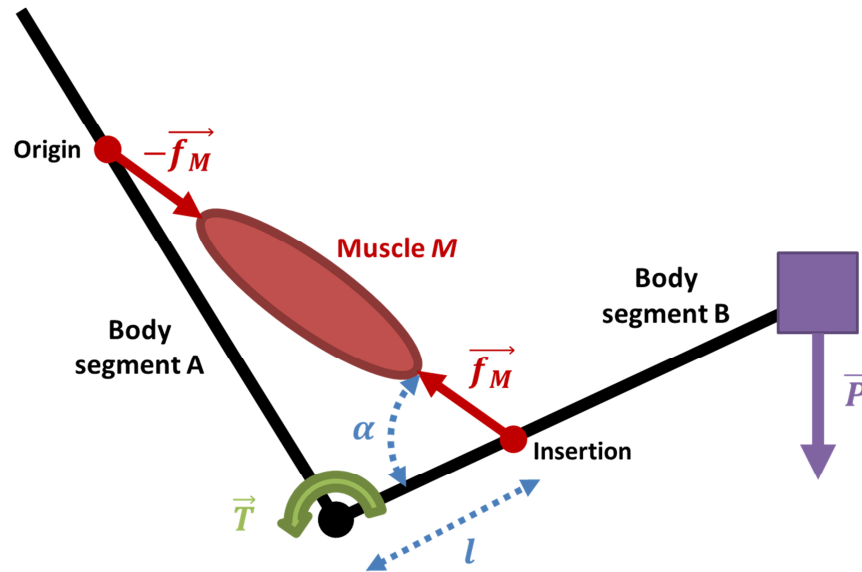


Figure 63: Relation between joint torque, muscle force and muscular lever arm. The muscle  $M$  exerts a force  $f_M$  to compensate the weight  $P$  of the object represented. In this 2D simplistic representation,  $T = f_M \times l \times \sin \alpha$  must be generated to lift the object, with  $l \times \sin \alpha$  the muscular lever arm of the muscle  $M$ . Adapted from Kroemer (1999).

An accurate representation of geometry is therefore important for estimating the muscle forces during a movement and/or an effort because it depends on the lever arms of muscles. Indeed, the distance between the lines of action of the muscles and the considered joint is relatively small. Consequently, a small error in the geometry can lead to a big error in the estimation of the lever arm and therefore in the calculation of muscle forces.

The general equation of movement using a musculoskeletal model can be expressed as follows (Pandy, 2001):

$$M(q)\ddot{q} + C(q, \dot{q}) + G(q) + R(q)f_{MT} + E = 0 \text{ (Eq. 7)}$$

Where

$q$  are parameters characterizing the movement (joint angles, natural coordinates ...)

$M$  is the mass matrix

$C$  is the centrifugal and Coriolis loading

$G$  is the gravitational loading

$E$  represents external forces

$R(q)f_{MT}$  represents muscular joint torques, where  $R$  is the matrix of muscular lever arms and  $f_{MT}$  are the muscle forces. Another definition is  $T_{MT} = R(q)f_{MT}$ , where  $T_{MT}$  are the joint torques.

## 2.4 Computation of the muscle forces

Several sub problems can be defined from Eq. 7, depending on the unknowns in the problem as well as the data available (see Erdemir, 2007 for a review):

- Inverse dynamics and static optimization: the muscle forces are computed from a measured motion ( $q$  and  $E$  are known,  $f_{MT}$  are unknown). In this approach, the muscle is considered as a simple force actuator and the optimization is linear.
- Forward dynamics: a motion is computed from known muscle forces. This approach uses EMG (ElectroMyoGram) data recorded during motion as an input to simulate a motion. Forward dynamics requires therefore a model of activation contraction dynamics to estimate the muscle forces from EMG data ( $q$  unknown,  $E$  and  $f_{MT}$  known). The optimization problem becomes large and non-linear, because it has the segment positions  $q$  and its derivatives as unknowns.
- Forward dynamics assisted data tracking: in this approach,  $q$ ,  $E$  and  $f_{MT}$  are known. Rather than solving the equation Eq. 7 using the inverse dynamics approach, an initial set of muscle activations are fed into a forward dynamics model of the musculoskeletal system. The solution is optimized using experimental data to find the muscle activations that best reproduce the experimental kinematics.
- Optimal control strategies: this approach is close to forward dynamics assisted data tracking as it is also based on a forward dynamics model. However, in this approach, the optimisation criterion is not limited to fit the experimental kinematics. Other criterion such as the minimization of the energetic cost of a motion (Anderson et al., 2001) can be used.

Another method was also proposed recently DeGroot et al (2009):

- Physiological inverse dynamics: as the inverse dynamics and static optimization approach, the muscle forces are computed from a measured motion ( $q$  and  $E$  are known,  $f_{MT}$  are unknown) but muscle dynamics with both activation and contraction dynamics is considered. This optimization problem is therefore non-linear, muscle dynamics introducing differential equations.

The inverse dynamics approach with static optimization is widely used, as the movement parameters  $q$  and external forces  $E$  can be easily measured experimentally using a motion capture system and force sensors. In this study, motion and external contact force data are

available for the muscle force computation using an inverse dynamics approach. Therefore, only this approach was developed.

In the inverse dynamics approach with static optimization, joint torques are first calculated using Eq. 8:

$$T_{MT} = M(q)\ddot{q} + C(q, \dot{q}) + G(q) + E \quad (\text{Eq. 8})$$

Joint torques  $T_{MT}$  are directly computed recursively at each joint by isolating each body segment one by one, starting from the most distal (on which the external forces are measured) to the most proximal. The muscle forces are calculated by solving Eq. 9:

$$f_{MT} = R(q)^{-1}T_{MT} \quad (\text{Eq. 9})$$

However, the calculation of the muscle forces is not unique. Indeed, the problem is underdetermined, which means that there are more unknowns (i.e. the muscles) than number of equations (i.e. degrees of freedom of the system). As a consequence, the matrix  $R$  is not invertible and the problem requires using optimization. The optimization problem can be formalized as:

*Minimize  $J(f_{MT})$  so that:*

$$T_{MT} = R(q)f_{MT}$$

$$0 \leq f_{MT} \leq f_{Max}$$

$$g(f_{MT}, q) \leq 0$$

$$h(f_{MT}, q) = 0$$

*With*

*$f_{Max}$  the maximum muscle force capacities of the considered muscles*

*(g,h) additional constraints depending on the specific requirements of the joint under investigation.*

There are several minimization criteria  $J$  in the literature such as (Erdemir, 2007):

- Minimization of the sum of the muscle forces or squared muscle forces
- Minimization of the sum of  $n^{\text{th}}$  power of muscle stresses
- Minimization of the sum of instantaneous muscle power
- Minimization of the maximal relative muscle load
- ...

One of the most frequently used criteria is the minimization of the sum of squared muscle stresses, i.e. muscle force divided by the physiological cross section area (PCSA) of the muscle (Crowninshield and Brand, 1981; Kaufman et al., 1991):

$$J(F_{MT}) = \sum_{i=1}^n \left( \frac{f_i}{PCSA_i} \right)^2$$

One of the advantages of this criterion is that the optimization problem becomes convex. Indeed,  $J$  is quadratic regarding  $f_{MT}$  and the constraint  $T_{MT} = R(q)f_{MT}$  is linear. Therefore, the problem always has a unique global solution.

### 3 Pedal force direction control by minimizing muscular activities

#### 3.1 Description of the musculoskeletal model used

A musculoskeletal model of the lower limb, developed at LBMC by Fraysse (2009) (Figure 64), was used in this work. Bone geometry was based on the data collected within the European project HUMOS 2 (Vein et al., 2005) and is composed of four rigid segments: pelvis, femur + patella, tibia + fibula and foot.

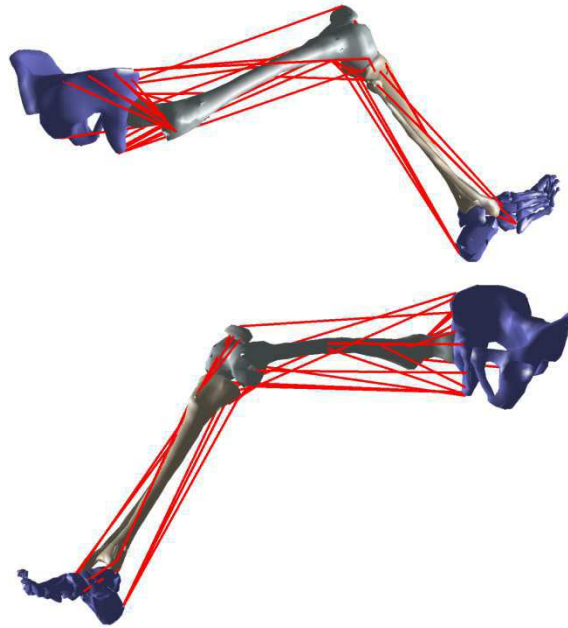


Figure 64: General views of the musculoskeletal model of the lower limb developed by Fraysse (2009).

The model includes 29 muscles for the lower limb, presented as well as their respective actions in Figure 65.

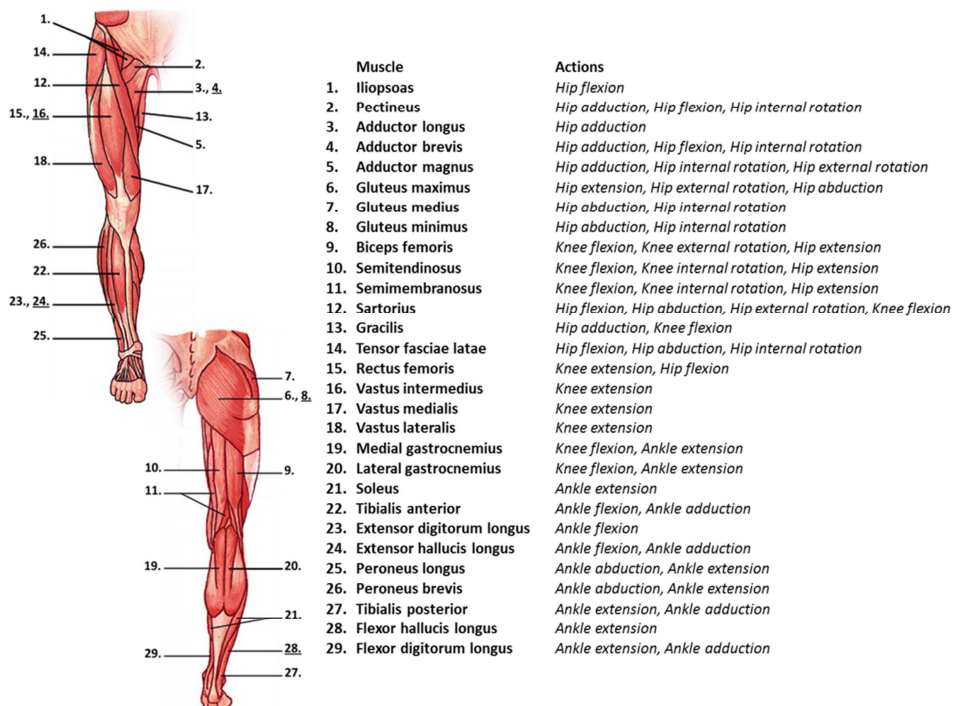


Figure 65: Muscles included in the musculoskeletal model developed by Fraysse (2009). The underlined numbers correspond to deep muscles, which are located underneath the surface muscles represented in the figure.

Muscles were modeled by their line(s) of action, i.e. 1D element. Muscles' origin, insertion and via-points were based on the lower limb model developed by Delp (1990) and, if necessary, adjusted to the bone geometry from HUMOS 2 on a case by case basis. Indeed, these adjustments were important to avoid incoherencies compared to the anatomic description of the muscles. The coordinates of each muscle's origin, insertion and via-points were expressed in the local coordinate system of the reference bone segment. For example, gluteus maximus's origin was expressed in the pelvis local coordinate system and its insertion in the femur local coordinate system.

For each muscle, a model with one contractile element was chosen. Force-length and force-velocity relationships, tendons, as well as excitation-contraction dynamics were not considered. Only the maximum isometric muscle force was considered. Muscles PCSAs (physiological cross section areas, i.e. area of the cross-sections perpendicular to the muscle fibers) were taken from data reported by Thorpe and al (1997). An inverse dynamics with static optimization approach was considered to compute the muscle forces. The computation of the muscle forces in this approach is an underdetermined problem (more unknowns than equations) requiring a resolution by optimization. The objective function used to compute the muscle forces was the minimization of squared muscle stresses,  $J = \sum_{i=1}^n \left( \frac{f_i}{PCSA_i} \right)^2$  (Crowninshield and Brand, 1981; Kaufman et al., 1991).

The musculoskeletal model was evaluated by Fraysse (2009) regarding the definition of the muscles by the analysis of the muscular lever arms and regarding the performance to reproduce joint maximal voluntary force by comparison to literature data (Chaffin et al., 1999). The muscular lever arms were showed in agreement with the physiological functions of each muscle. The prediction of joint maximal voluntary force was in agreement with the literature for average joint positions, but it was less accurate for joint positions close to the joint limits, especially for ankle extension. In the case of the clutch pedal operation, extreme joint positions could happen at the end of the pedal depression. However, the behavior of the model in estimating muscle forces during clutch pedal operation was also evaluated by Fraysse et al. (2007) using the data from the experiment of Wang et al. (2000). The activation patterns of the iliopsoas, the rectus femoris and the soleus were in agreement regarding their respective physiological function and the task. The patterns were not compared to EMG data because this type of data was not available..

### 3.2 Optimization problem

The aim was to explain the pedal force control by the minimization of the muscular activity as a potential pedal force control law. The optimization problem is then to find the pedal force direction that minimizes the muscular activities and it can be formalized as in Eq. 10:

$$\text{Minimize } W = \sum_{i=1}^{n \text{ muscles}} (\alpha_i)^2 = \sum_{i=1}^{n \text{ muscle}} \left( \frac{f_i}{f_i^{Max}} \right)^2 \quad (\text{Eq. 10})$$

With

$\alpha_i$ , the muscular activation level of the muscle  $i$

$f_i$ , the force from the muscle  $i$ ,

$f_i^{Max}$ , the maximum force capacity of the muscle  $i$ .

The muscle forces  $f_i$  were computed using the inverse dynamics with static optimization approach implemented in the musculoskeletal model.

In the present problem, both the data from ExpMax and ExpPcp of the FAC experiment were used. The joint angles, the pedal position and the pedal force in the rest posture were known. The design variable  $\overrightarrow{F_{SimMS}}$ , i.e. the pedal force simulated by minimizing the muscular activity, was constrained in the same way as in the pedal force direction simulation using the minimization of the joint torques, i.e. conservation of the tangential component, and the joint torques necessary to the muscle forces estimation were computed as in the previous simulation.

Here, only the joint torques generated by the muscles were considered in the muscle force computation. As the hip is modeled as a ball joint, it is considered that all the three hip joint torques are generated by the muscles. At the knee, Lloyd and Buchanan (2001) showed that knee muscles contraction provided only 11-14% of the abduction/adduction moment. As a consequence, it can be considered that the muscles do not generate the knee joint abduction/adduction moment but only flexion/extension and axial rotation moments. The same consideration can be applied for the ankle axial rotation moment as this moment is prevented by the bony structures of the ankle (shape of tibio-tarsal joint).

Then, a common value of the proportional factor  $K_{PCSA}$  was chosen to estimate the maximum force capacity of each muscle that would constrain the muscle forces  $f_i$  when computed by the static optimization. The value of  $K_{PCSA}$  was chosen such that the constraints on the muscle

forces  $f_i$  allow the static optimization to find a solution. The simulation was therefore tested using the data of the maximum pedal force exertion from the subject (subject 6) who had exerted the highest pedal force in ExpMax. By trial and test, it was found that  $K_{PCSA} = 50 \text{ N.cm}^{-2}$  allow the muscle force computation for this subject. As a consequence, this value of  $K_{PCSA}$  was applied to all subjects.

Finally, the geometry of the musculoskeletal model (e.g. the lever arm) was scaled to each subject of the Ifsttar/Renault experiment. The segments of the bone geometry were scaled according the dimensions of the corresponding body segment in the individualized RAMSIS manikin. As the muscles' origin, insertion and via-points were expressed in their respective reference bone segment local coordinate system, the same geometry-scaling factor was used to calculate the new coordinates of the muscles' characteristic points.

## 4 Results

### 4.1 Force force direction

The pedal force directions simulated by minimizing  $W$  (Eq. 10) ( $\theta_{F_{SimMS}}$  and  $\delta_{F_{SimMS}}$ ), were compared with experimental force directions ( $\theta_{F_{Exp}}$  and  $\delta_{F_{Exp}}$ ). The two sets of simulated data with the inputs from the maximum force exertion (ExpMax) and force perception (ExpPcp) trials, were statistically analyzed separately.  $\theta_{F_{SimMS}}$ , the simulated pedal force direction in XZ plane, and  $\delta_{F_{SimMS}}$ , the lateral deviation in XY plane were estimated using the same definition as in the previous section. The values of simulated normal and transversal force components as well as the experimental and simulated pedal force direction in XZ and XY planes are presented in Appendix. Figure 66 shows the comparison of pedal force direction in XZ plane between simulated and experimental data. For comparison purpose, the pedal force directions simulated by minimizing the joint torques (Sim1 in Chapter 2) ( $\theta_{F_{Sim}}$  and  $\delta_{F_{Sim}}$ ) are also presented.

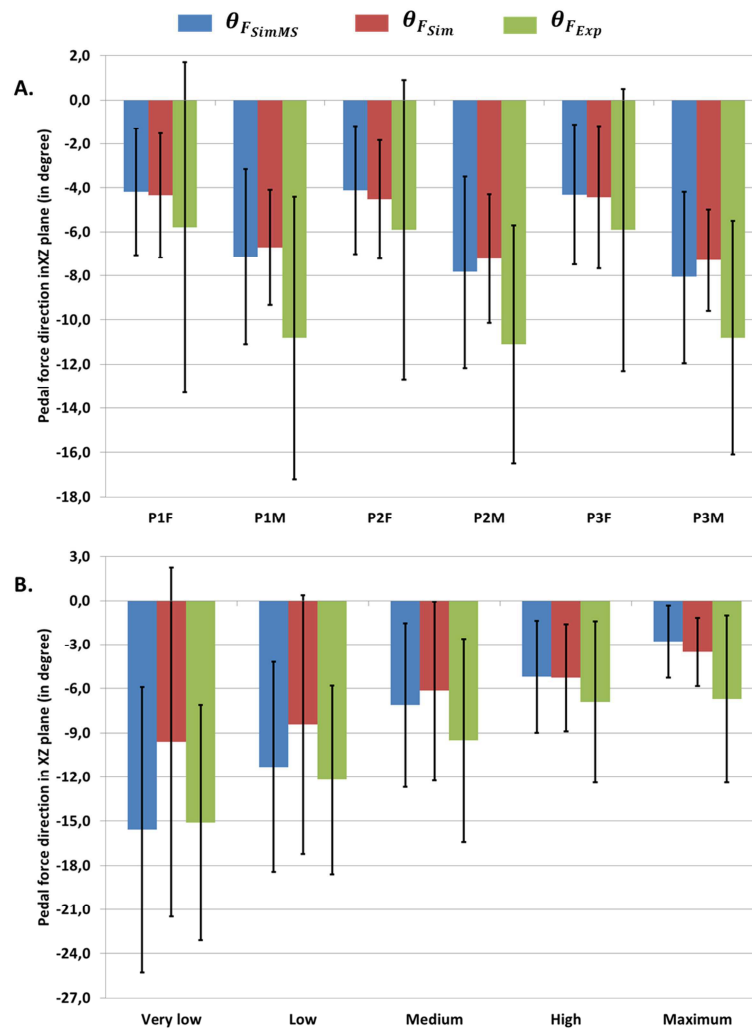


Figure 66: Means and standard deviations of pedal force direction in XZ plane from experiment, joint torque minimization-based simulation and muscular activity minimization based-simulation (respectively  $\theta_{F_{Exp}}$ ,  $\theta_{F_{Sim}}$  and  $\theta_{F_{SimMS}}$ ) for maximum pedal force exertion experiment (A) and pedal force perception experiment (B).

The pedal force direction in XZ plane simulated by minimizing muscular activity showed results similar to the ones by minimizing joint torques, especially for the maximum pedal force exertion data.  $\theta_{F_{SimMS}}$  and  $\theta_{F_{Sim}}$  are  $-6^\circ$  and  $-5.8^\circ$  on average respectively. Larger differences between the two simulations were found for the “very low” and “low” force levels. Interestingly,  $\theta_{F_{SimMS}}$  simulated by minimizing muscular activity were a little bit closer to  $\theta_{F_{Exp}}$  than  $\theta_{F_{Sim}}$  simulated by minimizing joint torques. For the medium force level, both simulations were quite similar. Note that both  $\theta_{F_{Sim}}$  and  $\theta_{F_{SimMS}}$  showed the same tendency as  $\theta_{F_{Exp}}$ : 1/ pedal force direction closer to the HipP<sub>app</sub> axis for mid-travel pedal positions than for end-travel pedal positions for maximum pedal force exertion, 2/ pedal force direction getting closer to the HipP<sub>app</sub> axis with force level, 3/ short women had an average force direction closer to the reference axis (Table 63 and Table 64 in Appendix).

Concerning the lateral deviation in XY plane, both simulations predicted a rightward (in the driver's point of view) lateral deviation contrary to experimental data that showed a leftward lateral deviation (Figure 67). Besides the average values of  $\delta_{F_{SimMS}}$  and  $\delta_{F_{Sim}}$  were close for both maximum pedal force exertion and pedal force perception data.

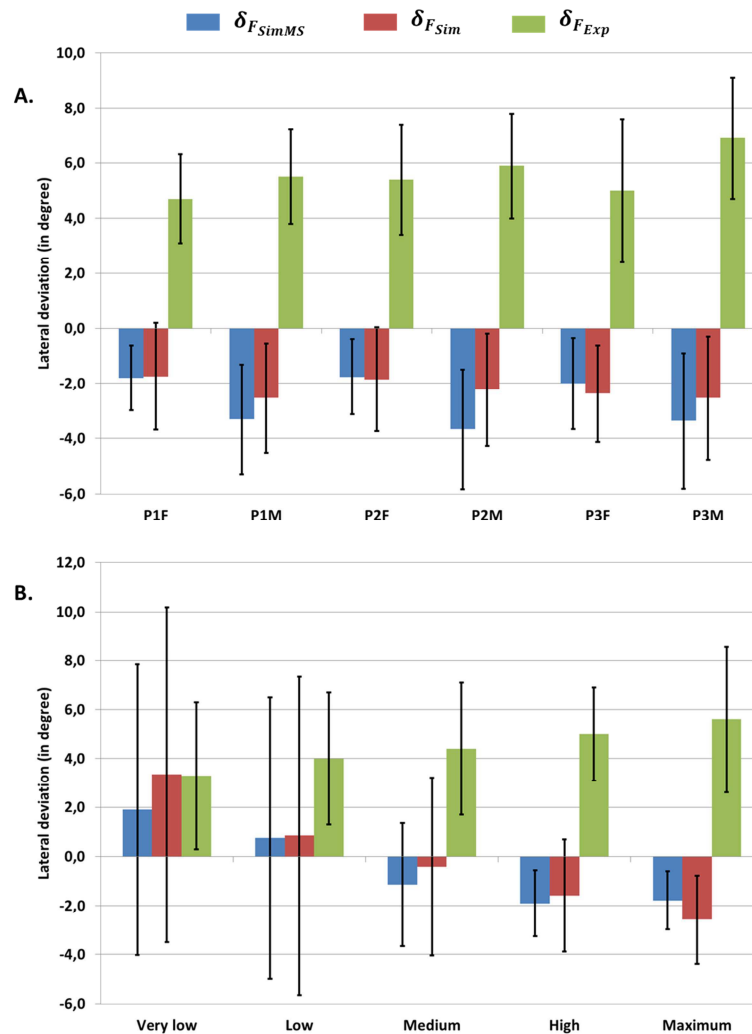


Figure 67: Means and standard deviations of pedal force lateral deviation in XY plane from experiment, joint torque minimization based simulation and muscular activity minimization based simulation (respectively  $\delta_{F_{Exp}}$ ,  $\delta_{F_{Sim}}$  and  $\delta_{F_{SimMS}}$ ) for A. maximum pedal force exertion experiment and B. pedal force perception experiment.

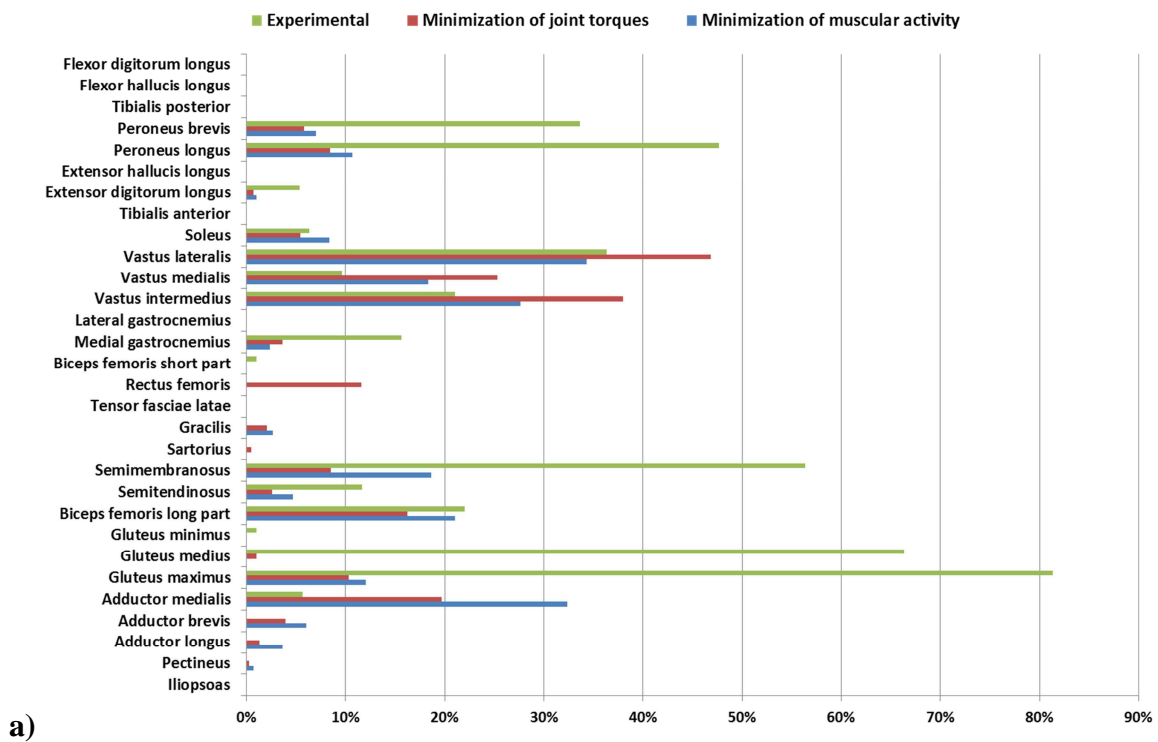
## 4.2 Muscle force patterns

One of the advantages to use a musculoskeletal model is the possibility for analyzing muscular activation patterns. An average male subject of the Ifsttar/Renault experiment was selected to illustrate the muscular activation patterns. The muscular activations were calculated for the selected subject using the experimental pedal force and the pedal forces simulated using the two proposed criteria. The posture, and so, the muscular lever arms used

for the muscle force computation were the same. Only the pedal force was different as an input.

First, the average muscular activation patterns corresponding to the experimental force ( $F_{Exp}$ ), the pedal force simulated by the minimization of muscular activity ( $F_{SimMS}$ ) and the pedal force simulated by the minimization of joint torques ( $F_{Sim}$ ) for maximum pedal force exertion at mid-travel (Figure 68a) and end-travel (Figure 68b) pedal position were analyzed. The muscular activation patterns show that the main muscles activated had a physiological function in agreement with the task:

- Soleus, peroneus longus and brevis are ankle extensors,
- Vastus lateralis, medialis and intermedius are knee extensors,
- Gluteus maximus, biceps femoris, semimembranosus and semitendinosus are hip extensors.



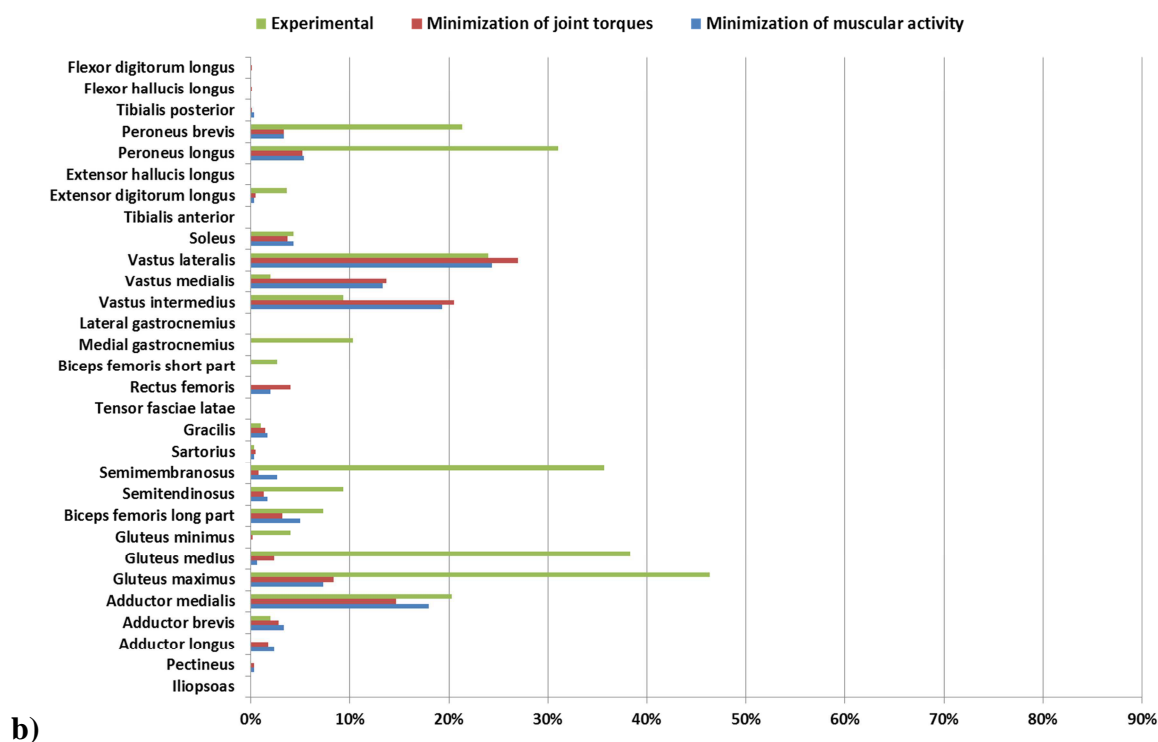


Figure 68: Average muscular activation levels for the experimental force, the pedal force simulated by the minimization of muscular activity and the pedal force simulated by the minimization of joint torques at (a) mid-travel and (b) end-travel pedal position.

Globally, the simulated pedal forces had lower muscle activation levels than experimental pedal force.  $F_{SimMS}$  and  $F_{Sim}$  showed similar activation patterns for both pedal positions. This can be explained by the fact that the two minimization criteria predicted similar pedal force directions. It can also be noticed that muscles were more activated for mid-travel pedal position than for end-travel position. This is in agreement with the fact that the subjects have on average exerted higher maximum pedal forces on mid-travel pedals.

Then, it can be observed that the hip adductors (adductor medialis, brevis and longus) were more activated by the simulated forces, whereas the experimental forces activated more the hip abductors (gluteus medius and maximus). This can be explained by the fact that experimentally the pedal force was directed leftward, i.e. in the direction of the hip abduction. On the other hand, the simulated pedal forces were directed rightward, which means in the direction of the hip adduction. The same explanation can be used for the average activation of the peroneus muscles which are responsible of the ankle eversion or abduction. It can also be observed that hip extensors (gluteus maximus, biceps femoris, semitendinosus, semimembranosus) were more activated than the knee extensors (rectus femoris and the three vastus) with the experimental forces. This is in agreement with the fact that the experimental pedal force directions were further from the  $HipP_{App}$  axis than the pedal force directions

simulated by either the minimization of joint torque or the minimization of muscular activity. Indeed, a pedal force direction further from the HipP<sub>App</sub> axis would cause higher hip joint torques and lower knee joint torques than a pedal force direction close the HipP<sub>App</sub> axis. However, as the contact pressure between the thigh and seat was only partly considered by removing the pedal force in rest position, the hip joint torques equilibrated by the muscle may not be reliable to propose further explanation.

For intermediate force level, the results of the two simulations only significantly differed for the “very low” and “low” force levels, for which  $\theta_{F_{SimMS}}$  were closer to  $\theta_{F_{Exp}}$  than  $\theta_{F_{Sim}}$ . Figure 69 showed the activation of the muscles corresponding to  $F_{Exp}$ ,  $F_{SimMS}$  and  $F_{Sim}$  for the “low” pedal force exertion.

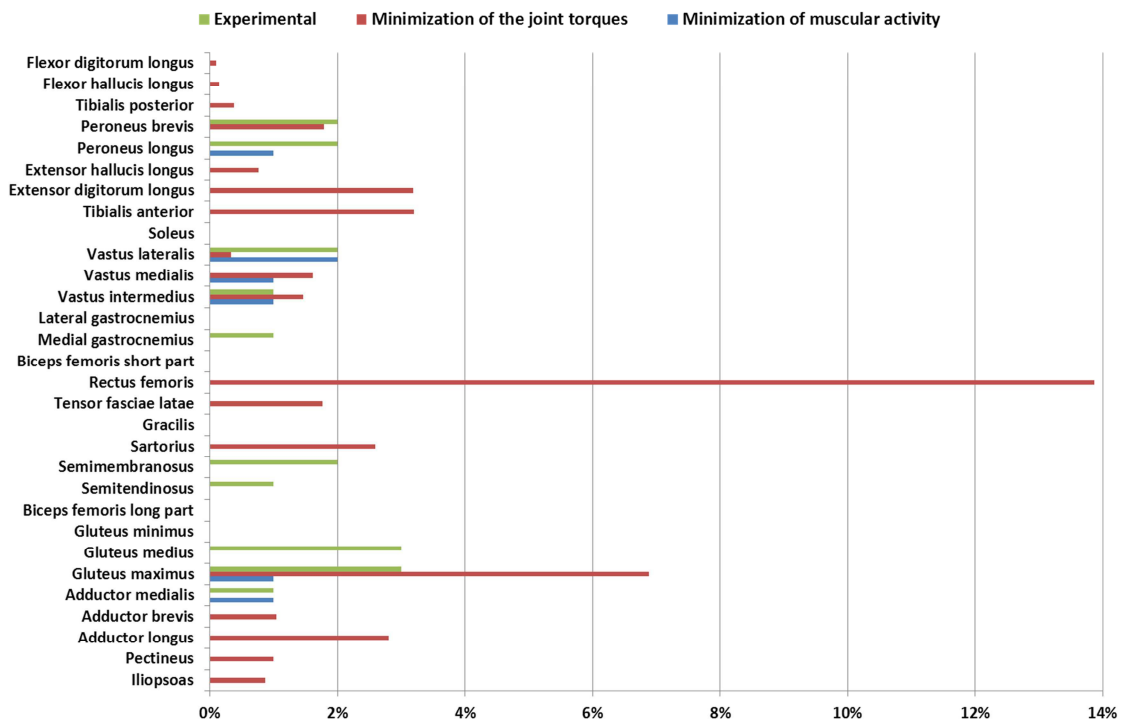


Figure 69: Muscular activation levels for the experimental force, the pedal force simulated by the minimization of muscular activity and the pedal force simulated by the minimization of joint torques (F<sub>Sim</sub>) at a low force level.

It can be noticed that  $F_{Sim}$  activated more muscles than  $F_{Exp}$  and  $F_{SimMS}$ . Moreover  $F_{Sim}$  caused higher activation than the two other forces, especially for the rectus femoris (14%) and the gluteus maximus (7%). On the opposite, the muscular activations from  $F_{Exp}$  and  $F_{SimMS}$  showed between 2% and 3% of muscular activation at maximum. Besides  $F_{Exp}$  and  $F_{SimMS}$  activated the same extensor muscles: the gluteus maximus for the hip, the vastus for the knee, the peroneus longus for the ankle. This illustrates the fact that  $\theta_{F_{SimMS}}$  were on average closer to  $\theta_{F_{Exp}}$  than  $\theta_{F_{Sim}}$ .

## 5 Discussion and conclusion

Using a musculoskeletal model of the lower limb and the criterion of minimization of muscular activity, the simulation predicted pedal force directions close to the ones predicted by the minimization of joint torques for maximum pedal force and pedal force perception exertions. But for low intermediate force levels, the minimization of the muscular activity showed results closer to the experimental one in the XZ plane than the other minimization criterion.

The proposed criterion is consistent with the minimization of the joint torques, at least at maximum force level. Indeed, at maximum force level, it can be considered that all muscles, which had a physiological function in agreement with the task, are activated. Thus minimizing the joint torques can be interpreted as minimizing the muscle forces at the joint. However, for intermediate force level, all muscles with a physiological function in agreement with the task may not be activated and there may be muscular recruitment that produces the necessary force at the joint minimizing the muscular activation. The results on the activation patterns showed that the minimization of the joint torques activated more muscles and in higher levels than the muscular minimization criterion. It may suggest that low intermediate force levels, reducing the joint load may be a motor control strategy more costly than minimizing the muscular activity. This would be consistent with the principle of minimum work, observed in biomechanical analysis of leg movements during clutch pedal operation (Wang et al., 2000) and can explain why the minimization of muscular activity had a pedal force direction close to experimental one in XZ plane.

For the lateral deviation, the comparison of the muscle activation patterns for maximum pedal force exertion showed that the experimental force caused on average higher activation levels than the simulated pedal force, especially in the hip and ankle abductor muscles. An explanation can be found in the analysis of the muscular lever-arms. Indeed, the muscle force computation depends highly on the lever-arms of the muscles (cf. Eq. 9 in this chapter). Considering that the lateral deviation is mainly due to hip abduction or adduction, Table 60 shows the lever-arm values for the main hip adductors and abductors of the selected subject for mid-travel and end-travel pedal position.

	Hip adductors			Hip abductors		
	Adductor longus	Adductor brevis	Adductor magnus	Gluteus maximus	Gluteus medius	Gluteus minimus
P1F	78.3	40.2	41.9	4.8	33.7	22.8
P1M	81.1	35.8	38.8	5.5	26.8	16.0
P2F	76.8	42.8	43.3	2.4	35.5	25.5
P2M	80.1	38.1	40.3	4.4	30.5	19.6
P3F	75.4	43.2	44.4	5.6	38.7	27.6
P3M	79.9	38.8	40.7	4.5	33.5	21.9

**Table 60: Lever-arm values for the main hip adductors and abductors of the selected subject for mid-travel and end-travel pedal position. The values are in mm.**

It can be noticed that the lever-arms for adduction are globally larger than the one for abduction. As a consequence, lower activation levels would be required from adductors than from the abductors to generate respectively adduction and abduction torques of the same magnitude. Minimizing the muscular activity would therefore rather support the adduction regarding the abduction if not constrained and thus predict a rightward pedal force direction than a leftward one.

Then, the behavior of the model was evaluated by Fraysse (2009) and showed that physiological functions of the muscles were respected. As a matter of fact, the analysis of the muscular patterns was consistent with the analysis of the pedal force direction. However, the muscular activation patterns were not compared to experimental EMG patterns in order to validate the output of the muscle force computation. In the Ifsttar/Renault experiment, no EMG were recorded but EMG were placed on biceps femoris (hip extensor and knee flexor), rectus femoris (hip flexor and knee extensor), tibialis anterior (ankle flexor) and lateral and medial gastrocnemius (knee flexor and ankle extensor) in the DHErgo experiment (Figure 70).

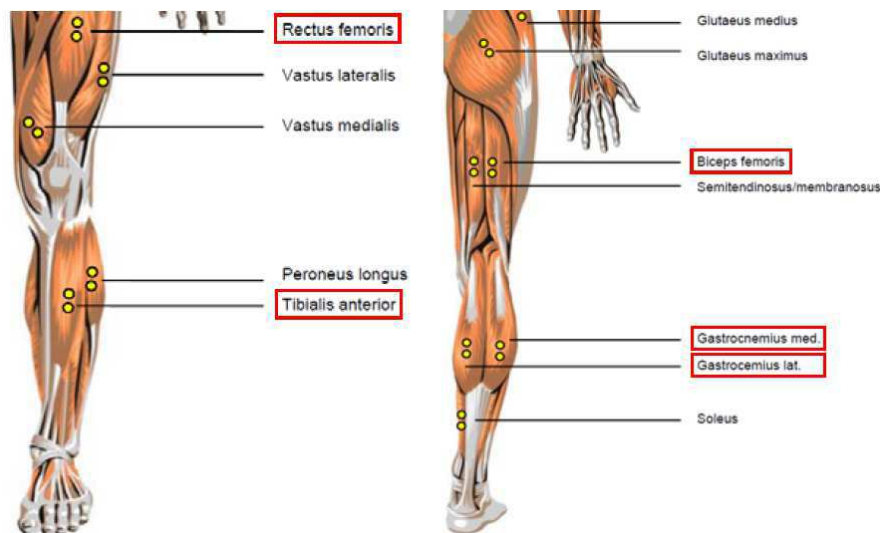


Figure 70: Muscles selected for EMG measurement in DHErgo experiment.

However, these EMG data were not comparable to the output of the muscle force computation. Indeed, the muscle force computation depends on the joint torques computation by inverse dynamics and as the seat/thigh contact force was not estimated during the clutch pedal operation in DHErgo experiment, the hip joint torques used in the muscle force computation were not reliable. Besides the most important muscles of the lower limb such as rectus femoris, biceps femoris and the lateral and medial gastrocnemius are bi-articular muscles, i.e. crossing two joints. As a result, an unreliable estimation of the hip joint torque would also affect the muscle recruitment at the knee and the ankle. Therefore the available EMG data were not suitable to validate the output of the muscle force computation.

Finally, the present work aimed at investigating the potential contributions of the musculoskeletal modeling for the understanding of the pedal force control. The proposed muscular optimization criterion was consistent with the need of reducing the joint load when increasing force exertion level and improved the results of the simulation of pedal force direction for intermediate force levels. However, the preferred pedal force direction in the XY plane was not explained by any of the minimization criteria. The study also showed that the validation of estimated muscle forces is, in particular a major issue, for the musculoskeletal model. Even if all external forces (especially contact forces) were known, a quantitative validation of the muscle force computed may be hard to achieve because the computation depends on the muscle lever-arms and on the maximum muscle force capacity (Scovil et al., 2006; Redl et al., 2007), which also means that the computation of muscle forces highly depends on the anthropometry and the strength capacity of the subject.

## 6 Appendix

### 6.1 Comparison of simulated and experimental pedal force directions

Table 61: Means and standard deviations of pedal force direction in XZ plane from experiment, joint torque minimization-based simulation and muscular activity minimization based-simulation (respectively  $\theta_{F_{Exp}}$ ,  $\theta_{F_{Sim}}$  and  $\theta_{F_{SimMS}}$ ) for a) maximum pedal force exertion experiment and b) pedal force perception experiment.

a)	$\theta_{F_{Exp}}$	$\theta_{F_{SimMS}}$	$\theta_{F_{Sim}}$
P1F	-5.8 ± 7.5	-4.2 ± 2.9	-4.3 ± 2.8
P1M	-10.8 ± 6.4	-7.1 ± 4.0	-6.7 ± 2.6
P2F	-5.9 ± 6.8	-4.1 ± 2.9	-4.5 ± 2.7
P2M	-11.1 ± 5.4	-7.8 ± 4.3	-7.2 ± 2.9
P3F	-5.9 ± 6.4	-4.3 ± 3.2	-4.4 ± 3.2
P3M	-10.8 ± 5.3	-8.1 ± 3.9	-7.3 ± 2.3
Short women	-5.9 ± 7.2	-3.1 ± 2.3	-3.3 ± 2.7
Average men	-7.4 ± 5.9	-6.2 ± 4.1	-6.3 ± 2.9
Tall men	-11 ± 6.1	-7.8 ± 3.6	-7.1 ± 2.2
All	-8.4 ± 6.7 <sup>G***, P***</sup>	-6.0 ± 3.9 <sup>G***, P***</sup>	-5.8 ± 3.1 <sup>G***, P***</sup>
b)	$\theta_{F_{Exp}}$	$\theta_{F_{SimMS}}$	$\theta_{F_{Sim}}$
Very low	-15.1 ± 8	-15.6 ± 9.7	-9.6 ± 11.9
Low	-12.2 ± 6.4	-11.3 ± 7.1	-8.4 ± 8.8
Medium	-9.5 ± 6.9	-7.1 ± 5.6	-6.2 ± 6.1
High	-6.9 ± 5.5	-5.2 ± 3.8	-5.3 ± 3.7
Maximum	-6.7 ± 5.7	-2.8 ± 2.5	-3.5 ± 2.3
Short women	-7.1 ± 6.6	-5.8 ± 7.7	-2.0 ± 4.6
Average men	-8.5 ± 7.1	-7.8 ± 7.2	-7.7 ± 7.5
Tall men	-12.1 ± 6.7	-8.4 ± 7.3	-7.7 ± 7.2
All	-9.5 ± 7.1 <sup>G***, P***</sup>	-7.5 ± 7.4 <sup>G***, P***</sup>	-6.1 ± 7.1 <sup>G***, P***</sup>

\*p<0.05, \*\*p<0.01, \*\*\* p<0.001. G: group of subjects; P: Pedal position; F: force level

Table 62: Means and standard deviations of pedal force lateral deviation in XY plane from experiment, joint torque minimization based simulation and muscular activity minimization based simulation (respectively  $\delta_{F_{Exp}}$ ,  $\delta_{F_{Sim}}$  and  $\delta_{F_{SimMS}}$ ) for a) maximum pedal force exertion experiment and b) pedal force perception experiment.

a)	$\delta_{F_{Exp}}$	$\delta_{F_{SimMS}}$	$\delta_{F_{Sim}}$
P1F	4.7 ± 1.6	-1.8 ± 1.2	-1.7 ± 1.9
P1M	5.5 ± 1.7	-3.3 ± 2.0	-2.5 ± 2.0
P2F	5.4 ± 2	-1.8 ± 1.4	-1.9 ± 1.9
P2M	5.9 ± 1.9	-3.7 ± 2.2	-2.2 ± 2.0
P3F	5 ± 2.6	-2.0 ± 1.7	-2.4 ± 1.8
P3M	6.9 ± 2.2	-3.4 ± 2.5	-2.5 ± 2.2
Short women	6.6 ± 1.5	-1.6 ± 1.5	-1.4 ± 2.2
Average men	6 ± 1.7	-2.5 ± 1.7	-1.9 ± 1.9
Tall men	4.4 ± 2.3	-3.6 ± 2.1	-3.1 ± 1.5
All	5.6 ± 2.1 <sup>G***, P***</sup>	-2.7 ± 2.0 <sup>G***, P***</sup>	-2.2 ± 2.0 <sup>G***</sup>

b)	$\delta_{F_{Exp}}$	$\delta_{F_{SimMS}}$	$\delta_{F_{Sim}}$
Very low	3.3 ± 3	1.9 ± 5.9	3.3 ± 6.8
Low	4 ± 2.7	0.7 ± 5.7	0.8 ± 6.5
Medium	4.4 ± 2.7	-1.1 ± 2.5	-0.4 ± 3.6
High	5 ± 1.9	-1.9 ± 1.4	-1.6 ± 2.3
Maximum	5.6 ± 3	-1.8 ± 1.2	-2.6 ± 1.8
Short women	6 ± 2.3	0.8 ± 6.3	1.4 ± 7.3
Average men	4.7 ± 2.1	-0.6 ± 1.9	-0.2 ± 2.8
Tall men	3.6 ± 2.6	-1.7 ± 2.2	-2.0 ± 3.2
All	4.7 ± 2.6 <sup>G***, P***</sup>	-0.7 ± 3.9 <sup>G***, P***</sup>	-0.5 ± 4.8 <sup>G***, P***</sup>

\*p<0.05, \*\*p<0.01, \*\*\*p<0.001. G: group of subjects; P: Pedal position; F: force level

## 6.2 Comparison of simulated and experimental normal and transversal forces

Table 63: Means and standard deviations of simulated (for muscular activity minimization and joint torques minimization) and experimental normal forces a) maximum pedal force exertion and b) pedal force perception experiments.

a)	Normal force (N)		
	Muscular activity minimization	Joint torque minimization	Experiment
P1F	-258 ± 117	-260 ± 119	-279 ± 150
P1M	-170 ± 86	-166 ± 82	-218 ± 114
P2F	-250 ± 122	-254 ± 123	-277 ± 155
P2M	-149 ± 84	-141 ± 72	-185 ± 97
P3F	-259 ± 135	-261 ± 133	-284 ± 159
P3M	-145 ± 86	-136 ± 79	-176 ± 106
Short women	-124 ± 89	-125 ± 87	-145 ± 103
Average men	-225 ± 123	-232 ± 124	-257 ± 163
Tall men	-247 ± 101	-236 ± 105	-287 ± 103
All	-205 ± 117 <sup>G***, P***</sup>	-203 <sup>G***, P***</sup> ± 117	-237 <sup>G***, P**</sup> ± 138

b)	Normal force (N)		
	Muscular activity minimization	Joint torque minimization	Experiment
Very low	-44 ± 22	-38 ± 27	-44 ± 23
Low	-60 ± 29	-57 ± 35	-63 ± 32
Medium	-91 ± 50	-93 ± 58	-100 ± 55
High	-152 ± 80	-156 ± 86	-167 ± 93
Maximum	-250 ± 114	-266 ± 123	-303 ± 144
Short women	-84 ± 82	-81 ± 86	-93 ± 85
Average men	-165 ± 128	-170 ± 134	-176 ± 155
Tall men	-161 ± 108	-173 ± 126	-203 ± 149
All	-141 ± 114 <sup>G***, P***</sup>	-146 <sup>G***, P***</sup> ± 125	-163 <sup>G***, P***</sup> ± 143

\*p<0.05, \*\*p<0.01, \*\*\* p<0.001. G: group of subjects; P: Pedal position; F: force level

Table 64: Means and standard deviations of simulated (for muscular activity minimization and joint torques minimization) and experimental transversal forces a) maximum pedal force exertion and b) pedal force perception experiments.

Transversal force (N)			
a)	Muscular activity minimization	Joint torque minimization	Experiment
P1F	18 ± 13	16 ± 23	-49 ± 27
P1M	43 ± 29	34 ± 32	-71 ± 40
P2F	18 ± 16	20 ± 22	-55 ± 30
P2M	45 ± 30	28 ± 27	-70 ± 38
P3F	18 ± 16	20 ± 18	-44 ± 34
P3M	37 ± 27	27 ± 26	-71 ± 40
Short women	13 ± 13	8 ± 16	-49 ± 32
Average men	26 ± 19	20 ± 24	-72 ± 37
Tall men	45 ± 28	40 ± 24	-58 ± 37
All	30 ± 25 <sup>G***, P***</sup>	24 <sup>G***</sup> ± 25	-60 <sup>G**, P**</sup> ± 37

Transversal force (N)			
b)	Muscular activity minimization	Joint torque minimization	Experiment
Very low	-1 ± 5	-3 ± 6	-4 ± 5
Low	1 ± 5	1 ± 7	-8 ± 7
Medium	6 ± 8	5 ± 12	-16 ± 12
High	13 ± 10	13 ± 16	-32 ± 21
Maximum	20 ± 17	30 ± 27	-62 ± 34
Short women	5 ± 9	3 ± 11	-22 ± 23
Average men	8 ± 12	8 ± 16	-36 ± 35
Tall men	14 ± 17	23 ± 28	-33 ± 35
All	10 ± 14 <sup>G***, P***</sup>	13 <sup>G***, P***</sup> ± 22	-31 ± 32 <sup>G*, P***</sup>

\*p<0.05, \*\*p<0.01, \*\*\* p<0.001. G: group of subjects; P: Pedal position; F: force level



## General conclusion and perspectives

<b>1</b>	<b><i>INTRODUCTION</i></b>	<b>187</b>
<b>2</b>	<b><i>BIOMECHANICAL APPROACH FOR EVALUATING MOTION RELATED DISCOMFORT</i></b>	<b>187</b>
<b>3</b>	<b><i>FORCE EXERTION-TASK CONTROL STRATEGY AND SIMULATION</i></b>	<b>189</b>
<b>4</b>	<b><i>PERSPECTIVES FOR INTEGRATION IN AUTOMOTIVE DESIGN PROCESS</i></b>	<b>191</b>



## 1 Introduction

In this PhD thesis, two research questions for digital human modeling were investigated:

- How to propose objective discomfort indicators to help the design engineers in their design selection process
- How to predict posture taking into account force exertion.

In this section, the main results are summarized. Then, the limitations of the study are discussed and then follow some perspectives for future work. Finally, short term perspective for industrial integration of the present work is proposed.

## 2 Biomechanical approach for evaluating motion related discomfort

In this study, the assumption was made that a better comfort may be obtained when people can make their own appropriate adjustments. A motion related discomfort modeling approach based on the concept of less-constrained movement has been proposed and illustrated by a case study of clutch pedal operation. The proposed approach is divided in two steps. First the identification of the relevant biomechanical parameters is performed by comparing imposed and less-constrained movements. The efficiency of this step mainly lies on an experimental design with the appropriate apparatus to control the critical design parameters of the investigated task. Second, the definition of the discomfort indicators is based on the use of cost functions as in many discomfort studies in the literature. Although the proposed approach is generic, the identified discomfort criteria are task-specific and test condition specific. Indeed, the proposed discomfort indicators may not be applicable to other situations where other pedal design parameters are adjustable. The method was also applied in the DHErgo project to an upper limb task (handbrake pulling) and a whole body movement (car ingress/egress).

In this work, less-constrained movements were used for identifying relevant biomechanical parameters in order to define discomfort indicators. In case of simulation using a DMH, the proposed indicators can be computed to compare several pedal design without the need of less-constrained movements. But the question how to simulate less-constrained motion remains open. Indeed, end-users could be interested in predicting less-constrained configuration. In case of the clutch pedal, the ranges of pedal adjustments observed experimentally were large and depended not only on pedal configuration but also on subject. A data-based approach as the one implemented in RP<sub>x</sub> could be proposed to predict less-

constrained motion. The general idea would be to separate imposed and less-constrained motion in the motion database. As the pedal position should remain free, the task descriptors should be the other controlled parameters of the task (subject characteristics, seat height, pedal resistance, travel length ...). Then, according to a new scenario (i.e. new task descriptors), a referential motion would be selected in the less-constrained motion database. Finally, the less-constrained movement for the new scenario could be predicted modifying the less-constrained movement of the referential pedal position. However such method would assume that an individual would adjust the pedal in the new scenario as in the referential motion. Actually, the pedal adjustment data from this study agree with this assumption as for example, pedal with lower seat height were lowered on average whereas pedal with higher seat height were moved up. But still, validation would be needed. Moreover, as for all data-based methods, the results would highly depend on the underlying dataset and it would be difficult to extrapolate outside the experimental conditions.

As far as the proposed discomfort indicators are concerned, there are two main issues remained open. First is how to combine the indicators to get a global evaluation of the proposed design. Actually, a global score is usually preferred by the engineers as it allows to quickly differentiate several design alternatives. Our proposed discomfort indicators may be efficient to compare some design propositions but they may not fulfill the expectations of industrials in terms of absolute ergonomic assessment. In this study, the attempt to propose a global score using the indicators and the discomfort ratings showed bad results. The poor reproducibility of the subject's ratings and the small size of subject sample could explain the poor results of the model. To improve the model, new experimentations would be required with a larger subject sample and also an efficient training of the subjects to use a rating scale to express their discomfort perception. Annett (2002) argued that comfort/discomfort assessment is as much a science as an art. How to combine these indicators into one global discomfort score certainly requires deep expertise in product design. These indicators could provide objective elements for an expert to form a global assessment of different design solutions. In this point of view, the proposed approach based on the definition of relevant objective individual indicators is not opposed but rather complementary to expertise.

Second is the dependency of the discomfort indicators computation with the motion simulation. The proposed discomfort indicators are based on biomechanical parameters dependent on movement, implying that the motion simulation should be experimentally validated when using a DHM. Besides, both kinematic and dynamic parameters should be considered. This is particularly important for the dynamic parameters such as joint torques. In

case of automotive control, the necessary force to apply on a control is usually known by the car manufacturer, for example, the pedal resistance along its travel path. But how a person will press the pedal to perform the task is more complex to estimate as the force direction is not strictly imposed by task. Any force that produces a component necessary for overcoming the pedal resistance is theoretically possible. And the computation of the joint torques highly depends on the control of the force direction. This is what connected the two parts of this PhD thesis. Biomechanics based discomfort modeling is one of the advantage of using a DHM, but its use is limited by the performance of DHM to simulate real task-related motions.

### 3 Force exertion-task control strategy and simulation

As a first step to improve the methods of posture prediction of force exertion-task, the mechanism of the force exertion on automotive control was investigated through the example of the clutch pedal. Using experimental data and biomechanical simulation, two aspects of the force exertion were investigated: the control of the force direction and the control of the posture. Interestingly, it was found that the pedal force direction and the postural adjustment were mainly explained by the need of reducing the joint load when increasing the force level. Besides, a simulation approach based on a musculoskeletal model and an optimization criterion minimizing the muscular activity improved the prediction of pedal force direction for low and intermediate force levels when compared to the minimization of joint torques with a multi-body model without muscles. However, it was also showed that the lateral deviation of the pedal force was not explained by any criteria of minimization, which suggests that the lateral force deviation may be controlled by other mechanisms.

The following step to this study would be to merge force direction and posture simulation methods into a unified one. As the study tends to suggest that minimization of joint load explain both force direction and posture adjustment, a first method would be to merge the two algorithms used in this work. Considering that the tangential force is imposed regarding experimental data, this new algorithm could be formalized as to predict both force direction and postural adjustment simultaneity:

$$\min G(\overrightarrow{\Delta Hip}, F_{Sim}^{Normal}, F_{Sim}^{Transversal}) = \min \left( \omega_{JT} * \sum_{Joint} \sum_{DoF} \left( \frac{T_{Joint}^{DoF}}{(T_{Joint}^{DoF})_{Max}} \right)^2 + \omega_{Dis} * \left( \frac{\|\overrightarrow{\Delta Hip}\|}{(\|\overrightarrow{\Delta Hip}\|)_{Max}} \right)^2 \right)$$

Or using a musculoskeletal model:

$$\min W(\overrightarrow{\Delta Hip}, F_{Sim}^{Normal}, F_{Sim}^{Transversal}) = \min \left( \omega_{Mus} * \sum_{i=1}^{n \text{ muscle}} \left( \frac{f_i}{f_i^{Max}} \right)^2 + \omega_{Dis} * \left( \frac{\|\overrightarrow{\Delta Hip}\|}{(\|\overrightarrow{\Delta Hip}\|)_{Max}} \right)^2 \right)$$

$\omega_{JT}$ ,  $\omega_{Dis}$  and  $\omega_{Mus}$  are the weight coefficients attributed respectively to the minimization of the joint torques, of the hip displacement and of the muscular activity in their respective objective functions. The design variables of both optimizations are  $\overrightarrow{\Delta Hip}$  the hip displacement,  $F_{Sim}^{Normal}$  the normal pedal force and  $F_{Sim}^{Transversal}$  the transversal pedal force. However, due to limited time, we have not tested this unified algorithm for prediction both force direction and posture. We strongly suggest a more realistic modeling the contacts with seat (seat-thigh contact and back-backrest contact). In DHErgo project, estimation of the contact forces was done using pressure maps. But many simplifying hypotheses were also done to estimate the impact of the contact on the hip joint. Currently, finite-element models such as Pam-Comfort, aim to predict the contacts with the seat for a seated individual. Based on finite elements modeling, this type of model takes into account the deformation of the flesh and of the seat regarding the mechanical properties of foam constituting the seat. However, the computation is relatively time consuming. Further developments are therefore needed.

The study also illustrates the strong relationship between posture, force capacity and force direction. Posture and force direction are interdependent and highly depend on the perception of the necessary force regarding the force capacity. Knowing the strength of all joints in every posture would allow to predict realistic force direction and posture regarding the force requirements for any task but also maximum force exertion capacity. However, joint strength is currently collected only using a heavy time-consuming experimental protocol. Considering that muscular strength vary greatly depending on a high number of factors such as posture, joint or the limb considered, subject, a large amount of data is required to get a full characterization of an individual. A solution to the characterization of joint strength may come from the use of musculoskeletal model. Indeed, considering that the muscles lever arms acting on a joint depends on posture; a few but well-chosen maximum joint torque data could be enough to scale some of the musculoskeletal model's parameters and therefore, the scaled model should be able to predict maximum joint torque in new postures. An attempt to develop

such method was performed during this PhD thesis (Pannetier et al., 2011). The results were encouraging but far from being used in simulation and further investigations are needed.

#### **4 Perspectives for integration in automotive design process**

In the current state of knowledge, the simulation of pedal force exertion using optimization criteria may not fulfill the car manufacturers' expectations. But using the data available in the FAC project, a data-based approach could be proposed. First the posture database has to be structured considering the usual motion descriptors as well as the force level perception. Then using a motion modification method as the one implemented in RPx, the posture could be predicted. Second, an interpolation method such as the one proposed by Wang et al. (2010) could be used to estimate the force magnitude and direction within the experimental space. This method could be implemented for clutch pedal but also for handbrake and gear lever as these two controls were also investigated in the FAC project. In case of the clutch pedal, as the posture and the pedal force are estimated, the discomfort indicators could also be estimated. Using this approach, a realistic pedal force exertion task and its discomfort assessment could be proposed. The main limitation of this method would be the same as all data-based method, which is the high dependency regarding the underlying dataset.



# Synthèse

<b>1</b>	<b>INTRODUCTION</b>	<b>195</b>
1.1	MANNEQUINS NUMERIQUES ET EVALUATION ERGONOMIQUE DES COMMANDES AUTOMOBILES .....	195
1.2	CONTEXTE DE L'ETUDE ET OBJECTIF DE LA THESE .....	196
<b>2</b>	<b>IDENTIFICATION DE CRITERES OBJECTIFS D'INCONFORT A PARTIR DU MOUVEMENT « MOINS CONTRAIT »</b>	<b>198</b>
2.1	INTRODUCTION .....	198
2.2	METHODES ET PROCEDURES EXPERIMENTALES.....	198
2.3	ANALYSE DE LA GENE RESSENTIE.....	200
2.4	ANALYSE DU MOUVEMENT DE DEBRAYAGE.....	202
2.5	ANALYSE DE L'EFFORT APPLIQUE SUR LA PEDALE .....	204
2.6	DEFINITION D'INDICATEURS D'INCONFORT POUR LE DEBRAYAGE .....	206
<b>3</b>	<b>CAPACITE MAXIMUM, PERCEPTION ET CONTROLE DE LA DIRECTION DE L'EFFORT SUR PEDALE</b>	<b>207</b>
3.1	INTRODUCTION .....	207
3.2	METHODES ET PROCEDURES EXPERIMENTALES.....	207
3.3	OBSERVATIONS EXPERIMENTALES.....	209
3.4	SIMULATION DE LA DIRECTION D'EFFORT ET DE L'AJUSTEMENT POSTURAL.....	212
<b>4</b>	<b>MODELE MUSCULO-SQUELETTIQUE ET CONTROLE DE LA DIRECTION D'EFFORT</b>	<b>215</b>
4.1	INTRODUCTION .....	215
4.2	SIMULATION DE LA DIRECTION D'EFFORT .....	215
<b>5</b>	<b>CONCLUSION GENERALE</b>	<b>217</b>



## 1 Introduction

La technologie de la simulation numérique devient incontestablement un enjeu majeur pour l'industrie automobile, en particulier pour la conception des véhicules. L'utilisation de modèles numériques du corps humain devrait, à terme, faciliter considérablement le travail de conception et limiter le recours aux tests sur maquettes physiques grandeur nature. L'objectif de ces mannequins numériques est de prendre en compte des facteurs humains en amont d'un projet de conception de produit. Dans le cadre de la conception de commandes automobiles, il s'agit en particulier de considérer la dynamique du mouvement et la force exercée lors de l'utilisation pour prédire le mouvement et l'inconfort associé.

L'objectif de cette partie est de souligner les limitations actuelles des mannequins numériques par rapport à la conception des commandes automobiles afin de définir les objectifs de ce travail de thèse.

### 1.1 Mannequins numériques et évaluation ergonomique des commandes automobiles

Considérant les caractéristiques techniques d'une commande automobile et leurs effets sur l'utilisateur, les besoins des ingénieurs en conception pour améliorer l'ergonomie des commandes sont :

- Des critères objectifs d'inconfort pour identifier et corriger les sources d'inconfort
- Des efforts sur commande réalistes (magnitude et direction)
- Des postures d'utilisation réalistes

#### 1.1.i Limitations des mannequins actuels utilisés dans l'automobile

Actuellement, trois éditeurs se partagent le marché des mannequins numériques : Siemens avec Jack™, Dassault Systèmes avec Human Builder™ et Human Solutions avec Ramsis™. Ces trois mannequins numériques intègrent des outils spécifiques à l'évaluation ergonomique d'un véhicule (enveloppe d'atteinte, analyse de champs de vision, ...) mais aussi des méthodes de prédiction de posture de conduite. Cependant, les méthodes proposées ne prennent pas ou peu en compte l'effet de la production d'un effort sur la posture. Par ailleurs, l'identification d'indicateurs d'inconfort pertinents à partir de ces mannequins est relativement difficile pour les non-experts en ergonomie.

### **1.1.ii Modélisation de l'inconfort**

L'inconfort, qui doit être différencié du confort, est une notion subjective, fonction d'une multitude de facteurs. Les hypothèses les plus souvent émises sont qu'il résulte entre autres de facteurs biomécaniques tels que les interactions mécaniques avec l'environnement et les contraintes mécaniques internes affectant le système musculo-squelettique. Les modèles d'inconfort doivent d'une part prédire l'inconfort ressenti lors d'une tâche mais aussi permettre l'identification des sources de la gêne en vue d'une correction. La principale difficulté réside donc dans l'identification de critères d'inconfort. Chaque tâche ayant ses propres contraintes, ces indicateurs sont par définition spécifiques à une tâche. Néanmoins, l'identification des critères peut reposer sur une approche générique pour pouvoir être étendu à un large panel de mouvement.

### **1.1.iii Relation entre l'effort et la posture**

La production d'un effort et l'ajustement postural sont intimement liés que ce soit par les caractéristiques d'une tâche (force à appliquer, direction de l'effort, position de l'effecteur, ...) ou par les capacités physiques d'une personne considérée. La simulation de posture et d'effort réalistes sur une commande automobile passe donc par la collecte de données d'effort dans des conditions expérimentales proche de la réalité mais aussi par une meilleure compréhension des mécanismes de contrôle moteur en jeu lors de la réalisation d'une tâche.

## **1.2 Contexte de l'étude et objectif de la thèse**

L'étude présentée dans ce manuscrit hérite d'une longue collaboration entre Renault et l'IFSTTAR sur les problématiques d'évaluation ergonomique des véhicules, avec à la fin des années 80 avec le développement du mannequin numérique MAN3D et plus récemment, suite au projet européen REALMAN, celui d'un outil de simulation de mouvement appelé RPx. L'approche proposée pour la simulation de mouvement et la prédiction d'inconfort dans RPx étant principalement cinématique et donc pas adaptée à des tâches impliquant une production d'effort, un projet de collecte de données de capacités d'effort sur commandes automobile (projet FAC) a donc été lancé par Renault et l'IFSTTAR en 2008. La même année, les deux entités se sont par ailleurs engagées avec d'autres partenaires universitaires et industriels européens dans un projet de recherche soutenu par l'UE visant entre autres à développer des méthodes de simulation de mouvement et de prédiction de l'inconfort prenant en compte la dimension dynamique d'un mouvement ou d'une tâche.

Débuté à la fin du projet FAC et en parallèle du projet DHErgo, cette thèse a pour objectif de développer les modèles biomécaniques de l'homme pour l'évaluation ergonomique des commandes automobiles. L'objectif de cette thèse est double. Il s'agit d'une part de proposer une méthode générique d'identification de critères d'inconfort pertinents pour évaluer une tâche et d'autre part, de comprendre les mécanismes de contrôle de la force et de la posture durant une tâche en vue d'améliorer les méthodes de simulation de mouvement. Une approche combinant expérimentation et modélisation a été choisie. La pédale d'embrayage et le mouvement de débrayage ont par ailleurs été retenus pour l'étude.

## 2 Identification de critères objectifs d'inconfort à partir du mouvement « moins contraint »

### 2.1 Introduction

Du point de vue d'un ingénieur conception, le problème n'est pas de distinguer un produit bien conçu d'un produit mal conçu mais plutôt de pouvoir choisir le meilleur design pour un produit parmi un ensemble de solutions potentielles. La réalisation d'une tâche étant plus ou moins contrainte par l'environnement, on peut supposer que la gêne ressentie diminuerait dans le cas où l'utilisateur pourrait effectuer ses propres ajustements. Ces mouvements « moins contraint » pourraient alors être utilisés comme mouvement de référence pour évaluer de nouvelles solutions de design. Dans cette étude réalisée dans le cadre du projet européen DHErgo, le concept de mouvement « moins contraint » ou « neutre » (Dufour and Wang, 2005) a été utilisé pour identifier des paramètres biomécaniques pertinents pour la définition d'indicateurs d'inconfort du mouvement de débrayage.

### 2.2 Méthodes et procédures expérimentales

#### 2.2.i Mesures expérimentales

Un conformateur à géométrie variable possédant les éléments importants de l'habitacle d'un véhicule (siège, volant, repose-pied, pédales d'accélération et d'embrayage) a été utilisé dans cette expérimentation. L'ensemble des éléments du conformateur ont été positionné autour d'un point H de référence lié au siège, défini à partir du mannequin de référence SAE J826. Six configurations pédales d'embrayage fournies par les constructeurs automobile impliqués dans DHErgo (BMW, PSA et Renault) ont été choisies pour couvrir l'espace de configuration présent dans les véhicules actuels : 5 configurations limites (BMW1, BMW2, BMW4, PCA1 et REN3) et une configuration centrale (PCA2) (Figure 71).

Pour limiter les combinaisons de personnalisation et faciliter le processus d'ajustement pour le sujet, seule la position de la pédale a été laissée comme paramètre ajustable par les sujets. Pour chaque configuration, les sujets ont donc testé une position de pédale imposée et une moins contrainte pour laquelle ils pouvaient réaliser des ajustements. Afin d'estimer la répétabilité du mouvement et des notes d'inconfort, la configuration centrale PCA2 a été testée trois fois. En outre, l'ordre des essais était randomisé pour chaque sujet.

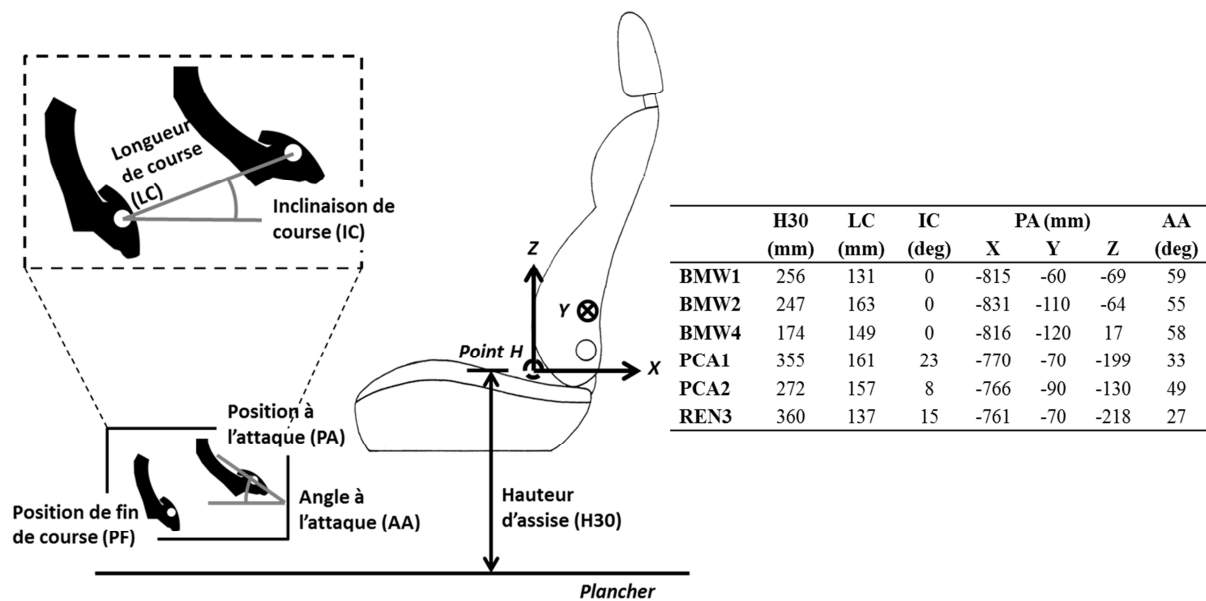


Figure 71: Paramètres de définition des pédales d'embrayage utilisées dans DHErgo

Vingt sujets volontaires (5 femmes et hommes âgés, 5 femmes et hommes jeunes) ont pris part à l'expérimentation. Due à la faible taille de l'échantillon, seuls des sujets ayant des statures appartenant au 50<sup>ème</sup> centile de leur groupe anthropométrique respectif ont été sélectionnés pour conserver une certaine homogénéité. Tous les sujets étaient des conducteurs expérimentés et ne présentait aucun troubles musculo-squelettiques.

Au cours de cette expérimentation, plusieurs types de données ont été recueillis :

- Des données anthropométriques décrivant chaque sujet
- Des données de capacités fonctionnelles (butées articulaires et de couples articulaires) du membre inférieur pour chaque sujet
- Des notes d'inconfort ainsi que leur explication au travers d'un QCM pour chaque essai
- Les trajectoires des 40 marqueurs réfléchissants placés sur le sujet ainsi que les 35 autres placés sur le conformateur enregistrées d'un système optoélectronique VICON pour chaque essai
- Les efforts appliqués sur la pédale au cours de chaque essai enregistré à l'aide d'un capteur de force tri-axe
- Des données de nappes de pression placées sur le siège pour chaque essai

### **2.2.ii** *Traitement des données*

A partir des dimensions anthropométriques collectées et du module Bodybuilder du logiciel Ramsis, un avatar de chaque participant a été créé. Ce modèle individualisé a été ensuite exporté dans le logiciel RPx pour une étape visant à définir la position des marqueurs placés sur le participant dans le repère du segment auquel ils appartiennent. Le principe consiste à superposer, dans un espace calibré, une représentation schématique du modèle sur différentes prises de vue à la posture du participant.

La cinématique du mouvement a été reconstruite par cinématique inverse à partir d'une méthode d'optimisation qui minimise l'écart entre la position des marqueurs réels mesurés et des marqueurs virtuels liés au mannequin numérique. Puis, les couples articulaires ont été calculés par dynamique inverse à partir de la cinématique du mouvement, des efforts externes et des propriétés massiques et inertielles des segments corporels. Les efforts articulaires ont été calculés itérativement à chaque instant en isolant les segments corporels du plus distal au plus proximal.

Deux instants-clés du mouvement de débrayage ont par ailleurs été définis pour chaque essai pour faciliter l'analyse. Le premier correspond au début de course, i.e. quand le pied gauche commence à appuyer sur la pédale et le second à la fin de course.

### **2.3** *Analyse de la gêne ressentie*

Le questionnaire d'inconfort utilisé dans l'expérimentation avait pour but de recueillir la gêne ressentie au cours du mouvement de débrayage à l'aide d'une échelle de notation, mais aussi d'obtenir des indications des effets des paramètres de configuration de la pédale (siège, position de la pédale en début/fin de phase d'appui, longueur/inclinaison de la course, résistance de la pédale) sur l'inconfort à travers des questions à choix multiples. En outre, dans le cadre de l'utilisation du concept de mouvement moins contraint, l'analyse des réponses devrait permettre d'identifier quel(s) réglage(s) ont été fait par les sujets ainsi que d'expliquer l'effet de ces ajustements sur la perception de la tâche. Les réponses au questionnaire ont donc été analysées en fonction de trois variables indépendantes : le groupe de sujets (âgés/jeunes femmes/hommes), la configuration de pédale et le type de configuration (imposée ou moins contrainte).

#### **2.3.i** *Evaluation des paramètres de configuration*

Pour les questions à choix multiples, les effets des trois variables (groupe de sujets, la configuration, le type de configuration) ont été analysés à l'aide des tableaux de fréquence.

Pour chaque question et variable, un test du  $X^2$  a aussi été effectué pour tester l'hypothèse d'indépendance des distributions de lignes et de colonnes. L'analyse a porté en particulier sur la perception de la position de la pédale en début et fin de course ainsi que la perception de la résistance de la pédale.

Six questions ont été posées pour évaluer les positions de début et de fin de la pédale en fonction de sa hauteur, sa distance et de sa position latérale. Pour chaque question, trois réponses possibles ont été proposées aux sujet: trop élevée/bon/trop basse pour hauteur de la pédale, trop loin/bon/trop près pour la distance, trop à gauche/bonne/trop à droite pour la position latérale. Le test du  $X^2$  a montré des effets importants du type de configuration sur la position de la pédale en début et fin de course. En début de course, les configurations de pédales imposées ont été jugées trop élevées, trop près et trop sur la droite, alors que les configurations moins contraintes ont été évaluées comme bonne dans les trois directions pour plus de 90% des essais. Cependant, l'ajustement de la pédale n'a pas amélioré pour autant la perception de la position de fin de course. Au lieu de cela, les configurations de pédales moins contraintes ont été plus souvent perçues comme « trop basse » et « trop éloigné » que les configurations imposées. Par conséquent, les sujets ont eu tendance à améliorer le début de course au détriment de la fin.

L'évaluation de la résistance de la pédale a été faite en utilisant l'échelle CR10 de Borg avec 5 niveaux de perception d'effort : très faible/faible/moyen/élevé/très élevé. La plupart des réponses ont qualifié la résistance comme étant moyenne (54%) et dans une moindre mesure comme faible (26%) ou élevé (18%). Seule la configuration a eu un effet sur la perception de la résistance de la pédale. BMW4 a été jugée comme ayant la pédale la moins dure alors que PCA1 et REN3 ont été évaluées comme étant les pédales les plus dures.

L'influence du siège, la longueur de la course de la pédale ainsi que son inclinaison ont également été évalués par les sujets. Pour plus de 90% des réponses, le siège n'a eu aucun effet sur la perception de l'inconfort. La course de la pédale d'embrayage a été estimée soit trop longue, soit à une bonne longueur à peu près 50-50. L'inclinaison de la course a été la plupart du temps estimée (72%) comme bonne.

### **2.3.ii** *Analyse des notes d'inconfort*

Lors de chaque essai, il a été demandé aux sujets d'évaluer la gêne ressentie lors du débrayage à l'aide d'une échelle de notation de type CP50, 0 pour une gêne imperceptible à 50 pour une gêne extrêmement élevée.

La répétabilité des sujets à noter l'inconfort a été évaluée en calculant l'écart maximum à la moyenne sur les trois répétitions de la configuration PCA2. Pour plus de la moitié des sujets, cet écart était supérieur à 5, signifiant un potentiel saut de catégorie d'inconfort entre deux répétitions.

Etant par définition indépendante, les effets des trois variables (groupe de sujets, la configuration, le type de configuration) sur la note d'inconfort ont été analysées par analyse de variance. Les résultats montrent une influence statistiquement significative des trois variables ( $p < 0.001$ ). En particulier, les configurations moins contraintes ont en moyenne été évaluées comme moins inconfortable que celle imposées. En outre, la configuration a, elle aussi, une importante influence sur la note, BMW1 étant la configuration générant le moins de gêne et PCA1 et REN3 celles en causant le plus.

### 2.4 Analyse du mouvement de débrayage

Les mouvements de débrayage enregistrés ont été analysés pour expliquer la gêne ressentie par les sujets. Tout d'abord, dans la mesure où l'ajustement de la pédale à entraîner une amélioration du début de course au détriment de la fin, les postures à ces deux instants-clés vont être analysées en comparant les mouvements moins contraints avec ceux imposés. Ensuite, comme il est apparu que la perception de la résistance de la pédale dépendait principalement de la configuration, la force appliquée sur la pédale (amplitude et direction) ainsi que ses répercussions au niveau des couples articulaires vont être analysées. Ces analyses doivent permettre d'identifier les paramètres biomécaniques pertinents pour la définition d'indicateurs d'inconfort du mouvement de débrayage.

#### 2.4.i Comparaison des mouvements de débrayage imposés et moins contraints

Au niveau de l'ajustement de leur position, les pédales ont en moyenne été déplacées de 8.8 mm vers l'avant, 21 mm vers la gauche et 16.8 mm vers le bas. Globalement, les sujets ont tous eu tendance à ajuster la pédale dans la même direction, c'est-à-dire plus loin du siège, plus bas et plus à gauche.

Les angles articulaires de la jambe gauche ont été analysés au début et en fin de course (Figure 72). Des tests t appariés ont été effectués pour estimer s'il existait des différences significatives entre les angles articulaires pour les pédales imposées et ceux pour les pédales moins contraintes. Les tests ont montré des différences significatives en termes d'angles de flexion/extension pour les trois articulations du membre inférieur (hanche, genou et cheville) ainsi qu'en termes d'angle d'abduction/adduction de hanche. L'ajustement de la position de la

pédale a conduit à une diminution de la flexion des articulations de la hanche, du genou et de la cheville, à l'attaque, et une augmentation de l'extension de ces articulations à la fin de l'enfoncement de la pédale, en particulier pour la cheville. En outre, le déplacement sur la gauche de la pédale pour les configurations moins contraintes a entraîné une augmentation de l'abduction de la hanche.

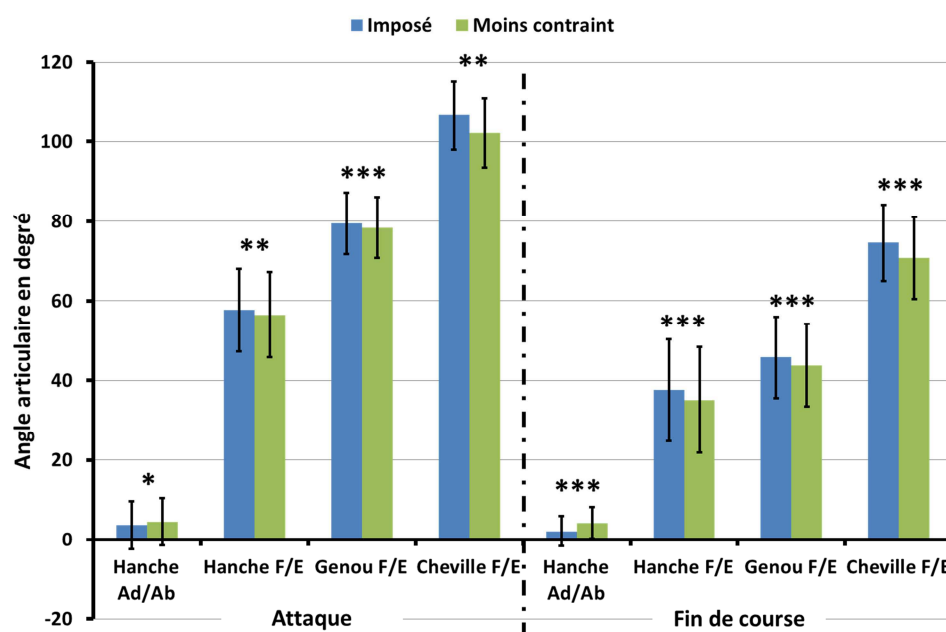


Figure 72: Angles articulaires moyens pour les pédales imposées et moins contraintes à l'attaque et en fin de course : adduction/abduction (Ad/Ab) de la hanche, flexion/extension (F/E) de la hanche, flexion/extension (F/E) du genou et flexion/extension (F/E) de la cheville (\* $p < 0.05$ , \*\* $p < 0.01$ , \*\*\*  $p < 0.001$ )

#### 2.4.ii Ajustement de pédale et perception d'inconfort

Au niveau des angles articulaires, la comparaison entre les configurations imposées et celles librement ajustées a montré des différences plus importantes pour la cheville. A partir des données de butées articulaires recueillies, il a été constaté que, contrairement aux autres articulations, l'angle de la cheville était très proche de sa limite dorsiflexion à l'attaque pour les configurations imposées ( $106.6^\circ \pm 8.6$  pour une butée à  $122^\circ \pm 5$  en dorsiflexion). Les sujets ont donc pu ajuster la position de la pédale de manière à réduire l'angle de flexion dorsale de la cheville. L'abduction de la hanche a également augmenté au début et à la fin du débrayage pour les configurations moins contraintes. Ce paramètre est particulièrement sujet au réglage latéral de la position de la pédale. Par conséquent, le réglage latéral de la pédale peut être dû à une préférence des sujets à appuyer sur la pédale vers la droite, i.e. vers l'extérieur.

## 2.5 Analyse de l'effort appliqué sur la pédale

La résistance de la pédale d'embrayage était modélisée à l'aide d'un ressort simple. Par conséquent, l'effort maximum au cours du débrayage intervenait en fin de course, ce qui en fait un instant-clé d'intérêt pour l'analyse de l'effort appliqué sur la pédale. La force enregistrée par le capteur d'effort 3D a par ailleurs été décomposée en 3 composantes : la force tangentielle (parallèle à la course de la pédale et donc motrice), la force normale (perpendiculaire à la course de la pédale et donc non motrice) et la force latérale qui complète le trièdre direct (Figure 73a). La direction de la force appliquée sur la pédale a été définie et analysée en comparaison avec l'axe passant par le centre articulaire de la hanche et le point d'application, i.e. l'axe  $HP_{App}$ . Deux types d'angle ont été calculés. Le premier dans le plan XZ du repère expérimental,  $\theta_{F_{Exp}}$  (Figure 73b), correspondant à la direction principale de l'effort (forces tangentielle + normale) a été défini comme l'angle entre la force et l'axe  $HP_{App}$ . Le second dans le plan XY,  $\delta_{F_{Exp}}$  (Figure 73d), représentant la déviation latérale de l'effort (forces tangentielle + latérale) a été défini par rapport à l'axe X du repère. La déviation latérale de la jambe  $\delta_{HP_{App}}$  (Figure 73c) a aussi été évaluée.

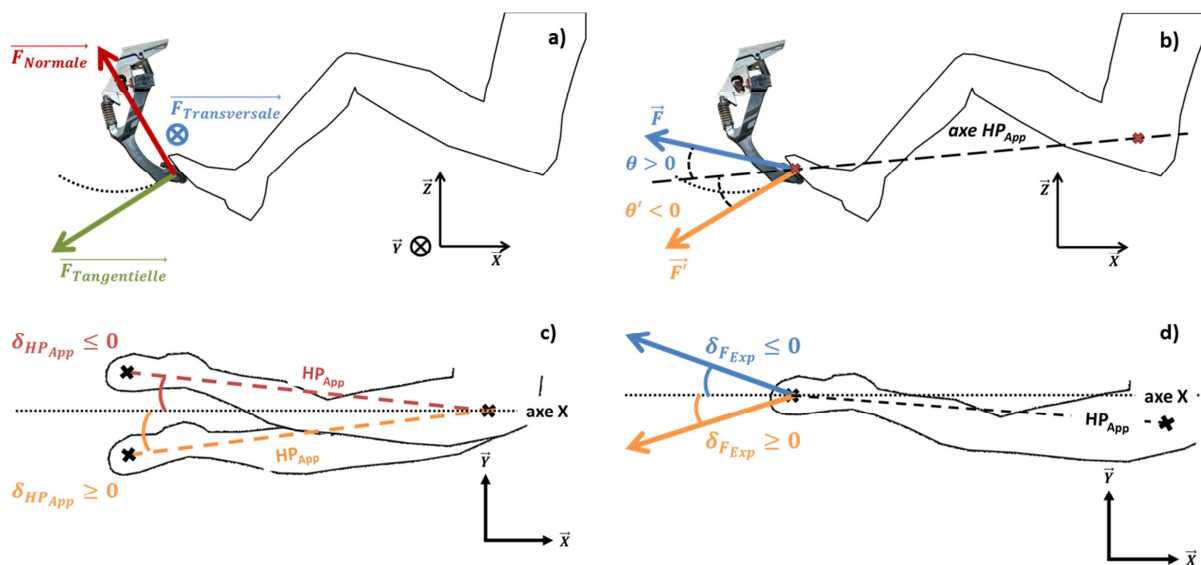


Figure 73: Analyse de la force appliquée à la pédale : a) Décomposition de la force, b) Définition de la direction d'effort dans le plan XZ, c) Déviation latérale de la jambe gauche et d) Déviation latérale de la force appliquée.

### 2.5.i Influence des variables contrôlées sur la force appliquée à la pédale

Un effet important de la configuration sur la résultante de force et ses composantes a été trouvé. La résultante de l'effort sur la pédale varie de 166 N (BMW4) à 184 N (REN3) en moyenne. Le groupe de sujets a également un effet significatif, en particulier sur les composantes tangentielles et normales. En effet, les sujets jeunes ont plus sollicité la

composante normale de l'effort que les sujets âgés. Par ailleurs, seul un effet significatif du type de configuration a été observé sur la composante latérale de la force appliquée sur la pédale.

En moyenne,  $\theta_{F_{Exp}}$  est de  $-5.6^\circ$ . Comme pour la résultante des efforts et ses composantes, la configuration et le groupe de sujet ont une influence importante sur  $\theta_{F_{Exp}}$ , contrairement au type de configuration. BMW4 est la configuration pour laquelle la direction d'effort est la plus éloignée de l'axe  $HP_{App}$  ( $-9^\circ$ ). A l'opposé, PCA1 et REN3 ont des directions d'effort moyennes proches de l'axe d'intérêt, respectivement  $-3^\circ$  et  $-1.6^\circ$ . En outre les sujets âgés présentaient des directions moyennes d'effort plus proches de l'axe de la hanche que les sujets jeunes. Pour les déviations latérales de la force  $\delta_{F_{Exp}}$  et de la jambe  $\delta_{HP_{App}}$ , les trois variables (groupe de sujets, configuration et type de configuration) ont eu un effet significatif. Fait intéressant, la force appliquée sur la pédale était orientée vers la droite alors que la jambe l'était vers la gauche, en particulier pour les configurations imposées. Les sujets n'ont donc pas appliqué leur effort dans l'axe de poussée définie par la direction  $HP_{App}$ .

### 2.5.ii *Couples articulaires au niveau de la cheville et du genou*

Comme les forces de contact entre la cuisse et le siège n'ont pas été estimées, les couples articulaires de la hanche n'ont pas été pris en compte. Seuls les couples articulaires de flexion/extension ont été étudiés car l'opération de pédale d'embrayage a été considérée comme étant principalement une opération de flexion/extension. En moyenne, les couples au genou et à la cheville présentaient des valeurs respectives de  $-19$  Nm et  $-11$  Nm. L'analyse des résultats a montré que les couples articulaires du genou et de la cheville ont été significativement affectés par la configuration de la pédale et un groupe de sujets, mais pas selon le type de configuration. En particulier, BMW4 est la configuration générant le moins de couple au genou, i.e.  $-12$  Nm, alors que PCA1 et REN3 sont celles qui en génèrent le plus, respectivement  $-25.4$  Nm et  $-27.4$  Nm. Les autres configurations ont des valeurs autour de la moyenne.

### 2.5.iii *Effort sur pédale et inconfort*

La configuration a eu des effets importants sur l'effort appliqué sur la pédale (résultante, composantes et direction) et sur les couples articulaires (genou et cheville). L'analyse de l'inconfort a montré que la configuration a également eu des effets importants sur la perception de la résistance de la pédale ainsi que sur les notes d'inconfort. Par conséquent, les corrélations entre les forces tangentielle et normale, la direction de la force, les couples articulaires (genou et cheville) et les notes CP50 ont été étudiés (Table 65).

Table 65: Matrice de corrélation avec les coefficients de Pearson-Bravais.

	$F_{Normale}$	$F_{Tangent.}$	$\theta_{F_{Exp}}$	Couple <sub>Genou</sub>	Couple <sub>Cheville</sub>	Notes CP50
$F_{Normale}$	1	<b>-0.1327*</b>	<b>0.8286***</b>	<b>-0.7848***</b>	<b>0.7137***</b>	0.0723
$F_{Tangent.}$		1	0.093	<b>-0.236***</b>	<b>-0.2493***</b>	-0.0611
$\theta_{F_{Exp}}$			1	<b>-0.8364***</b>	<b>0.6541***</b>	-0.0062
Couple <sub>Genou</sub>				1	<b>-0.5564***</b>	<b>-0.1489*</b>
Couple <sub>Cheville</sub>					1	<b>0.1205*</b>
Notes CP50						1

\*p&lt;0.05, \*\*p&lt;0.01, \*\*\* p&lt;0.001.

Seuls les couples articulaires sont significativement corrélés avec notes d'inconfort, en particulier pour le genou. Le couple articulaire du genou est également significativement corrélé avec les composantes tangentielles et normales de force appliquée sur la pédale, ainsi qu'avec la direction d'effort. Ainsi, pour chaque configuration, on peut supposer qu'il existerait une direction optimale d'effort, contrôlée par la composante normale de l'effort, qui minimiserait le couple au niveau du genou et donc qui minimiserait la gêne ressentie. La sollicitation de la composante normale de l'effort (composante non motrice) peut aussi expliquer les effets du groupe de sujets sur les différentes composantes de l'effort et les couples articulaires, en particulier par le fait que cette composante était plus sollicitée par les sujets jeunes que par les sujets âgés.

## 2.6 Définition d'indicateurs d'inconfort pour le débrayage

A partir des précédents résultats d'analyse, plusieurs indicateurs d'inconfort ont été retenus :

- 7 indicateurs cinématiques, i.e. les angles de flexion/extension en début et fin de course pour la hanche, le genou et la cheville ainsi que la position latérale du pied
- 2 indicateurs dynamiques, i.e. les couples articulaires du genou et de la cheville en fin de course

Les indicateurs cinématiques ont été définis à l'aide de fonctions de coût en terme d'inconfort et les indicateurs dynamiques ont été définis en normalisant les couples articulaires par les valeurs de couples isométriques maximum collectées pour chaque sujet. Ces indicateurs pourraient en particulier servir à la comparaison de différentes configurations de pédale d'embrayage dans le but de sélectionner la meilleur du point de vue de la gêne ressentie.

### 3 Capacité maximum, perception et contrôle de la direction de l'effort sur pédale

#### 3.1 Introduction

Simuler de façon réaliste la posture adoptée par un individu à l'aide d'un mannequin numérique est un des points critiques inhérents à l'utilisation des mannequins numériques pour l'évaluation ergonomique. Pour les tâches impliquant la production d'un effort telles que la manipulation des commandes automobiles, l'individu adapte non seulement sa posture aux contraintes géométriques, mais aussi au niveau qu'il doit appliquer pour réaliser la tâche. La plupart des mannequins numériques existants utilisés dans l'industrie automobile pour l'évaluation ergonomique d'un produit ou d'un poste de travail ont une approche cinématique du mouvement humain sans tenir compte des efforts en jeu. Dans le contexte de la simulation réaliste de la manipulation de commandes automobiles, les stratégies de contrôle de posture et de l'effort sur la pédale ont été étudiées à partir de données expérimentales de capacité d'effort collectées dans le projet FAC, afin de proposer des améliorations des mannequins numériques pour la simulation de tâches automobiles.

#### 3.2 Méthodes et procédures expérimentales

Un conformateur à géométrie variable a été utilisé pour définir différentes configurations de conduite. L'ensemble des éléments du conformateur (siège, volant, plancher, pédale d'embrayage, levier de vitesse et frein à main) ont été positionnés autour d'un point H de référence lié au siège, défini à partir du mannequin de référence SAE J826. Trois configurations de pédale d'embrayage ont été sélectionnées par Renault, représentant les trois gammes de véhicules majoritaires chez le constructeur (compact, berline et monospace). Pour chaque configuration, deux positions-clés ont été retenues pour l'expérimentation (milieu et fin de course), donnant ainsi 6 positions statiques à tester par les sujets (Figure 74).

Trente sujets volontaires ont pris part à l'expérimentation : 10 femmes de petite taille (5<sup>ème</sup> centile de la population française en termes de stature), 10 hommes de moyenne taille (50<sup>ème</sup> centile) et 10 hommes de grande taille (95<sup>ème</sup> centile). Tous les sujets étaient des conducteurs expérimentés et ne présentaient aucun trouble musculo-squelettique.

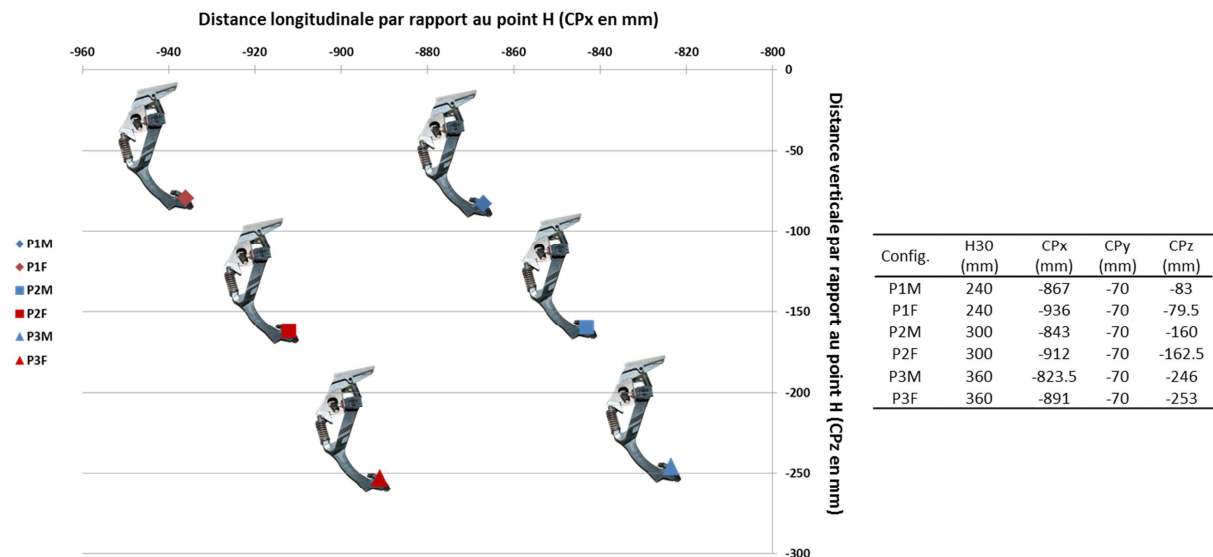


Figure 74: Définition des configurations de pédale testées dans le projet FAC

L'expérimentation a été divisée en deux parties. La première, appelée ExpMax, avait pour objectif de collecter des données d'effort maximum isométrique sur les six configurations définies précédemment. La deuxième partie, appelée ExpPcp, avait pour objectif de collecter de données de perception d'effort. Seule la position P2F a été testée dans cette partie suivant 5 modalités d'effort (très faible, faible, moyen, fort et maximum) choisis à partir de l'échelle CR10 de Borg.

Au cours de cette expérimentation, plusieurs types de données ont été recueillis :

- Des données anthropométriques décrivant chaque sujet
- Les trajectoires des marqueurs réfléchissants placés sur le sujet ainsi que ceux placés sur le conformateur enregistrées d'un système optoélectronique VICON pour chaque essai
- Les efforts appliqués sur le plancher (pied droit), sur la pédale d'embrayage (pied gauche), sur le volant (main gauche) et sur le levier de vitesse (main droite) au cours de chaque essai.

L'axe principal de recherche étant l'étude des efforts appliqués sur la pédale, seules les données d'effort sur la pédale d'embrayage ont été considérées.

La méthodologie globale de traitement des données pour la reconstruction mouvement était la même que celui utilisé sur les données de l'expérimentation précédemment présentée. Par ailleurs, la force appliquée sur la pédale a été déterminée en utilisant la méthode plateau. Les participants avaient pour instructions d'appliquer le niveau de force requis (de très faible à

maximum) aussi vite que possible et de le maintenir pendant 5 secondes. La valeur moyenne de chaque essai a été calculée à partir de 1.5s à 4.5s.

### 3.3 Observations expérimentales

Les postures et les efforts collectés au cours de l'expérimentation ont été analysés par analyse de la variance suivant 2 variables indépendantes : le groupe de sujet et la position de la pédale pour les données provenant d'ExpMax et le groupe de sujet et le niveau d'effort pour les données d'ExpPcp. En outre, Les efforts enregistrés sur la pédale au cours des essais ont été analysés suivant la décomposition aussi utilisée dans la précédente étude : force tangentielle, normale et latérale.

#### 3.3.i Capacités d'effort maximum sur pédale statique

Globalement, il a été observé que la capacité d'effort des sujets était plus importante pour les pédales en position mi-course, en moyenne 735 N, que pour celles en fin de course, en moyenne 600 N. Les femmes de petite taille ont affiché une capacité de force significativement plus faible que les 2 groupes d'hommes, 450 N en moyenne contre plus de 700 N. Dans le même temps, peu de différences en termes de capacité d'effort ont été trouvées entre les hommes, quel que soit leur stature. Les effets du groupe de sujets et de la position de la pédale sur la résultante des efforts et ses trois composantes ont par ailleurs été trouvés comme étant significatifs.

Comme pour l'expérimentation du projet DHErgo, la direction de l'effort a été analysée d'une part à l'aide de l'angle entre la force et l'axe hanche-point d'application et d'autre part, en comparant les déviations latérales de l'effort et de la jambe gauche. En moyenne, la direction d'effort était plus proche de l'axe  $HP_{App}$  pour les pédales en fin de course que pour les pédales à mi-course, respectivement  $-6^\circ$  et  $-11^\circ$ . En outre, les femmes de petite taille avaient en moyenne une direction d'effort plus proche de l'axe  $HP_{App}$  que les hommes, en particulier les hommes de grande taille. Au niveau de la déviation latérale, la principale observation est que quel que soit la position de la pédale ou le groupe de sujets, l'effort appliqué sur la pédale est orienté vers la gauche alors que la jambe était orientée vers la droite du point de vue du conducteur.

3.3.ii Perception d'effort sur pédale statique

Efforts normalisés et direction d'effort

Sans surprise, la résultante des efforts a significativement augmenté avec le niveau de force, quel que soit le groupe de sujets. En outre, si on considère les efforts normalisés, on peut constater que la loi de perception des efforts est indépendante du groupe de sujets.

Au niveau de la direction d'effort en fonction du niveau d'effort, on peut observer que la direction de la force appliquée tend à se rapprocher de l'axe  $HP_{App}$  lorsque le niveau d'effort augmente. Par ailleurs, quel que soit le niveau d'effort, la direction de l'effort est orientée vers la gauche alors que la jambe est orientée vers la droite du point de vue du conducteur.

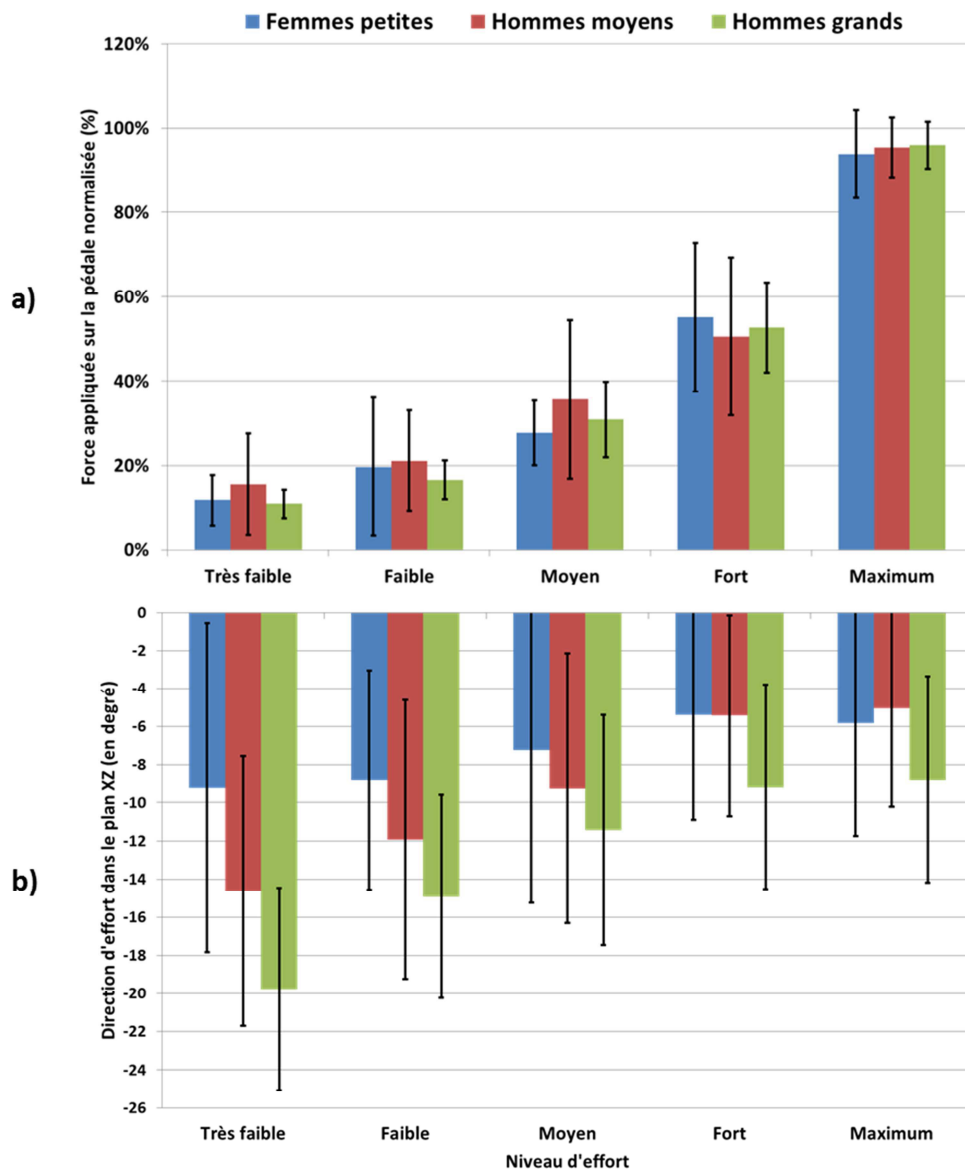


Figure 75: Perception d'effort sur pédale statique : a) Evolution de l'effort normalisé et b) Evolution de la direction d'effort en fonction du niveau d'effort et du groupe de sujets

### Ajustement postural

L'ajustement postural en fonction du niveau d'effort a été estimé à l'aide des postures de mannequins numériques obtenues pour chaque essai après la reconstruction de mouvement par cinématique inverse. Grâce à l'analyse vidéo, il a été observé que les sujets avaient tendance à se lever du siège avec l'augmentation du niveau de force. Par conséquent, le déplacement du bassin ainsi que les variations des angles des articulations du membre inférieur ont été analysés.

Les déplacements du bassin sur les axes x, y et z du repère expérimental ont été calculés pour chaque sujet et chaque niveau de force par rapport à une position de repos enregistrée avant la séance des essais perception de la force. Globalement, on peut constater que les sujets ont ajusté leur posture en déplaçant leur bassin vers l'arrière, vers le haut et légèrement vers la droite avec l'augmentation du niveau de la force.

Comme les sujets ont ajusté leur position en déplaçant leur bassin vers l'arrière, vers le haut et vers la droite, quatre angles articulaires ont été considérés:

- Les angles de flexion/extension de la hanche, du genou et de la cheville
- L'angle abduction/adduction de la hanche

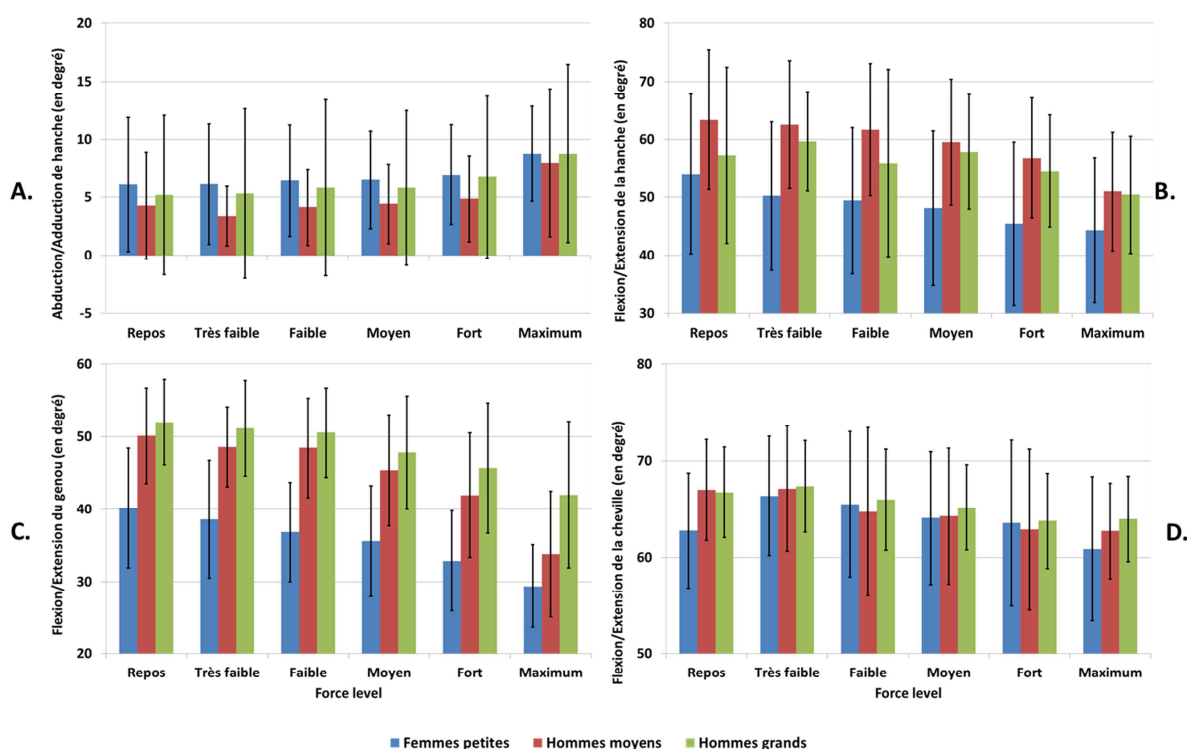


Figure 76: Variation des angles d'abduction/adduction de la hanche, de flexion/extension de la hanche, du genou et de la cheville pour les 3 groupes de sujets.

Tout d'abord, il peut être observé que l'adduction de la hanche a augmenté de façon significative seulement au niveau de la force maximale, de 5-6° à 8.5°. Les angles de

flexion/extension de la hanche, du genou et de la cheville ont diminué avec le niveau de force. Les variations d'angles entre la posture de repos et celle d'effort maximum étaient de  $-9.5^\circ$ ,  $-12.2^\circ$  et  $-3^\circ$  respectivement pour la hanche, le genou et la cheville, montrant ainsi que les sujets ont étendu leur jambe gauche avec l'augmentation du niveau de la force. Parmi les trois articulations du membre inférieur, des variations angulaires élevées ont été observées pour la hanche et du genou à la différence de la cheville. Il peut également être remarqué que les angles de flexion/extension de la hanche et du genou des femmes de petite taille étaient significativement plus faibles que ceux des hommes, ce qui traduit le fait que les femmes ont en moyenne plus tendu leur jambe gauche que les hommes.

### 3.4 Simulation de la direction d'effort et de l'ajustement postural

#### 3.4.i Hypothèse de simulation

Wang et al. (2000) ont suggéré dans leur étude que le contrôle de la direction d'effort sur une pédale reposait sur le principe de minimisation des couples articulaires du membre inférieur. Néanmoins, l'hypothèse n'a été validée qu'avec un modèle biomécanique 2D alors les résultats expérimentaux montrent que la déviation latérale de la force n'est pas négligeable. Par ailleurs, les observations expérimentales tendent à montrer que l'ajustement postural pourrait aussi s'expliquer par la nécessité de réduire le chargement articulaire. En effet, lorsque l'on augmente le niveau d'effort, l'extension de la jambe tend à vouloir diminuer les bras de levier de la force au niveau du genou et de la hanche.

#### 3.4.ii Simulation de la direction d'effort

Le but de cette première simulation est de calculer la direction d'effort à posture et force tangentielle imposées qui minimisent les couples articulaires. Le problème a été formalisé de la façon suivante :

$$\text{Trouver } F_{Sim}^{Normale} \text{ et } F_{Sim}^{Transversale} \text{ qui minimisent } G = \sum_{Articulation} \sum_{DDL} \left( \frac{T_{Art.}^{DDL}}{(T_{Art.}^{DDL})_{Max}} \right)^2$$

Les couples articulaires  $T_{Art.}^{DDL}$  calculés dans la simulation pour les trois articulations du membre inférieur sur 7 degrés de liberté ou DDL : 3 pour la hanche, 2 pour le genou (pas d'abduction/adduction) et 2 pour la cheville (pas de rotation axiale). Ils ont aussi été normalisés dans la fonction objectif G en utilisant des valeurs maximales de couples de la littérature.

Les directions d'effort simulées ont été ensuite comparées à celles expérimentales. En ce qui concerne l'angle par rapport à l'axe  $HP_{App}$ , les résultats de la simulation ont montré les

mêmes tendances observées expérimentalement, i.e. une direction d'effort plus proche de l'axe  $HP_{App}$  pour les pédales en fin de course et une direction d'effort se rapprochant de l'axe  $HP_{App}$  avec l'augmentation du niveau d'effort. L'écart entre les résultats de simulation et les données expérimentales est en particulier plus important pour les efforts « très faible » et « faible », environ  $5^\circ$ , que pour les efforts « maximum », environ  $3^\circ$ . Cet écart vient d'une sous-estimation par la simulation de la composante normale de l'effort qui contrôle la direction dans le plan sagittal. Cette sous-estimation pourrait venir du fait que les contacts entre le siège et la cuisse au cours des essais n'étaient pas connus.

En ce qui concerne la déviation latérale de l'effort, la simulation a prédit une orientation vers la droite alors qu'expérimentalement, l'effort était orienté vers la gauche. Ce résultat sous-entend que la déviation latérale de l'effort n'est pas contrôlée par la minimisation des couples mais potentiellement par un autre mécanisme que les données actuelles ne permettent pas d'identifier.

### 3.4.iii Simulation de l'ajustement postural

Le but de cette deuxième simulation est de calculer le déplacement de la hanche gauche à direction d'effort imposée qui minimise à la fois les couples articulaires et le déplacement de la hanche. Du fait qu'expérimentalement les sujets se sont principalement reculés et élevés, le déplacement simulé a été contraint dans le plan sagittal sur une droite définie telle que  $\frac{\Delta x}{\Delta z} = \tan 35^\circ$ .

Ce second problème a donc été formalisé de la façon suivante :

$$\text{Trouver } \Delta x \text{ et } \Delta z \text{ qui minimisent } H = \sum_{\text{Articulation}} \sum_{DDL} \left( \frac{T_{Art.}^{DDL}}{(T_{Art.}^{DDL})_{Max}} \right)^2 + 0.5 * \left( \frac{\sqrt{\Delta x^2 + \Delta z^2}}{100} \right)^2$$

Les pondérations de la fonction objectif pour les parties minimisant les couples articulaires et le déplacement de la hanche ont été choisies arbitrairement en partant du fait que la minimisation des couples était prioritaire. La limite de déplacement a été fixée à 100 mm en se basant sur les résultats expérimentaux. Par ailleurs, contrairement à la première simulation, une seconde optimisation a été nécessaire pour pouvoir estimer H. En effet, à chaque itération, il est nécessaire de calculer une nouvelle posture qui prenne en compte le déplacement imposé. Ce problème a été résolu en utilisant une méthode de résolution itérative classique basée sur la pseudo-inverse de la matrice jacobienne.

Globalement, les mêmes ordres de grandeur de déplacement de la hanche ont été trouvés par simulation comparés aux données expérimentales. En outre, la simulation a correctement prédit le fait que le déplacement de la hanche augmentait avec le niveau de force. La

simulation donne également une assez bonne prédiction des trois principaux angles articulaires en fonction du niveau de force. Les résultats montrent que l'ajustement postural est le fruit d'un compromis entre la réduction du chargement articulaire et le déplacement du bassin, en particulier pour les niveaux de force intermédiaires. La fonction multi-objectif utilisée dans la simulation met aussi en avant le fait que le besoin de réduire le chargement articulaire augmenterait avec le niveau d'effort.

## 4 Modèle musculo-squelettique et contrôle de la direction d'effort

### 4.1 Introduction

L'analyse du contrôle de la direction d'effort dans la partie précédente a montré que la minimisation des couples articulaires pouvait globalement expliquer l'orientation de la force dans le plan sagittal mais pas la déviation latérale. Par ailleurs, il a été montré que le critère de minimisation des couples articulaires donnaient de meilleurs résultats pour les efforts maximum que pour les niveaux d'effort intermédiaires.

Dans cette partie, nous allons utiliser un modèle musculo-squelettique et considérer la minimisation de l'activité musculaire comme loi de contrôle moteur de la direction d'effort. Ce critère a été choisi car son interprétation vis-à-vis de la minimisation des couples articulaires semble plus facile. Le but est d'évaluer l'apport d'un modèle musculo-squelettique par rapport à un modèle corps rigide classique pour la simulation de posture.

Le modèle musculo-squelettique utilisé pour cette étude a été développé à l'IFSTTAR par Fraysse (2009) au cours de sa thèse.

### 4.2 Simulation de la direction d'effort

La simulation reprend le principe de la simulation basée sur la minimisation des couples articulaires qui a été présentée dans la partie précédente et a été formalisée de la manière suivante :

*Trouver  $F_{SimMS}^{Normale}$  et  $F_{SimMS}^{Transversale}$  qui minimisent  $W = \sum_{i=1}^n \text{muscles} (\alpha_i)^2 = \sum_{i=1}^n \text{muscle} \left( \frac{f_i}{f_i^{Max}} \right)^2$*

Pour chaque muscle  $i$ , l'activation musculaire  $\alpha_i$  est définie comme le rapport de la force musculaire  $f_i$  (calculée par le modèle musculo-squelettique) sur la capacité maximale d'effort du muscle  $f_i^{Max}$  (proportionnelle à la section physiologique transverse du muscle issue de la littérature).

Globalement, les directions d'effort prédites par la simulation utilisant le critère de minimisation des activités musculaires sont proches de celles prédites par la minimisation des couples, que ce soit pour les essais de capacités d'effort ou ceux de perception. En particulier, la présente simulation prédit une déviation latérale de l'effort vers la droite et non vers la gauche comme cela est le cas expérimentalement. Néanmoins, le critère musculaire améliore la prédiction de la direction d'effort dans le plan sagittal pour les efforts très faibles et faibles par rapport au précédent critère. Pour ces niveaux faibles d'effort, l'analyse des profils

d'activation musculaire a par ailleurs montré que la minimisation des couples articulaires avait tendance à activer plus de muscles et à des niveaux plus élevés que le critère de minimisation musculaire, suggérant que réduire le chargement articulaire peut être une stratégie de contrôle moteur plus coûteuse que de minimiser l'activité musculaire pour des niveaux d'effort peu élevé.

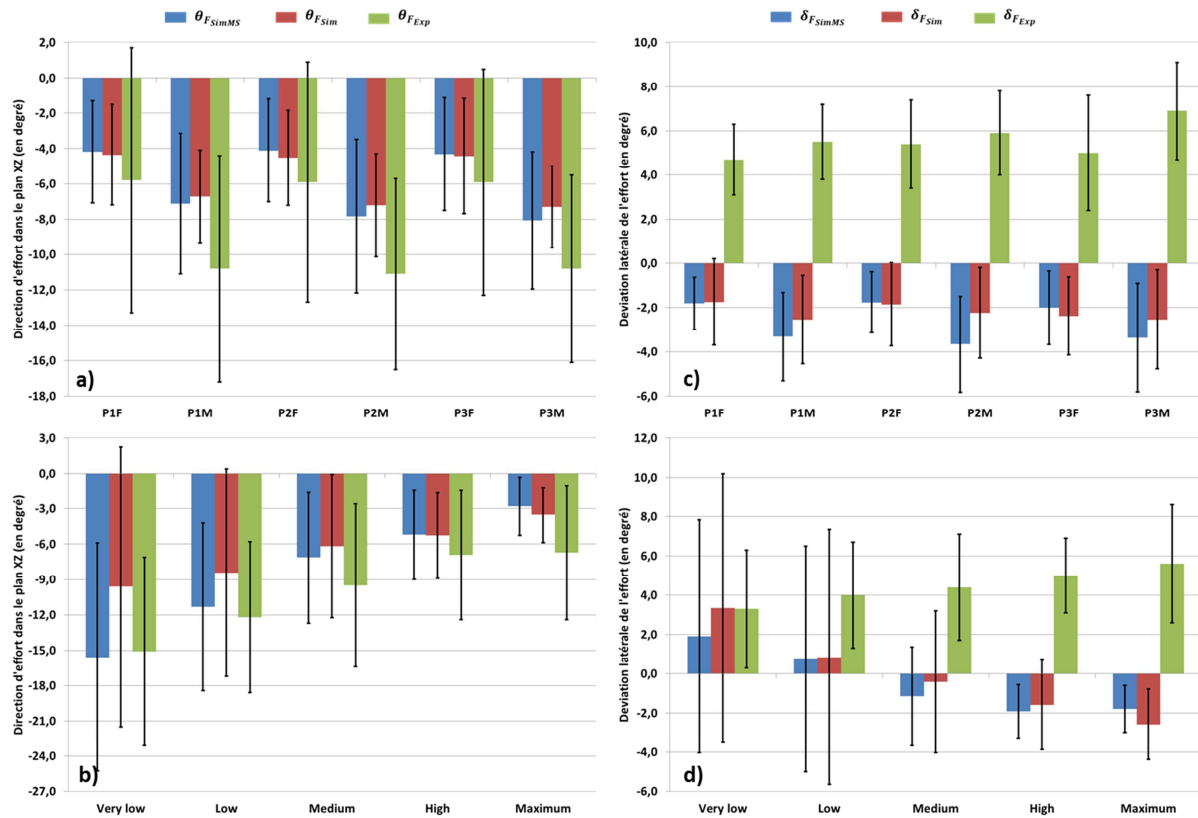


Figure 77: Comparaison des directions d'effort dans les plans XZ (a pour les essais de capacité d'effort et b pour les essais de perception) et XY (c pour les essais de capacité d'effort et d pour les essais de perception) issues des données expérimentales (en vert), de la simulation par minimisation des couples articulaires (en rouge) et de la simulation par minimisation de l'activité musculaire (en bleu)

## 5 Conclusion générale

Cette thèse a été réalisée dans le contexte du développement des modèles numériques biomécaniques de l'homme pour l'évaluation ergonomique des produits. Les questions de recherche de l'étude se sont focalisées en particulier sur deux points :

- Comment proposer des indicateurs objectifs de la gêne ressentie pour aider les ingénieurs dans leur processus de sélection du meilleur design de produit ?
- Comment prédire la posture d'un individu en tenant compte de l'effort exercé ?

La définition d'indicateurs objectifs de l'inconfort à partir de paramètres biomécaniques n'est pas chose aisée. De nombreux paramètres biomécaniques peuvent être pris en considération. Dans cette étude, nous avons fait l'hypothèse qu'un meilleur confort d'utilisation pouvait être obtenu quand les gens sont à même de faire leurs propres réglages. Un modèle d'inconfort basé sur le concept du mouvement moins contraint a été proposé et illustré par un cas d'étude sur le mouvement de débrayage. Les paramètres pertinents ont été identifiés en comparant des configurations imposées et moins contraintes. Bien que l'approche proposée soit générique, les indicateurs d'inconfort identifiés sont spécifiques à la tâche et dépendants des conditions d'essai. En effet, comme seule la position de la pédale a été considérée comme paramètre ajustable, les indicateurs proposés peuvent ne pas être applicable à d'autres situations dans lesquelles d'autres paramètres de conception seraient ajustables.

Mais la manière de simuler des mouvements moins contraints reste en question. En effet, les utilisateurs finaux pourraient être intéressés à prédire les moins contraint de configuration. De notre point de vue, une approche basée sur des données telle que celle mis en œuvre dans RPx pourrait être proposé pour prédire de tels mouvements. Il reste que comme pour toutes les méthodes basées sur des données, les résultats dépendent fortement de l'ensemble de données sous-jacent et il sera difficile d'extrapoler en dehors des conditions expérimentales.

Ensuite, une question est de savoir comment combiner les indicateurs pour obtenir une évaluation globale d'un produit. Un score global est généralement préféré par les ingénieurs car il permet de différencier rapidement plusieurs alternatives de conception. Nos indicateurs d'inconfort proposés peuvent être efficaces pour comparer des propositions de design, et ne répondent donc pas complètement aux attentes des industriels en matière d'évaluation ergonomique absolue. De notre point de vue, notes globales et indicateurs ne sont pas fondamentalement opposés les uns aux autres, mais doivent être considérés comme des outils complémentaires pour l'évaluation ergonomique de produits. Ainsi ces indicateurs pourraient

fournir des éléments objectifs pour un expert pour former une méthode d'évaluation globale d'un design de produit.

Enfin, les indicateurs de gêne proposés sont basés sur les paramètres cinématiques et dynamiques d'un mouvement expérimental, ce qui implique que la simulation de mouvement utilisant un mannequin numérique doit être validée expérimentalement aussi bien du point de vue de la cinématique que de la dynamique. Ceci est particulièrement important pour les paramètres dynamiques tels que les couples articulaires car leur calcul dépend fortement du contrôle de la direction de la force. C'est sur ce point en particulier que les deux parties de cette thèse se relient.

Dans une première étape visant à améliorer les méthodes de prédiction de posture impliquant la production d'un effort, le mécanisme de production d'effort sur une commande automobile a été étudié à travers l'exemple de la pédale d'embrayage. En utilisant des données expérimentales et de la simulation biomécanique, deux aspects de la production d'effort ont été étudiés: le contrôle de la direction d'effort et le contrôle de la posture.

Un des principaux résultats de cette étude est que la direction de la force appliquée sur la pédale ainsi que l'ajustement postural sont principalement expliqués par la nécessité de réduire le chargement articulaire lorsque l'on augmente le niveau de force demandé. Par ailleurs, l'utilisation d'un modèle musculo-squelettique avec un critère d'optimisation minimisant l'activité musculaire a permis d'améliorer la prédiction de la direction d'effort pour des niveaux de force de faible intensité par rapport à un critère de minimisation des couples articulaires et à un modèle multi-corps sans muscles de l'homme. Néanmoins, aucune des approches de simulation proposées n'a permis d'expliquer la déviation latérale de l'effort sur la pédale, ce qui suggère que la direction de la force latérale peut être contrôlée par d'autres mécanismes. L'étape suivante de cette étude serait donc de mettre en place une méthode permettant de prédire simultanément la direction d'effort et l'ajustement postural. L'étude tendant à montrer que la réduction du chargement articulaire explique à la fois le contrôle de la direction et celui de la posture, il pourrait donc être envisagé dans un premier temps de fusionner les deux algorithmes utilisés dans ce travail. Reste qu'une des principales difficultés de la simulation pour les commandes automobile est la gestion des contacts entre l'individu et le siège. Pour cela, une modélisation plus réaliste des contacts avec le siège est nécessaire.

## References

- Abdel-Malek, K., Arora, J., 2008. Physic-Based Digital Human Modeling: Predictive Dynamics. In: Duffy, V.G., Handbook of Digital Human Modeling: Research for Applied Ergonomics and Human Factors Engineering. CRC Press, Inc. Boca Raton, FL, USA, Part 5.
- Anderson, F.C., Pandy, M.G., 2001. Dynamic optimization of human walking. *Journal of Biomechanical Engineering* 123, 381–390.
- Annett, J., 2002. Subjective rating scales: science or art?. *Ergonomics*, 45 (14), 966-987
- Armstrong, T.J., Buckle, P., Fine, L.J., Hagberg, M., Jonsson, B., Kilbom, A., Kuorinka, I. A.A., Silverstein, B.A., Sjøgaard, G., Viikari-Juntura, E.R.A., 1993. A conceptual model for work-related neck and upper limb disorders. *Scandinavian Journal of Work, Environment and Health* 19, 73–84.
- Ausejo, S., Wang, X., 2008. Motion capture and human motion reconstruction. In: Duffy, V.G., Handbook of Digital Human Modeling: Research for Applied Ergonomics and Human Factors Engineering. CRC Press, Inc. Boca Raton, FL, USA, pp. 38-1-38-14
- Ayoub, M. M., Gidcumb, C. F., Reeder, M. J., Beshir, M. Y., Hafez, H. A., 1981. Development of an Atlas of Strengths and Establishment of an Appropriate Model Structure. *Anatomy and physiology human factors engineering & man and machine system*.
- Bubb, H., 2003. Research for a strength based discomfort model of posture and movement. International Ergonomics Association XVth Triennial Congress, August 24-29, 2003, Seoul.
- Borg, G., 1998. Borg's perceived exertion and pain scales. Human Kinetics Publishers.
- Bubb, H., Fritzsche, F., 2008. A Scientific Perspective of Digital Human Models. In: Duffy, V.G., Handbook of Digital Human Modeling: Research for Applied Ergonomics and Human Factors Engineering. CRC Press, Inc. Boca Raton, FL, USA, Part 3.
- Chaffin, D. B., 1997. Development of computerized human static strength simulation model for job design. *Human Factors and Ergonomics in Manufacturing*, 7(4), 305–322.
- Chaffin, D., Andersson, G., Martin, B., 1999. *Occupational Biomechanics*, 3<sup>rd</sup> Edition. J. Wiley & Sons, New York, NY.
- Chaffin, D.B., 2005. Improving digital human modeling for proactive ergonomics in design. *Ergonomics*. 48(5) 478-491.
- Chaffin, D.B., 2008. Some Requirements and Fundamental Issues in Digital Human Modeling. In: Duffy, V.G., Handbook of Digital Human Modeling: Research for Applied Ergonomics and Human Factors Engineering. CRC Press, Inc. Boca Raton, FL, USA, Part 2.
- Chateauroux, E., Wang, X., Trasbot, J., 2007. A database of ingress / egress motions of elderly people. SAE International conference and exposition of Digital Human Modeling for Design

- and Engineering, University of Washington, Seattle, Washington, USA, June 12-14, 2007, SAE Paper 2007-01-2493.
- Chevalot, N., Wang, X., 2004. An experimental investigation of the discomfort of arm reaching movements in a seated position. *SAE Transactions* 113, 93–103.
  - Chung, M.K., Lee, I., Kee, D., 2005. Quantitative postural load assessment for whole body manual tasks based on perceived discomfort. *Ergonomics*, Vol.48, No.5, 492-505.
  - Crowninshield, R.D., Brand R.A., 1981. A physiologically based criterion of muscle force prediction in locomotion. *Journal of Biomechanics*;14:793–801
  - Cruse, H., Wischmeyer, E., BrÄ¼wer, M., Brockfeld, P., Dress, A., 1990. On the cost functions for the control of the human arm movement. *Biological Cybernetics* 62, 519–528.
  - Daams, B. J., 1994. Human force exertion in user-product interaction. *Backgrounds for design*. Delft: Fac. of Industrial Design Engineering, Delft Univ. of Technology
  - Das, B., Wang, Y. 2004. Isometric Pull-Push Strengths in workspace: 1 Strength Profiles. *International Journal of Occupational Safety and Ergonomics*, 10, 1, 43-58.
  - Das, B., Wang, Y. 2004. Isometric pull –push strengths in workspace: 2 Analysis of spatial factors. *International Journal of Occupational Safety and Ergonomics*, 10, 1, 59-64.
  - De Groote, F., Pipeleers, G., Jonkers, I., Demeulenaere, B., Patten, C., Swevers, J., De Schutter, J., 2009. A physiology based inverse dynamic analysis of human gait: potential and perspectives. *Computer Methods in Biomechanics and Biomedical Engineering*, 12(5), 563-574
  - De Looze, M.P., Kuijt-Evers, L.F.M., Van Dieën, J.H., 2003. Sitting comfort and discomfort and the relationships with objective measures. *Ergonomics* 46, 985–997.
  - Dellman, N.J., Haslegrave, C.M., Chaffin, D.B., *Working postures and movements: tools for evaluation and engineering*. CRC Press, London.
  - Delp, S.L., 1990. Surgery simulation: a computer graphics system to analyze and design musculoskeletal reconstructions of the lower limb. Ph.D. Thesis, Stanford University, Stanford, California.
  - Dessailly, E., 2008. Analyse biomécanique 3D de la marche de l' enfant déficient moteur. Thèse de doctorat, Université de Poitiers.
  - DHErgo, 2010. D17. Data for Case Studies 1.
  - Dickerson, C.R., Martin, B.J., Chaffin, D.B., 2006. The relationship between shoulder torques and the perception of muscular effort in loaded reaches. *Ergonomics*, Vol. 49, No. 11, 1036–1051.
  - Doriot, N., Chèze, L., 2004. A three-dimensional kinematic and dynamic study of the lower limb during the stance phase of gait using an homogeneous matrix approach. *IEEE Trans Biomed Eng* 51 (1), 21–27.

- Dufour, F., Wang, X., 2005. Discomfort assessment of car ingress/egress motions using the concept of neutral movement. *SAE Transactions* 114 (6), 2905–2913.
- Dumas, R., Cheze, L., Verriest, J.-P., 2007. Adjustments to Mc Conville et al. and young et al. body segment inertial parameters. *Journal of Biomechanics* 40, 543-553.
- Erdemir, A., McLean, S., Herzog, W., Van der Bogert, A.J., 2007. Model-based estimation of muscle forces exerted during movements. *Clinical Biomechanics* 22, 131-154.
- Faraway, J., 2000. Modeling reach motions using functional regression analysis. *SAE Technical Paper* 2000-01-2175.
- Fathallah, F. A., Chang, J. H., Berg, R. L., Pickett, W., Marlenga, B., 2008. Forces required to operate controls on farm tractors: Implications for young operators. *Ergonomics*, 51 (7), 1096-1108.
- Fraysse, F., Wang, X., Cheze, L., 2007. Estimation of the Muscle Efforts of the Lower Limb During a Clutch Pedal Operation. In: *SAE International Conference on Digital Human Modeling* (SAE Paper 2007-01-2487).
- Fraysse, F., 2009. Estimation des activités musculaires au cours du mouvement en vue d'applications ergonomiques. Mémoire de thèse de l'Université Claude Bernard Lyon 1.
- Gallagher, S., Moore, J. S., Stobbe, T. J., 1998. Physical strength assessment in ergonomics. American Industrial Hygiene Association, Fairfax, Virginia.
- Haslegrave, C. M., 1995. Factors in the driving task affecting comfort and health. In: *3rd International Conference on Vehicle Comfort and Ergonomics*. pp. 223–230.
- Haslegrave, C. M., 2004. Force exertion. In: Dellman, N.J., Haslegrave, C.M., Chaffin, D.B., *Working postures and movements: tools for evaluation and engineering*. CRC Press, London, pp. 367-402.
- Helander, M.G., Zhang, L., 1997. Field studies of comfort and discomfort in sitting. *Ergonomics* 40, 895–915.
- Hignett, S., McAtamney, L., 2000. Rapid entire body assessment (REBA). *Applied Ergonomics* 31 (2), 201 – 205.
- Hoffman, S.G., Reed, M.P., Chaffin, D.B., 2007. Predicting force-exertion postures from task variables. *Technical Paper* 2007-01-2480. SAE International, Warrendale, PA.
- Hoffman, S.G., 2008. Whole-body postures during standing hand-force exertions: development of a 3D biomechanical posture prediction Model. PhD Dissertation. The University of Michigan, Ann Arbor, MI.
- Institut Français du textile et de l'habillement (IFTH), 2006. Campagne Nationale de Mensuration
- Jung, E. S., Choe, J., 1996, Human reach posture prediction based on psychophysical discomfort. *International Journal of Industrial Ergonomics*, 1996, Vol.18, p.173-179.

- Kapandji, I., 1994. *Physiologie articulaire Vol. 2: Membre inférieur*, 5th Edition. Maloine, Paris, France.
- Karhu, O., Kansii, P., Kuorinka, I., 1977. Correcting working postures in industry: A practical method for analysis. *Applied Ergonomics* 8 (4), 199 – 201.
- Kaufman, K.R., An, K.N., Litchy, W.J., Chao, E.Y.S., 1991. Physiological prediction of muscle forces—II. Application to isokinetic exercise. *Neuroscience*, 40:793–804
- Kee, D., Karwowski, W., 2001. The boundaries for joint angles of isocomfort for sitting and standing males based on perceived comfort of static joint postures. *Ergonomics*, 2001, Vol. 44, No. 6, 614-648.
- Kee, D., Karwowski, W., 2003. Ranking systems for evaluation of joint and joint motion stressfulness based on perceived discomforts. *Applied Ergonomics* 34, 167-176
- Kee, D., Lee, I., 2012. Relationships between subjective and objective measures in assessing postural stresses. *Applied Ergonomics*, 43 (2), 271–276.
- Kim, J.H., Yang, J., Abdel-Malek, K., 2009. Multi-objective Optimization Approach for Predicting Seated Posture Considering Balance. *International Journal of Vehicle Design* 51(3/4), 278–291
- Kroemer, K. H. E., 1970. *Die Messung der Muskelstärke des Menschen. Methoden und Techniken*. Bremerhaven: Wirtschaftsverl. NW (Forschungsbericht/Bundesanstalt für Arbeitsschutz und Unfallforschung).
- Kroemer, K.H.E., 1971. Foot operation of controls. *Ergonomics*, 14(3), 333–361.
- Kroemer, K. H. E., 1999. Assessment of human muscle strength for engineering purposes: a review of the basics. *Ergonomics*, 42 (1), 74-93.
- Kuijt-Evers, L.F.M., Bosh, T., Huysmans, M.A., de Looze, M.P., Vink, P., 2007. Association between objective and subjective measurements of comfort and discomfort in hand tools. *Appl. Ergon.* 38 (5), 643e654.
- Kumar, S., 2004. *Muscle strength*. Boca Raton: CRC Press.
- Lara-Lopez, A., Aguilera-Cortes, L., Barbosa-Castillo, F. 1999. Measurement of forces applied to handgrips and pedals for a sample population of Mexican males. *Applied Ergonomics* 30, 173-176.
- Liu, G., Mc Millan, L., 2006. Estimation of missing markers in human motion capture. *The Visual Computer*, 22 (9), 721-728.
- Lloyd, D.G., Besier, T.F., 2003. An EMG-driven musculoskeletal model to estimate muscle forces and knee joint moments in vivo. *Journal of Biomechanics* 36, 765–776.
- Lloyd, D.G., Buchanan, T.S., 2001. Strategies of muscular support of varus and valgus isometric loads at the human knee. *Journal of Biomechanics* 34:1257–1267

- Ma, L., Zhang, W., Chablat, D., Bennis, F., Guillaume, F., 2009. Multi-objective Optimization Method for Posture Prediction and Analysis with Consideration of Fatigue Effect and Its Application Case. *Computers and Industrial Engineering* 57, 1235–1245.
- Manal, K. and T. S. Buchanan, 2003. A one-parameter neural activation to muscle activation model: estimating isometric joint moments from electromyograms. *Journal of Biomechanics* 36, 1197-202.
- Marler, R.T., Arora, J.S., Yang, J., Kim, H.-J., Abdel-Malek, K., 2009. Use of Multi-objective Optimization for Digital Human Posture Prediction. *Engineering Optimization* 41(10), 295–943
- Marler, R.T., Knake, L., Johnson, R., 2011. Optimization-Based Posture Prediction for Analysis of Box Lifting Tasks. *Digital Human Modeling, HCII 2011*, 151–160.
- McAtamney, L., Corlett, E. N., 1993. Rula: a survey method for the investigation of work-related upper limb disorders. *Applied Ergonomics* 24 (2), 91 – 99.
- Mehta, C.R., Tiwari, P.S., Rokade, S., Pandey, M.M., Pharade, S.C., Gite, L.G., Yadav, S.B., 2007. Leg strength of Indian operators in the operation of tractor pedals. *International journal of industrial Ergonomics*, 37, 283-289.
- Mick, F., 1995. Eine experimentelle Untersuchung der Korrelation von Komfortempfinden und Handhabungskräften an Pedalen. Diplomarbeit, Technische Universität, Munich.
- Mital, A., Kumar, S. 1998. Human muscle strength definitions, measurement and usage : Part I - Guidelines for the practioner. *International Journal of Industrial Ergonomics*, 22, 101-121.
- Mital, A., Kumar, S., 1998. Human muscle strength definitions, measurement and usage : Part II – The scientific basis (knowledge base) for the guide. *International Journal of Industrial Ergonomics*, 22, 123-144.
- Monnier, G., Renard, F., Chameroy, A., Wang, X., Trasbot, J., 2006. Motion simulation approach integrated into a design engineering process. *SAE International conference and exposition of Digital Human Modeling for Design and Engineering*, Lyon, France, July 4-6, 2006, SAE Paper 2006-01-2359.
- Monnier, G., Wang, X., Beurier, G., Trasbot, J., 2007. Coordination of spine degrees of freedom during a motion reconstruction process. *SAE International conference and exposition of Digital Human Modeling for Design and Engineering*, University of Washington, Seattle, Washington, USA, June 12- 14, 2007, SAE Paper 2007-01-2454.
- Monnier, G., Wang X., Trasbot, J., 2008. RPX: A motion simulation tool for car interior design. In: Duffy, V.G., *Handbook of Digital Human Modeling: Research for Applied Ergonomics and Human Factors Engineering*. CRC Press, Inc. Boca Raton, FL, USA, Part 31.
- Mortimer, R.G., Segel, L., Dugoff, H., Campbell, J.D., Jorgeson, C.M., Murphy, R.W., 1974. Brake force requirement study: driver-vehicle braking performance as a function of brake system design variables. National Highway Safety Bureau U.S Department of transportation.

- Occhipinti, E., 1998. OCRA: a concise index for the assessment of exposure to repetitive movements of the upper limbs. *Ergonomics* 41 (9), 1290–1311.
- Pandy, M.G., 2001. Computer modeling and simulation of human movement. *Annu. Rev. Biomed. Eng.* 3, 245–273.
- Pannetier, R., Robert, T., Holmberg, J., Wang, X., 2011. Optimization-based muscle force scaling for subject specific maximum isometric torque estimation. *ISB Congress 2011, Brussels, 3-7 July 2011*.
- Park, W., Chaffin, D., Martin, B.: Toward memory-based human motion simulation: development and validation of a motion modification algorithm. *IEEE Transactions on Systems, Man, and Cybernetics-Part. A: Systems and Humans* 34(3), 376–386 (2004)
- Pheasant, S., Harris, C., 1982. Human strength in the operation of tractor pedals. *Ergonomics*, 25, 1, 53–63.
- Redl, C. et al. Sensitivity of muscle force estimates to variations in muscle-tendon properties (2007) *Human Movement Science*, 26 (2), pp. 306-319.
- Reed, M.P., Manary, M.A., Flannagan, C.A.C., and Schneider, L.W., 2002. A statistical method for predicting automobile driving posture. *Human Factors*. 44(4): 557-568.
- Sanders, M. S., Mc Cormick, J., 1993. *Human Factors in Engineering and Design*, 7th edition (New York: McGraw-Hill).
- Schmidt, M. W., López-Ortiz, C., Barrett, P. S., Rogers, L. M., Gruben, K. G., 2003. Foot force direction in an isometric pushing task: prediction by kinematic and musculoskeletal models. *Experimental Brain Research*, 150(2), 245-254.
- Scovil, C.Y., Ronsky, J.L. Sensitivity of a Hill-based muscle model to perturbations in model parameters (2006) *Journal of Biomechanics*, 39 (11), pp. 2055-2063.
- Seidl, A., 1994. *Das Menschmodell Ramsis: Analyse, Synthese, und Simulation dreidimensionaler Körperhaltungen des Menschen [The man-model RASMSIS: Analysis, Synthesis, and simulation of three-dimensional human body postures.]*, Doctoral Dissertation, Technical University of Munich.
- Seitz, T, Recluta, D, Zimmermann, D and Wirsching, H-J., 2005. FOCOPP - An approach for a human posture prediction model using internal/external forces and discomfort. *Proceedings of the SAE Digital Human Modeling Conference*.
- Shen, W., Parsons, K.C., 1997. Validity and reliability of rating scales for seated pressure discomfort. *International Journal of Industrial Ergonomics*, 20, 441-461.
- Soechting, J.F., Buneo, C.A., Herrmann, U., Flanders, M., 1995. Moving effortlessly in three dimensions: does Donders' law apply to arm movement? *The Journal of Neuroscience*, September, 15(9), 6271-6280.
- Southall, D., 1985. The discrimination of clutch-pedal resistances. *Ergonomics*, 28(9), 1311–1317.

- Thorpe, S.K., Li, Y., Crompton, R.H., McNeill, A. R., 1997. Stresses in human leg muscles in running and jumping determined by force plate analysis and from published magnetic resonance images. *J. Exp. Biology* 201, 63-70.
- Uno, Y., Kawato, M., Suzuki, R., 1989. Formation and control of optimal trajectories in human multi-joint arm movements: Minimum torque-change model. *Biological Cybernetics*. 61, 89-101.
- Van Sint Jan, S., 2007. *Color atlas of skeletal landmark definitions*. Churchill Livingstone, Elsevier, Philadelphia.
- Veldpaus, F.E., Woltring, H.J., Dortmans, L., 1988. A least-squares algorithm for the equiform transformation from spatial marker co-ordinates. *Journal of Biomechanics*, 21 (1), 45-54.
- Verriest, J.P., Wang, X., Trasbot, J., Tessier, Y., 1994. Application of a 3D human model to computer aided ergonomic design of vehicles, in proc. of FISITA'94: Engineering for Customers, pp 53-61, Int. Academic Publishers, Beijing, 1994.
- Vezin, P., Verriest, J.P., 2005. Development of a set of numerical human models for safety. *Proceedings of the 19th International Technical Conference on the Enhanced Safety of Vehicles*, Published by U.S. Department of Transportation NHTSA, Paper No 163.
- Vink, P., Hallbeck, S., 2012. Editorial: Comfort and discomfort studies demonstrate the need for a new model. *Applied Ergonomics*, 43 (2), 271–276.
- Wang, X., Verriest J.P., 1998. A geometric algorithm to predict the arm reach posture for computer-aided ergonomic evaluation. *The Journal of Visualization and Computer Animation*, 9, 33-47.
- Wang, X., Verriest, J.-P., Lebreton-Gadegbeku, B., Tessier, Y., Trasbot, J., 2000. Experimental investigation and biomechanical analysis of lower limb movements for clutch pedal operation. *Ergonomics* 43, 1405–1429.
- Wang, X., Breton-Gadegbeku, B. L., Bouzon, L., 2004. Biomechanical evaluation of the comfort of automobile clutch pedal operation. *International Journal of Industrial Ergonomics* 34 (3), 209 – 221.
- Wang, X., Bullock, M. I., 2004. Pedal operation. In: Dellman, N.J., Haslegrave, C.M., Chaffin, D.B., *Working postures and movements: tools for evaluation and engineering*. CRC Press, London, pp. 190–211.
- Wang, X., Chevalot, N., Monnier, G., Trasbot, J., 2006. From motion capture to motion simulation: an in-vehicle reach motion database for car design. *SAE 2006 Transactions Journal of Passenger Car – Electronic and Electronic Systems* , SAE Paper 2006-01-2362. pp.1124-1130.
- Wang, X., Chevalot, N., Trasbot, J., 2008. Prediction of in-vehicle reach surfaces and discomfort by digital human models. *SAE Technical Paper* 2008-01-1869.

- Wang, X., 2008a. Contribution à la simulation du mouvement humain en vue d'application en ergonomie. HDR de Biomécanique. Université Claude Bernard Lyon 1, IFSTTAR, LBMC, UMR\_T9406.
- Wang, X., 2008b. Discomfort Evaluation and Motion Measurement. In: Duffy, V.G., Handbook of Digital Human Modeling: Research for Applied Ergonomics and Human Factors Engineering. CRC Press, Inc. Boca Raton, FL, USA, Part 25.
- Wang, X., Barelle, C., Pannetier, R., Numa, J., 2009. Capacités musculaires des membres inférieurs et supérieurs appliquées aux commandes automobiles et leur perception d'effort. Rapport Contrat Projet Renault F08-22.
- Wang, X., Barelle, C., Pannetier, R., Numa, J., Chapuis, T., 2010. A data-based approach for predicting hand and foot maximum force on a control: Application to hand brake. 3rd AHFE International Conference 2010, Miami, USA, 17-20 July 2010.
- Wang, X., Pannetier, R., Burra N. K., Numa, J., 2011. A Biomechanical Approach for Evaluating Motion Related Discomfort: Illustration by an Application to Pedal Clutching Movement. 14th International Conference on Human-Computer Interaction, Orlando, 9-14 July 2011.
- Winkel, J., Westgaard, R., 1992. Occupational and individual risk factors for shoulder neck complaints: Part II – The scientific basis (literature review) for the guide. International Journal of Industrial Ergonomics 10, 85–104.
- Wirsching, H.J., Engstler, F., 2012. New enhancements and validation of force based posture and discomfort predictions. IEA World Congress on Ergonomics, Recife, Brazil, 12-16 february 2012.
- Yang, J., Marler, R.T., Kim, H., Arora, J., Abdel-Malek, K., 2004. Multi-Objective Optimization for Upper Body Posture Prediction. In: 10th AIAA/ISSMO Multidisciplinary Analysis and Optimization Conference, Albany, New York, USA, August 30-September 1, 2004.
- Zacher, I., Bubb, H., 2004. Strength based discomfort model of posture and movement. Digital Human Modeling for Design and Engineering Symposium Proceedings, June 15-17, 2004, Oakland University, Rochester, Michigan, USA. SAE Paper 2004-01-2139.
- Zajac, F.E., 1989. Muscle and tendon: properties, models, scaling, and application to biomechanics and motor control. Crit. Rev. Biomed. Eng. 17, 359–411.
- Zhang, L., Helander, M., Drury, C., 1996. Identifying factors of comfort and discomfort. Human Factors 38, 377–389.
- Zhang, X., Chaffin, D., 2000. A Three-Dimensional Dynamic Posture Prediction Model For Simulating In-Vehicle Seated Reaching Movements: Development and Validation. Ergonomics Vol 43, 1314.

## Personal publication

- **Pannetier, R.**, Burra, N. K., Numa, J., Robert, T., Wang, X., 2011. Effects of free adjustment in pedal position on clutching movement and perceived discomfort. IEA DHM 2011. 1<sup>st</sup> International Symposium on Digital Human Modelling, 14-16 June 2011.
- **Pannetier, R.**, Robert, T., Holmberg, J., Wang, X., 2011. Optimization-based muscle force scaling for subject specific maximum isometric torque estimation. ISB Congress 2011, Brussels, 3-7 July 2011.
- **Pannetier, R.**, and Wang, X., 2012. Development of objective discomfort evaluation indicators for a task-oriented motion using less constrained motion concept: application to automotive pedal clutching task. IEA World Congress on Ergonomics, Recife, Brazil, 12-16 february 2012.
- Wang, X., Barelle, C., **Pannetier, R.**, Numa, J., Chapuis, T., 2010. A data-based approach for predicting hand and foot maximum force on a control: Application to hand brake. 3<sup>rd</sup> AHFE International Conference 2010, Miami, USA, 17-20 July 2010.
- Wang, X., **Pannetier, R.**, Burra N. K., Numa, J., 2011. A Biomechanical Approach for Evaluating Motion Related Discomfort: Illustration by an Application to Pedal Clutching Movement. 14<sup>th</sup> International Conference on Human-Computer Interaction, Orlando, 9-14 July 2011.